

Laser desorption
mass spectrometric studies
of artists' organic pigments

Nicolas Wyplosz

Cover illustration: detail from *The Astronomer* (ca. 1660) by Gerard Dou (1613-1675). Reproduced with permission of the Stedelijk Museum De Lakenhal, Leiden, The Netherlands.



The work described in this thesis was performed at AMOLF (FOM Institute for Atomic and Molecular Physics), Kruislaan 407, 1098 SJ, Amsterdam, The Netherlands. It is part of the research program of Priority Program MOLART (Molecular aspects of Ageing in Painted Works of Art) of the NWO (Nederlandse Organisatie voor Wetenschappelijk Onderzoek) and of the research program nr. 28 and 49 (Mass Spectrometry of Macromolecular Systems) of the FOM (Stichting voor Fundamenteel Onderzoek der Materie).

ISBN 90-77209-02-6

© Nicolas Wyplosz

Laser desorption
mass spectrometric studies
of artists' organic pigments

ACADEMISCH PROEFSCHRIFT

ter verkrijging van de graad van doctor
aan de Universiteit van Amsterdam
op gezag van de Rector Magnificus
prof. mr. P.F. van der Heijden,
ten overstaan van een door
het college voor promoties ingestelde commissie,
in het openbaar te verdedigen
in de Aula der Universiteit
op donderdag 20 november 2003 te 11.00 uur
door

Nicolas Wyplosz
geboren te Parijs (Frankrijk)

Promotiecommissie:

Promotor:

Prof. Dr. J.J. Boon

Copromotor:

Prof. Dr. ing. R.M.A. Heeren

Overige commissieleden:

Prof. Dr. J.R.J. van Asperen de Boer

Dr. S. Ingemann

Prof. Dr. P.G. Kistemaker

Prof. Dr. C.G. de Koster

Prof. Dr. N.H. Tennent

Dr. J. Wouters

Faculteit der Natuurwetenschappen, Wiskunde en Informatica

MOLART and MOLART Reports

MOLART - Molecular Aspects of Ageing of Painted Art - was a 5-year cooperative project between art historians, restorers, analytical chemists and technical physicists funded by the Dutch Organisation for Scientific Research (NWO). Technical support and advice was given by Shell-SRTCA (Amsterdam), AKZO-NOBEL (Arnhem), Instituut Collectie Nederland (ICN, Amsterdam) and the Dutch art museums. The project was launched on 1 February 1995 and ended in early 2003. The object of MOLART was to contribute to the development of a scientific framework for the conservation of painted art on the molecular level. The focus of MOLART was the determination of the present chemical and physical condition of works of art produced in the period from the 15th to the 20th century. Studies of historical paint manufacturing and workshop practice must give insight into the nature of the painters' media and the painting technique used originally. Fundamental studies on varnishes, paint, and colorants are undertaken to understand the molecular aspects of ageing since this is thought to be a main cause for the continued need to treat paintings.

This report is the eighth in a series of MOLART reports that will summarise all research results obtained in the course of the project. Information about MOLART can be obtained from the project co-ordinator Prof. Dr. J.J. Boon, FOM-Institute for Atomic and Molecular Physics, Kruislaan 407, 1098 SJ Amsterdam, The Netherlands, boon@amolf.nl.

1. Molecular studies of fresh and aged triterpenoid varnishes, Gisela A. van der Doelen, 1999. ISBN 90-801704-3-7
2. A mathematical study on craquelure and other mechanical damage in paintings, Petri de Willigen, 1999. ISBN 90-407-1946-2
3. Solvent extractable components of oil paint films, Kenneth R. Sutherland, 2001. ISBN 90-801704-4-5
4. Molecular changes in egg tempera paint dosimeters as tools to monitor the museum environment, Oscar F. van den Brink, 2001. ISBN 90-801704-6-1
5. Discoloration in renaissance and baroque oil paintings, Margriet van Eikema Hommes, 2002. In Press: Archetype Publications, London.
6. Analytical chemical studies on traditional linseed oil paints, Jorrit D.J. van den Berg, 2002. ISBN 90-801704-7-X
7. Microspectroscopic analysis of traditional oil paint, Jaap van der Weerd, 2002. ISBN 90-801704-8-8

Forthcoming

9: Molecular studies of Asphalt, Mummy and Kassel earth pigments: characterisation, identification and effect on the drying of traditional oil paint, Georgiana M. Languri. (forthcoming 2004), PhD Dissertation. University of Amsterdam.

10: Analysis of diterpenoid resins and polymers in paint media and varnishes with an atlas of mass spectra, Klaas Jan van den Berg. (forthcoming 2003).

Published MOLART reports can be ordered from Archetype Publications, 6 Fitzroy Square, London W1T 5HJ, England, Tel: +44 207 380 0800 Fax: +44 207 380 0500, info@archetype.co.uk, or from FOM.

Contents

Chapter 1 : Introduction	1
1.1. Introduction	2
1.2. Structure of an easel painting	3
1.3. Traditional and modern organic pigments	4
1.4. Categories of pigments under investigation	6
1.5. Deterioration of organic pigments	8
1.6. Investigation of organic colouring materials in conservation science	8
1.6.1. Rationale	8
1.6.2. Methodology	9
1.6.3. Restriction of the analytical approach	10
1.6.4. Molecular analysis of artists' organic pigments	11
1.7. LDMS of organic colouring materials, a rationale	13
1.8. Thesis outline	14
1.9. Main results and implications for painting studies	15
Chapter 2 : Principles and instrumentation of LDMS	17
2.1. Introduction	18
2.2. Laser Desorption Mass Spectrometry for Surface Analyses	19
2.3. Principles of LDMS	21
2.3.1. Formation of characteristic ions in LDMS	21
2.3.2. Laser desorption and ionisation (LDI)	22
2.3.3. Matrix-assisted laser desorption/ionisation (MALDI)	26
2.3.4. LDI and MALDI of paint materials	28
2.4. Instrumentation for the analysis of paint cross-section	29
2.4.1. Mass analysers	29
2.4.2. Time-of-flight Mass Spectrometer: Set-up and operation	30
2.4.3. Ion Trap Mass Spectrometer: Set-up and Operation	37
2.4.4. Multiple stage experiment with the ITMS	42
2.5. Conclusion	44
Chapter 3 : An experimental strategy for LDMS of paint materials	45
3.1. Introduction	46
3.2. Sample and sample mounting	46
3.2.1. Sample holders	46
3.2.2. Level differences	48
3.3. Laser-sample interaction	50
3.4. Shot-to-shot variations	56
3.5. TOF-MS versus ITMS: pressure and time-scale	59
3.6. Ion collection in the ITMS analyser: LMCO	60
3.7. CID experiments with the ITMS analyser	62
3.8. Conclusion	64

Chapter 4 : LDMS of flavonoids	65
4.1. Introduction:	66
4.2. Flavonoid pigments	68
4.2.1. Materials and practice	68
4.2.2. Molecular analysis of flavonoids and flavonoid pigments	69
4.3. Experimental	70
4.3.1. Instrumental set-ups	70
4.3.2. Flavonoid samples	71
4.3.3. Sample preparation	72
4.3.4. Mass calibration	72
4.4. Characterization of flavonoid aglycones with LDMS	73
4.4.1 Laser Desorption and Ionisation (LDI)	75
4.4.2 Matrix Assisted Laser Desorption Ionisation (MALDI)	79
4.5. Multiple-stage LDI–ITMS	81
4.5.1 LDI-ITMS of kaempferol	81
4.5.2 LDI-ITMS of luteolin and fisetin	84
4.5.3 DTMS and DTMS/MS of kaempferol	86
4.5.4 LDI-ITMS of quercetin and morin, apigenin and genistein	86
4.5.5 Influence of the collisional energy in MS/MS experiments	88
4.6. Characterisation of flavonoid-O-glycosides	89
4.6.1 LDI	89
4.6.2 MS/MS	91
4.7. Analysis of complex samples	92
4.7.1 Weld extracts	92
4.7.2 Flavonoid lakes	93
4.8. Analysis fibres dyed with flavonoids	94
4.9. Investigation of cross-sectioned samples	95
4.10. Conclusion	95
Chapter 5 : LDMS of anthraquinones	97
5.1. Introduction	98
5.2. Anthraquinone pigments	98
5.2.1. Materials and practice	98
5.2.2. Molecular analysis of anthraquinone pigments	101
5.3. Experimental	102
5.3.1. Instrumental set-ups and mass calibration	102
5.3.2. Samples	102
5.4. LDI and MALDI of Alizarin	103
5.4.1. Synthetic alizarin	103
5.4.2. LDI of an alizarin lake	106
5.5. Alizarin lake in oil paint	108
5.6. Analysis of natural dyed fibres	108
5.7. Conclusion	110

Chapter 6 : LDMS of indigoids	111
6.1. Introduction	112
6.1.1. Materials and practice	112
6.1.2. Technical investigation of indigo in Conservation Sciences	114
6.1.3. LDMS of indigo and indigo-containing samples	115
6.2. Experimental	115
6.2.1. Samples	115
6.2.2. Instrumental set-ups	116
6.2.3. Sample preparation	117
6.2.4. Mass calibration	118
6.3. Analysis of synthetic indigo	118
6.3.1. LDI-TOF-MS	118
6.3.2. MALDI-TOF-MS	122
6.3.3. Multiple-stage LDI-ITMS	123
6.3.4. LD-EI with the ITMS	126
6.3.5. Conclusion	126
6.4. Analysis of natural indigos	126
6.5. LDMS of indigo at the surface of dyed fibres	128
6.6. LDMS of indigo in oil paint	129
6.6.1. LDMS of indigo/lead white mixtures	130
6.6.2. Effect of laser power density	134
6.6.3. Influence of the ratio of lead white to indigo	135
6.6.4. LDMS of aged indigo/linseed oil mixtures	136
6.6.5. LDMS of an indigo/linseed oil/lead white mixture	138
6.6.6. Conclusion	139
6.7. Spatially-resolved LDMS of cross-sections	140
6.8. Conclusion	142
Chapter 7 : LDMS of modern synthetic pigments	145
7.1. Introduction	146
7.2. Samples	149
7.2.1. Azo pigments	150
7.2.2. Phthalocyanines	150
7.2.3. Quinacridones	152
7.2.4. Perylene red pigment	153
7.2.5. Dioxazine pigment violet PV23	154
7.2.6. Diketopyrrolo Pyrrole Pigment Red PR 254	155
7.2.7. Acrylic polymer emulsions (commercial tube paints)	155
7.3. Experimental conditions	155
7.4. Analysis of reference samples	156
7.4.1. Naphthol AS pigment red PR188	157
7.4.2. Diarylide pigment yellow PY83	158
7.4.3. Cu-Phthalocyanine green PG7	159
7.4.4. Cu-Phthalocyanine green PG36	162
7.4.5. Quinacridones:PV19, PR206, PR207 and PR209	163
7.4.6. Perylene pigment red: PR 178	165

7.4.7.	Dioxazine pigment violet PV23	165
7.4.8.	Diketopyrrolo Pyrrole Pigment Red PR 254	166
7.4.9.	Conclusions	167
7.5.	Acrylic polymer emulsions and oil paints	167
7.5.1.	Phthalocyanine acrylic emulsion paints	167
7.5.2.	Azo, quinacridone, dioxazine, perylene, DPP, anthraquinone	171
7.5.3.	Oil paints	175
7.5.4.	Conclusions	175
7.6.	Spatially-resolved LDMS analysis of cross-sectioned paint samples	176
7.6.1.	Reconstructed stacks of phthalocyanine layers	176
7.6.2.	Samples removed from easel paintings	177
7.7.	Conclusions	178
Chapter 8 : Surface preparation of paint cross-sections		181
8.1.	Introduction	182
8.2.	FTIR-imaging and LD-ITMS	183
8.3.	Evidence of smearing	183
8.4.	A new sample preparation	186
8.5.	Analyses after polishing	189
8.6.	Conclusion	190
8.7.	Acknowledgements	190
Bibliography		191
Summary		198
Samenvatting		202
Résumé		206
Dankwoord		210
Curriculum Vitae		212

Glossary

AFM	atomic force microscopy
CCD	charge-coupled device
CI	color index number
CID	collision-induced dissociation
DHB	2,5-dihydroxybenzoic acid
DIC	differential interference contrast
DTMS	direct temperature-resolved mass spectrometry
EI	electron ionisation
ESI	electrospray ionisation
FAB	fast-atom bombardment
FTIR	Fourier transform infrared spectroscopy
GC	gas chromatography
HPLC	high performance liquid chromatography
IR	infrared
ITMS	ion trap mass spectrometry
LD	laser desorption
LDI	laser desorption and ionisation
LDMS	laser desorption mass spectrometry
LMCO	low mass cut-off
MALDI	matrix-assisted laser desorption/ionisation
MCT	mercury-cadmium-telluride
MS	mass spectrometry
MS/MS or MS ²	two-stage mass spectrometry
MS ⁿ	multiple-stage mass spectrometry
Nd:YAG	neodymium-doped yttrium aluminium garnet
PEG	polyethylene glycol
PPG	polypropylene glycol
RF	radio frequency
TIC	total ion current
TLC	thin-layer chromatography
TOF-MS	time-of-flight mass spectrometry
SIMS	secondary ion mass spectrometry
VIS	visible
UV	ultraviolet
XY and XYZ	two and three-dimensional translational motion

Chapter 1

Introduction

The technical investigation of organic pigments in easel paintings is not without problems. Pigments have complex chemical compositions; details of their manufacturing processes are generally unknown and dramatic transformations of the colouring properties are observed with the passing of time. Characterisation of the chemical composition is greatly complicated by the particularly small size and complex arrangement of the samples available for analysis. Microscopic samples are preferably studied as paint cross-sections, but the finest methods of molecular analysis available today (chromatography and mass spectrometry) are not very compatible with this sampling method. In practice, investigation of organic pigments in cross-sections remains often inconclusive by the lack of a suitable method of analysis. This dissertation explores a new approach to the analysis of organic pigments found in easel paintings, using laser desorption mass spectrometry (LDMS). LDMS makes it possible to investigate the surface of paint cross-section with a spatial-resolution down to 10 μm utilising the analytical method of mass spectrometry.

Chapter 1 rationalizes the purpose of our study and outlines the main results that will be presented. Basic information is provided on artists' organic pigments and the analytical methodology used today for their molecular investigation in the field of the Conservation Sciences. After identification of the limitations of the current techniques we will explain the new prospects offered by the utilization of LDMS.

1.1. Introduction

Easel paintings represent an essential part of our cultural heritage and have a major artistic and historical significance. Undoubtedly, it is imperative to best conserve this heritage for generations to come. In the last decades, scientific studies are playing an increasing role in the conservation of works of art¹⁻⁶. There is notably a growing interest in the characterisation of paint materials and the elucidation of their ageing mechanisms. Advances in the techniques of investigation are giving more insight into these complex issues and the development of new analytical methodology is an important task of conservation scientists⁷⁻⁹.

Technical investigations of organic colouring materials in works of art concern principally their identification, the investigation of their degradation processes and the prevention of their further degradation. Investigation of easel paintings is particularly problematical because colouring materials are present in very small quantities, thoroughly mixed with many other compounds, and because ageing phenomena have often resulted in molecular degradation and fading of the original colours. In addition, samples removed for analysis are very small in size and have an intricate multi-layered structure, which represents a real challenge for the analytical chemist. Samples are usually prepared as thin or cross-sections to be investigated by microscopic techniques, and large collections of sectioned samples are kept today in conservation laboratories.

Several analytical techniques provide the conservation scientist with molecular information on the organic pigments. The best information is obtained at the moment with chromatography and mass spectrometry, but these techniques cannot be applied to the study of cross-sections, and paint samples are usually dissected prior to investigation. Microscopy and spectroscopy are the methods of choice for the study of sectioned samples, but they do not provide the same degree of information. In many cases, organic pigments are not present in sufficient quantity for detection and strong interferences of the other paint materials can impair the analysis. Therefore, the characterisation of organic pigments in easel painting samples often remains speculative or relies on circumstantial evidence provided by the identification of the inorganic substrate used as a “carrier” of the colour. Characterisation of very thin organically pigmented layers (in tens of micrometers), which cannot be accurately dissected, and the study of the influence of the different materials on each other (within or between layers) remain almost impossible to address at a molecular level. So, there is a great need for an analytical technique that could perform molecular identification of very small

amounts of organic pigments, present in complex mixtures of aged materials, preferably using samples in the form of thin or cross-sections.

This thesis presents research into the application of Laser Desorption Mass Spectrometry (LDMS) to the study of such samples. Sections 1.2. to 1.4. outline the general characteristics of the preparation and use of organic pigments in easel paintings, as well as the particular deterioration issues involved. Section 1.5. gives a brief overview of the different analytical methods currently in use for the study of organic pigments, and rationalises the use of LDMS by describing the perspective offered by this novel method of analysis. Finally section 1.6. and 1.7. specify the experiments addressed in this thesis and outline the results obtained.

1.2. Structure of an easel painting

Painting materials studied in the framework of the MOLART project (see preamble) cover the period of time ranging approximately from the 15th to the 20th century. During this period, painting techniques, materials and studio practice have evolved continuously¹⁰⁻¹⁵. Every artist has its own style, and it is hardly an exaggeration to say that the chemical composition of each work of art is unique. However, the great majority of easel paintings share common characteristics and samples under investigation in this thesis present habitually a multi-layered arrangement. In the sectioned view shown Figure 1.1, we give a schematic example of the structure of an easel painting to illustrate the spatial distribution of the different paint materials.

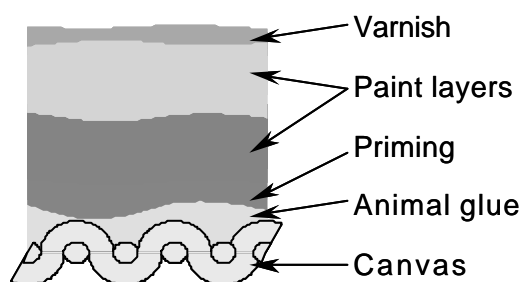


Figure 1.1 Typical build-up of an easel painting (in cross-section).

In this depiction, preparation layers (called *ground* or *priming*) are applied on a support, for instance a canvas stretched onto a wooden frame. These layers make the surface of the support less absorbent and sufficiently smooth to receive the paint layers. A preparatory drawing, sketched with a piece of charcoal or a pencil, is made on this ground layer. On top of these preparative layers, the various

Chapter 1

coloured paint layers are found. Finally, a protective varnish layer - a natural resin, possibly pigmented - contributes to the final appearance of the painting.

Coloured paint layers are made from ground pigments* mixed with a binding medium, commonly egg tempera or a drying oil (such as linseed oil), or a modern synthetic polymer or composite. Each of these layers contains different components. Paint layers are placed in a highly heterogeneous fashion on the surface of the support and their thickness typically varies from a few to hundreds of micrometers. Organic colouring materials are found entangled in a complex array of inorganic and organic paint materials. Organic lakes were particularly appreciated for their use in transparent top layers known as *glazes*. Such pigments were added in low concentrations to the medium and applied as a relative thin layer where their refractive index was matched with the organic binder. Light passes through this film and reflects from the layer beneath it, providing a unique effect of transparency.

1.3. Traditional and modern organic pigments

Pigments traditionally employed in easel paintings are for the most part mineral matter (such as ultramarine, azurite, ochre, sienna, umber) or the result of (al-) chemical synthesis (such as lead white, lead-tin yellow, Prussian blue, vermilion, smalt, verdigris). A few pigments however were organic in nature and were prepared from plants or animals. The vast majority of these colouring

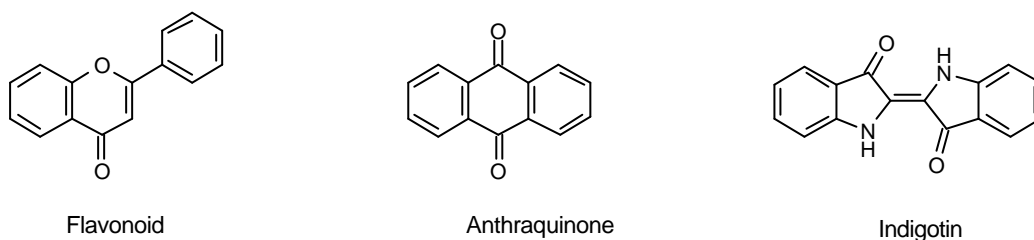


Figure 1.2 *Molecular structures of the three prevalent traditional organic pigments: flavonoid, anthraquinone and indigo.*

materials belong to the chemical classes of flavonoids (yellow), anthraquinones (red), and indigoids (blue), with basic molecular structures shown in Figure 1.2. Their colouring properties are known since antiquity in many civilizations. These

* Distinction should be rigorously made between pigments, which are insoluble discrete particles in suspension in the medium, and dyes, which are soluble in their medium of application. However, some colouring materials (such as indigo) can be found both in suspension or dissolved in oil.

dyes are largely used for textiles ^{16, 17}. In Table 1.1, some prevalent biological sources used in easel paintings are listed ¹⁶.

Organic reds	<ul style="list-style-type: none"> • Madder root (<i>Rubia tinctorium</i> L.) • Kermes insects (<i>Kermes vermilio</i> Planchon) • American cochineal (<i>Dactylopius coccus</i> O. Costa) • Polish cochineal (<i>Porphyrophora polonica</i> L.) • Indian Lac (<i>Kerria lacca</i> Kerr) • Brazil wood (<i>Caesalpinia brasiliensis</i> L.)
Organic yellows	<ul style="list-style-type: none"> • Weld (<i>Reseda luteola</i> L.) • Persian berries (Rhamnaceae species), e.g. Common Buckthorn (<i>Rhamnus catharticus</i> L.) • Black oak (<i>Quercus velutina</i> Lam.) • Young fustic (<i>Cotinus coggygria</i> Scop.) • Old fustic (<i>Chlorophora tinctoria</i> L.)
Organic blues	<ul style="list-style-type: none"> • Indigo (<i>Indigofera tinctoria</i> L.) • Woad (<i>Isatis tinctoria</i> L.)

Table 1.1 *Prevalent natural sources of traditional organic colouring material used in European easel paintings.*

The palette of artists' colours dramatically changed after the emergence of chemical synthesis in the late 19th century. First synthetic organic pigments appeared with the pioneering works of Perkin, Bayer, Graebe and Liebermann ¹⁸. Colouring materials traditionally obtained from natural sources, such as indigo and alizarin, were soon artificially produced in large quantities and at low costs. Synthetic techniques have considerably improved over the years and have led to the production of a broadening diversity of new pigments. Entirely new classes of molecules have been discovered, and the spectrum of colours traditionally available was dramatically enlarged. Some principal classes of modern pigments used today in paint formulation are phthalocyanines, quinacridones, perylene and azo dyes, with basic molecular structures exemplified in Figure 1.3. Exact or similar synthetic equivalents to traditional colouring materials have been found, and production from animal or vegetable sources has been virtually supplanted. Today, synthetic organic pigments represent the largest part of the commercially available artists' colours ¹⁸⁻²¹.

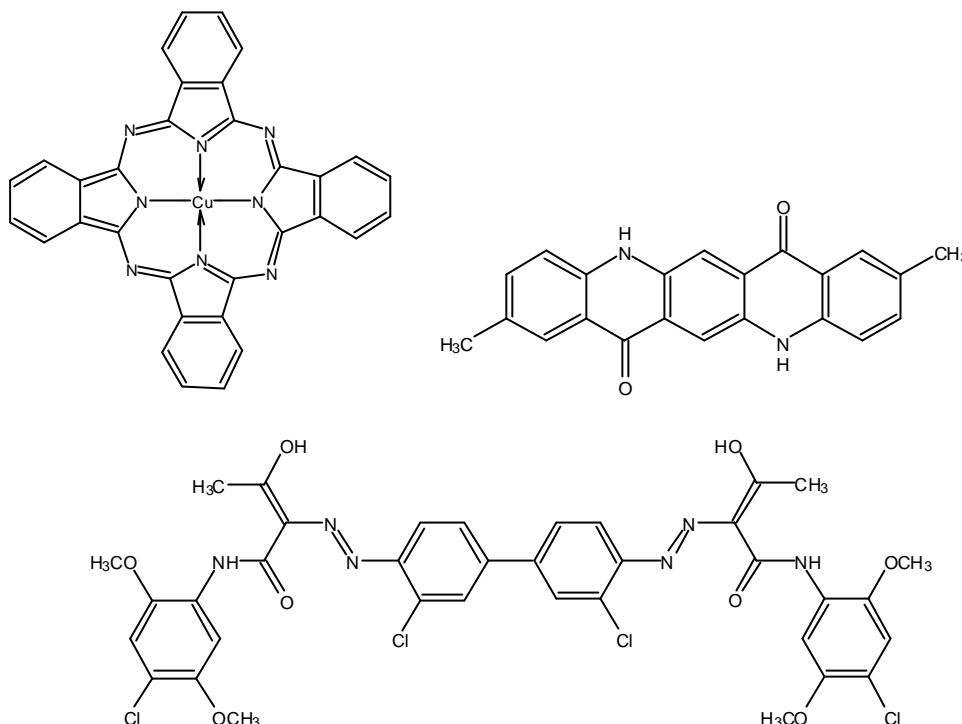


Figure 1.3 Modern pigments: example of a phthalocyanine (C.I. PB15), a quinacridone (C.I. PR122), and an azo dye (C.I. PY83).

1.4. Categories of pigments under investigation

Analytical issues in the study of artists' organic pigments strongly depend on their manufacturing methods and use. Three groups of pigments must be distinguished for technical investigations: *traditional* organic pigments divided in (1) *mordanted* colouring materials and (2) *non-mordanted* colouring materials, and (3) modern *synthetic* pigments.

First of all, it is necessary to make a distinction between traditional organic pigments and modern synthetic pigments. Colouring materials used to produce traditional organic pigments were obtained from plants and animals. The colouring compounds were not isolated in pure form. Colours from biological sources have a complex composition varying as a function of many factors such as species, geographical origin, period of crop, etc. Habitually no documentation has been recorded concerning the pigments components and their manufacturing process and only the guidelines of the preparation are known from documentary sources. Modern synthetic pigments on the contrary are the result of controlled chemical

reactions. They have a considerably higher degree of purity, although extra components might have been added to confer better chemical or physical properties to the pigments. Pigment composition is usually indicated on the paint tubes, but more detailed information about the manufacturing process is proprietary and rarely available.

Among the organic colouring materials obtained from biological origin, a further distinction must be made between flavonoid and anthraquinone dyestuffs on the one hand and indigo on the other hand. Flavonoid and anthraquinone dyestuffs, that are soluble in water, are found in paintings in a manufactured insoluble form called *lake*^{22, 23}. Only indigo, does not require this way of preparation. To prepare a lake, dyestuffs are first extracted in solution from the plants' raw material. The colouring material in solution in this plant extract is then adsorbed onto, or co-precipitated with an inert inorganic substrate, called *mordant*. This operation renders the dyestuff insoluble as particles coloured with the dye. The mordanted dyestuff is collected, washed and dried as a solid coloured pigment. This technique is commonly used in the dyeing of textile, where mordanting is used to fix the dye onto the textile fibres. Different types of substrates were used; some mainly consisted of hydrated alumina, derived from rock alum, whereas others were calcareous (e.g. chalk or gypsum). The substrate could be added in excess to improve the working properties of the pigment, and would serve then as *extender*. Lakes prepared by the addition of alkali and hydrated alumina (called *true lakes*) involve a *complexation* between the colouring material and the metal ion produced by alum. If the lake is made by adding only calcium carbonate or calcium sulphate and omitting the alkali, no complexation takes place and the colouring material is simply *absorbed* onto the substrate. Preparation of organic lakes for artists is rarely documented. Their original chemical composition in easel paintings is unknown. The preparation of the indigo pigment stands apart as it implies an oxido-reduction reaction. The reduced form of indigo, indoxyl, is obtained by fermentation of plant material. Indoxyl is colourless and soluble in water. Indigo is formed by oxidation of indoxyl on exposure to air (dehydrogenation with atmospheric oxygen). Indigo is much simpler in composition than organic lakes, but since adulteration was common, the pigment can be of variable quality.

Various authoritative publications listed in the reference section provide extensive information concerning the history and use of artist's pigments for easel paintings^{11, 16, 21, 24-28}, as well as the photo-physics and photo-chemistry of colouring materials^{29, 30}.

1.5. *Deterioration of organic pigments*

A serious problem encountered in easel paintings is the fugitive character of organic pigments. Deterioration is mainly caused by light and is noticed by the transformation of pigments into discoloured products, a process called *fading*. In time, discoloration of pigments causes fundamental changes in the appearance of easel paintings³¹⁻⁴³. Examples have been reported where colours have completely faded away. Madder containing glazes on lead white often suffer³⁹ while green paints made with stable blue and unstable flavonoids may turn blue.

Colour stability in organic pigments is a complex matter. It is not only the property of the colouring dyestuff, but part of a system comprising the pigment substrate and the other paint materials surrounding the pigment (medium and inorganic pigments). For instance, it was observed that when lakes are used in pigment mixtures rather than as surface glazes, their propensity to lose their colour is reduced³¹. The surrounding matrix with which they are mixed probably protects them from photo-oxidative damage. In contrast, the use of strongly scattering white pigments is known to play a deleterious role⁴⁴. From more general literature we know that atmospheric pollutants, the nature of the paint medium, the pigment volume concentration, the paint thickness, etc. might influence the chemical degradation of the pigment. The rate of fading can be reduced thanks to ultra-violet filtration. The original appearance of faded areas in easel paintings has been reconstructed recently with the aid of computers³¹.

1.6. *Investigation of organic colouring materials in conservation science*

1.6.1. *Rationale*

There are at least three main reasons for investigating artist's organic coloring materials at a molecular level.

1. *Understanding of the history and character of easel paintings:* Authentication of paint ingredients serves the attribution of the painting, the better understanding of artist's techniques, the history and use of paint materials, the prediction of the appearance changes over the course of time due to material deterioration; and tells whether a pigment is original or was added during a successive restoration.

2. *Selection of appropriate methods for restoration treatment:* It can tell the restorer whether a paint layer should be removed and determine if any chemical treatments being considered are likely to be harmful to the colorant identified.
3. *Establishment of appropriate methods for the care and preservation of easel paintings:* The study of degradation processes can tell to what extent pigments may be sensitive to deleterious environmental conditions (light heat, gaseous pollutants in the atmosphere, etc) and may help in the prevention of their further degradation.

1.6.2. Methodology

Two complementary analytical approaches are commonly employed to investigate artist's organic colouring materials in conservation science.

The first approach concerns the investigation of simplified model systems prepared in the laboratory. Models have been used extensively to study the degradation behaviour of organic pigments. For this purpose, paint components are manufactured after ancient recipes. The preparation of these so-called *reconstructions* or *mock-up samples* is supported by research on documentary sources to match as closely as possible the original composition of the paint. In an attempt to reproduce the natural degradation of paint materials, samples are *artificially aged* by subjecting them to different types of controlled environments (light, temperature, relative humidity, etc.). Ageing behaviour is inferred by comparing colour measurements or molecular analyses performed on fresh and aged samples.

The second approach concerns the investigation of easel paintings themselves⁴⁵. Methods of investigation are often classified according to their sample requirements. Several *non-invasive* methods exist that do not induce any damage to the easel paintings. Nevertheless more detailed investigations are often necessary, which only *invasive* methods of investigations can provide. For this purpose it must be decided to remove samples from representative areas of the painting. This operation is only possible after detailed discussions with the curator and the restorer. Sample removal is evidently realised with the worry to minimise the damage to the painting, and only the very minimum amount of material is removed. The operation is generally realised during restoration, after the varnish layer has been removed giving better access to the paint layers. A chip of paint of microscopic size, i.e. barely visible to the naked eye, is then carved out with the help of a scalpel under a high magnification microscope. Samples are removed

Chapter 1

from the most inconspicuous areas, preferably from the edge of the painting or along a crack. The amount of material is generally limited to some micrograms.

These samples are usually investigated in the form of *embedded cross-sections* since this form of preparation gives access to the build-up of the different layers. Samples are embedded in a supportive resin and the resulting blocks are polished or sectioned. Sectioned samples come in the form of a small block of embedding synthetic resin (typically a few cubic millimetres) displaying the flat-sectioned surface of the paint sample. This operation considerably facilitates the sample manipulation.

Bulk analysis is performed to provide better sensitivity, or with techniques unable to characterise embedded cross-sections. Where possible, the different layers of the paint sample are dissected into isolated fragments prior to analysis. In this way, it is possible to retain a certain degree of structural information (build-up of the materials within the sample) and to limit the complexity of the analytical results. In any case, the correlation between molecular information and physical structure of the sample is somewhat approximate, especially in comparison to studies of embedded cross-sections. Dissection of samples of such tiny size is admittedly a difficult operation, and it is not always possible, even to expert hands, to isolate one single layer.

Different degrees of molecular information can be sought according to the quantity and complexity of the samples available, and their method of preparation. A first approximation to the identification of organic pigments requires the characterisation of the chemical nature of the substance. Indirect characterization is often based on the identification of an inorganic substrate, inferring the presence of an organic pigment, or on the identification of an inorganic pigment, excluding the presence of an organic pigment. Finer molecular information can determine the biological origin of an organic pigment (e.g. whether a red organic pigment is from animal or vegetable origin, and in the best case its exact biological origin). Characterization of the degradation products has been demonstrated with reconstructed models ⁴⁶, but has never been attained with samples removed from easel paintings.

1.6.3. *Restriction of the analytical approach*

In principle, the organic pigments can be investigated with a large array of modern analytic methods. Freeman ⁴⁷ recently gave an overview of the prevalent techniques used in the study of synthetic colorants, whereas Stoecklein ⁴⁸ reviewed the methods used in the field of forensic science. The particular characteristics of

easel paintings samples pose however various limitations that hinder investigations in various ways and considerably narrow down the alternatives.

First of all, the composition of traditional organic pigments is expectedly rather complex. Early recipes make it clear that considerable variation in the sources of the dyestuffs, in the chosen substrate and in the mode of preparation are possible. Furthermore, organic pigments in easel paintings are found in complex mixtures of paint materials distributed in a heterogeneous way. Generally no information is available about the manufacturing of the pigment nor the original composition of paintings. Additional materials (binders, fillers, adulteration products) thoroughly mixed with organic pigments in the paint layers can induce strong interference and mask the signal of the organic dyestuff. Identification is moreover complicated by the low quantity of organic pigment material relative to the substrate/extender and in the case of lakes by the complexation reaction. Finally, degradation of the materials is assumed to induce dramatic transformations of the chemical composition of paint components, while their mechanism is presently hardly understood.

A second group of restrictions is due to the microscopic size of the sample. Minute samples are difficult to handle and quantities of materials available are insufficient for many analytical techniques. When prepared as cross-section, only surface techniques of investigation are possible. Many techniques that prove under other circumstances perfectly efficient in the study of organic pigments, fail to produce clear results with microgram amounts of materials, in microscopic, heterogeneous and multi-layered samples, and with specimens prepared as embedded sections. This also holds for the study of mordant dyes in historical fabrics. In this case the small size of the sample and very low amounts of colouring material are often a limitation for successful analysis.

1.6.4. Molecular analysis of artists' organic pigments

A few analytical techniques however suit the investigation of artists' organic pigments. A good overview of these techniques can be found in monographs by Schweppe^{17, 49}.

Optical microscopy is generally used first for the determination of particle colour, form, distribution, refractive index, oil absorption and grinding properties. The technique provides highly valuable information about inorganic pigments but is far less conclusive for organic pigments. The transparent character of organic lakes makes them particularly difficult to detect. In glazes, layers are very small and the pigment is found in very low concentration. Modern synthetic pigments which have very small grain sizes (sometimes below 1 μ m) cannot be identified.

Chapter 1

Chemical microscopy (sublimation test, staining test and solubility test) is useful to reveal the presence of organic pigments, and leads only in favourable cases to identification. Scanning electron microscopy with electron-induced X-ray microanalysis (EDX) is ideal to study morphological features in addition to permitting elemental analysis of paint fragments. EDX is a particularly sensitive method for the detection of inorganic pigments, and serves also as a tool for the characterization of the substrate of organic lakes (giving indirect evidence for the use of organic materials).

Various spectroscopic methods of investigation are useful in the identification of organic pigments: absorption spectroscopy (Visible, UV, IR) ^{8, 50-54}, X-ray fluorescence spectrometry (XRF), Fluorescence spectroscopy ^{50, 51, 55-57}, Raman ^{51, 58} and FTIR spectroscopy ^{19, 59-67}. Colour and spectral reflectance measurements in the visible and near ultraviolet range provide a very accurate tool for the study of colour permanence and fading. FTIR and Raman allow the determination of functional groups in an organic sample. FTIR is highly successful with pure pigments and can be advantageously combined with microscopy for the study of cross-sections. However, it has limited success when applied to the analysis of pigment in a binding medium, because of its low sensitivity and poor resolution ¹⁹. 3D-fluorescence ^{50, 56, 57} and photoluminescence spectrometry (PLS) ^{68, 69} are useful non-destructive alternatives, but they contribute not much to a thorough molecular characterization.

Chromatography and mass spectrometry (possibly hyphenated) are certainly the methods of choice for the analysis of organic pigments at a molecular level. Successful results are obtained with thin layer chromatography (TLC) ⁷⁰, HPLC (High Performance Liquid Chromatography ⁷¹⁻⁷⁹, GCMS (Gas Chromatography Mass Spectrometry), DTMS (Direct-Temperature resolved Mass Spectrometry) ^{19, 80}, Py-GC ^{38, 81}, Py-GC-MS ^{19, 80} and SIMS ⁸².

All these techniques are capable of dealing with the micrograms amounts of sample available in easel painting analysis. Chromatography offers a high sensitivity in the study of multicomponent samples. Mass spectrometry provides particularly detailed chemical information by determination of the molecular weight and structural assignment on the basis of fragment ions. Disadvantages of chromatographic and mass spectrometric techniques are found in the need for sample preparation. Dissection of the paint layers and extraction ⁸³ of the colouring materials is not always possible. Derivatization prior to chromatographic analysis often used to improve the results is also problematic with samples in very small quantities that are part of complex mixtures. The spatially-resolved analysis of the surface of a paint cross-section requires a different approach.

1.7. LDMS of organic colouring materials, a rationale

Mass spectrometry is well-established for the analysis of dyes, and literature on the subject is considerable. Van Breemen⁸⁴ has reviewed the various ionisation techniques. He notably stressed that none of them are suitable for the analysis of all classes of dyes. In his review the successful use of FAB*, ESI and APCI or direct coupling with chromatography such as LCMS in the investigation of the various classes of colouring materials has been described in detail. In the field of conservation science, traditional organic dyes have been studied with ESI and APCI/ITMS^{32, 46} and DTMS³⁷. However, all previous mass spectrometric studies are destructive for the sample, and all ionisation techniques used so far are incompatible with embedded cross-sections.

The potential of surface mass spectrometry for the study of complex multi-component solid samples have been demonstrated with techniques such as LDMS, SIMS and FAB⁸⁵. Here laser beams (LDMS) or particle beams (SIMS and FAB⁸⁵) are used to sample a solid surface with high spatial resolution. Particle beams offer higher spatial resolution (about 1µm) and are particularly well suited for elemental analysis. Lately, elemental imaging of surfaces is possible with commercially available TOF-SIMS instrumentation. LDMS has proved to be a valuable technique for mapping of organic macromolecules on a solid surface. Spatial resolutions down to about 20 µm are currently achieved, and automated measurements have been proposed⁸⁶.

Few researchers have addressed the topic of laser desorption of organic pigments and little is known about the behaviour of these pigments under the different desorption and ionisation conditions. Bennett⁸⁷ has used LDI for the analysis of mixtures of modern synthetic organic pigments. Each mixture studied contained up to four pigments that could be identified using mass spectrometry. Several laser shots were used and the resulting mass spectra were averaged to produce a mass spectrum with a good signal-to-noise ratio. Quantitative analysis was not carried out because of differences in the ionisation efficiencies of the different dyes. Dale⁸⁸ used two-step laser desorption photo-ionisation to examine azo, anthraquinone or phthalocyanine dyes. MALDI of azo dyes has been reported by Sullivan⁸⁹.

LDMS, which combines the detailed analytical information of MS and the possibility to study surfaces⁸⁷, appears therefore as an adequate technique to study organic pigments in easel paintings and paint reconstructions. LDMS also could be an effective way to sample and analyse dyes directly from the surface of fibres. Thus far, this potential has hardly been exploited.

* FAB: Fast Atom Bombardment, SIMS: Secondary-ion Mass Spectrometry

1.8. Thesis outline

In this thesis, we have investigated the viability of surface LDMS for the study of organic pigments. LDMS was developed for spatially-resolved molecular analysis of small surface areas (down to 10 μm). Two ionisation techniques were tested for *in-situ* mass spectrometric analysis: laser desorption/ionisation (LDI) and matrix assisted laser desorption and ionisation (MALDI). Spatially-resolved laser sampling was also used in an attempt to analyse pigments by mass spectrometry directly from the surface of sectioned samples. Attention was focussed on the study of organic pigments in complex mixtures and the effect of the surface composition on the mass spectrometry of paint samples and dyed fibres. This endeavour is part of a more general scheme, which includes TOF-SIMS for elemental mapping as well as other novel surface analytical techniques, such as imaging-FTIR and imaging reflection VIS/UV fluorescence micro-spectroscopy. Results of this research are the topic of other volumes of the MOLART series⁹⁰.

Chapter 2 introduces the use of lasers in combination with analytical mass spectrometry, describing the options chosen in our experiments (type of laser and ionisation techniques) and defining the characteristics of our spatially-resolved ionisation systems (versatility, spatial resolution). It introduces the ITMS and TOF-MS instruments that we have used to investigate natural and synthetic organic pigments, and stresses the performance of the ITMS in MS/MS mode. The development of a sample holder for the study of cross-sections is also discussed. Chapter 3 discusses more specifically various experimental issues in order to establish the optimal analytical conditions for the characterisation of organic colouring materials by LDMS.

Chapter 4 to 7 are concerned with the analysis of four different groups of organic pigments. Mordanted colouring materials are addressed in chapter 4 (flavonoids) and 5 (anthraquinones). In chapter 6, the investigation is focussed on indigo (a non-mordanted pigment). Finally, chapter 7 deals with LDMS of various modern synthetic organic pigments. In these chapters, we will also consider the influence of surrounding materials on the desorption of organic pigments (matrix effects), in particular lead white and aged linseed oil. Some paint samples and paint cross-sections will be discussed. Wool fibres dyed with indigo or anthraquinones are interrogated by means of spatially-resolved LDMS.

In Chapter 8, a new polishing procedure is presented for the preparation of paint cross-sections for LDMS analysis. Results are demonstrated with FTIR-imaging, differential interference contrast microscopy and interference profilometry.

1.9. *Main results and implications for painting studies*

Adaptation of the LDMS technique to the study of easel painting materials has produced contrasting results. On the one hand, the technique provides a valuable tool for the mass spectrometric study of artists' materials, but on the other hand analyses results at times in complex spectra or are simply unsuccessful.

For pure reference materials direct laser desorption and ionisation (LDI) works very well and abundant signal can be detected by the mass analysers. Comparison between ionisation techniques showed that the LDI of organic pigments provides detailed structural information without the use of a matrix (MALDI). The strong laser-sample interaction in the case of organic pigments highly simplifies the investigation of the surface of paint materials because no matrix is necessary. A wide range of traditional and modern organic pigments found in paintings could be therefore straightforwardly analysed both with the TOF-MS and the ITMS analysers. In the latter case, the abundant number of ions reaching the detector makes it possible to further perform multiple-stage experiments (MS^n) that may provide additional analytical information. This was illustrated by the differentiation of three flavonoid isomers – luteolin, morin and kaempferol - on basis of their fragmentation pattern. As each isomer is characteristic of a different plant, these results augured the possibility of identifying the biological origin of a pigment or a dye from the characterization of diagnostic components. In an MS^4 -experiment it was possible to follow the fragmentation route of indigotin. Interesting results were also obtained for the characterisation of flavonoid glycosides through MS/MS. However these results had to be toned down by inconclusive MS/MS experiments conducted with other flavonoid isomers such as quercetin and morin, or apigenin and genistein. Finally it appears that, if in theory the biological origin of a pigment could be identified, this would not be the case in all instances.

A further step was taken by attempting the identification of plant extracts and organic pigments in the form of lakes, and of dyestuff at the surface of dyed fibres. Luteolin was positively identified in a weld extract which proved that the technique is valuable in the case of plant extract. Comparison of indigo pigments of synthetic and natural origins indicated that LDMS could be used for their differentiation. Several colouring materials such as indigo or alum-mordanted flavonoid were successfully identified by direct LDI from the surface of a fibre. These encouraging results showed that LDI could be used for direct identification of dyes on textiles in particular for the study of complex samples where current techniques such as chromatography failed to produce conclusive information. Spectra of madder lakes showed that the complex form could be observed. Indigo

Chapter 1

was positively analysed in mixtures with lead white and oil. Modern pigments were easily identified in acrylic polymer emulsions.

Unfortunately it was not possible to reveal the complex form of a weld lake by any of the LDMS approaches. This negative result limits the prospect of characterizing yellow organic pigments in easel painting samples by LDMS since yellow organic colouring materials were mostly used in the form of lakes. In addition, analytical information provided by LDMS does not match results obtained by chromatographic techniques. Here only the major components could be identified whereas chromatography has been proved to identify additionally minor components.

In many instances LDMS was successfully used for the investigation of the local molecular composition of the surface of paint samples. In the case of paint cross-sections however, spatially-resolved LDMS gave only limited results. Positive results were shown in the case of indigo-containing mixtures and with a few samples from museum collections, showing that the approach is meaningful in the study of artists' materials. However, all samples investigated did not deliver conclusive spectra. An explanatory hypothesis assumes that only the paint material revealed at the surface can be successfully ionised and detected. More research will be needed to understand these limitations and to fully capitalize upon the capabilities offered by the LDMS techniques.

Chapter 2

Principles and instrumentation of spatially-resolved Laser Desorption Mass Spectrometry

Laser Desorption Mass Spectrometry (LDMS) is a promising analytical technique for the investigation of samples taken from easel paintings. It provides the means to chemically characterise solid samples, including non-volatile and thermally labile molecules, with a high spatial resolution. The analytical work presented in this thesis addresses the application of LDMS to the investigation of the local molecular composition of the surface of paint samples and paint cross-sections. Chapter 2 introduces the LDMS techniques employed in this study and explains the instrumental options taken. It describes two LDMS set-ups tested that can perform spatially-resolved analysis of paint cross-sections. We will outline the different desorption and ionisation techniques employed and discuss their potential for the study of paint materials. The principles of the two mass analysers, namely a Time-of-flight Mass Spectrometer (TOF-MS), and an Ion Trap Mass Spectrometer (ITMS) will be described. Particular attention is paid to the operation of the ITMS in multiple-stage (MS^n) experiments.

2.1. Introduction

In Chapter 1, LDMS⁹¹⁻⁹³ has been described as a promising analytical tool for the study of paint materials found in easel paintings because it combines the advantage of laser micro-probing and mass spectrometric analysis. Probing in the micrometric range with a focussed laser beam provides sufficient resolution to investigate individual layers in paint samples (Figure 2.1). Mass spectrometry is a well-established technique for the investigation of paint materials at a molecular level^{19, 46, 80, 94-97}.

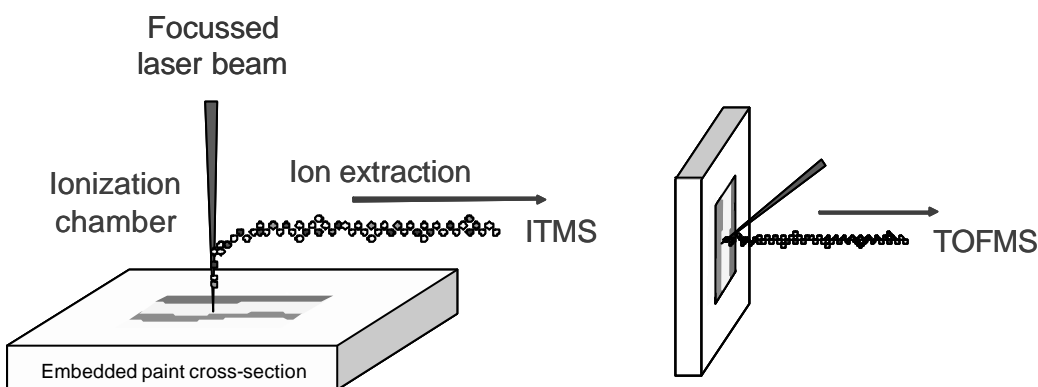


Figure 2.1 Principles of spatially-resolved LDMS of the surface of a paint cross-section. Laser desorption makes it possible to directly analyse sample material from the surface of an embedded paint cross-section. Ions produced from the surface of the paint cross-section in the ionization chamber are transferred to the analyser for mass separation and detection. (A) ITMS configuration (B) TOF-MS configuration.

In the field of Conservation Science, previous attempts to investigate paint cross-sections at a molecular level were often hindered by the lack of adequate analytical instrumentation. Surprisingly enough, spatially-resolved LDMS was – to the knowledge of the author – only applied to the analysis of preservatives in archaeological wood⁹⁸. The objective of this thesis is therefore to explore spatially-resolved LDMS as an analytical method for the investigation of the local molecular composition of the surface of paint samples. The use of LDMS is expected to give new insight into complex analytical questions that were difficult or impossible to address so far.

Different LD techniques and different mass analysers have already been successfully employed to locally convert and analyse molecules from complex surfaces. Van Vaeck ⁹⁹ has reviewed the instruments and methodology, as well as the various applications of laser-microprobe mass spectrometry.

In this thesis two mass analysers were utilised for LDMS of paint materials, namely an Ion Trap Mass Spectrometer (ITMS) and a Time-of-Flight Mass Spectrometer (TOF-MS). The external ion source ITMS arrangement has been designed specifically for the investigation of paint cross-sections and preliminary results concerning surface analysis of paint material were first demonstrated in 1999 by Van Rooij ¹⁰⁰. In the meantime we have adapted a commercial TOF-MS to perform similar types of analysis. Investigations of paint samples with LDMS are performed in combination with other innovative imaging techniques, i.e., FTIR-imaging for the investigation of molecular functional groups distribution ⁹⁰ and TOF-SIMS-imaging for mapping elemental and low molecular weight components ¹⁰¹.

In this chapter we will introduce the different desorption and ionisation techniques employed in our LDMS studies and discuss their respective benefits and limitations for the investigation of artists' paint materials. Subsequently, the principles of time-of-flight and ion trap mass spectrometry are introduced and their complementary character is clarified. Finally the performance of the ITMS analyser in multiple-stage MS experiments (MS^n) is examined and the particular significance of this instrument for LDMS investigations of complex paint materials is explained.

2.2. Laser Desorption Mass Spectrometry for Surface Analyses

Laser beams are coherent, monochromatic, directional and intense beams of photons ¹⁰². Soon after the development of the first commercial lasers in the 1960s, mass spectrometrists realised the benefits for volatilisation and ionisation of analytes ¹⁰³⁻¹⁰⁵. The first uses of lasers in mass spectrometry concerned the vaporisation of graphite, the elemental analysis of metals, isotope ratio measurements and pyrolysis. In the 1970s, laser-induced desorption was applied to volatilise macromolecules with little structural damage. The use of Laser-Desorption Mass Spectrometry (LDMS) quickly gained considerable importance as tool for the study of organic and inorganic materials. The real breakthrough came by the end of the 1980s with the introduction of matrices to assist the production of gaseous ions in Matrix Assisted Laser Desorption and Ionisation (MALDI) experiments ¹⁰⁶. The discovery of MALDI dramatically extended the range of samples amenable to molecular characterisation and widely spread the use

Chapter 2

of laser in mass spectrometry as a *soft ionisation* technique. Today lasers are routinely used for the production of stable ions from non-volatile, polar, thermally labile, and high molecular weight organic materials.

The laser desorption and ionisation technique is part of a wider array of soft ionisation techniques available in mass spectrometry in which energy is transferred to the condensed phase under various conditions ¹⁰⁷. Chemical ionisation (CI), field desorption (FD) and plasma desorption (PD), as well as fast atom bombardment (FAB) - making use of a focussed atom beam for desorption and ionisation - and secondary ion mass spectrometry (SIMS) - with a focussed beam of ions, are only a few examples.

At the same time, mass spectrometrists took advantage of the laser properties to develop “non-destructive*” microprobing. Focussed laser beams are used to perform surface chemical analysis with high spatial resolution, a technique also known as laser microprobe mass analysis (LAMMA). The lateral resolution of a laser microprobe can be ideally pushed to the diffraction limit (which depends on the laser wavelength), but a good balance between analytical sensitivity and spatial resolution is generally obtained in routine analysis with beams of a few tens of micrometers in diameters.

Van Vaeck ⁹⁹ surveyed the analytical features of LDMS (lateral resolution, sensitivity, etc) in comparison with other methods currently used for local surface analysis: electron probe X-ray microanalysis (EPXMA), Auger electron spectroscopy, electron spectroscopy for chemical analysis (ESCA) and secondary ion mass spectrometry (SIMS) which provide information on the elemental or inorganic sample composition, micro-Raman and micro-FTIR. A comprehensive overview of surface characterisation techniques has been recently edited ⁸⁵, with a section specifically dedicated to the investigation of the molecular composition.

Microprobe LDMS is especially useful in elemental and inorganic analysis and in the characterisation of complex mixtures and of adsorbates on solid surfaces. Van Vaeck ⁹⁹ reviewed the applications of LDMS for organic and inorganic analysis whereas surface analysis of molecular species was discussed in a recent tutorial by Hanley ¹⁰⁸. In this thesis, microprobe LDMS is exclusively used in the forward geometry with the laser hitting the sample surface directly. Transmission geometry also exists with the laser hitting the back of a thin section. Successive spot analyses, obtained by scanning the surface with the laser beam, provide chemical imaging. Late developments of the method took good advantage of motorised micro-positioning and automated data acquisition ⁸⁶.

* In analytical chemistry parlance *non-destructive* means that the bulk of the sample is recoverable after analysis, in contrast to other analytical techniques. Strictly speaking, a distinction is made with *non-intrusive* techniques, which indicates that the analysis procedure leaves the object under investigation undamaged.

According to the type of desorption and ionisation procedure, different types of analytical information can be obtained. High laser power is useful for the speciation of inorganic substances. Spectra primarily contain signals from elemental ions. Identification of inorganic compounds has to be done by means of elemental ratios. Low laser power, especially in combination with the use of a matrix is appropriate for non-volatile and thermally labile species. Today, local analysis with microprobe MALDI-MS is used in numerous technological and fundamental fields¹⁰⁹: in biomedicine and biology for the study of toxic elements, drugs, and metabolites at the cellular level in thin tissue sections, in environmental research to characterise individual aerosol particles, in material technology to research microscopic heterogeneities and surface anomalies, in the production of polymers to detect the inadequate dispersion of reagents, etc.

In this thesis both LDI and MALDI experiments with a UV laser operating at low laser power will be used for the study of traditional and modern organic pigments. We will look at the possibility to identify these pigments as such and mixed with inorganic pigments and organic (oil) and synthetic (acrylic) media. LDI will be explored for the investigation of organic pigments at the surface of paint cross-sections because the technique is selective and leaves the arrangement of the sample undisturbed for subsequent analyses. The technique will be also applied to analyse dyed fibres in the investigation of historical textiles. MALDI can be used for the investigation of higher molecular weight species, in particular paint media and their additives.

2.3. *Principles of LDMS*

2.3.1. *Formation of characteristic ions in LDMS*

LDMS analysis of samples in the condensed-phase (solids and liquids) consists of three successive steps: (1) volatilisation (2) ionisation and (3) analysis of gas-phase ions on the basis of their mass-to-charge ratio. Gaseous ions are first formed in an ionisation chamber - external to the analyser - by irradiation with the laser beam. Subsequently, ions are introduced in the mass analyser for detection.

Desorption with a laser can bring simultaneously a variety of particles in the gas phase: atoms, molecules, molecular fragments, and polymeric species in neutral or ionised state. Electrons, radicals and even large clusters can be also present. In this cloud of material, called the *laser plume*, numerous physical and chemical reactions can take place. Collisions between neutral and charged particles

Chapter 2

(i.e. primary ions) as well as energy redistribution (i.e. metastable ions) can lead to the formation of new ions^{99, 110, 111}. Among all this desorbed material, analytical information is exclusively obtained from ions (either positive or negative) falling within the mass range of the analyser. Various methodologies exist to optimise ionisation and detection efficiency, including the recourse to matrices (MALDI), and the use of auxiliary ionisation techniques to excite desorbed neutrals to the ionised state by post-ionisation¹¹².

In a mass spectrum, every ion detected is informative. Two classes of diagnostic ions can be distinguished. The first class of ions includes intact molecular ions that directly communicate the mass of the complete molecule, and pseudo- (or quasi-) molecular ions $[M+X]^+$ from which the mass of the original molecule is easily deduced. The second class comprises specific fragment ions that provide structural information on the molecule. A sufficient variety of characteristic ions is necessary for the identification of the molecule. Excessive molecular fragmentation and rearrangement should be nevertheless avoided as this complicates the spectra and their interpretation (as this is generally the case in SIMS experiments). Conversely the presence of intact molecular ions is particular helpful.

The goal of LDMS analyses is therefore twofold: (1) to produce ions in sufficient amounts for their detection and (2) to provide information characteristic for the molecular structure. Several intricate and concomitant processes are responsible for the formation of gas-phase ions and factors affecting the mass spectra are manifold. The best experimental conditions must be sought depending on the type of analyte (e.g. absorption spectrum, form and size of the sample) and the analytical issue at stake. Different desorption and ionisation methodologies can be employed with our two LDMS instruments. A variety of laser wavelengths are available from ultraviolet to infrared, with different power and irradiance characteristics. Samples can be investigated with direct laser desorption and ionisation (LDI), or if necessary with post-ionisation of the neutral fraction using electron ionisation (LD-EI). Alternatively, a matrix can be mixed with or applied on top of a sample to assist the desorption ionisation process in Matrix-Assisted Laser Desorption/Ionisation (MALDI). In the next sections, we introduce the fundamentals of these different experimental approaches.

2.3.2. Laser desorption and ionisation (LDI)

In Laser Desorption and Ionisation (LDI), Figure 2.2, a short laser pulse is employed for the formation of gaseous analyte ions. The interconnection between the desorption and ionisation processes is complex and still not completely

understood. The photon density of the laser beam determines the type of laser-solid interaction. At photon densities below the desorption threshold, no material is removed from the surface. At a photon density above the desorption threshold but below the ablation threshold, volatilisation and fragmentation of individual intact molecules takes place. At extreme photon densities, ablation^{113, 114} starts to occur that can lead to a combination of atomisation and the expulsion of macroscopic parts of the sample surface. The transition from the desorption to the ablation regime is not clearly defined and will vary from sample to sample. Moreover, as the photon density of subsequent laser shots is not uniform across the laser beam, the different regimes can occur simultaneously and are physically separated in the illuminated area.

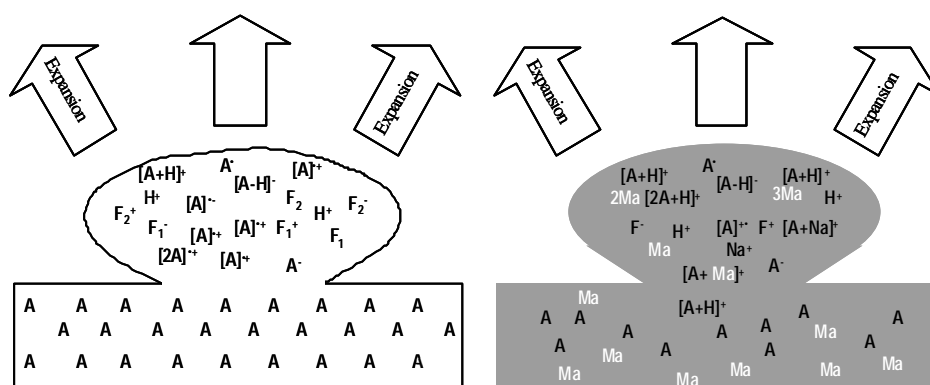


Figure 2.2 (1) LDI process with dominant formation of molecular ions of the analyte $[A]^{2+}$, $[A+H]^+$, $[A-H]^-$, along with fragments (F^+ or F^-). (2) MALDI processes with dominant formation of pseudo-molecular ion of the analyte $[A+H]^+$ with limited fragmentation. The matrix (Ma) is represented in gray.

Various ionisation mechanisms are assumed to contribute to some extent to the formation of diagnostic ions, and different tentative models have been proposed in the literature^{99, 111}. Two principal ion formation mechanisms can be outlined however:

The laser pulse acts both as the desorption and ionisation agent. Different excitation processes are possible (Figure 2.3) all leading to combined desorption and *photo-ionisation* of the analyte and the formation of radical cations $M^{\dot{+}}$ (and $M^{\dot{-}}$)

Ions are formed by *photochemical ionisation* either in the gas or in the condensed phase. Ion-molecule reactions are responsible for the formation of secondary ions such as protonated molecules $[M+H]^+$ and cationized molecules, e.g. $[M+Na]^+$ and $[M+K]^+$. High neutral pressure in the plume can additionally lead

to the formation of clusters such as $[2M+H]^+$. Photochemical ionisation is particularly enhanced in the MALDI process (see below).

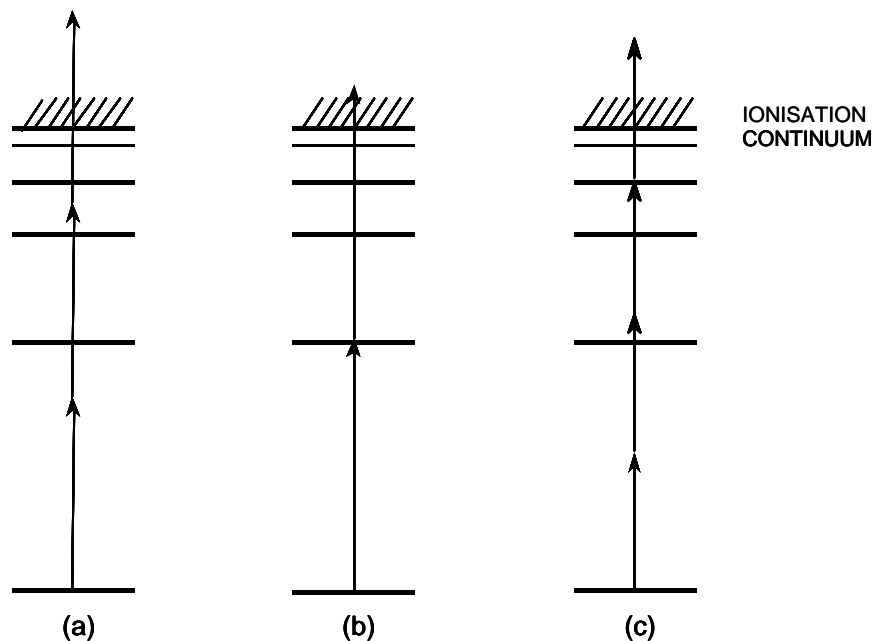


Figure 2.3 Energy-level diagrams (after Lubman) showing multi-photon ionisation (MPI) transitions for (a) non-resonant multi-photon ionisation (b) resonant two-photon ionisation and (c) resonance-enhanced multi-photon ionisation (REMPI).

Rapid and intense energy deposition is necessary to induce laser desorption of solid analytes and avoid excessive sample consumption at the same time. This requirement is met by high energy densities and short pulse widths (typically 500 fs – 500 ns) supplied by pulsed lasers*. Since desorption is not necessarily a resonant process, wavelengths ranging from the far UV to the far IR regions can be employed. Common types of lasers used are CO₂ lasers with output at 10.6 μm ; Er-YAG lasers at 2.94 μm ¹¹⁵; frequency-tripled or quadrupled Q-switched Nd:YAG lasers at respectively 355 nm and 266 nm; Nitrogen lasers at 337 nm; excimer lasers with variable gas mixtures operating at wavelengths ranging from about 190-350 nm.

* Three parameters are necessary to describe a pulsed LD experiment: *energy* of the laser pulse (in J), *pulse duration* in seconds (generally given in ns), and *surface area* of irradiation in m^2 (generally given in μm^2 or mm^2). These parameters can be combined to give the laser *power* = energy / duration (in J/s), the *irradiance* (or *intensity*) = power / surface (in W/m^2), and the *fluence* (or energy flux) = energy / surface (in J/m^2). The photon energy is proportional to the *wavelength* according to the relation $E=h\nu$.

Focussing optics serve to reduce the size of the laser beam and increase the photon flux. Highly focussed beams (ca. 10 μm) are used for spatially-resolved measurements, whereas larger spot sizes can be preferred to examine contaminants that sparsely cover a surface or to ensure a larger ion production or better surface coverage.

The laser power density*, that determines both the desorption rate and the energy deposition in the desorbed species, greatly affects the spectral information. In the low laser power density range, soft ionisation can lead to the formation of intact molecular ions as will be discussed in more detail in Chapter 3.

One important aspect of LDMS of organic components is the fact that the analytical information varies with the laser wavelength. Two wavelength ranges can be roughly distinguished to outline general features of the desorption and ionisation processes¹¹⁰:

1) *In the ultraviolet (UV) range* photons of short wavelength are sufficiently energetic to excite the electronic state of the analyte molecules. Laser energy which is absorbed by the surface - typically in the range of $10^8\text{W}/\text{cm}^2$ for heating rate of $10^6\text{K}/\text{s}$ - induces desorption through internal energy conversion into *rovibrational energy*. Ideally, rapid energy delivery during laser-solid interaction could overcome the forces that bind the sample molecules together in the matrix without inducing fragmentation. Ejection of high molecular-weight ions and neutrals is caused by the shock wave in the peripheral region of the laser spot, imparting kinetic energy. In practice however, although molecules can be brought intact into the gas phase, a certain degree of fragmentation is unavoidable. Desorption of the molecules from the surface can be accompanied by a transition to the ionic state (ejection of an electron), a process known as *laser desorption ionisation* (LDI). The LDI process, which depends on the photon energy, can be the result of either single photon or multiphoton excitation. Since photon density is very high within the laser beam, there are significant chances of more than one photon being absorbed by a molecule before internal energy conversion returns it to the electronic ground state. An electronically excited molecule will ionise either by absorption of additional photons such that the sum of the energy of the absorbed photons exceeds its ionisation energy (Figure 2.3), or through a gas-phase ion-molecule reaction leading to a cationized species. Multi-photon ionisation is proved particularly efficient when resonance conditions apply, a process known as resonance-enhanced multi-photon ionisation (REMPI). REMPI is a very sensitive and a very selective technique¹¹⁶. However the low selectivity of non-resonant

* Photon *energy* absorption by the analyte is controlled during measurements by tuning the fluence of the laser, but it is important to remember that the energy of the photons remains unchanged because it is fixed by the laser wavelength.

ionisation better suits the study of paint materials since it provides, despite its lower sensitivity, a wider range of analytical information.

2) *In the infrared (IR) range*, energy deposition induces desorption through rovibrational excitation. This generally results in a much higher thermal decomposition in comparison to UV-LDI. Heating rates are much smaller (10^3K/s) than in the UV range because usually less energy is absorbed at longer wavelengths. Photon energy is generally not sufficient to directly produce molecular ions because of the lack of electronic excitation. For that reason IR-LD results essentially in the vaporisation of neutral species. Auxiliary forms of ionisation are then necessary such as the use of a matrix for IR-MALDI experiments, or the use of post-ionisation of the desorbed neutrals for temporally and spatially separated two-step desorption/ionisation¹¹⁷.

2.3.3. *Matrix-assisted laser desorption/ionisation (MALDI)*

In early years, the application of LDMS to the characterisation of solid samples was quite limited as many components were not amenable to formation of gaseous ions by laser desorption, or the high energy required for desorption induced excessive fragmentation. Optimisation of the laser wavelength (to match the sample absorption maximum and increase selectivity) and the use of post-ionisation techniques on the neutral vapours offered only limited improvement. The introduction of matrices to assist the LDI process^{103, 106, 118}, a technique referred to as Matrix-Assisted Laser Desorption/Ionisation (MALDI) represented a significant advance, and considerably extended the range of LDMS applications. Soft ionisation provided by MALDI quickly evolved to a prevailing routine method for the study of complex macromolecules⁹⁹. Present investigations with MALDI address the structural characterisation of synthetic polymers and biomolecules such as proteins and nucleic acids. Exceptional highlights include characterisation of DNA with molecular weights of several 100 kDa, detection of femtomoles quantities of large biomolecules like proteins, and analyses of complex protein mixtures.

In order to desorb intact non-volatile and thermolabile molecules, it is necessary to introduce energy in the system in such a way that thermal decomposition is prevented. The principle of MALDI (Figure 2.2) is to incorporate the sample to be characterised in a light absorbing liquid or solid matrix with a low boiling point. The matrix, which is a highly UV/IR-absorbing compound, serves to absorb sufficient laser radiation to induce vaporisation and moderate the excitation of the analyte molecules. This absorption by the matrix controls the energy

subsequently deposited in the sample molecules, which are mainly converted to intact pseudo-molecular ions, such as $[M+H]^+$, $[M+Na]^+$ and $[M+K]^+$.

The mechanism that promotes the ionisation of the macromolecule in the matrix is not clearly understood but is commonly believed to involve photo-ionisation combined with ion-molecule reactions with an excited matrix molecule in the gas-phase. Zenobi *et al.*¹¹¹ have recently reviewed the mechanism of MALDI ion formation, distinguishing (1) *primary ion formation*, such as multi-photon ionisation, energy pooling, excited-state proton transfer, disproportionation reactions, desorption of pre-formed ions and thermal ionisation and (2) *secondary ionisation reactions* in the MALDI plume, such as gas-phase proton transfer, gas-phase cationization and electron transfer.

A detailed account of photo-ionisation and subsequent ion-molecule reactions in MALDI is beyond the scope of this chapter, but we can summarise the combined contribution of all these different processes by pointing to the formation of three principal types of analyte ions. (1) Proton-transfer (in primary ion formation or secondary reactions) is possibly the most frequently proposed MALDI ionisation model. According to the direction of the proton-transfer (matrix to analyte, or analyte to matrix) the process results in protonation $[M+H]^+$ or deprotonation $[M-H]^-$ of the analyte. (2) Cationized molecules are believed to result principally from ion-molecule reactions in the gas phase. Ubiquitous Na^+ and K^+ impurities are sufficient to give strong alkali cationized signals, e.g. $[M+Na]^+$ and $[M+K]^+$. (3) Ionisation of the matrix followed by electron transfer from analyte to the matrix radical cation lead to the formation of the analyte radical cation $M^{\cdot+}$. This process can happen if the analyte has a lower ionisation potential than the matrix and is therefore not commonly observed.

Although some fragmentation is generally unavoidable MALDI optimises the production of gaseous molecular ions, and molecular (pseudo) ions dominate the mass spectra. Large, non-volatile, labile molecules can be transferred into the gas phase as intact ions. Sometimes, the analyte may form adduct ions with molecules of the matrix. Matrix related ions are generally confined to low m/z values (typically below m/z 1000). Under best circumstances, ionisation yields can be improved by several orders of magnitude and the shot-to-shot reproducibility is generally far superior to LDI. At the same time the minimal laser power density required for production of molecular ions is reduced. Additives can be also employed to promote the cationization of the molecular ion.

Sample preparation is crucial to the success of the method and the size of the resulting signal varies greatly with the matrix used. It is thus important to carefully select the matrix compound in relation to the analytical problem. The bulk of MALDI studies has been achieved with UV laser radiation that provides

Chapter 2

the rapid heating necessary to reduce the likelihood of thermal decomposition and structural fragmentation¹¹⁹. Spectacular results obtained first with MALDI in the ultraviolet regions were later followed with successful investigation in the infrared regions¹¹⁵.

2.3.4. LDI and MALDI of paint materials

UV-LDI and UV-MALDI seem very promising techniques for the study of organic pigments in paint cross-sections. UV-LDI is particularly attractive since it makes it possible to sample the surface of cross-sections directly, i.e. without further preparation. In addition, when low laser power is employed, only minimal amounts of material are removed leaving the sample “intact” for other methods of analysis. In the case of complex heterogeneous mixtures such as paint cross-sections, the volatility, thermal stability and absorption characteristics of the different components might differ greatly. Therefore the laser wavelength used for LD is essential as it determines the desorption and ionisation efficiency for each of the individual components. Predictably, electronic excitation provided by the UV laser used at low laser power is not likely to volatilise the paint medium effectively. Polymerised and oxidised binding media (dried and cross-linked oils) and varnishes (terpenes) are highly polar components or have high molecular weights. The formation of abundant inter-molecular bonds decreases the volatility of these compounds considerably. In this case rovibrational excitation provided by an IR laser would be far more appropriate to break molecular bonds and yield good analytical results. However, the high thermal excitation provided by the IR laser is expected to lead to more fragmentation (laser induced pyrolysis). As a result, the study of complex heterogeneous mixtures brings up the question of preferential desorption ionisation. Ion formation, which depends on the local energy deposition, is directly affected by the type of materials in the immediate vicinity of the analyte. Sample morphology and surface texture might be also influential. In samples made up of elements with very different physical properties and first ionisation potentials (IP), the ionisation yield of one component or a group of components could be much larger than the rest, providing *selective analysis*. If the laser wavelength would correspond to the sample absorption maximum, LDI would be greatly enhanced.

UV-MALDI has already been successfully employed in our laboratory for the study of paint materials containing large macromolecular systems such as aged media (oxidised linseed oil, and egg tempera), varnishes (terpenic resins and synthetic polymers) and cross-linked matrices, and to investigate complex ageing processes such as oxidation and polymerisation. Results have been recently

presented by Van den Brink ⁹⁷ on egg lipids and their oxidation products in fresh and artificially aged paint reconstructions. In this procedure, the matrix is thoroughly mixed with the analyte (extracts of reconstructed samples) and samples are deposited as thin film on a stainless steel probe. In view of these promising earlier results, MALDI will be applied in this thesis to the investigation of organic pigments. The use of a matrix, which is likely to promote the formation of intact molecular ions, can be particularly beneficial to studies of organic pigments (1) with MS/MS where the parent ion is isolated as precursor ion for subsequent fragmentation with CID, and (2) in complex mixtures (e.g. with lead white, oil or acrylic media, additives) where higher molecular weight and non-volatile materials are found. In addition, one might reasonably assume that the use of a matrix could assist the desorption of the components at the surface of paint cross-sections. Therefore the possibility to deposit matrix in solution on the surface of paint samples to perform *spatially-resolved MALDI* of paint-cross sections is explored in this thesis (Chapter 5). Evidently, the matrix should not infiltrate the whole sample since redistribution of the soluble elements is not wanted. The objective is to produce a thin film of matrix crystals at the surface of the section. It will be shown in the case of organic pigments that in LDI the pigment acts as its own *intrinsic* matrix. This particularity makes it possible to obtain with LDI results as good as in MALDI. Preference will then go to the LDI procedure that saves the complications related to the use of an additional matrix.

2.4. Instrumentation for the analysis of paint cross-section

2.4.1. Mass analysers

In the study of paint cross-sections, pulsed lasers are required because they produce the adequate laser power and wavelength for desorption and ionisation and limit the sample consumption ⁹¹.

Scanning MS analysers that separate ions *in space* work well with continuous wave (CW) lasers because a relatively steady ion current is generated, allowing time for the mass spectrum to be scanned. However, in the shorter time scales provided by pulsed lasers, they fail to obtain a complete mass spectrum.

Two types of analysers that work in a pulsed fashion, with *cumulative and time-based* separation, overcome this limitation and afford appropriate mass detection: Time-of-flight Mass Spectrometers (TOF-MS) and Trapped Ion systems, *viz.* Ion Trap Mass Spectrometer (ITMS) and Fourier Transform

Chapter 2

Cyclotron Resonance Mass Spectrometer (FT-ICR-MS). Although FT-ICR-MS systems outperform ITMS systems in many aspects, their use is nevertheless more complex and they are less cost-effective.

In our laboratory, two instruments were developed to perform LDMS of paint cross-section, one with a TOF-MS analyser and one with an ITMS analyser. The two instruments present many similarities. In both cases, ions are produced in an ionisation chamber situated outside the mass analyser by means of a pulsed laser with a focussed beam. Whereas the TOF-MS is a commercially available instrument, which needed only a minor adaptation of the sample holder, the ITMS arrangement has been designed specifically for the spatially-resolved LDMS investigation of paint cross-sections. The functioning of Time-of-Flight and Ion Trap Mass Spectrometers has been extensively reviewed in the literature¹²⁰⁻¹²⁵ and only the basic operating concepts relevant to the discussion of our analytical work are provided here.

TOF-MS provides rapid analysis with high transmission and hence sensitivity, together with panoramic spectrum registration. The absence of high mass detector limits is particularly useful in the study of high molecular paint components (oils, proteins, synthetic polymers). Commercial software provides easy manipulation of the sample holder and data acquisition.

The home-build ITMS instrument provides moderate mass-resolution and mass-accuracy but offers the significant advantage of ion manipulation. Multiple-stage analysis (MS^n) in the ITMS provides the means to investigate ionic structures in greater detail. It is for instance possible to distinguish between isobaric molecules as will be demonstrated in Chapter 4 for yellow organic pigments with the identification of structural isomers. Ion isolation in the trap will also be particularly advantageous in the study of complex mixtures. Possible limitations with the ITMS arise from trapping efficiency with ion packets of broad kinetic-energy range, and from its limited dynamic range.

2.4.2. *Time-of-flight Mass Spectrometer: Set-up and operation*

The TOF-MS experimental set-up (Figure 2.4) is a commercial Bruker Biflex TOF-MS (Bruker-Franzen Analytik, Bremen). The ion source is developed for (MA)LDI experiments where samples are deposited as a thin film on a stainless steel probe. The regular Bruker probe has a cylindrical shape with a circular flat surface of 30 mm in diameter. The probe is introduced in the ionisation chamber through a vacuum lock and positioned in focus of the laser beam. The ion source consists of a positively or negatively charged metal electrode, i.e., the sample

probe, and a grounded accelerating grid at a distance of about 2 cm. Possible accelerating potentials are in the range of +25/-20kV.

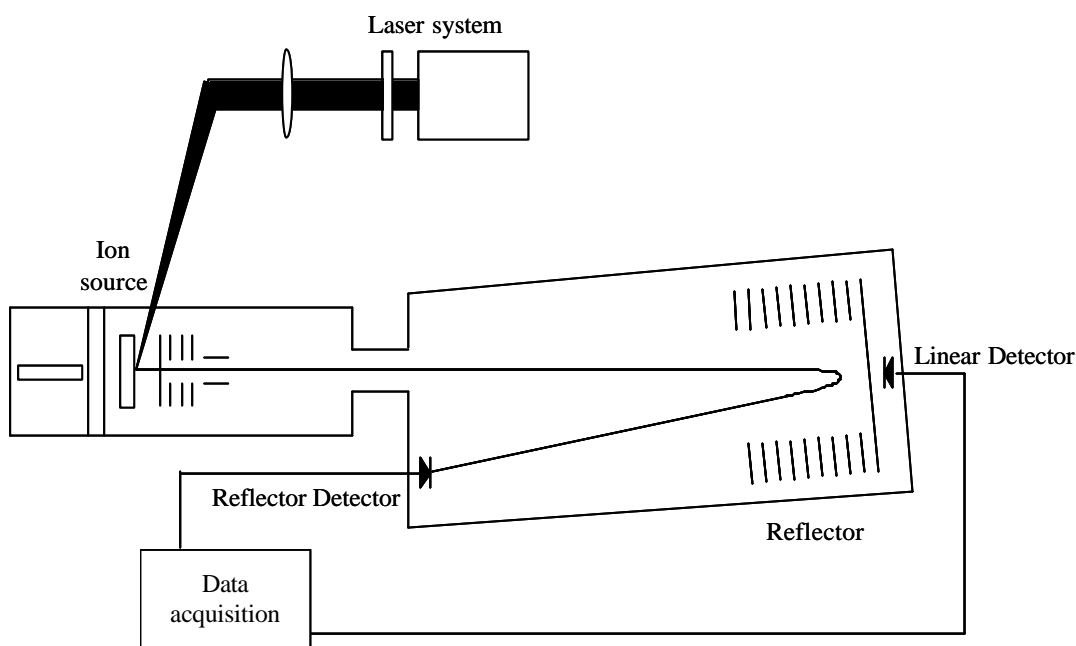


Figure 2.4 Schematic diagram of the Reflection-Time-of-Flight MS (Re-TOF-MS)

Microscopic probe positioning is possible at any place on the circular surface thanks to an XY sample manipulator and the digital output of a CCD (Charge Coupled Device) camera for observation. The ionisation chamber is maintained at a pressure of 10^{-7} mbar by means of a turbopump. The laser is a nitrogen discharge (N_2) laser that produces pulses of ultraviolet (UV) light with a wavelength of 337 nm (3,68eV), pulse-energy of 150-200 mJ and average duration below 4 ns. Repetition rate is typically 1-2 Hz. An attenuator allows fine adjustment of the laser fluence (Figure 3.4). The laser beam diameter is roughly estimated to some tens of micrometers. Data is processed with the Bruker software XMASS. The laser beam impinges on the sample at an angle of ca. 60° with respect to the surface normal (Figure 2.1). Figure 2.5 shows a picture of the instrument and a schematic diagram of the source configuration.

Essentially a TOF-MS is a very precise timekeeper. It separates ions of different mass-to-charge ratios (m/z) by making use of their mass dependent velocity after they have been accelerated to the same kinetic energy (Figure 2.6) In other words, the mass of an ion is deduced from its flight-time from the ion source to the detector (hence the name *time-of-flight*).

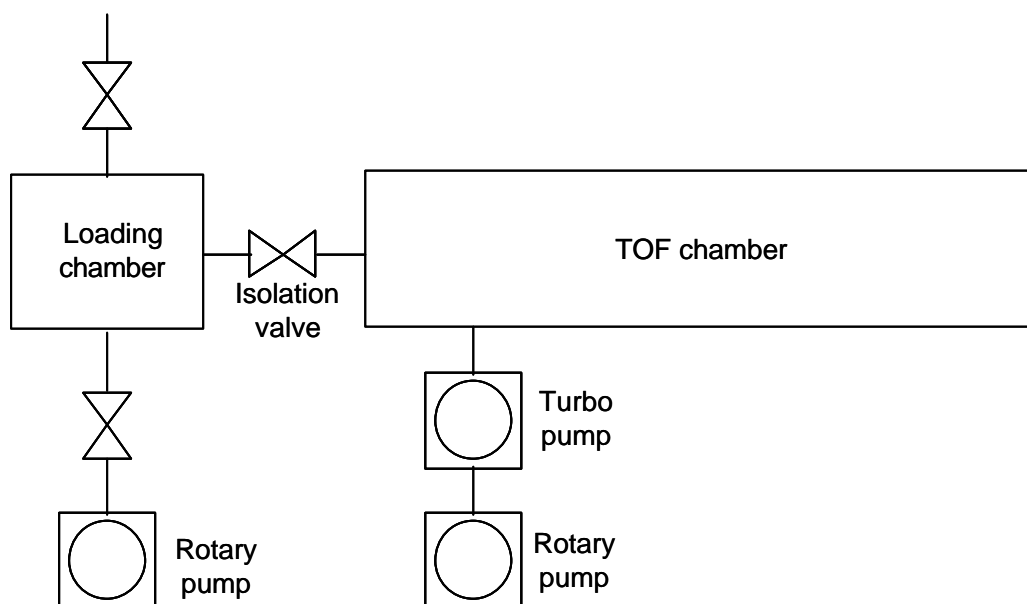
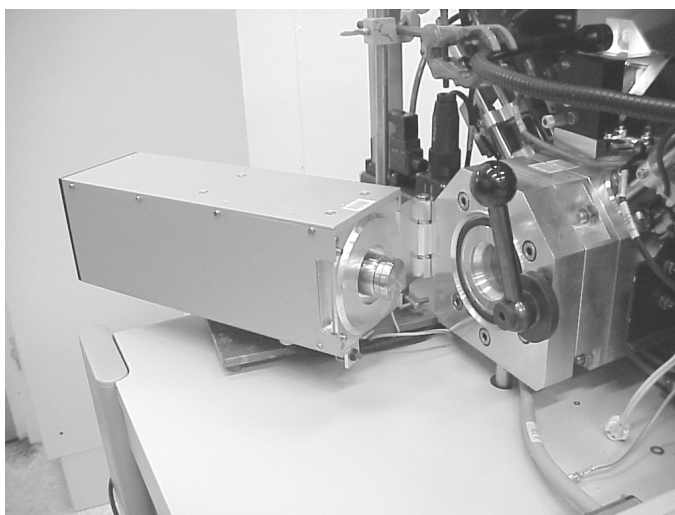


Figure 2.5 *Sample exchange chamber (vacuum lock) of the TOF-MS and schematic diagram of the sample introduction chamber.*

The firing of the laser in a pulsed laser desorption experiment marks a precisely defined time of ion generation for time of flight analysis. A detector positioned at the end of the ion trajectory determines the flight time for each ion created during the desorption and ionisation event. Detection occurs through an electron multiplier, which feeds the signal to a 1 GHz transient recorder. During the LD process ions are formed in different time domains, different positions and with a distribution of kinetic energy. All these processes result in a broadening in arrival times of ions with the same mass at the detector and adversely affect the

mass resolution. For example, the ion formation time is known to exceed the laser pulse length, and/or the irregularities of the surface of the sample – a particularly likely feature of paint cross sections or bunch of dyed fibres – causing a spread in flight times as the path-length will depend on the location where the ions are produced. Here a combination of delayed and pulsed ion extraction scheme (PIE or time-lag focussing) is employed to correct for the effects of temporal, spatial and initial kinetic energy distribution (Figure 2.7). An extraction pulse is applied after firing of the laser to ensure that all ions get the same additional kinetic energy.

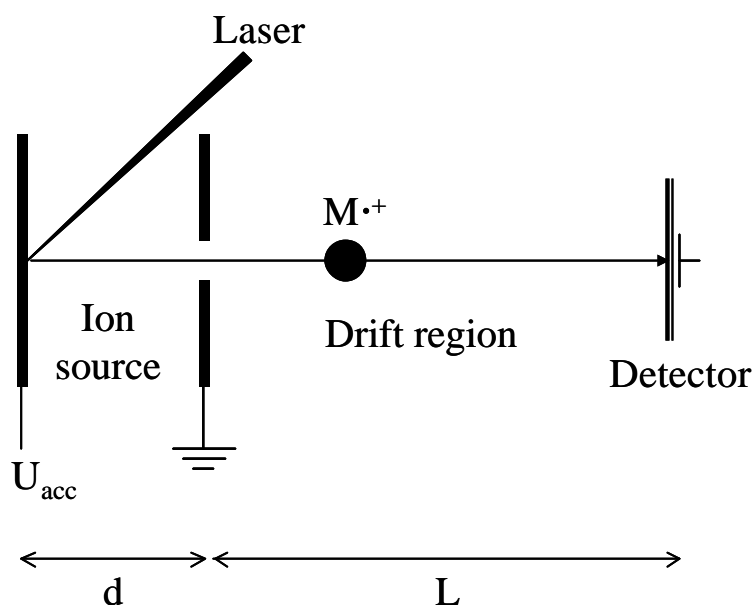


Figure 2.6 *Basic principle of a TOF mass spectrometer in the linear mode: ions are produced in the ion source with a focused laser beam. In the source region, ions are accelerated in an electric field U over a distance d . Ions are then separated according to their mass-dependent flight-time over a distance L in the field-free drift region. Ion counting is achieved with a multi-channel plate detector at the end of the flight tube.*

This fast extraction pulse ensures a well-defined time focus and compensates for the time spread in ion generation. Adding a delay between the firing of the laser and the extraction pulse corrects for the initial spread in kinetic energy. In this case after ion generation the ions travel a short distance between the sample surface and the extraction electrode before the pulsed extraction field is applied. During this time delay the ions with a higher kinetic energy will travel a longer distance than the low kinetic energy ions. Therefore the faster ions will experience a lower extraction potential compared to the low kinetic energy ions,

resulting in a compensation of the total flight time spread for the different initial kinetic energies. All ions will reach the entrance of the detector at the same time, the so-called *time focus*. Space focussing is obtained with a two-stage extraction set-up and compensates for the different locations where ions are formed.

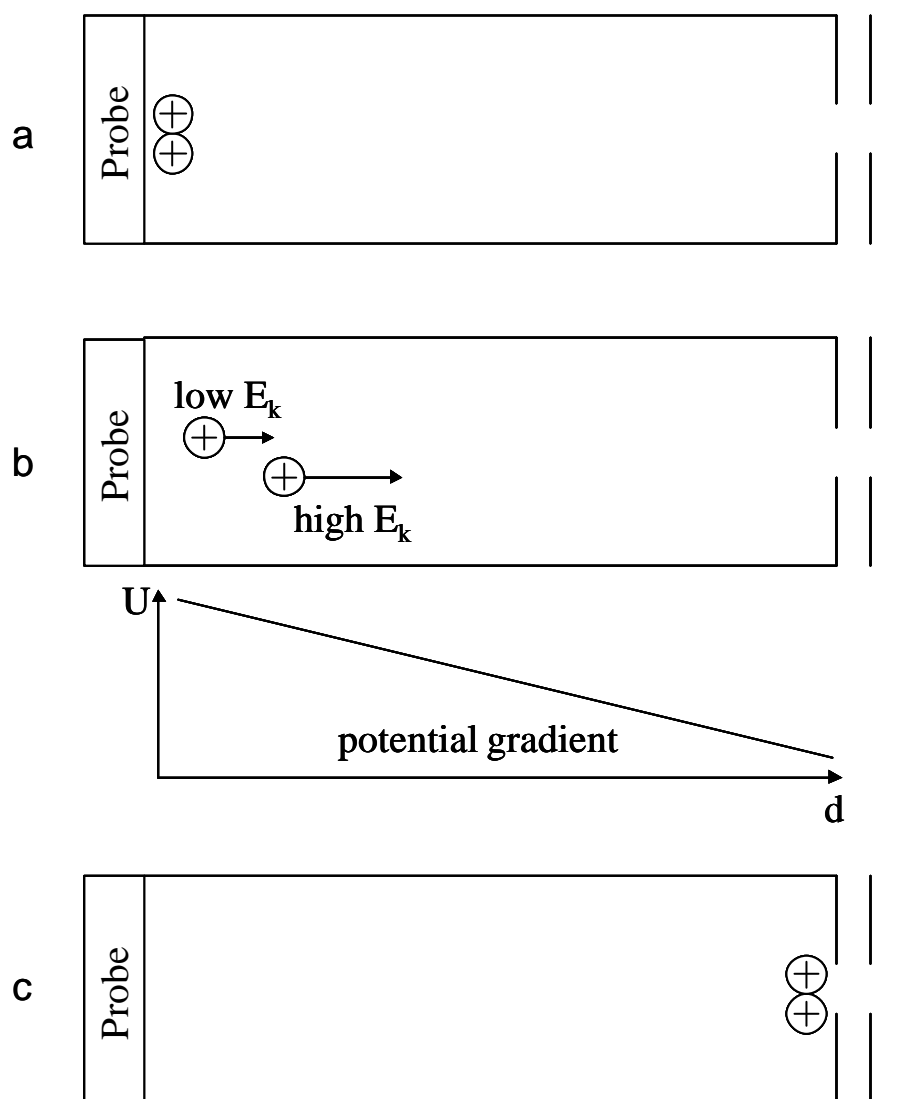


Figure 2.7 *Higher mass resolution is obtained with time-lag focussing: pulsed and time-delayed extraction compensate for the spatial, temporal and initial kinetic energy distribution of isobaric ions. (a) two ions are formed at the surface of the sample (b) ions of different kinetic energy are corrected by a gradient of potential and (c) enter simultaneously in the flight tube of the analyser.*

Due to the consideration above, delayed extraction is used to improve the mass resolution of the system. Delayed extraction also leads to a diminution of local pressure upon acceleration, which lowers collision activation in the extraction and acceleration process, resulting in ions with lower internal energies. This in turn reduces the degree of fragmentation in the TOF-MS mass spectra.

Resolution

Mass resolution depends on a number of parameters in the TOF-MS system. The digitisation hardware has an effect on time resolution and is given by the sample frequency of the transient recorder. The accelerating voltage has an additional influence as it determines the initial kinetic energy. The higher the kinetic energy the less relevant the initial kinetic energy spread is. Typically, at a sample frequency of 1GHz (1 ns bins) we achieve a resolution of $(m/\Delta m)_{50\%} = 10,000$ resolution in the pulsed extraction mode. This provides sufficient resolution to reliably resolve the isotope ratios necessary to support the assignment of the peaks. Note that in a TOF-MS mass resolution depends on the mass range selected. Over the total mass range between 0-500,000 Da we see a drop in resolution to approximately 1000.

Reflectron

In reality ions of a same mass-to-charge ratio do not have exactly the same kinetic energy at the entrance of the drift region, even after time-lag focussing. This depends essentially on the exact location where the ions are formed and to a smaller extent on space charge effects, i.e., the action of electrostatic repulsion forces in the ion cloud. For a same mass-to-charge ratio faster high-energy ions will reach the detector sooner than slower low-energy ions. The kinetic energy spread results in poorer mass resolution.

A correction of the energy dispersion is achieved by reflecting the ions in a small angle with an electrostatic field, as depicted in Figure 2.8¹²⁶. Inside the reflector a homogeneous electric field is applied to retard and reflect the ions. Ions with same mass-to-charge ratio but higher kinetic energy penetrate deeper into the reflector compared to their less energetic counterparts. Therefore, the faster moving ions have further to travel, thus spending more time in the reflectron. This compensates also for the kinetic energy dispersion and ensures that ions of same mass-to-charge ratio reach the detector at the same time, which leads to a significant improvement in resolution. Whereas metastable fragmentation due to post source decay (PSD) does not become apparent in the linear mode because the fragment and the parent ions move with the same velocity, a reflectron instrument

will separate the parent and product ions of different mass, based on their kinetic energy differences. As a result the residence time of parent and fragment ion in the reflectron will be different. The linear mode offers however higher sensitivity despite its lower resolution features and is often preferred in the study of large analyte ions.

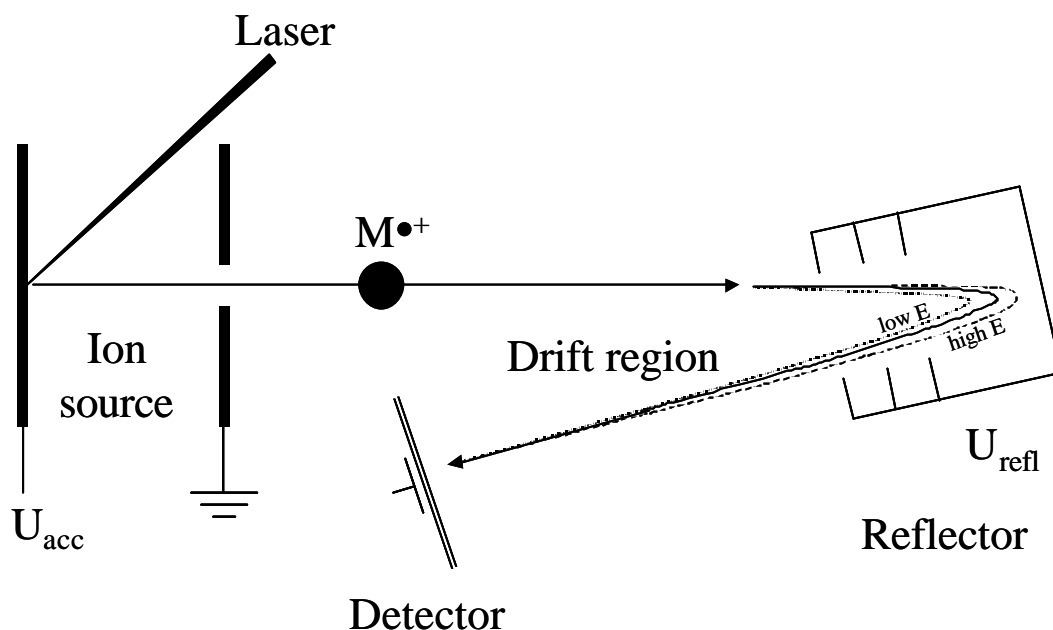


Figure 2.8 *Basic principle of a TOF mass spectrometer in the reflection mode. During their travel in the field-free drift region ions cross the reflector region where the electric field U_{refl} compensate small differences in initial kinetic energy.*

Calibration

External mass calibration is performed before each series of measurements to obtain optimal mass accuracy. Deviation within a series of measurements is considered negligible. A mixture of two samples of polyethylene glycol (PEG) presenting two molecular weight distributions of average m/z 400 and 1000 respectively serve as calibrant for all types of analyte. For the calibration, a MALDI measurement is carried out with a mixture of a 1mM ethanolic solution of PEG and a 1M ethanol solution of 2,5-dihydroxybenzoic acid (DHB). A thin film of calibrant is deposited on the surface of the probe in a similar fashion as for the analyte. The mixture is first deposited with a pipette and the ethanol vehicle is

subsequently left to evaporate. Differences in laser power and sample preparation can produce differences in the desorption process. Similar experimental conditions for the analysis of calibrant and analyte (thickness of the film, attenuation of the laser power) are therefore the best guarantee to optimise the mass accuracy. For this reason, the calibrant is deposited in the appropriate groove situated at the same level as the surface of the sectioned sample when a paint cross-section is investigated (see section 3.2).

Calibration is achieved with the DHB and the PEG spectral data using typically 5 to 10 peaks at regular intervals on the m/z range [0-1500]. Sufficient mass accuracy was obtained (ca. 50 ppm at mass 1000) with external calibration alone, and internal calibration involving the mixing of standard compounds with the unknown analyte was not necessary at this stage of the investigations.

The exact position of impact of the laser beam on the probe is determined prior to analysis. This is achieved by spotting a thin layer of an opaque calibrant (e.g. PEG or lead white) on the probe. After desorption of this opaque calibrant a clearly visible empty space is left at the location of impact. The exact position of impact is then marked on the screen of the camera monitor. Accurate positioning of the probe under the laser beam is then possible, and individual particles of the analyte (typically 10-50 micrometers for ground pigments) or a single fabric fibre can be targeted. Adjustment of the camera output (sharpness, clarity and centring) is necessary before each set of analyses to guarantee correct observation of the sample, and accurate targeting of the sample with the laser. Constant attention was also given to the size of the focus and form of the laser beam.

2.4.3. Ion Trap Mass Spectrometer: Set-up and operation

Our second experimental set-up is an external ion source – ion trap mass spectrometer (Figure 2.9 and Figure 2.10) which has been specifically designed for surface LDMS of paint-cross sections. The mass analyser is a commercial Ion Trap Mass Spectrometer (ITMS), from an Esquire® instrument (Bruker-Franzen Analytik, Bremen). The Ion Trap Mass Spectrometer is composed of an ionisation source, a storage cell, and an ion detector. The cell itself is composed of three electrodes: a central ring electrode flanked by two end-cap electrodes (Figure 2.11). The rest of the instrumentation consists of an ionisation chamber where analyte gaseous ions are produced and a series of electrostatic lenses, which transfer these ions to the ITMS for mass spectrometric analysis. Two vacuum pumps maintain the whole system at low-pressure (measured at $2 \cdot 10^{-6}$ mbar in the ionisation region).

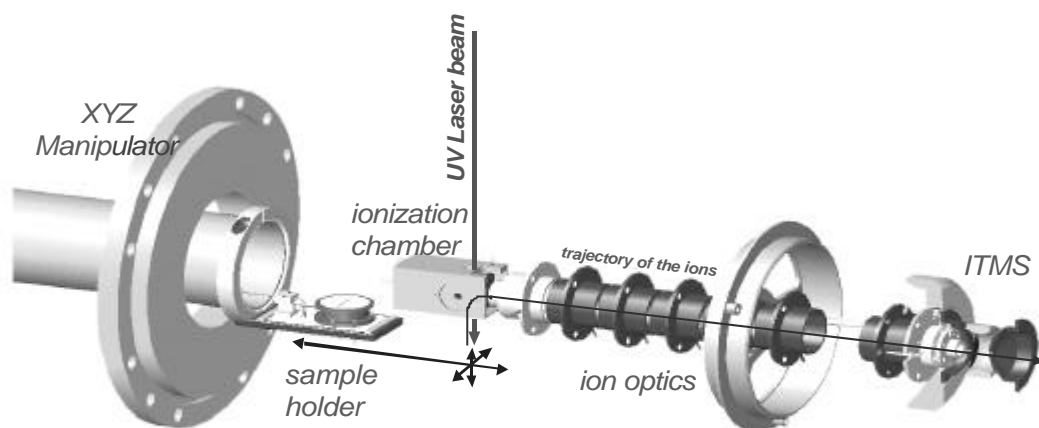


Figure 2.9 *The external ion-source Ion Trap Mass Spectrometer built at AMOLF. The sample is positioned under the laser beam with micrometric precision. Ions are produced from the surface of the paint sample (thin film on a metallic probe or an embedded cross-section) and transferred to the ITMS for MS or tandem MS analysis.*

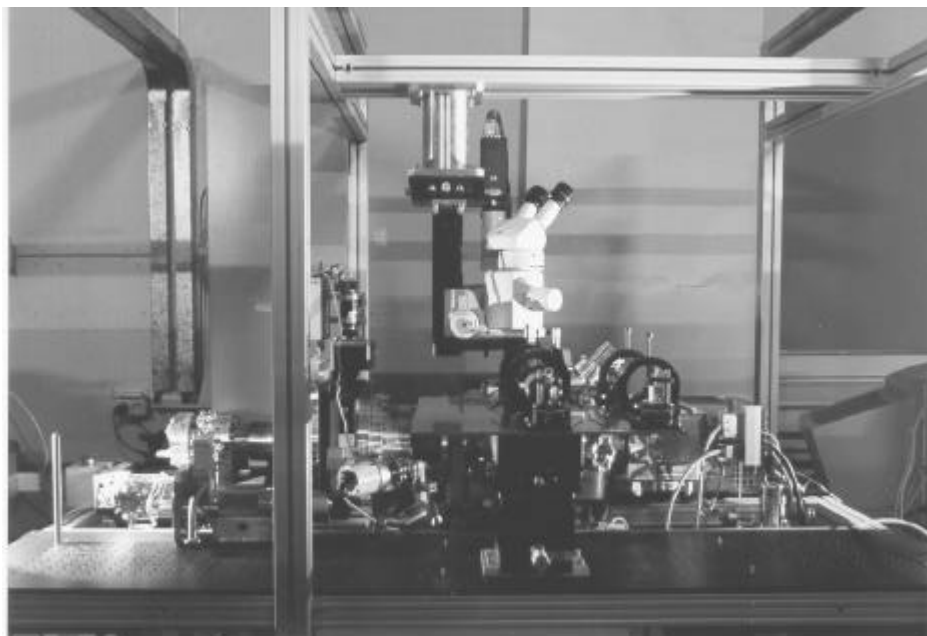


Figure 2.10 *ITMS set-up comprising a XYZ manipulator, a pulsed Nd:YAG laser and an optical microscope equipped with a CCD camera.*

The ionisation chamber was designed to indiscriminately perform non spatially-resolved analysis on direct insertion probes and spatially-resolved analysis on the surface of paint samples. For non-spatially-resolved analysis, a solution or suspension of the sample is deposited on the 3 mm diameter tip of a stainless steel direct insertion probe and the additional solvent is left to evaporate.

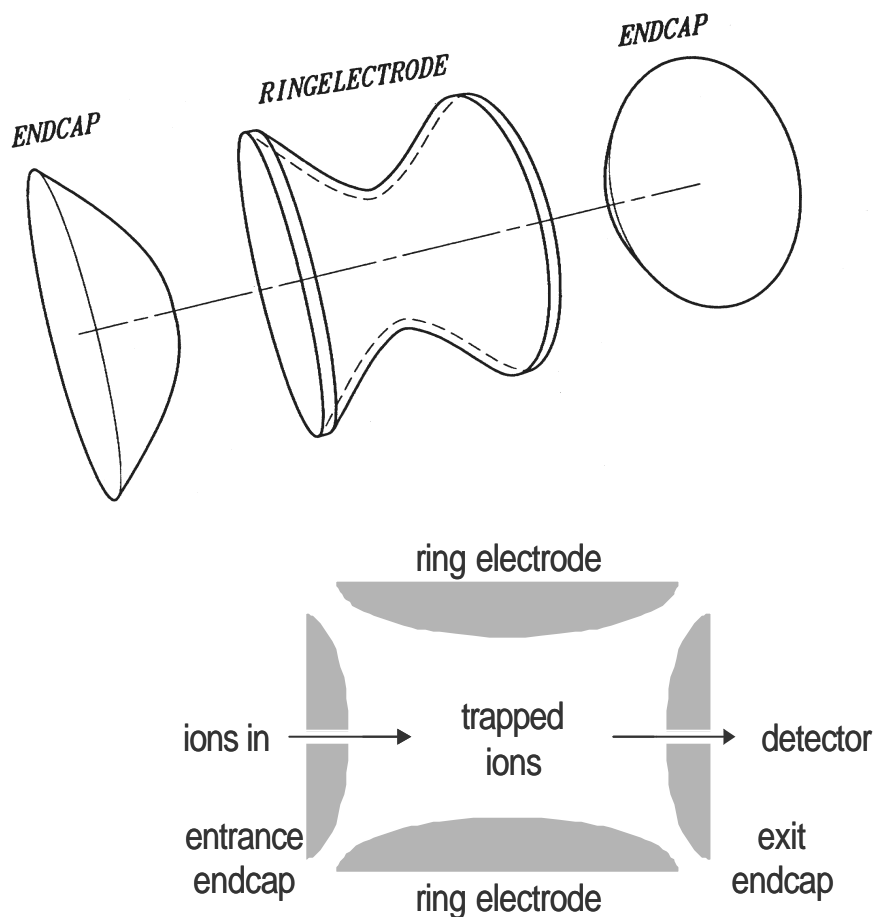


Figure 2.11 *ITMS cell with its three electrodes. Ions are introduced through the entrance endcap and detected after expulsion through the exit endcap.*

The probe is first introduced in a lateral transit chamber, which serves as vacuum lock. When the vacuum lock has been pumped down, the probe is introduced inside the ionisation chamber in the focus of the laser beam. For spatially-resolved analysis, paint cross-sections are first introduced in a sample exchange chamber, which also serves as vacuum lock. When the exchange

Chapter 2

chamber has been pumped down, the sample is translated inside the ionisation chamber with an XYZ manipulator. The software-controlled XYZ manipulator has a micrometric lateral precision. Thanks to an optical microscope equipped with a CCD camera the sample can be accurately positioned in the focus of the laser beam.

The frequency-tripled output of a Quanta-Ray GCR-11 (Spectra-Physics Inc) pulsed Nd:YAG laser was used for desorption and ionisation. It produces pulses of ultraviolet laser light with a wavelength of 355 nm (3,49eV), a tuneable pulse-energy of maximum 60 mJ, and duration of 5 ns (also available are the principal emission wavelength at 1064 nm and the second harmonic at 532 nm). Repetition rate is typically 1-2 Hz. The laser beam is directed onto the sample perpendicular to its surface, or at 45° in the non-spatially-resolved source (Figure 2.12).

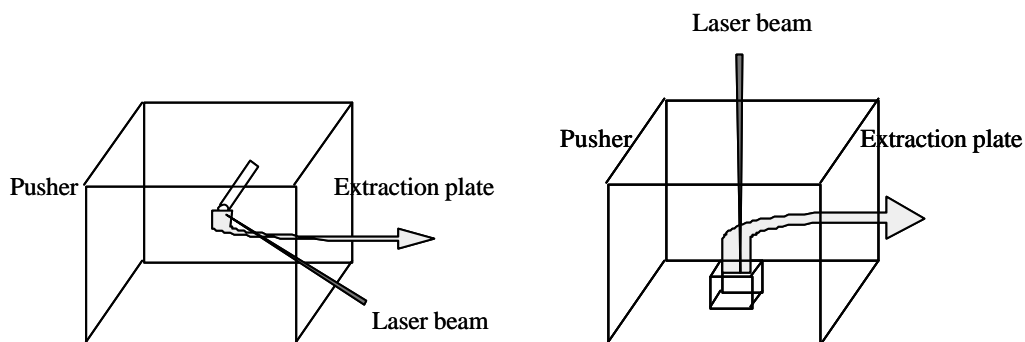


Figure 2.12 *ITMS source configurations: (left) direct insertion probe with a laser at 45° and (right) embedded paint sample with a laser at 90°*

The spot diameter on target was measured to be approximately 10 μm in the spatially resolved measurements and 1 mm in the non spatially-resolved measurements. As the laser beam hits the surface, material is vaporised from the surface of the sample and expands in the ionisation chamber. Gaseous neutrals can be post-ionised with an electron ionisation beam (LD-EI). Ions are then extracted from the ionisation chamber and transferred into the ITMS via the ion transfer lenses. Long transfer time in the ITMS set-up - in seconds compared to microseconds in the TOF-MS - and high pressures increase the probability of ion-molecule reactions in the gas-phase and thermalisation of internal energy.

Applying an appropriate radio frequency (RF) electric potential to the ring electrode, while the two end-cap electrodes are grounded, creates a trapping potential well within the cell. When gaseous ions are introduced in the cell, ions

within a certain mass-to-charge range find a stable motion regime and remain confined in the cell (Figure 2.13). The cell is hence appropriately named an *ion trap*. Trajectories of the ions in the trap describe complex three-dimensional 8-shaped revolutions referred to as Lissajous figures. Helium gas introduced in the cell enhances the trapping efficiency by reducing the initial velocity of the ions without inducing fragmentation (ion damping).

The conditions for stable ion motion within the cell electrodes depends on

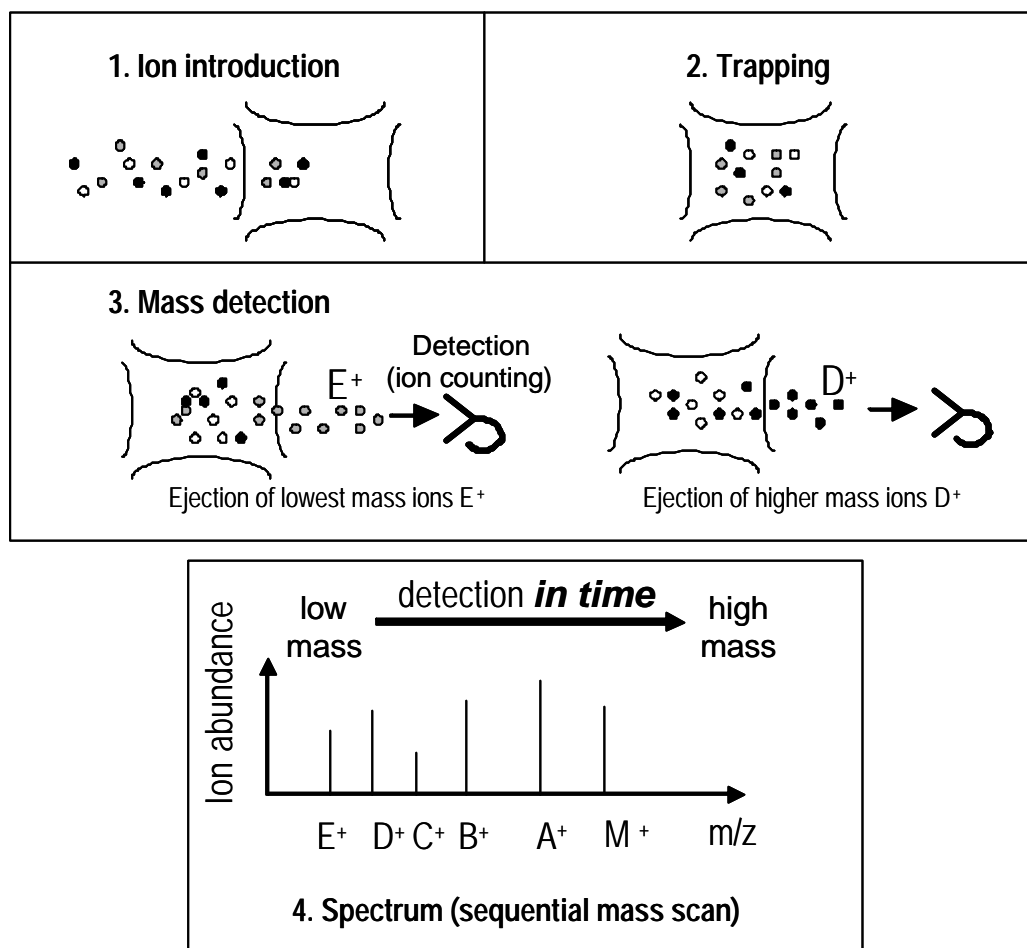


Figure 2.13 Sequence of events during an MS experiment in an ITMS: (1) ions enter the ITMS (1) and are trapped (2). Mass detection of the trapped ions (3): ions E^+ of lowest m/z are ejected from the ITMS and detected, ions D^+ of higher m/z , and subsequently ejected and detected, and so on with higher and higher m/z : ions C^+ , ions B^+ , ions A^+ , up to ions M^+ (molecular ions). The counting of ions by the detector is realised by the successive ejection/detection events in time. Results are displayed in the form of a mass spectrum (4) which displays the amount of ions as a function of their mass/charge ratio.

the one hand on the physical and functional parameters of the trap (i.e., size and form of the cavity, potentials applied, pressure in the trap, amplitude and frequency of the RF field, etc.) and on the other hand on ion parameters (i.e., mass/charge ratio, introduction direction and velocity, total amount of ions introduced in the trap, etc.). Frequency and amplitude of the RF field during ion injection impose a lower mass limit of trapping, called low mass cut-off (LMCO), and also determine the efficiency of the trapping for each m/z . In our experiments the low-mass cut-off ranged typically from m/z 50 up to m/z 100 (i.e. ions below these masses are not trapped). A difference in trapping efficiency is the combined effect of flight time differences during ion transport and intermittent periods of trapping (duty cycle). During the ion transport between the ion source and the trap, ions of different m/z travel at a different speed, which results in a time spreading of the ion cloud. For example, with a kinetic energy spread of 1%, an ion of m/z 1000 will arrive at the ion trap analyser 90 μs after the laser has fired during a time period of ca. 1.5 μs . An ion of m/z 100 will arrive at the ion trap analyser 29 μs after the laser has fired during a time period of ca. 200 ns only (assuming an average kinetic energy of 100eV and a flight path of 40 cm). Since the ion trap fulfils the trapping condition at a particular RF amplitude, trapping is only achieved on periodic time interval. This is responsible for a ca. 50% ion loss in transmission. Accordingly differences in trapping efficiency will be observed for different m/z . Optimal trapping conditions of the ions will be sought by tuning the LMCO, hence limiting the m/z range for panoramic registration.

Ions successfully trapped in the storage cell are available for subsequent mass spectrometric experiments, i.e., their separation and detection according to their mass-to-charge ratio. Changing the ion trajectory stability condition in the cell by modifying the trapping potential makes it possible to induce the ejection of ions of a particular m/z toward the detector. In practice, the ion population is ejected from the trap in order of incremental mass toward the detector for ion counting. In other words, an MS experiment consists of an incremental mass-scanning of the trapped ion population *in time*. The resulting detector-signal is converted into a mass spectrum, i.e., a graph displaying the ion counts as a function of the mass-to-charge ratio (m/z). As a matter of fact, the great majority of ions detected in this work are singly charged ($z=1$).

2.4.4. Multiple stage experiment with the ITMS

Trapped ions can be investigated in *multiple-stage MS* experiments (also called tandem-in-time or MS^n). MS^n experiments are based on successive ion isolation and ion fragmentation events (Figure 2.14).

Isolation of ions of one particular m/z is achieved by mass-selectively ejecting all other ions from the trap by applying the appropriate auxiliary RF voltage to the end caps. After this operation, a mass scanning of the ion population would theoretically result in a single peak for the selected m/z . In practice the m/z range of isolation is rather a Gaussian distribution with $\Delta m/z$ of circa 10 Da.

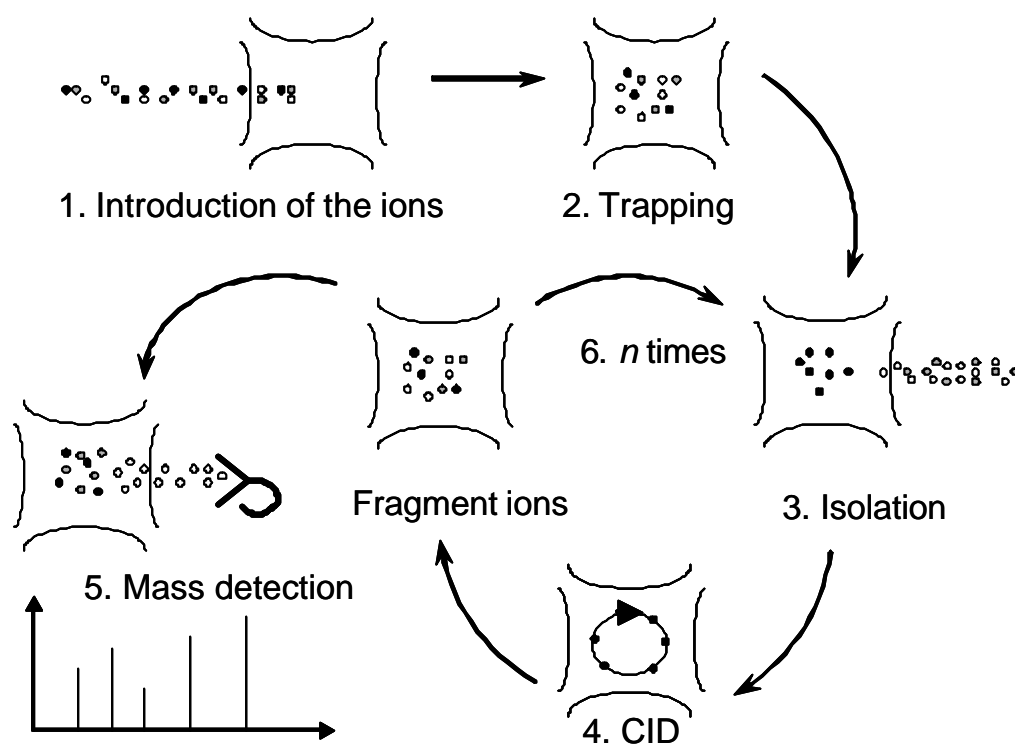


Figure 2.14 Sequence of events during an MS/MS experiment: ions enter the ITMS (1) and are trapped (2). Isolation of a particular series of ions (3), fragmentation of the selected ions (4), mass detection (5) i.e. same operation as in figure 2.13(3), or selection of a particular series of fragment ions for further MSⁿ analysis (6).

Mass-selective fragmentation of ions is accomplished through an operation called *collisional induced dissociation* (CID). In CID the secular motion of a particular ensemble of ions in the trap is resonantly accelerated at a specific frequency. Multiple low-energy collisions with inert background (helium) gas molecules cause the internal energy of these ions to build up, which eventually results in their fragmentation. Stable fragment ions resulting from the collisional induced dissociation stay confined in the trap. The population of ions resulting from fragmentation depends on the choice of the CID conditions, i.e., type and pressure of background gas, and the duration and amplitude of excitation.

The population of fragment ions is then mass-selectively ejected from the trap, resulting in a MS/MS or MS² spectrum. The isolation and fragmentation operation can be reiterated up to several (*n*) times before recording the mass spectrum which produces an MS^{*n*} spectrum.

Strictly speaking, the isolation step does not require the performance of MS/MS experiments, as only a specific secular frequency is excited making CID a mass-selective operation. However, the isolation step is profitable to the analyst as fragmentation can be performed on a 'purified' starting material (similar to a chromatographic step) and yields clear MS/MS spectra. In particular, ejection of the major components can be beneficial to proper detection of the minor constituents. Isolation of a precursor ion makes the link between parent and daughter ions evident.

2.5. Conclusion

Two instruments were described that apply LDMS to the study of artists' paint materials and cross-sectioned samples removed from easel paintings. Short (pulsed) bursts of energy from focused UV laser beams result in the local formation of ions from a solid sample for mass analysis, and limit at the same time the sample consumption. TOF-MS and ITMS analysers that pair particularly well with the use of pulsed lasers were employed for mass detection. The combined use of micro-positioning and imaging components makes it possible to accurately localise the area of interest and focus the laser beam for sampling. TOF-MS is preferred for quick and panoramic mass scanning of the analyte, whereas ITMS is dedicated to multi-stage MS experimental studies used to investigate molecular fragmentation patterns and complex mixtures of samples. Two LD processes are used for the investigation of paint materials: LDI for the selective desorption of organic pigments, and - where the utilisation of a matrix is possible - MALDI for the study of paint materials containing large macromolecular systems.

Chapter 3

An experimental strategy for LDMS investigations of paint materials and paint cross-sections

LDMS analyses of paint materials critically depend on the optimisation of the desorption and ionisation parameters. In this chapter we will discuss the effect of several experimental parameters, such as the laser power density, the repetition rate of the laser shots, the ITMS mass cut-off, and the CID conditions for MS/MS experiments, and determine their influence on the quality of the LDMS data. In addition we will discuss significant issues such as the laser power threshold, the shot-to-shot variation of the ion formation, the measurement of isotope patterns and the rate of ablation. The aim of this study is to establish the optimal experimental approach for spatially-resolved LDMS of artist's materials.

3.1. Introduction

A great variety of experimental parameters influence the outcome of an LDMS analysis. Formation of ions at the sample surface depends on the photon-sample interactions, which is governed by sample arrangement, laser wavelength, laser power density and repetition rate, surface temperature, chemical composition and surface morphology. As LDMS aims at the determination of the local chemical composition of the surface, it is imperative to establish what experimental parameters to use to answer a particular analytical issue. For instance questions such as what is the power density best used for the structural analysis of fragile organic pigments in a complex matrix, what is the smallest pigment particle that can be observed, etc, have to be addressed.

In this chapter we will discuss the method to obtain optimum LDMS conditions for the investigation of paint materials and paint cross-sections. We will emphasise the surface properties of the sample, the mounting of the sample in the MS holder, the influence of the laser power density, the close repetition of laser shots, the mass cut-off and collision-induced dissociation parameters of the ITMS analyser. Examples of LDI and MALDI analyses of paint materials will be presented to illustrate these different issues. As a result, an optimal strategy to perform LDMS of paint materials and paint cross-sections is established.

3.2. Sample and sample mounting

3.2.1. Sample holders

A large variety of sample types is investigated by LDMS in this thesis. They include reference materials, calibrants, liquid oil pigment mixtures, cardboard coated with one or several layers of pigmented medium, paint cross-sections and dyed fibres with threads of a few tens of micrometers in diameter. These samples have to be mounted accurately in the focus of the desorption laser beam in the ion source. Two sample holders compatible with both the TOF-MS and the ITMS ionisation sources were designed to make LDMS possible with samples of all different kinds.

The first and most common sample arrangement (Figure 3.1.A) is the use of a metallic substrate. A standard sample holder is used mainly for the analysis of

reference materials with LDI and MALDI. Sample deposition is facilitated by the application of a droplet of a solution or a suspension of the analyte under study, resulting in a thin layer of analyte on the metallic surface of the probe after evaporation of the solvent (Figure 3.2.A). Analyses of these thin layers are particularly successful in the case of organic pigments. The usage of thin films greatly enhances the signal in comparison with powder of coarser grain sizes, thicker films, or paint samples of larger dimension.

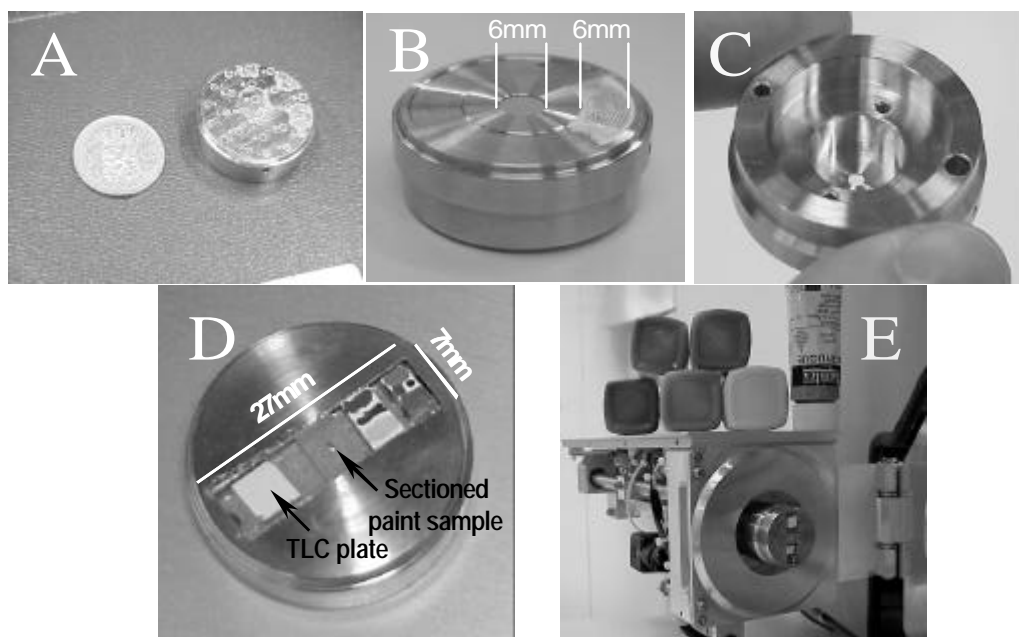


Figure 3.1 (A) Commercial LDMS probe surface with 26 pre-defined sample positions for the study of thin films and absorbed particles. (B) Home-built LDMS probe for the study of paint cross-sections and paint reconstructions on a cardboard support, front side. A calibrant has been deposited in the appropriate groove. (C) Back side showing the cavity where the sample is introduced and fastened with a back spring. (D) Home-built LDMS probe for the study of paint cross-sections and samples deposited on a TLC plate (E). Probe holder with the XYZ manipulation system.

An alternate approach was developed to minimise the dispersion of the sample at the surface of the probe. Small TLC plates (ca. 5x5x1.3mm) coated with cellulose were mounted on a home-built sample holder as shown in Figure 3.1 D. To facilitate the mounting of a TLC plate, the standard TOF-MS sample holder was equipped with a 1.3 mm deep groove. TLC plates are fastened using double-sided sticky tape (Figure 3.2 B). A small aliquot of a sample solution is subsequently deposited on the surface of the TLC plate. The higher surface tension of the cellulose surface ensures a minimum dispersion of the sample leaving a concentrated spot of analyte. This preparation is especially useful when only small

Chapter 3

amounts of material are available in dilute solution. The ionisation efficiency is similar compared to the use of a metallic substrate. The TLC plates offer the added advantage of providing a disposable substrate for the analyte, which eliminates the possibility of probe contamination from previous analysis.

In a similar fashion, cross-sections can be fastened in the groove of this sample-holder using double-sided adhesive tape (Figure 3.2 C). This configuration necessitates the correct trimming of the cross-section block of resin to fit the size and depth of the groove. The main drawback of this method is that when the front and back surface of the mounted samples are not parallel, differences in the z-axis position of the laser focus along the sample surface will occur. Larger samples such as embedded cross-sections that cannot be thinned down, irregular samples, painted cardboard and textile fibres require a different sample holder altogether.

We developed a sample holder for this purpose as shown in Figure 3.1.B and C. The sample holder has a cylindrical cavity of 12 mm in diameter and 6 mm in height with a circular aperture of 8 mm in diameter. A resin block, a piece of painted cardboard or a fibre thread is clamped inside the cavity with the aid of a back spring (Figure 3.2 D and E). The spring-loaded clamping of the sample in the cavity ensures that the sample surface is parallel to the surface of the probe holder and limits the z-motion of the surface during sample positioning. A groove in the surface of the probe allows the deposition of a calibrant at the exact same level as the sample surface. Home-made sample holders have the same dimensions as the regular sample holder and are introduced in exactly the same fashion in the mass analyser (Figure 3.1 E).

3.2.2. *Level differences*

Correct positioning in the z-axis (axis of the extraction) of the samples in the ionisation source of the TOF-MS is essential. Differences in ionisation positions are expected to induce shifts in the flight-time that reduce the mass resolution. Tests were designed and conducted to establish whether such a negative effect could be observed within a range of a few millimetres. No significant shift was observed for level differences within 0.1mm-range. We explain this restricted effect by the combination of delayed and pulsed extraction. For z-coordinates differences in excess of 0.1mm a significant mass shift is observed. A shift of 2 Da for 0.2mm and 10 Da for 1.3mm has been determined at a mass of 1000 Da. This has dramatic effect in the analysis of textile fibres as will be discussed in more detail in Chapter 6. The calibrant groove designed in the spring-loaded probe holder ensures the same z-coordinate for the analyte and the calibrant.

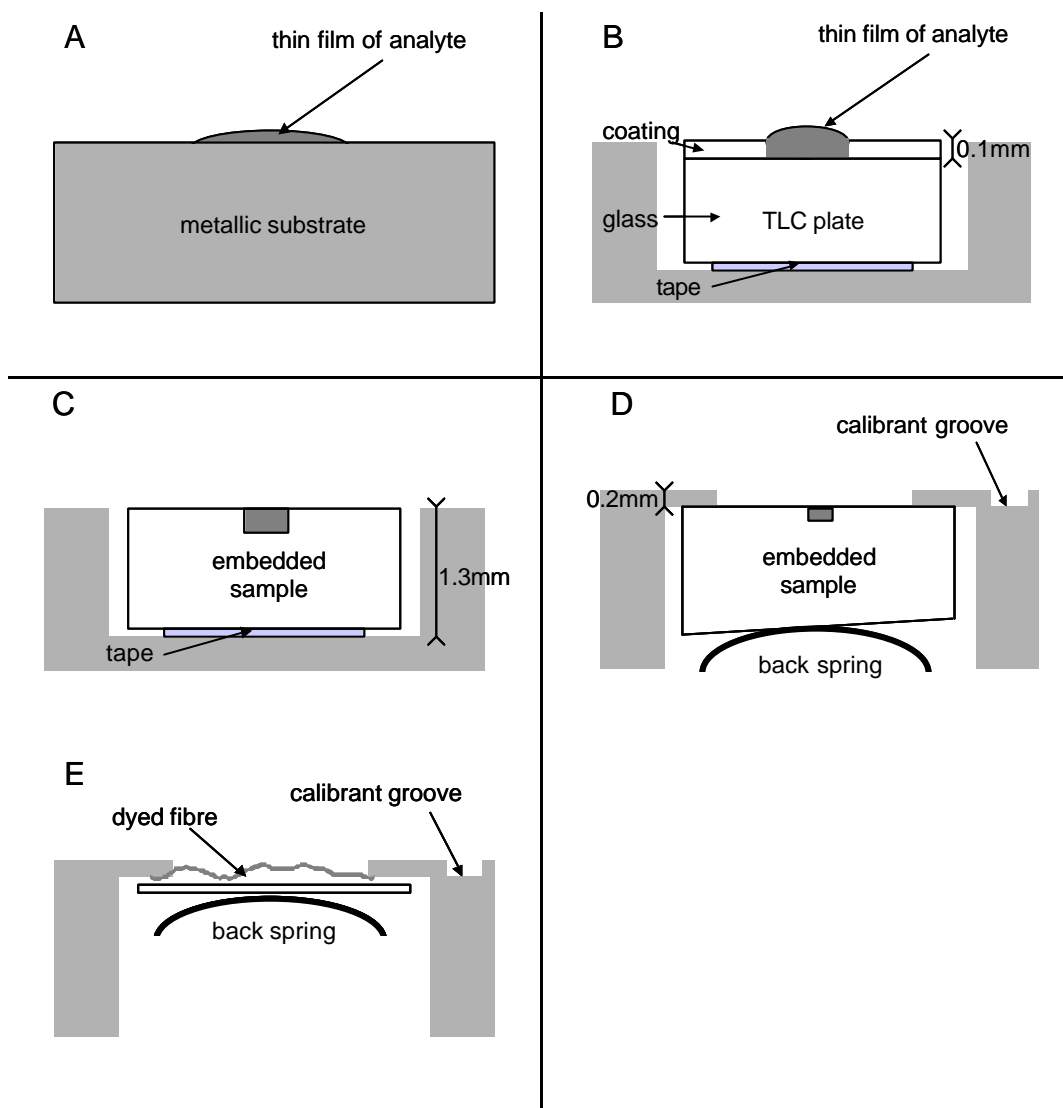


Figure 3.2 *Different probe holders for spatially-resolved analysis of paint materials with TOF-MS and ITMS: (A) thin film deposited on a metallic probe (B) TLC plate and (C) embedded paint cross-section stuck on the probe (D) embedded paint cross-section and (E) fibre clamped in the holder's cavity.*

3.3. *Laser-sample interaction*

The amount of energy deposited into the sample is a key to the understanding of the interaction between the laser beam and the sample surface. In this section we will describe the parameters that determine how much laser energy is converted into internal energy of surface molecules i.e., the amount of energy deposited.

Energy deposition at the surface of the sample depends both on macroscopic properties and on molecular structure of the sample surface (chemical composition of the different compounds). The macroscopic properties include the composition and complex arrangement of the layers, which is expected to influence the propagation of light at the surface of the section through different reflection, scattering and refraction properties, and surface corrugation. The different molecular structures in complex samples lead to different molecular absorbances at different wavelengths. For that reason a mixture of various paint materials can hinder or inversely promote the LDI process (acting as intrinsic matrix). The type of medium, as well as the pigment-to-medium ratio in a coloured layer will determine the energy transfer efficiency in the desorption process (from the photons to the analyte molecules). High heterogeneity of the sample is expected to induce differences in photo-chemical and photo-physical processes from spot to spot at the surface of the sample, and possibly from shot to shot resulting in laser ablation.

The amount of internal energy deposited and dissipated in the surface will affect the ionisation efficiency, the degree of fragmentation, the desorption rate and the overall interaction volume. Broadly speaking, two power density domains can be distinguished¹¹⁰. In the low power domain ($<10^8$ W/cm²) evaporation of surface layers is obtained, partially in the form of intact neutral and ionised molecules. In this domain the evaporation process is rather reproducible and volume of material ablated is kept small, typically in the order of μm^3 . There is usually no noticeable damage to the sample following a single pulse. Ionisation efficiency - i.e., the ratio of ions to neutrals - is low (of the order of 10^{-5}) but the mild conditions assure the generation of diagnostic ions from organic compounds up to a few 1000s Da. In higher power domains, elemental ions and small molecular fragment ions are mainly desorbed, and ionisation yields are increased. The dimension of the ablation crater scales with the power density. The analyte volume desorbed per laser shot (crater volume) from a sample surface depends on a variety of parameters, the type of analyte, the surface condition of the sample and the characteristics of the laser beam (laser-target angle, density, etc). In the low laser power domain, very small

ablation volumes ($<\mu\text{m}^3$) are not easily determined and the size of ablation craters is rather estimated with the surface diameter of the impact. The size of the laser beam does not provide a precise indication of the crater diameter since the desorption rate varies over the irradiated surface area. A rough estimation of the interaction area is given by the observation of the fluorescence spot provided by the sample under laser irradiation. A more accurate estimation is obtained by measuring the diameter of a discoloured area left on a photosensitive paper, or the diameter of a hole in a thin film of reference material (Figure 3.3). In spatially-resolved analysis, the size of the UV laser beam will be made as small as possible to increase the spatial resolution. The laser optics limits the beam diameter to $40\mu\text{m}$ (estimated with the discoloration of photo-sensitive paper).

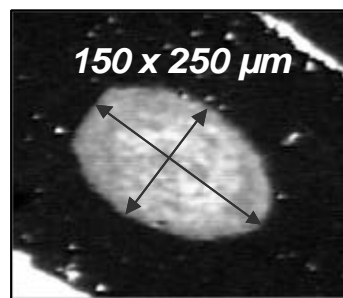


Figure 3.3 *Crater left at the surface of photo-sensitive paper showing the size of the laser impact for a defocused experiment.*

An experiment was performed where the laser energy of a UV laser beam working at 337nm was varied between 5 and $70\ \mu\text{J}$ under the same focussing conditions (Figure 3.4). Tuning of the laser energy is obtained by attenuating the laser beam with an optical filter positioned in its path. 0% attenuation corresponds to full transmission of the laser light whereas 50% attenuation means that approximately half of the light emitted by the UV laser is filtered before reaching the sample. This experiment demonstrated that the degree of discoloration varies more than the size of the discoloured area. It is not possible to evaluate the real size of the impact when low laser energies were employed since the spots are not clearly defined. For that reason all spot sizes in this thesis are related to the spot size at maximum laser energy. This implies that the actual spatial-resolution is probably lower than the quoted spot size at low laser energies.

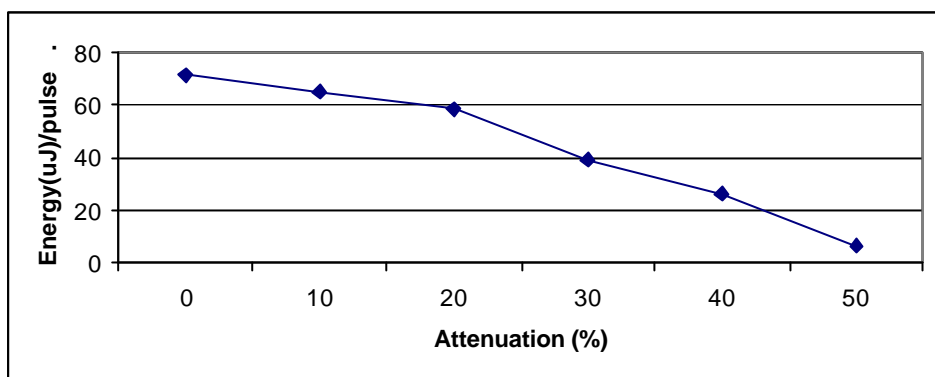


Figure 3.4 *Power density of the UV laser beam as a function of the energy attenuation provided by the laser optics. A 0% attenuation corresponds to the full energy delivered by the laser; at 50% attenuation about 90% of the laser energy is filtered out by the attenuator.*

In a typical LDMS experiment, it is difficult to determine prior to analysis how much energy per pulse should be applied to achieve precisely a given power density in the desorbed micro-volume. A strategy was devised in which the power density is progressively increased starting with a fully attenuated beam. After assessing the LDI threshold, the laser energy is set to an optimum value as described in the next example. This example illustrates the relationship between the laser power density and the spectral information for LDI of organic colouring compounds. Kaempferol, a yellow organic colouring material belonging to the flavonoids (see Chapter 4) was deposited as a thin film (approximately 10 μm) on a stainless steel probe and analysed by TOF-MS. The 337nm output of a nitrogen laser was focussed to the surface of the probe with a beam size of approximately 40 μm diameter.

In the lowest power density range (<10 μJ), energy deposition is insufficient to induce desorption/ionisation process and spectra display nothing but the instrument noise. It is not impossible that the laser removes material from the surface of the sample, but this material is not detected by the mass spectrometer. Different reasons could account for this absence of detection: (1) material is desorbed but not ionised, (2) ions are produced but do not reach the detector, (3) ions reach the detector but in insufficient amounts, i.e. below the detection limit, or outside the analyser mass detection range (the TOF-MS has theoretically no mass boundaries, but the ion injection conditions impose a low mass cut-off for the ITMS).

When a certain laser density is reached, called *LDI threshold* (ca. $10\mu\text{J}$ for kaempferol on stainless steel), sufficient energy is deposited into the analyte to produce observable gaseous ions and the mass spectrum displays a series of kaempferol peaks (Figure 3.5.A).

At this laser density level, the smallest quantity of internal energy is imparted to the molecules that lead to formation of intact molecular ions, i.e. the amount of fragmentation is low under these conditions. During the LDI process, both positive and negative ions are generated but ions with only one polarity are accelerated towards the detector. Successive analyses of the same compound reveals that the minimum laser power density required to detect the presence of the molecule (LDI threshold) depends on the arrangement of the sample film (thickness, size of the aggregates) and varies from one desorption spot to another.

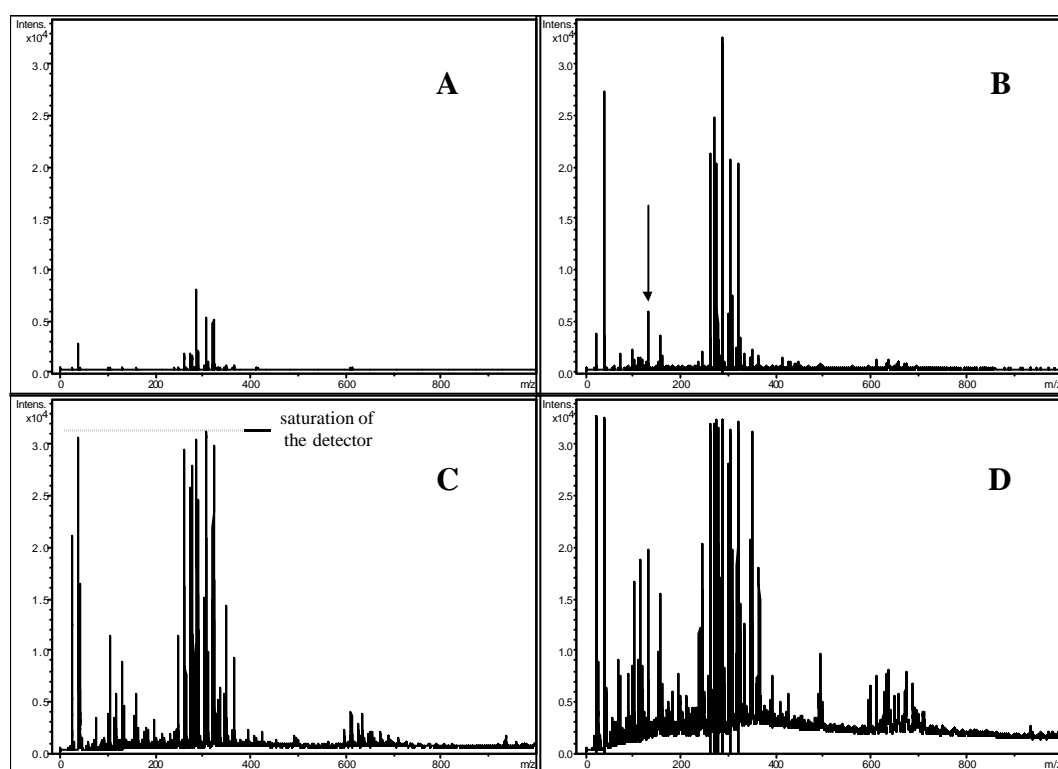


Figure 3.5 *Effect of laser density on the appearance of the LDI-TOFMS mass spectra in the case of kaempferol. Spectra at the desorption and ionisation threshold of $10\mu\text{J}$ (A); at higher density higher S/N is obtained and more fragmentation and dimers/clusters are observed (B), at even higher density the detector saturates but no additional analytical information is provided (C), highest laser densities lead to excessive fragmentation and dimerisation, with saturation of the detector (D).*

Inversely, different arrangements of the same compound produce different spectra (distribution and relative intensities of fragment ions) for an identical laser power density. For this reason, great care should be given to sample preparation and the exact value of LDI threshold laser power densities cannot be proposed. Although similar trends are observed comparisons between different components are difficult. An experiment where different reference organic pigments were deposited as thin films on stainless steel showed that under these conditions the LDI threshold energy fluctuates around 10 μJ .

The *threshold spectrum* of kaempferol in the positive mode (Figure 3.5.A) shows that low laser density LDI achieves soft ionisation. Absorption of the UV laser energy induces the formation of analyte radical cations $\text{M}^{\cdot+}$ and protonated and sodiated molecules $[\text{M}+\text{H}]^+$ and $[\text{M}+\text{Na}]^+$. Thermal ionisation of alkali contaminants - present in nearly all types of samples - generates alkali ions in high abundance. The spectrum displays also fragment ions and a few ions of higher molecular mass. Thermal energy imparted to the molecules during the LDI process is moderate and pyrolysis (fragmentation through thermal activation) is greatly minimised. Fragment ions with low relative abundances (0.5%) produce nevertheless sufficient evidence to positively identify kaempferol.

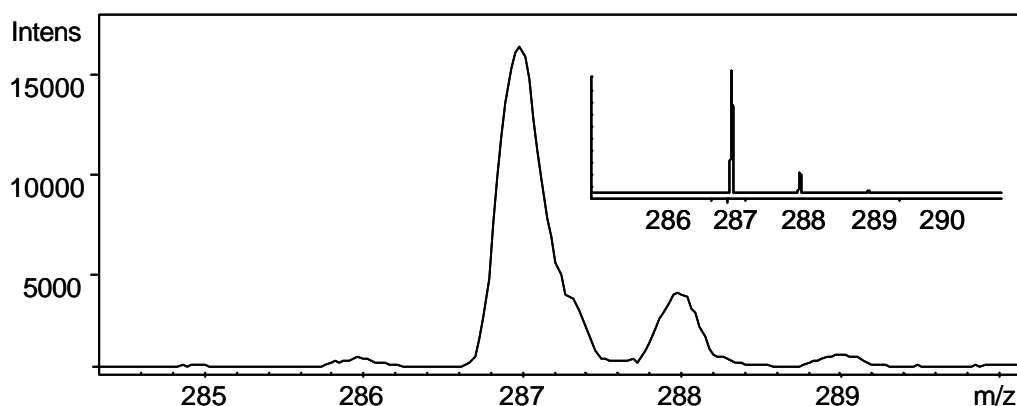


Figure 3.6 LDI-TOF-MS of kaempferol. In inset, the theoretical isotopic distribution.

A closer look at the region around the molecular mass (Figure 3.6) shows mostly protonated molecules $[\text{M}+\text{H}]^+$ and only few radical cations $\text{M}^{\cdot+}$. Peaks at 288 and 289 are attributed to the isotope ^{13}C , which occurs in a natural abundance of approximately 1.08 per cent*. *Isotopic distribution* for the 15 carbon atoms of the protonated ion of kaempferol of formula $\text{C}_{15}\text{H}_{11}\text{O}_6$ gives relative intensities of 100 for m/z M, 16.5 for m/z M+1, and 1.3 for m/z M+2. Isotopic distribution

* The most common isotope of carbon is ^{12}C , which nucleus has 6 protons and 6 neutrons, but about 1,08% of the natural carbon consist of the isotope ^{13}C , which has one more neutron in its nucleus.

provides essential information on the elemental composition and can be greatly contribute to the identification of the molecular structure¹²⁷

It is observed in Figure 3.5.B that an increase in the laser energy of 10% above the LDI threshold enhances directly the total number of ions collected by the detector. At the same time neutral pressure is increased and we observe enhanced rearrangement (cluster ions*) and oligomerization effects (dimers such as $[2M+H]^+$, $[2M+Na]^+$ are detected). At high laser power (Figure 3.5.C) mass resolution gets worse as the peak width becomes broader. A large ion population results in a broader spatial distribution of the ion cloud. Higher ionisation yields promote this broadening of the cloud through the so-called 'space-charge effect', that is an increase in repulsive forces between ions of the same charge. The detector saturates at approximately 30,000 counts, which makes measurements of relative intensities above 30,000 counts impossible. At even higher laser energy density (ca. 70 μ J) characterisation becomes even more difficult (Figure 3.5.D). Excessive fragmentation is observed in combination with the formation of dimers and higher oligomers (clustering). These clustering phenomena are attributed to the higher neutral pressure in the laser plume at these high energies. The increased degree of fragmentation is attributed to the higher amount of internal energy deposited into the surface. Rising the laser power density results also in increased sample consumption. High laser power density results eventually in serious damage of the sample surface, which is visible under the microscope.

In conclusion, these experiments show that ionisation yields and structural information are interrelated parameters which depend on the laser power density. Additional energy deposition amplifies the ion population (TIC) but promotes at the same time the formation of a variety of additional ionic species (dimers, fragment ions). By tuning the laser power density correctly, it is possible to obtain an optimal population of the characteristic ions. Low energy deposition during the desorption/ionisation process increases the probability to obtain molecular structure information by transferring intact molecular ions and diagnostic fragment ions into the gas phase. Furthermore, it limits the sample consumption and preserves the integrity of the specimen surface for further analyses[†]. Practice shows that sufficient variety of diagnostic ions with appropriate signal-to-noise ratio is obtained for laser power densities within a small range (<5%) above the LDI threshold value. Working in this energy domain provides the optimal balance between mass spectral information and sample consumption. Therefore this energy

* A cluster ion consists of the main building blocks or structural moieties of the original molecule.

† High irradiance LDI could be interesting for speciation of inorganic substances. However, other analytical techniques such as TOF-SIMS imaging (Heeren *et al.*) or SEM-EDX will be preferred in this case since they limit considerably the damage of the sample surface and provide a superior mass resolution.

domain was consistently chosen for performance of LDMS experiments on paint materials in this thesis.

3.4. Shot-to-shot variations

LDI experiments are usually performed with a series of several laser shots in close succession, and the resulting spectral information is averaged to produce a reliable mass spectrum. This practice is rationalised in the following experiment where we monitor the spectral information as a function of time during multiple-shot analyses. The flavonoid morin was deposited as a thin film on a stainless steel probe and analysed by LDI-ITMS. The UV laser was focussed to the surface of the probe and employed with a repetition rate of ca. 1 Hz. Phase-locking between the trap function (i.e. ion accumulation and scanning) and the laser triggering assured that for each laser shot the spectrum is recorded under the same time conditions. Since repeated laser shots increase the sample consumption, the number of laser shots (or duration of the LD process) should be theoretically kept as low as possible to prevent excessive damage of the sample surface.

Figure 3.7 shows the total ion current (TIC) of morin, recorded for 45 seconds with an uncorrected offset of circa 2000 counts for the background. During the time period $t=[0-18s]$, the laser is still idle and the background is recorded. At $t=18sec$ the UV laser (355nm) is switched on and the total number of ions detected increases shortly to an average value of 6000 counts. During the time period $t=[18-33s]$, the TIC curve displays a serrated profile with shot-to-shot variation in excess of 30% (i.e. three times larger than the background variation). In the ensuing period $t=[33-50s]$ shot-to-shot variations visibly subside with values mostly under 10% (i.e. comparable to the background variation).

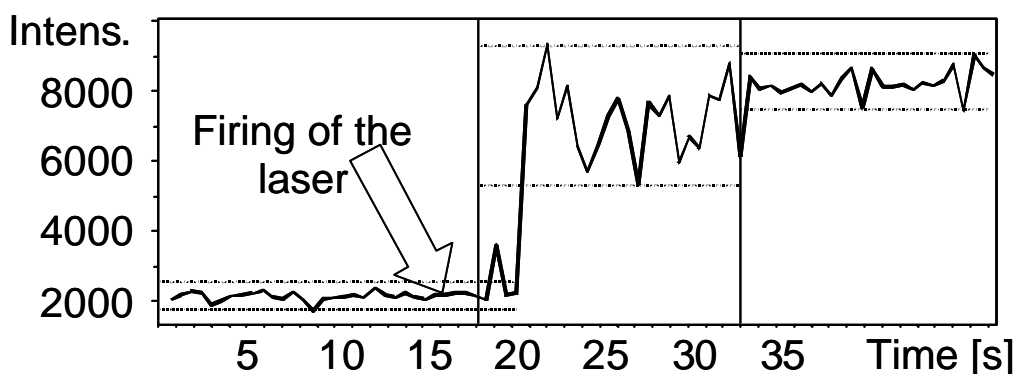


Figure 3.7 Total Ion Current (TIC) of morin in multiple-shot LDI-ITMS analyses at low laser power.

Laser hardware is considered to have only a negligible effect on the variation in TIC intensity since variation in power density from shot to shot should not exceed 1%. The TIC profile is rather explained by modifications in time of the photon-solid interaction as the distribution and relative intensities of analyte ions are slightly different from shot to shot (no modifications were induced in the experimental conditions during the measurement). Certain ions are only detected intermittently. In Figure 3.8 the spectra for two successive laser shots are shown in parallel. These irregularities are the direct consequence of shot-to-shot variations in energy absorption. In most cases the fragmentation pattern of a molecule is manifold and consists of different fragmentation pathways. The quantity of internal energy imparted to the molecules during the LDI process and subsequent collisions with neutrals (neutral pressure, ion neutral ratio) determines the most energetically favourable fragmentation pathways. Modification of the local surface configuration after each laser shot (ablation) is likely to slightly modify the conditions of energy absorption for the subsequent laser shots.

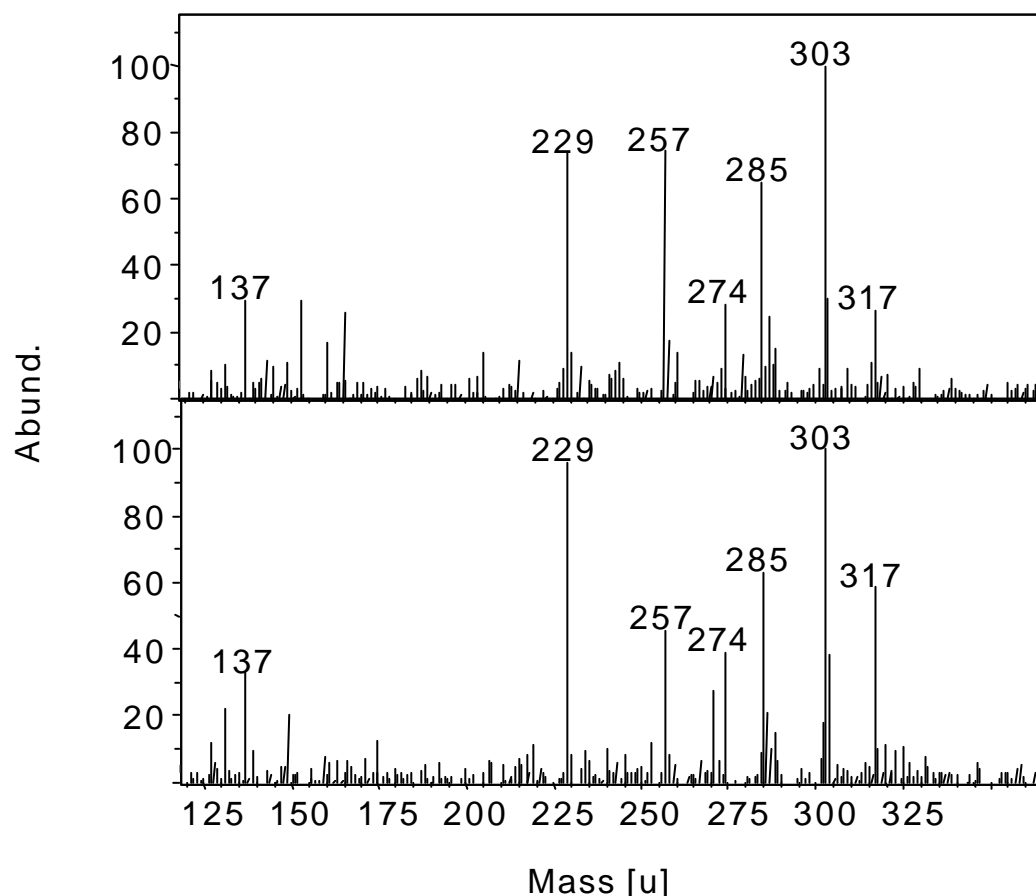


Figure 3.8 *Single ion current (SIC) of morin showing the shot to shot variation of the fragment distribution and relative intensity in LDI-ITMS.*

Chapter 3

We can clearly observe in Figure 3.7 that several laser shots (about five) are necessary before a representative TIC signal is obtained, and a few more (about ten) before this signal presents a steady profile. Several laser shots are clearly necessary to reach a steady state temperature at the surface of the sample. We propose that the delay in appearance of ions is caused by a temperature dependence of the ion production. As the temperature increases, a plasma cloud is formed near the surface of the sample. This idea has been proposed before to explain the formation of sodiated and potassiated species under CO₂ laser desorption/ionisation conditions¹¹⁰. Additional absorption of the UV laser radiation in the plasma cloud in our experiments could increase the ion production by ionising desorbed neutral molecules and by increasing the internal energy of the already existing ions. Temperature equilibrium is eventually reached.

At low laser density the sample depletion is rather slow and several hundreds of shots are necessary to observe a meaningful decrease of the TIC. The camera output does not offer sufficient magnification to accurately monitor the modification of the sample surface during a multiple-shots experiment. However, samples were examined after analysis under high magnification (x400) with an optical microscope and it was not possible to observe any damage on the sample surface after ten shots.

In conclusion, LDI experiments should take into account the delay in ion production and the shot-to-shot variations by oversampling. Scans should be averaged over several shots (typically about 10) to obtain representative mass spectra. In the case of automated-scanning experiments, a minimum amount of shots (between 5 and 10) should be used to reach the TIC steady state.

Paint cross-sections

The complex micro-morphology of paint cross-sections and the limited amounts of analyte represents a particular inconvenience to use multiple laser shots. Sectioned paint samples present a highly heterogeneous set of paint materials. Different chemical compositions are found at different spots on the sample surface, and deeper in the sample. Consequently, the composition of the analyte itself might change as the experiment goes along. In this case, recording spectra by averaging ion signal on several shots (for a fixed location) is problematical although it could contribute to statistically more relevant data. In general ablation volumes should be kept as low as possible to limit sample consumption and safeguard the integrity of the layered structure. On the other hand, if the compound of interest is not situated directly at the surface some etching of the surface layers is permissible.

3.5. TOF-MS versus ITMS: pressure and time-scale

Mass spectra obtained with the two mass analysers will be distinctively different, even for identical compounds measured under similar LDI conditions (Figure 3.9).

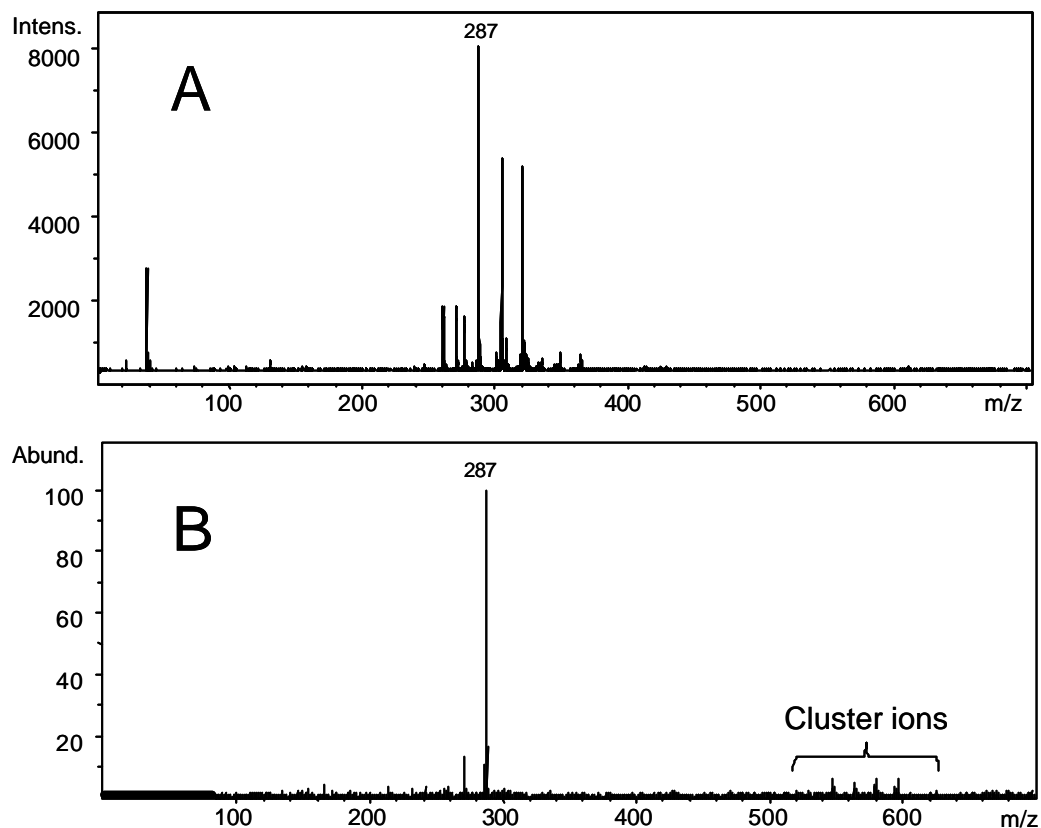


Figure 3.9 LDI of kaempferol at low laser power. The TOF spectrum (A) and the ITMS spectrum (B) that demonstrates the formation of cluster ions.

The two analysers differ in two important aspects. First, the analysers' pressures differ 5 orders of magnitude between both analysers. Secondly, the total analysis time varies between microseconds for the TOF-MS to seconds for the ITMS. These two differences lead to a different appearance of the analyte ions in the different mass spectra.

Pressure is measured at 10^{-3} mbar in the ITMS analyser compared to 10^{-7} mbar in the TOF-MS. High pressure in the analyser of the ITMS will lead to an increased collision rate of the trapped ions with the helium background gas. These collisions can have two effects, they can increase the amount of internal energy of the trapped ions leading to an increased degree of fragmentation. On the other

hand, the increased pressure can lead to the formation of cluster ions. In our experiments we observe that the increased pressure mainly leads to an increased relative amount of clusters in the ITMS under similar LDI conditions.

The period of time between ion formation and detection is significantly different in the TOF-MS and the ITMS experiments. In both cases we believe that difference in time definition of the initially-generated ion packet only plays a marginal role since extraction is delayed and pulsed. Transport time to the detector is estimated to be in the order of a microsecond in the TOF-MS compared to a few microseconds in the low-energy transport system of the ITMS (note that ions produced in the source of the spectrometer still have to be transported to the detector). The total analysis time in the TOF-MS is solely governed by this transport time. In the case of the ITMS, an additional accumulation, equilibration and detection time of ca. 1s is required and determines the total analysis time. During this extended time period, ions in the gas phase are likely to undergo further transformations such as fragmentation through collisions with neutrals and formation of cluster ions, or can be simply lost. This implies that the ion trap will detect the metastable ions formed in the LDI experiment that are not observed in the TOF-MS experiment.

3.6. *Ion collection in the ITMS analyser: LMCO*

Efficiency of the ion collection in the ITMS analyser must be optimised according to the type of analyte and the type of MS experiments. The different parameters that affect the ion collection efficiency are RF potential during ion accumulation, the ion kinetic energy and the pressure in the ion trap.

The trapping RF potential of the ITMS analyser is a periodical wave of 1Mhz. Ions can be accumulate in the ion trap only for a certain amplitude range of the RF signal. In Chapter 2 we have discussed the connection between the frequency and amplitude of the RF field during ion injection and the lower mass limit of trapping. The time domain acceptance of the ITMS can therefore be improved by modification of the low mass cut-off $M_{\text{cut-off}}^{100}$. This is illustrated with the following MALDI-ITMS analysis of polyethylene glycol (PEG) $\text{HO}[\text{CH}_2\text{CH}_2\text{O}]_n\text{H}$, the reference compound used as calibrant in our experiments. The PEG sample from Serva (Heidelberg) presents an average molecular weight of 400 Da. The matrix in the MALDI experiment was 2,5-dihydroxybenzoic acid (DHB) from Sigma, Inc. The polymer sample was prepared by mixing a 1M matrix solution in ethanol with an approximately 10g/L analyte solution in ethanol, yielding a molar ratio matrix/analyte of 1000/1. The analyte and the matrix were deposited as a thin film on a stainless steel probe. The UV laser was focussed to

the surface for LD and analyses were performed with the ITMS. In Figure 3.10 we can observe that MALDI spectra recorded for different values of $M_{\text{cut-off}}$ (70u and 100u) give a different peak distribution for the same PEG sample. This is evidence that trapping efficiency depends on $M_{\text{cut-off}}$. In practice it implies that optimisation of $M_{\text{cut-off}}$ is required, especially when the highest amount of one particular ion is desired to perform multiple-stage MS experiments.

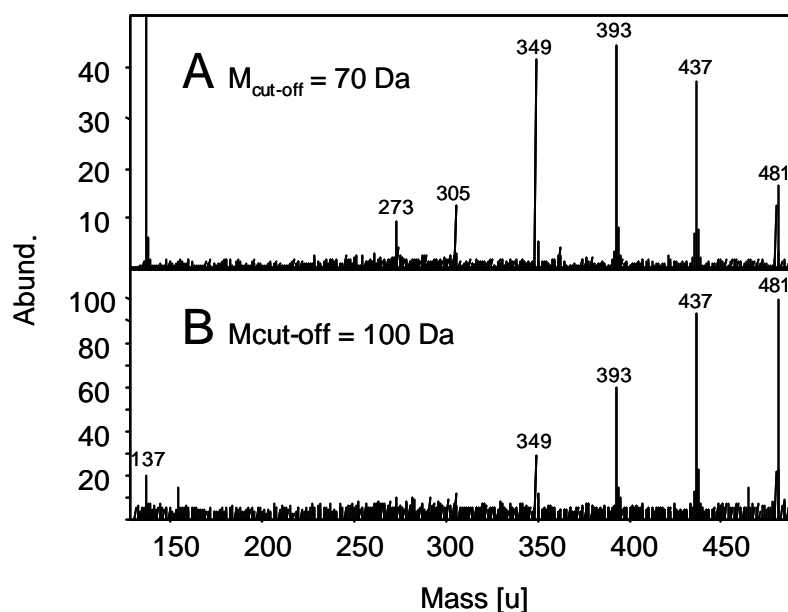


Figure 3.10 Collection efficiency of the ion trap: MALDI-ITMS of polyethylene glycol (PEG), $MW_{av}=400$, measured with $M_{\text{cut-off}}$ of 70 Da (A) and 100 Da (B) showing the dissimilar distribution of the ions collected.

The trapping characteristics also depend on the size of the ion cloud which is governed by the kinetic energy spread upon generation of the ions. Trapping efficiency will vary for the different part of the ion cloud (0 to 100%), and significant amounts of ions will be lost (50%) during collection. Narrow ion clouds (time distribution $<1\mu\text{s}$) are problematic since efficiency of the trapping depends strongly on the value of the RF amplitude when the cloud of ions reaches the entrance of the trap (in the worse case, no ions are trapped). Fortunately, the low energy ion transport system results in a kinetic broadening of the ion cloud. The laser is fixed in synchrony with the oscillation of the RF signal and it has been shown that the exact position of the pulse in the RF period does not change the reproducibility of the analysis. This indicates that the ion cloud must be wider (in time) than a number of RF cycles.

Finally, we should mention that correct trapping is only obtained for a limited ion population in the trap. For high quantities of ions (as discussed in previous paragraph) it is recommended to limit the ion introduction time, i.e. the

time period during which ions are allowed to enter the trap. This is achieved by applying a block voltage to the ion introduction lens. An excessive ion population in the trap induces a space-charge effect that modifies the trapping potential and results in a deterioration of performance of the ion trap.

3.7. CID experiments with the ITMS analyser

Ions trapped in the ITMS cell can be investigated in multiple-stage MS experiments (MS^n). Manipulation of the ions in the trap involves successive operations in time (isolation, excitation, detection) that can be modified in order to optimise the structural clues for molecular elucidation. In the illustrative MS/MS analysis presented here, molecular ions of the flavonoid compound kaempferol were investigated in a non-spatially resolved experiment. The laser was tuned at or slightly above the desorption-ionisation threshold where a continuous signal for the intact molecular ion is recorded (Figure 3.11.A).

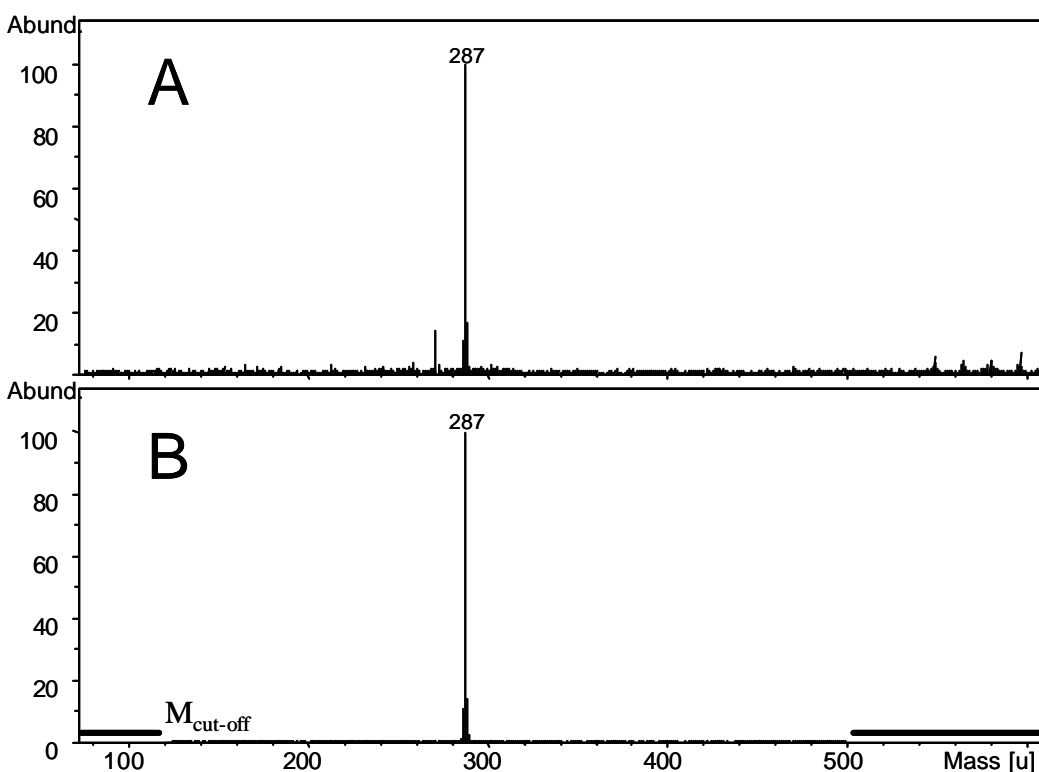


Figure 3.11 LDI-ITMS of kaempferol at the laser threshold: MS analysis (A) isolation of the pseudo-molecular ion m/z 287 at $M_{\text{cut-off}} = 125$ Da (B) demonstrating a clear increase of the signal to noise ratio.

When the sample is in excess the laser power density can be further increased in order to enlarge the precursor ions population. Slightly higher irradiance promotes the production of intact parent ions without excessive increase of the fragmentation. A $M_{\text{cut-off}}$ of 75 Da was chosen to obtain efficient trapping in the mass range of kaempferol (m/z 286). Figure 3.11.B shows the isolation step of the molecular ions. Isolation spectra are habitually recorded prior to CID experiments in order to optimise the population of the precursor ions. In this mode, all ions except the molecular ion of kaempferol are expelled from the trap. In practice, ions isolated in the trap are typically selected on a mass interval with a Gaussian distribution of $\Delta(m/z) = 10$ Da. Therefore, after isolation the spectrum still shows the isotopic distribution of the radical cation and protonated molecular ion of kaempferol on the interval [286-289]: $[M^{\cdot+}]$ and $[M+H]^+$ and their respective isotopes. After isolation a new $M_{\text{cut-off}}$ can be selected that best matches the next MS operation (for the purpose of this example $M_{\text{cut-off}} = 125u$). This MS/MS cut-off mass and the selected ion mass determine the RF characteristics (frequency, amplitude) of the excitation pulse used for CID. The S/N ratio is generally significantly increased after isolation. The transmission of the ITMS during isolation is theoretically integral, i.e. all ions are retained for subsequent manipulation which means an identical absolute intensity of the signal before and after isolation.

All MS/MS experiments in this thesis were performed with isolation of the precursor ions prior to fragmentation. This operation greatly simplifies the interpretation of the spectra since the relation between parent and daughter ions is unequivocal. However, in a CID experiment it would be fully possible in theory to fragment one or several specific ions without proceeding to a prior isolation.

The isolated protonated molecular ion of kaempferol (m/z 287) was fragmented using collisional induced dissociation (CID) in the trap cell. Fragmentation in the trap is obtained by resonantly accelerating the ions to induce multiple low-energy collisions with the surrounding helium gas. When the resonance excitation voltage is too small no fragmentation takes place, and the MS/MS spectrum is identical to the MS spectrum. With increasing excitation-voltage fragmentation occurs, first marginally, i.e. protonated molecular ions are still dominant, and then prevalently, i.e. protonated molecular ions are not observed anymore. The total amount of internal energy imparted during CID determines which fragmentation pathways will be taken. The composition of MS/MS spectra is therefore depending on the intensity of the controlled collisional-activation. If the excitation is too small, collisions fail to produce sufficient diagnostic fragment ions. Conversely, an excessive excitation hinders the formation of diagnostic fragment ions and the MS/MS spectrum is useless. Correct CID intensity must be sought for each particular compound (see section 4.5.4). As

for single MS experiments, exact reproducibility of the MS/MS sequence of events is not expected. Distribution and relative intensities of fragment ions slightly vary from shot to shot and it is wise to average the spectrum over several shots.

The MS/MS experiment can be reiterated several times to investigate the fragmentation of the molecular ion. Fragment ions are then further investigated in an additional CID experiment (MS^n). (Section 6.3.3 discusses an MS^4 experiment with indigo). MS/MS can be used for structural studies of organic pigments in the presence of a complex matrix or medium. To optimise the structural information acquired in MS/MS two approaches are possible. In the first one, the CID amplitude is optimised to obtain a good balance in the MS/MS spectrum composition between molecular ions and diagnostic fragment relative intensities. In a second approach, a complementary set of spectra at different CID amplitudes can be produced and the sum of this information is used for interpretation. Quantitative determination seems excluded.

3.8. Conclusion

In LDMS analysis, structural information can be optimised by correct preparation of the sample and tuning of the experimental parameters. New probes were designed specifically to accommodate various forms of samples within the two mass spectrometers. Deposition of the sample as a thin film on a metallic support or a TLC plate coated with cellulose provides good ionisation yields. In the case of paint cross-section, great care should be given to obtain surfaces as smooth as possible. Tuning the laser power density near to slightly above the laser desorption and ionisation threshold value offers the best conditions for the formation of intact molecular ions and limited fragmentation. At the same time, low laser power density guarantees smallest deterioration of the sample. Conversely high laser power should be avoided since excessive molecular fragmentation makes the interpretation of the spectra more difficult. Experimental results have shown that optimal desorption and ionisation conditions are obtained in experiments where multiple laser shots are used in close succession. In LDMS experiments performed with the ITMS, ion introduction times and mass cut off must be tuned to optimise the spectral information. Best multi-stage MS experiments are obtained by optimising the density of the ion population of the precursor ions trapped in the cell and then tuning the CID condition to achieve satisfactory fragmentation of the parent ions.

Chapter 4

An LDMS investigation of traditional colouring materials - Part I: Flavonoids *

In this chapter LDMS experiments on flavonoid compounds are reported. Successful LDI and MALDI analyses performed with the ITMS and TOF-MS analysers demonstrate the applicability of LDMS techniques to the analysis of organic yellows. Results are shown on a series of reference flavonoid compounds, plant extracts and lake reconstructions. Multiple-stage mass spectrometry is employed to identify different flavonoid aglycone isomers and investigate flavonoid-O-glycosides. Desorption and ionisation with an UV laser (337nm and 355nm) is a feasible approach for in-situ sampling from a complex surface with a spatial-resolution down to 10 micrometers. Spatially-resolved LDMS results the characterization of flavonoids on single dyed fibres are demonstrated.

* This chapter is based on the publication: Wyplosz, N., Heeren, R.M.A., van Rooij, G. and Boon, J.J.: Analysis of Natural Organic Pigments by Laser Desorption Mass Spectrometry: A Preliminary Study to Spatially Resolved Mass Spectrometry, *Dyes in History and Archaeology* 16/17 (2002), 187-198, Archetype Publications.

4.1. Introduction:

Flavonoids are yellow organic colouring materials traditionally used to prepare artists' pigments and textile dyes^{1, 2, 5, 16, 22, 27, 28, 69, 128}. Their poor lightfastness has been known for a long time and the visible degradation of their colour in museum objects with age is a serious concern for conservation scientists^{31-33, 35, 39}. A great number of publications are available on the occurrence, medicinal importance or structural determination of flavonoids^{129, 130}, and a range of chromatographic and mass spectrometric techniques are routinely used for their analysis^{87, 131-138}. In the field of conservation science, however, only few techniques have been proved successful for the investigation of flavonoid yellows^{23, 32, 37, 46, 51, 59, 67, 76, 77, 79, 139}

Identification of organic pigments in paintings remains particularly problematic since colouring materials are generally present in very small quantities, mixed with a medium and entangled in a complex layered structure. In addition, original colours have often dramatically faded away and pigments are hardly observable anymore. The nature of the flavonoid/substrate/medium systems in easel paintings is still incompletely understood and their complex degradation mechanisms have been hardly addressed at all.

Results presented in the literature concern the study of flavonoid reference compounds^{39, 128}, dyes extracted from fibres³⁷, and paint samples. Chromatography and mass spectrometry provide sufficiently detailed information for positive characterisation of flavonoids and the investigation of their degradation mechanisms^{46, 140}. Unfortunately, analytical procedures used so far necessitate to first dissect the coloured layers, or to extract and derivatize the colouring material. As a result, investigation of museum objects often fails by lack of sufficient amounts of material, and analyses are not possible with embedded paint cross-sections³¹. For this reason, the presence of yellow pigments in paint samples is commonly inferred from circumstantial evidence provided by identification of materials traditionally used as a substrate for the flavonoids.

In this chapter we examine the applicability of LDMS for the identification of flavonoid dyestuffs traditionally used in easel paintings. LDMS investigation is performed with LDI and MALDI on ITMS and TOF-MS analysers. Analysis will focus first on a series of flavonoid aglycones present in plants used to prepare the organic yellow pigments. The molecular structures of these flavonoids are shown in (Figure 4.1). Positive identification of structural isomers is particularly problematic in mass spectrometry since molecules have the same elemental composition hence the same molecular mass. The use of multiple-stage mass

spectrometry (MS^n) performed with the ITMS will be demonstrated in the case of luteolin, kaempferol and fisetin, three flavonoid compounds with the same molecular mass that only differ by the position of one of their four hydroxyl groups (Figure 4.1). This analytical approach will be also applied to the characterization of the aglycone moiety of a flavonoid-O-glycoside as well as a flavonoid lake manufactured in the laboratory after traditional recipes. Spatially-resolved LD is demonstrated with the *in-situ* investigation of dyed textile fibres. This straightforward procedure eliminates the use of extraction and derivatization of the colouring materials prior to fibre analysis.

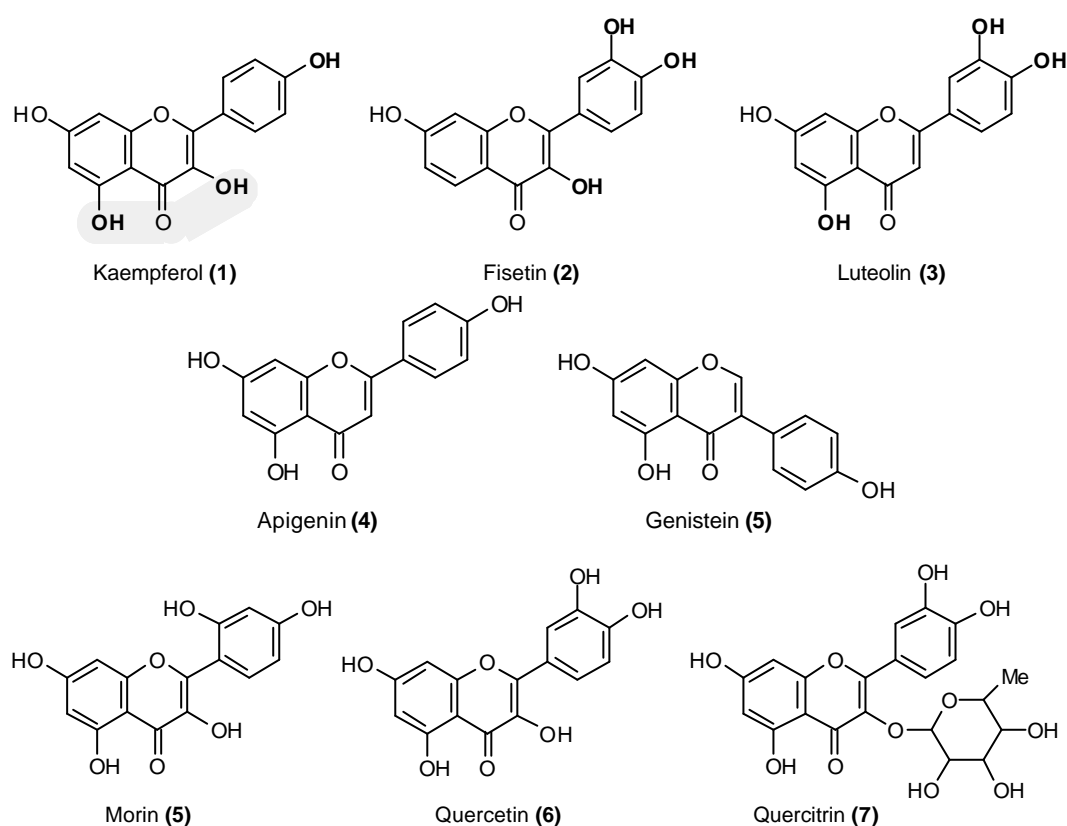


Figure 4.1 Molecular structure of flavonoid compounds studied by LDMS, with their corresponding molecular masses: kaempferol (286 Da), luteolin (286 Da) and fisetin (286 Da); apigenin (270 Da) and genistein (270 Da); morin (302 Da) and quercetin (302 Da); and quercitrin a quercetin rhamnoside (448 Da). Note the different positions of the hydroxyl groups in (1), (2) and (3), and of the B ring in (4) and (5).

4.2. Flavonoid pigments

4.2.1. Materials and practice

Yellow organic colouring materials are known since the antiquity and have been used both as dyes for textiles and pigment for paintings. The principal sources of organic yellows are plants containing colouring materials belonging to the chemical class of flavonoids (from the Latin *flavus*: yellow). Flavonoids are extremely widespread in the vegetable reign and can be extracted from a vast number of plants. Only a few biological sources, however, contain colouring materials that were considered sufficiently light fast for use in the preparation of artists' pigments. Some of the most widespread traditional sources for artists' pigments were: weld (*Reseda luteola* L.), buckthorn berries (of the genus *Rhamnus*), dyer's broom (*Genista tinctoria* L.), young fustic (*Cotinus coggygria* Scop.), old fustic (*Chlorophora tinctoria* L.), and black oak (*Quercus velutina* Lamk.) in use since the end of the 18th century.

Colouring materials present in these plants belong essentially to the three flavonoid groups of flavones, flavonols and isoflavones. Figure 4.2 shows the basic molecular structures and labelling system of these flavonoid groups. Molecular structures are all based on a phenyl group (ring marked B) attached to a 4H-1-benzopyran-4-one (rings marked A and C). When the phenyl group is bound in position 2 the flavonoid belongs to the group of *flavone*, and when it is bound in position 3 the flavonoid belongs to the group of *isoflavone*. When the C-ring of a flavone molecule is oxygenated in position 3, it belongs then to the group of *flavonols*. Additional oxygenation of the A- and B-rings does not alter the flavonoid type nomenclature.

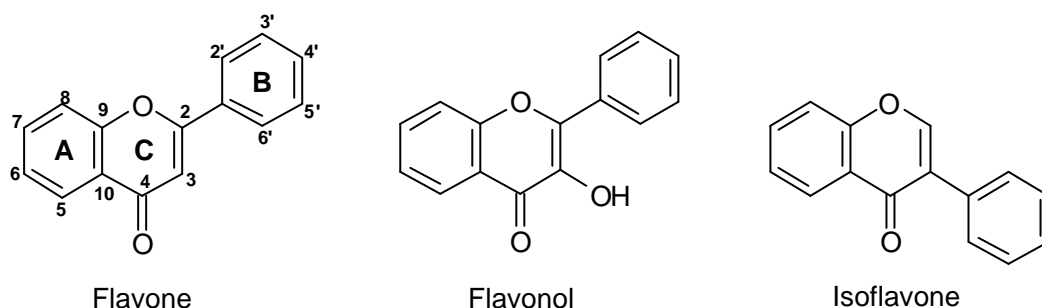


Figure 4.2 Basic molecular structure and nomenclature of flavones, flavonols and isoflavones.

In the plant sources considered in this study, flavonoid molecules possess various types of substitutions, notably hydroxylation, methoxylation, and glycosylation. The type and position of the substituents confer specific chromophoric properties to the molecule. Flavonoids, in which one or more of the hydroxyl groups are bound to one or more sugars are called *flavonoid-O-glycosides*, whereas flavonoids without attached sugars are called *aglycones*. Plant extracts used in the production of yellow lakes may contain flavonoids of different types - either in the form of aglycones or in the form of glycosides - and in different concentrations. The presence of each of these various compounds influences the colour characteristics of the pigment. If the lake manufacturing process involves hydrolysis of the plant extract, glycosidic bonds are broken in the process, which yields the corresponding aglycone moiety*.

4.2.2. Molecular analysis of flavonoids and flavonoid pigments

Flavonoids constitute a considerable group of naturally occurring phenols with more than 5000 different structures already identified. Flavonoids receive increasing interest due to their medicinal properties. They possess antioxidant activity and exhibit anti-tumour, antibacterial, and antiviral effects. Identification of flavonoids and their glycosides are a growing topic in analytical chemistry and the literature on the subject is quite extensive. Instrumental analysis of flavonoids is quite wide-ranging and includes notably chromatographic methods such as HPLC or GC, spectroscopic methods such as UV, IR, NMR and MS and the combination of them, for instance HPLC/UV, HPLC/MS, MS/MS, etc.

In the last decade, investigation of flavonoids with mass spectrometric techniques has received considerable attention since it provides detailed structural information with only micrograms amounts of samples. Ionisation techniques used in mass spectrometry of colouring materials have been reviewed by Van Breemen⁸⁴. Gas-phase ionisation techniques such as electron impact (EI) and chemical ionisation (CI) exclusively used until the 1980's are still very common today (for instance with APCI). Various desorption ionisation and ion evaporation methods were introduced later and eliminated the need for derivatization: field desorption, plasma desorption, fast atom bombardment (FAB) or liquid secondary ion mass spectrometry (liquid SIMS), thermospray, ion spray, electrospray (ESI) and laser desorption (LD).

Literature concerning the investigation of flavonoid compounds in Conservation Science is nevertheless particularly scarce. Analyses of flavonoid

* In the case of dyed fibres, analytical procedures involving the use of alkali to extract the colouring material can break the glycosidic bond and yield the corresponding aglycone.

Chapter 4

fabric dyes were reported with UV-VIS spectroscopy¹⁴¹ and non-destructive analyses of yellow lake have been presented using photo-luminescence spectrometry (spectro-fluorometry)^{128, 142}. Deterioration of flavonoids in laboratory models has been investigated with colour measurements³⁹. Mass spectrometry (DTMS³⁷, ESI and APCI-ITMS⁴⁶), and photodiode array HPLC^{37, 76} which combines the advantage of simultaneous separation and quantification have shown very promising results. Unfortunately, none of these techniques enable the structural analysis of flavonoids directly from the surface of the sample. The objective of this chapter is therefore to explore LDMS for the investigation of flavonoids directly from complex surfaces such as thin films and dyed fibres.

4.3. Experimental

4.3.1. Instrumental set-ups

Analyses were performed at two different wavelengths in the ultraviolet range: at 355 nm (Q-switched Nd:YAG laser) on the ITMS and at 337 nm (N₂ laser) on the TOF-MS. Desorption and ionisation was performed directly (LDI) or with the assistance of a matrix (MALDI). Measurements were performed either in positive or in negative mode. Note that LDMS investigations were evenly divided between the TOF-MS and the ITMS analysers, and unless otherwise stated – notably in MSⁿ experiments – the choice of the analyser was determined by the availability of the instrumentation. For a detailed description of both instruments we refer the reader to Chapter 2.

Comparative measurements were also performed with Direct Temperature Mass Spectrometry (DTMS) on a sector instrument JEOL SX102-102A (BEBE) to obtain better insight into the effects of ionisation and fragmentation processes. Samples are deposited at the tip of a direct insertion probe fitted with a resistively heatable platinum/rhodium (9/1) filament (100 µm diameter). The probe filament was temperature programmed to heat at a rate of 0.5 A min⁻¹ (approximately 8°C s⁻¹) to a final temperature of about 800°C. Ions were generated by electron impact ionisation (EI).

4.3.2. Flavonoid samples

Reference flavonoid compounds include apigenin, genistein, fisetin, kaempferol, luteolin, morin, quercetin and its glycoside quercitrin. Their molecular structure is shown in Figure 4.1. All these flavonoid compounds are found in plants traditionally used to prepare organic yellow pigments²⁸.

- Kaempferol, found in the weld plant (*Reseda luteola* L.) in the form of kaempferol-3-glucosid-7-rhamnosid, and in the common buckthorn (*Rhamnus catharticus* L.) in the form of kaempferol-7-methylether (rhamnocitrin).
- Fisetin, a major compound of the young fustic (*Cotinus coggygia* Scop.).
- Luteolin, a major compound of the weld plant (*Reseda luteola* L.) and found as glycoside in the dyer's broom (*Genista tinctoria* L.).
- Apigenin, a major compound of the weld plant (*Reseda luteola* L.).
- Genistein, found in the dyer's broom (*Genista tinctoria* L.).
- Morin, a major compound of the old fustic (*Chlorophora tinctoria* L.).
- Quercetin and its glycoside quercitrin, two major compounds of the black oak (*Quercus velutina* Lamk.).

Apigenin and luteolin are flavones, genistein is an iso-flavone, and fisetin, kaempferol, morin, quercetin and quercitrin belong to the flavonols (hydroxyl group in position 3). Reference samples were obtained from Sigma and Fluka and were used without further purification.

Yellow lakes studied in this chapter were manufactured by A. Wallert (Rijksmuseum, Amsterdam) according to traditional recipes found in documentary sources. Colouring material is extracted with an alkaline aqueous solution of K_2CO_3 from the appropriate dried parts of the plant (traditionally the alkaline solution was a lye made from wood ash or stale urine). Aluminium hydrate in the form of alum ($AlK(SO_4)_2 \cdot 12H_2O$) is added to induce the formation of an $Al(OH)_3$ substrate that precipitates with the colouring material fixed onto it. Aluminium forms a complex with the colouring materials. In the process of textile dyeing, the coordination of the complex anchors the colouring material to the fabric. $Al(OH)_3$ formed in excess in the process might also serve as substrate by absorption of colouring materials. The precipitate is eventually washed and dried leading to the solid coloured pigment.

Using traditional recipes, alum-mordanted wool was dyed with quercetin at the National Museum of Scotland, and the samples were kindly supplied by Ester Ferreira. At first, mordanted wool was prepared with alum (potassium aluminium sulphate $KAl(SO_4)_2$) and potassium hydrogen tartrate. The wool was then died

Chapter 4

with a 1 μ M bath of quercetin. The experimental methods have been described more fully in the literature^{79, 143}.

4.3.3. Sample preparation

Samples in Laser Desorption and Ionisation (LDI) experiments were deposited as a thin or thick film on a stainless steel probe. For thin films, a few micrograms of the sample were mixed with ethanol (the molarity does not matter here). Generally, the analyte powder incompletely dissolved and the suspension was homogenised using a vortex mixer. About 5 microliters of this solution or suspension were deposited onto the probe with a pipette and dried in vacuum. Evaporation of the ethanol vehicle leaves the particle adsorbed at the surface of the probe. For thick films a few micrograms of pigment were deposited directly on the surface. A few microliters of ethanol were deposited to disperse and adsorb the sample at the surface of the probe. The MALDI experiments were exclusively performed using 2,5-dihydroxybenzoic acid (DHB) as a matrix. DHB serves as a proton donor and produces $[M+H]^+$ ions of the analyte. DHB itself produces ions in the low molecular mass range that can be easily identified. A thin layer of the sample is first absorbed on the surface of the probe as for LDI experiments. Subsequently, a thin matrix layer is deposited on top of the sample. This approach was chosen to mimic as much as possible the way in which a matrix would be applied when analysing a paint cross-section.

Flavonoids on wool fibres were analysed *in-situ*, the sample fibres being clamped at their two ends in the probe cavity. Individual fibres can be fastened in close contact with the metallic substrate provided that the two ends are correctly secured. In the case of a bunch of fibres all the threads cannot possibly be positioned in contact with the substrate. Fibres are therefore not all in the same plane, and some might even be loose at one end. When strands of millimetric thickness are studied, the surface of the sample bulges out of the sample cavity. A single fibre of ca 10-30 micrometers in thickness can be easily localised under microscopic magnification and positioned in the laser beam thanks to the XY manipulation system of the probe. The diameter of the laser beam corresponds approximately to the thickness of the individual fibres.

4.3.4. Mass calibration

A mass calibration for TOF-MS measurements was realised before each series of measurements to obtain optimal mass accuracy. Two samples of

polyethylene glycol (PEG) with a molecular weight distribution of averaging m/z 400 and 1000 respectively served as calibrant. MALDI measurements were performed with a mixture of a 1mM ethanol solution of PEG and a 1M ethanol solution of DHB. The mixture was deposited on the surface of the probe and the ethanol vehicle was left to evaporate. Calibration was realised with peaks from the DHB and the PEG at regular intervals in the m/z range [0-1500].

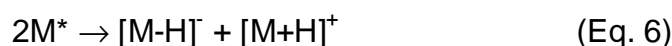
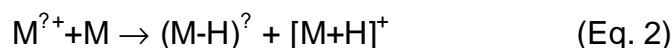


Table 4.1 *Activation and ionisation mechanisms.*

4.4. *Characterization of flavonoid aglycones with LDMS*

A first series of experiments was conducted to assess the potential of LDMS in the investigation of flavonoid aglycones. Samples include kaempferol, fisetin, luteolin, apigenin, genistein, morin and quercetin. Analytes were analysed in LDI and MALDI experiments with the two mass analysers – TOF-MS and ITMS – and for different laser power density ranges. Multiple-stage mass spectrometry (MS^n) was performed on the ITMS to provide additional structural information. DTMS analyses with the sector instrument in MS and MS/MS mode were performed additionally to confirm the results obtained with LDMS.

Particular attention is given to the mass spectral information as a function of the flavonoid group since previous MS studies have shown that aglycones within a same group have similar fragmentation patterns^{131, 132}. Flavonoid aglycones analysed include two flavones (apigenin and luteolin), four flavonols (fisetin, kaempferol, morin, and quercetin) and one isoflavone (genistein). The possibility to distinguish between flavonoid structural isomers (molecule of

	Flavonols				Isoflavone			Flavones		
	Quercetin	Morin	Kaempferol	Fisetin	Genistein	Luteolin	Apigenin			
302	302	286	286	286	270	-	-	M ⁺		
303	303	287	287	287	271	287	271	[M+H] ⁺		
321	321	305	305	305	289	305	289	[M+H ₂ O+H] ⁺		
325	325	309	309	309	293	309	293	[M+Na] ⁺		
341	341	325	325	325	-	325	309	[M+K] ⁺		
657	657	611	611	611	579	617	522	Dimeric clusters		
968	966	935	902	887		919	799	Trimeric clusters		
-	-	-	286			286	-	M ⁺		
303	303	287	287			287	271	[M+H] ⁺		
-	-	305	305		data non available	305	289	[M+H ₂ O+H] ⁺		
325	325	309	309		available	309	293	[M+Na] ⁺		
341	341	325	-			-	309	[M+K] ⁺		
656	-	-	-			-	-	Dimeric clusters		
-	-	941	-			903	-	Trimeric clusters		

Table 4.2 *Principal characteristic ions of investigated flavonoids in LDI and MALDI-TOF-MS.*

identical mass but different structures) was researched, as this information would make it possible to trace the biological origin of a natural organic yellow pigment. Flavonoid aglycones under investigation here include isomers belonging either to the same flavonoid group or to different groups: kaempferol, fisetin and luteolin at m/z 286; apigenin and genistein at m/z 270, morin and quercetin at m/z 302 (Figure 4.1).

4.4.1 Laser Desorption and Ionisation (LDI)

Samples were all prepared and measured under the same experimental conditions. Photoionisation spectra were obtained for each sample working at low laser power density. High intensity of the signal gives evidence for good response of the flavonoid at both 337nm (nitrogen laser in TOF-MS experiments) and 355nm (Nd:YAG laser in ITMS experiments). This is explained by the highly conjugated structure of the flavonoid compounds and their strong absorption in the UV range (one of their biological functions). LDMS spectra obtained for the different flavonoids present many similarities (Table 4.1). Kaempferol is presented as a representative case.

LDI-TOF-MS

A typical photoionisation spectrum of kaempferol obtained with LDI-TOF-MS is shown in Figure 4.3.A. Three different regions can be distinguished, which correspond to different ionisation mechanisms. A series of peaks in the range of the molecular mass (m/z 286 and above) represent the bulk of the signal observed in this spectrum. In the lower mass range [m/z 0-286] a few fragment ions are observed at m/z 143, 165, 229 and 271 as well as sodium and potassium ions. Only few ions with very low abundances corresponding to dimeric species are observed in the mass region from m/z 600-650. Such a spectral distribution – with prevalent detection of intact-molecules – is evidence for a soft ionisation process. In the mass spectrum, we can identify different ionisation processes.

In the range of the molecular mass, the radical cation M^{2+} is observed at m/z 286 with only a negligible abundance. Dominant peaks at m/z 287, 309 and 325 are assigned to the protonated molecule $[M+H]^+$ at m/z 287, the sodiated molecule $[M+Na]^+$ and a water adduct $[M+H+H_2O]^+$. The simultaneous formation of the radical cation, protonated and sodiated ions indicates that different ionisation processes take place at the same time during LDI.

The negligible proportion of ions detected at m/z 286 corresponds to direct ionisation to the radical cation M^{2+} . Energy of one single photon (3,68eV) emitted

by the nitrogen laser at 337nm is not sufficient to ionise the flavonoid compounds* . The radical cation must result from a multi-photon ionisation (MPI) process (Table 4.1).

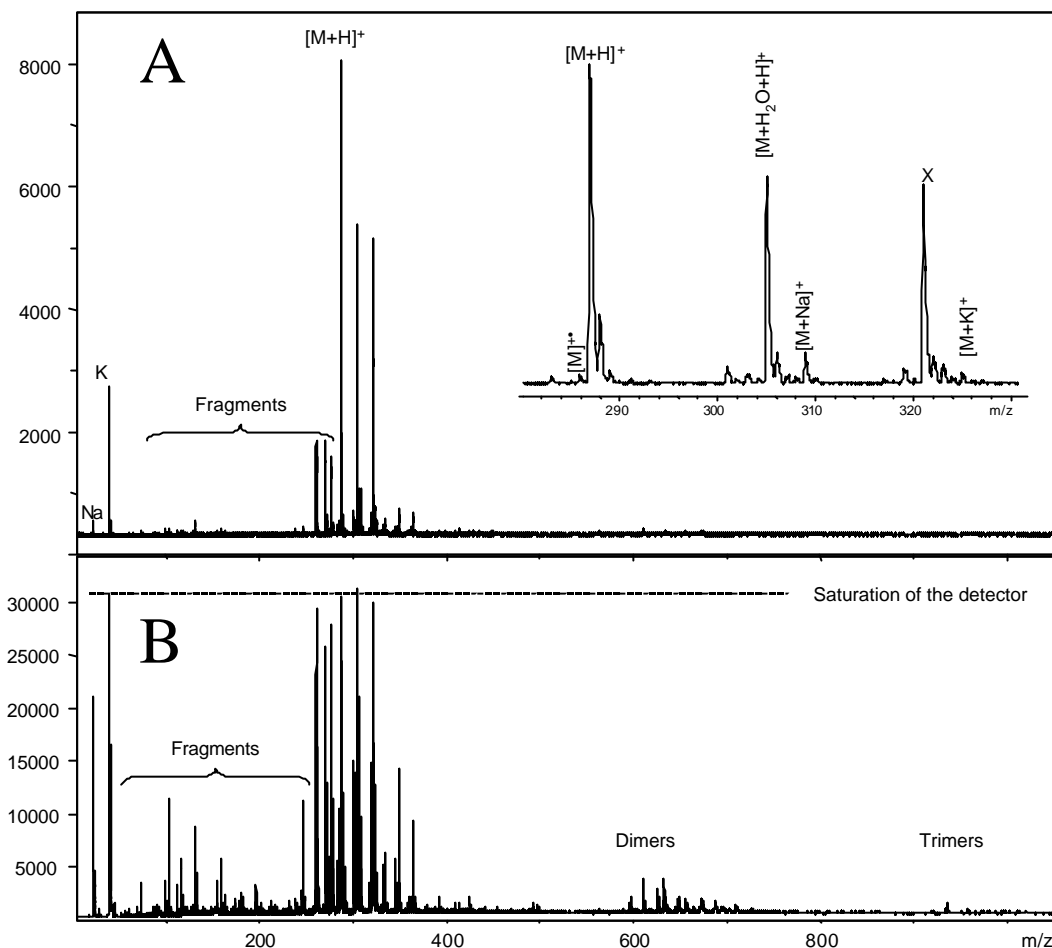


Figure 4.3 Direct LDI-TOFMS of pure kaempferol with a UV laser emitting at 337nm: just above the desorption threshold (A) and with a higher laser power (B). In both cases, 150 shots were accumulated and averaged to improve the signal to noise ratio. Note that at high laser power the detector reaches saturation around 30000u.

To explain the formation of protonated molecules, we propose that kaempferol acts as its own proton donor^{111, 119}. The conjugated structure of the flavonoid molecule combined with the various hydroxyl substituents makes the molecule a good proton donor. Supportive evidence is provided by the negative ion spectrum, where intense peaks at m/z 285 (base peak) and 286 (50% relative

* The ionisation potential (IP) of kaempferol in the gas phase is estimated - through comparison with molecules of similar structures to be in the order of 7-8eV. Photon ionization at UV wavelength of 337nm (3,68eV) and 355nm (3,49eV) requires therefore at least two photons. In the condensed phase, it is more likely that LDI of kaempferol requires more than two photons.

intensity) are assigned to the radical anion M^{2-} and to the deprotonated molecule $[M-H]^-$. We speculate that the formation of $[M-H]^-$ results from electron capture from the intermediate species $(M-H)^?$. The great simplicity of the negative ion spectrum suggests that this mode could be preferred for rapid identification.

Cationization by alkali ions is common in LDMS experiments and formation of sodium and potassium adducts is explained by the presence of sodium and potassium in the sample. This is supported by intense peaks at m/z 23 and 39 assigned to Na^+ and K^+ . Formation of sodium and potassium adducts most probably corresponds to alkali ion attachment to neutrals in the ablation region, or desorption of pre-formed salts from the condensed-phase.

At higher laser power densities (Figure 4.3.B) the desorption and ionisation process becomes more energetic and new features can be observed in the spectra. Ion intensities increase significantly and the general profile of the spectra becomes more complicated as numerous additional ions are detected.

Groups of ions are observed in the mass spectral region where dimers and trimers are expected. All ions assigned in these regions have a sodium or potassium ion incorporated. We assume that this condition is necessary for the stability of the dimeric species. Peaks at m/z 595 and 611 are assigned to the sodiated and potassiated adduct of the dimer $[2M+Na]^+$ and $[2M+K]^+$. A majority of the additional peaks can be assigned to species containing more than one alkali ion. For instance a peak at m/z 617 is assigned to the ions $[(M-H)Na(M)]Na^+$. This complex dimeric species is the result of sodium ion attachment on a salt molecule composed of deprotonated molecules and a sodium ion. The relative abundance of these ions significantly increases when higher laser power densities are employed.

Additional dimeric species with multiple alkali atoms are assigned at m/z 633 to $[(M-H)K(M)]Na^+$, at m/z 649 to $[(M-H)K(M)]K^+$, at m/z 655 to $[(M-H)Na(M-H)K]Na^+$, at m/z 671 to $[(M-H)K(M-H)K]Na^+$. With high laser power density, the same phenomenon is observed in the mass range corresponding to trimeric species. Ions are assigned at m/z 903 to $[(M-H)Na(M)(M)]Na^+$, at m/z 919 to $[(M-H)K(M)(M)]Na^+$, at m/z 935 to $[(M-H)K(M)(M)]K^+$, at m/z 957 to $[(M-H)K(M-H)K(M)]Na^+$.

We propose that formation of such ions is the result of laser-solid interaction in the condensed-phase during LDMS analysis with laser shots in close succession (typically 2Hz in this series of TOF-MS experiments). Formation of these ions is explained by pre-formation in the ablation region of excited species $[M-H]^?$ followed by subsequent dimerisation and alkali attachment.

Identical formation of dimeric and trimeric species with multiple alkali ions was also observed for the two isomers of kaempferol, i.e. luteolin and fisetin, as well as for the other flavonoid species.

LDI-ITMS

Kaempferol was deposited on the probe in an identical fashion as for TOF-MS experiments and analysed with the ITMS slightly above the desorption ionisation threshold. Figure 4.4.A demonstrates that the pure reference compound is successfully desorbed and ionised with a Nd:YAG laser operating at 355nm yielding the same protonated molecule as in the LDI-TOF-MS spectra. In the threshold spectrum, a strong preponderance of protonated molecules, negligible radical cation and fragment ions is evidence for a soft desorption and ionisation mechanism in good agreement with the LDI-TOF-MS results. Characteristic fragment ions (not visible in Figure 4.4.A), are detected at m/z 121, 153, 165, 213, 259 and 271 with a relative abundance <1%.

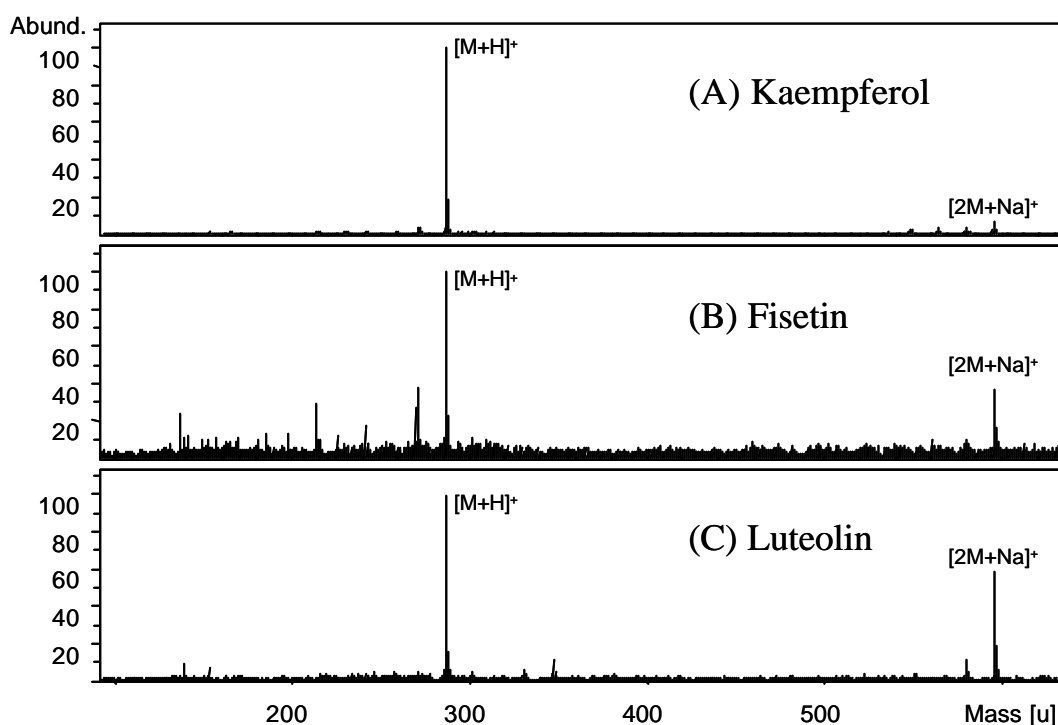


Figure 4.4 LDI-ITMS of kaempferol (A), fisetin (B) and luteolin (C).

In the higher m/z range, the sodiated dimer $[2M+Na]^+$ is detected at m/z 595. This further supports the hypothesis of Na^+ ion incorporation in the clusters. Additional ions at m/z 580, 564 and 548 are presently unidentified. The stability of the sodiated dimer was demonstrated in an MS/MS experiment where fragmentation of the dimeric species (m/z 595) yielded fragment ions assigned to the loss of one and two carbonyls.

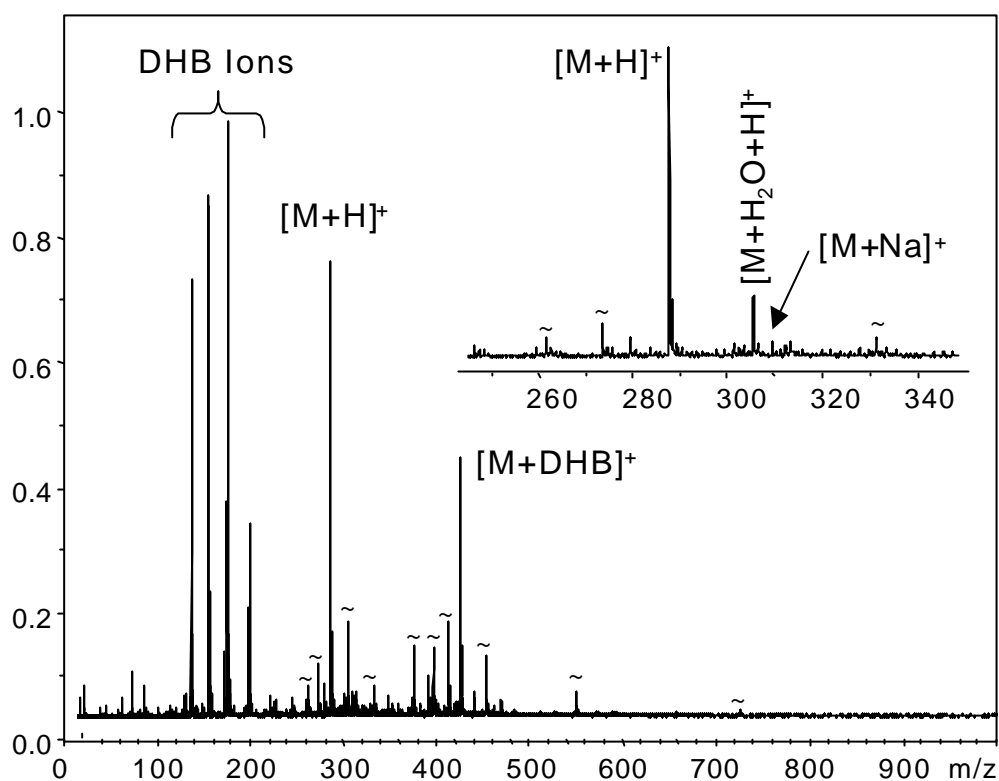


Figure 4.5 MALDI-TOF of pure Kaempferol in a 2,5-DHB matrix. 150 shots were accumulated to obtain this spectrum at similar laser power densities used to obtain Figure 4.4. The peaks marked with “~” are matrix peaks that were also found in the blank matrix experiments.

In conclusion, LDI-ITMS and LDI-TOF-MS experiments performed at low laser power density provide similar structural information. Mass spectra display essentially protonated molecular ions $[M+H]^+$ with little additional diagnostic fragment ions. As a result, LDI spectra do not provide sufficient structural information to positively distinguish between different structural isomers. In order to increase the structural information in LDI experiments, the MS/MS capabilities of the ITMS were therefore employed (Section 4.5). For this purpose, a series of additional MS experiments were first performed in order to select optimal LDI experimental conditions (pressure, laser power density, etc) to optimise the production of precursor $[M+H]^+$ ions for MS/MS experiments.

4.4.2 Matrix Assisted Laser Desorption Ionisation (MALDI)

MALDI-TOF-MS and MALDI-ITMS experiments – with DHB as a matrix – were conducted with the same series of flavonoid samples and results were compared with LDI data. A representative MALDI-TOF-MS spectrum at low

laser power density, illustrated with kaempferol (Figure 4.5), shows the flavonoid aglycone to be almost exclusively detected as the protonated molecule. Similar to the LDI experiments both water and sodium adducts are found (Table 4.1). An abundance of matrix-related peaks is detected that can be readily assigned through comparison with a matrix blank experiment. In contrast to the LDI experiments, oligomeric clusters are not observed. This supports our earlier assumption that these species are formed by laser-solid interaction in multiple shot analyses. Absorption of the photon energy by the DHB matrix prevents these phenomena. In MALDI-ITMS, the soft nature of the MALDI process is confirmed since

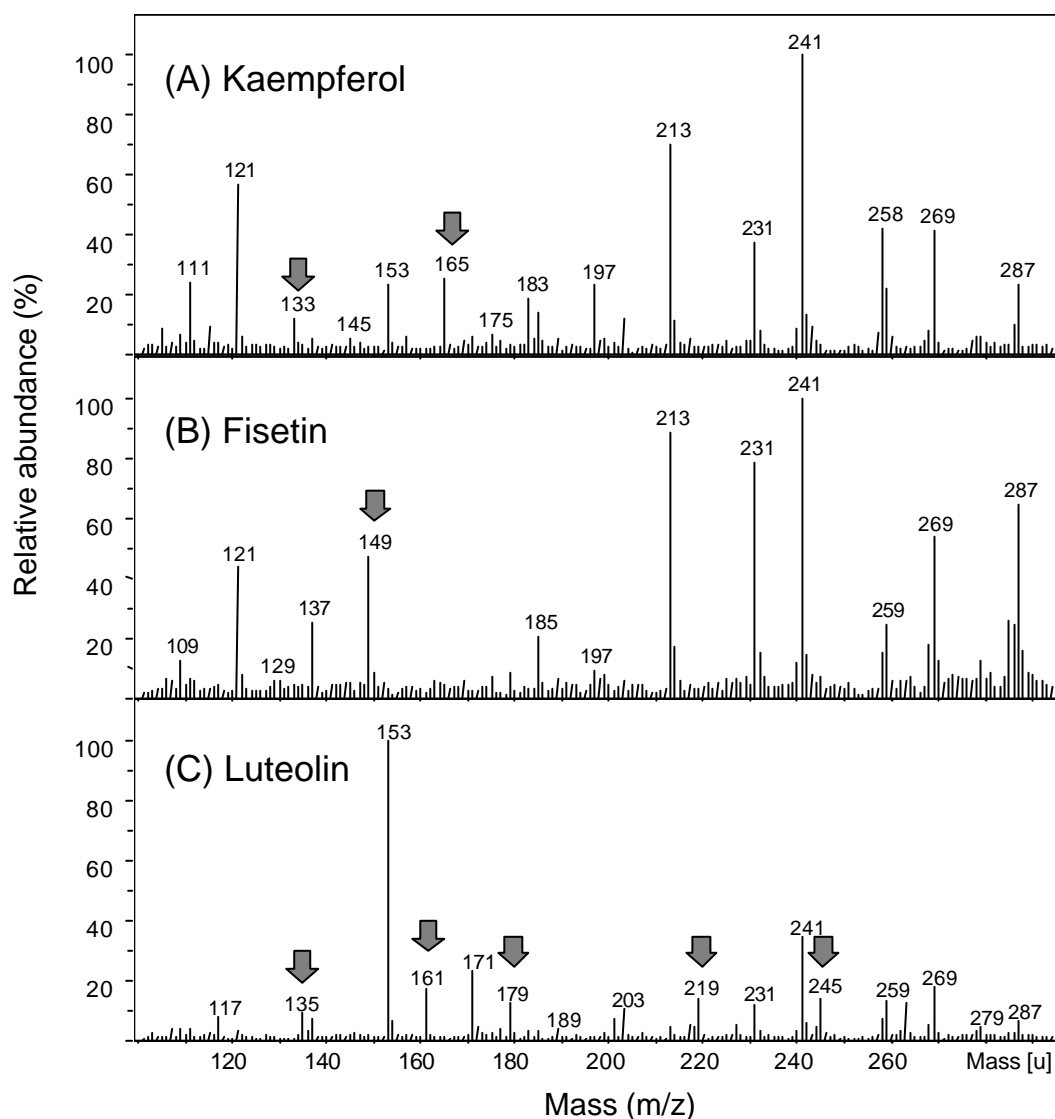


Figure 4.6 *Low-energy CID spectra of the protonated molecular ion of the three structural isomers kaempferol, luteolin and fisetin in an MS/MS experiment with the ITMS. Diagnostic fragment ions marked with an arrow make it possible to distinguish the three isomers.*

kaempferol shows up exclusively as protonated and sodiated molecular ions, whereas fragment ions are almost totally absent. The matrix (DHB) is essentially observed by a peak at m/z 137, whereas in MALDI-TOF-MS the distribution of matrix ions is much broader.

4.5. Structural analysis of flavonoid aglycones with multiple-stage LDI-ITMS

LDMS data presented above are not informative enough to conclusively differentiate flavonoid of the same elemental composition in samples with an unknown composition. The isolation and dissociation capabilities of the ITMS were therefore employed for structural examination of flavonoid isomers. A standard multiple-stage mass spectrometric strategy described in Chapter 2, involving sequential ionisation, purification, dissociation and product ion detection, was employed in these LDI-ITMS experiments. Tuning the laser power density slightly above the desorption threshold allows for minimal internal energy deposition in the analyte molecules and limited sample consumption. Multiple-stage DTMS experiments with a sector instrument were additionally performed to better understand the formation of ions in LDMS experiments.

4.5.1 Multiple-stage LDI-ITMS of kaempferol

Protonated molecules of kaempferol (m/z 287) were isolated in the ITMS cell and fragmented using collisional induced dissociation (CID). Spectra of the isolated species were recorded to confirm that the parent ion was correctly isolated. Selection of the ion in the trap was achieved within a standard range of $\Delta m/z=10\text{Da}$. The base peak after isolation is the protonated molecule, but a minor contribution of the radical cation cannot be avoided*.

Figure 4.6.A shows the MS/MS spectrum of kaempferol at low energy CID averaged over several laser shots with optimised conditions (resonance excitation voltage and low mass cut-off). Results obtained at low-energy CID are found to be in good agreement with fragmentation of the molecular ion obtained by FAB tandem mass spectrometry reported by Ma *et al.*¹³⁵.

* The isolation capabilities of the ITMS in this experiment have a mass range of approximately 10Da, which means that the protonated molecule is not isolated from the radical cation. In the CID experiment only the protonated molecules at m/z 287 are excited and fragmented however.

Fragment ions are labelled according to the nomenclature proposed by these authors (Figure 4.7). The $^{i,j}A^+$ and $^{i,j}B^+$ labels indicate fragment ions containing intact A and B rings, respectively. The superscripts i and j indicate the position of the C-ring bonds that have been broken. The additional loss of small neutral molecules such as CO from $^{i,j}A^+$ is simply noted $^{0,2}A^+-CO$. For simplicity, the ions formed by the direct loss of radicals or small neutral molecules (e.g. a carbonyl) from the radical cation $[M+H]^+$, are not indicated with special labels.

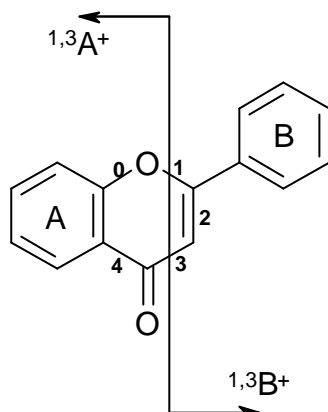


Figure 4.7 Nomenclature (according to Ma): cleavage of the C ring in 1/3 yield $^{1,3}A^+$ (fragment with intact A ring) and $^{1,3}B^+$ (fragment with intact B ring).

The low-energy CID spectrum of $[M+H]^+$ of kaempferol is illustrated in Figure 4.6.A. Main characteristic fragment ions are listed in Table 4.3. Ions corresponding to the (combined) loss of H_2O and CO from the protonated molecule $[M+H]^+$ were assigned to the following fragment ions: $[M+H-H_2O]^+$ at m/z 269, $[M+H-CO]^+$ at m/z 259, $[M+H-H_2O-CO]^+$ at m/z 241, $[M+H-2CO]^+$ at m/z 231 and $[M+H-H_2O-2CO]^+$ at m/z 213.

The presence of an intense peak at m/z 258 can be explained in different ways. This ion can simply be the result of the loss of a carbonyl from radical cations that have not been discarded from the trap during the isolation step. Since the population of radical cations was low in the MS spectrum after isolation, we rather assume that the loss of carbonyl from the protonated molecule is accompanied by the loss of a proton. Experiments were performed with DTMS to support this assumption (see below).

The remaining fragment ions can be explained by two different fragmentations of the C-ring, namely cleavage in 1/3 and cleavage in 0/2. The fragmentation pathway with the 1/3 cleavage corresponds to a retro Diels-Alder fragmentation (Figure 4.8). Fragment ions resulting from this cleavage are identified as $^{1,3}A^+$ at m/z 153, $(^{1,3}B^+-2H)$ at m/z 133 and $(^{1,3}A^+-C_2H_2O)$ at m/z 137. Fragment ions resulting from the 0/2 cleavage are identified as $^{0,2}A^+$ at m/z 165, $(^{0,2}A^+-CO)$ at m/z 137 and $^{0,2}B^+$ at m/z 121. Ma *et al.*¹³⁵ have proposed a fragmentation pathway, involving the protonation at the C-3 and C-2 position

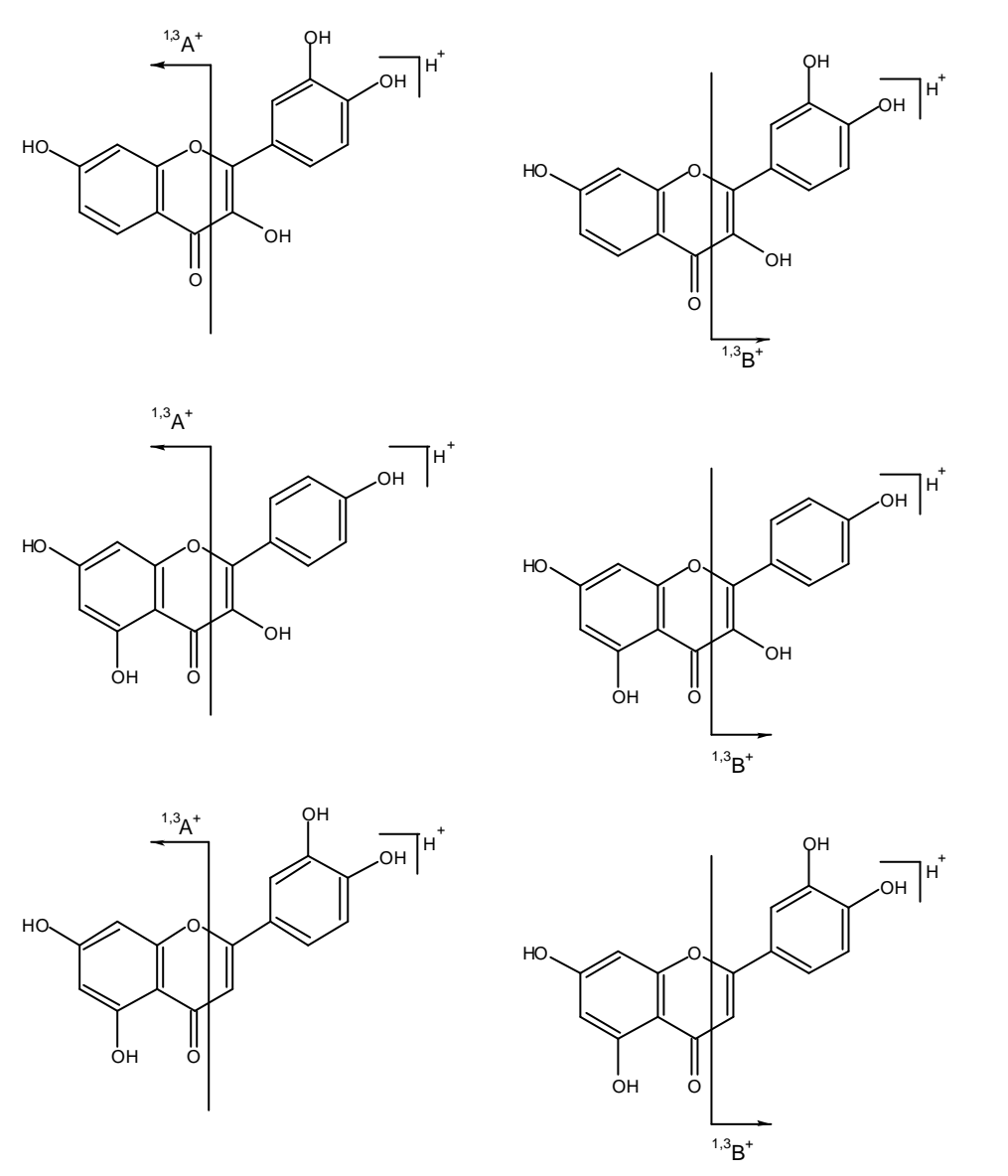


Figure 4.8 Comparison of the retro Diels-Alder fragmentation of protonated fisetin, kaempferol and luteolin showing the similarity and dissimilarity of the resulting $^{1,3}A^+$ and $^{1,3}B^+$ fragment ions.

followed by cleavage of bonds 0 and 2 in the C-ring. This mechanism would be characteristic of flavones.

Advantageously, these diagnostic ions contain intact A and B rings that provide us with information concerning the oxygenation pattern in the parent ions. In this case, structural information is sufficient to positively identify kaempferol.

4.5.2 Multiple-stage LDI-ITMS of luteolin and fisetin

MS/MS experiments were conducted under identical conditions with fisetin and luteolin, two structural isomers of kaempferol (Figure 4.1). Fisetin belongs like kaempferol to the group of flavonols, whereas luteolin is a flavone.

	Kaempferol	Fisetin	Luteolin
$[M+H-H_2O]^+$	269	269	269
$[M+H-CO]^+$	259	259	259
$[M+H-C_2H_2O]^+$		245	245
$[M+H-H_2O-CO]^+$	241	241	241
$[M+H-2CO]^+$	231	231	
$[M+H-C_2H_2O-C_2H_2]^+$			219
$[M+H-H_2O-2CO]^+$	213	213	
$[M-C_2H_2O-C_2H_2O]^+$			203
$^{0,2}A^+$	165	149	
$^{0,2}A^+-CO$	137	121	
$^{1,3}A^+$	153	137	153
$^{1,3}A^+-C_2H_2O$	111		
$^{0,4}B^+$			179
$^{0,4}B^+-H_2O$			161
$^{0,2}B^+$	121	137	137
$^{1,3}B^+$			135
$^{1,3}B^+-2H$	133	149	

Table 4.3 Attribution of the fragment ions in the CID spectra of luteolin, fisetin and kaempferol (labelling according to the nomenclature proposed by Ma et al.).

The low-energy CID spectra of (pseudo)-molecular ions of the three structural isomers are illustrated in Figure 4.8, and a comparative overview of main characteristic fragment ions is given in Table 4.3. It is apparent that the multiple-stage MS spectra of the three isomers are sufficiently different for positive discrimination. Diagnostic fragment ions used to distinguish the three isomers are marked in Figure 4.8 with a grey arrow.

Fisetin presents a fragmentation pattern characteristic of flavonols and a parallel can be directly established with kaempferol to assign the different characteristic fragment ions. On basis of their MS/MS spectra, the two molecules can be unequivocally distinguished. The number of hydroxyl group substituents present on the A-ring for the two isomers is immediately revealed through cleavage of the C-ring. For instance, kaempferol, that is doubly oxygenated on positions 5 and 7, yields $^{0,2}A^+$ fragment ions at m/z 165, whereas fisetin, that is only oxygenated on position 7 yields $^{0,2}A^+$ fragment ions at m/z 149.

Luteolin has a different fragmentation pattern specific for the flavone group (Figure 4.7). A third fragmentation route involving cleavage of two C–C bonds at position 0/4 of the C ring is additionally observed. This pathway corresponds, like the cleavage in 1/3, to a retro Diels-Alder fragmentation. The peak observed at m/z

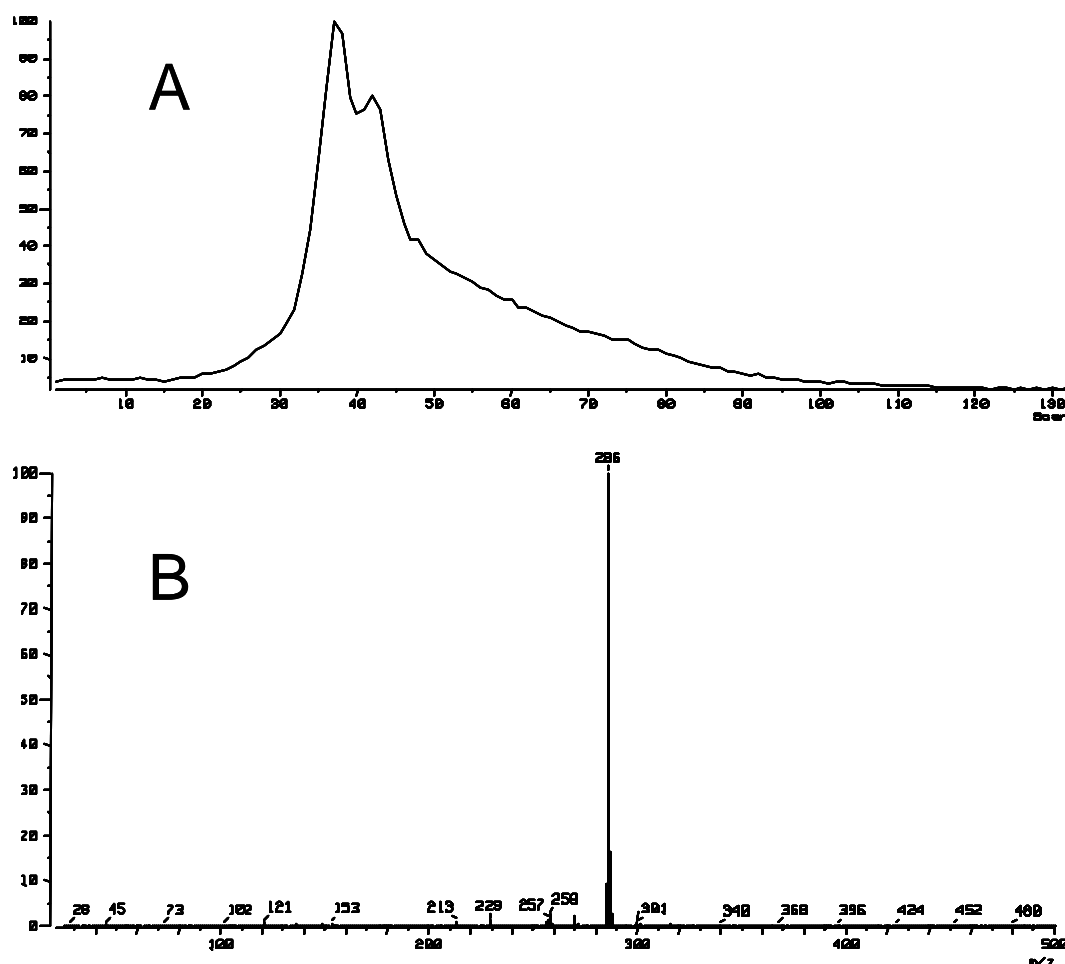


Figure 4.9 *DTMS of kaempferol performed at 16eV electron impact ionisation with a JEOL SX 102A double focusing mass spectrometer with B/E geometry. Total Ion Current (A) and mass spectrum (B).*

Chapter 4

161, corresponding to (${}^{\beta,4}\text{B}^+-\text{H}_2\text{O}$) fragment ions is distinctive of luteolin and is not observed in the spectrum of the two other isomers. A second characteristic difference for molecules belonging to the flavone group concerns the absence of a hydroxyl group in position 3. A loss of 42 Da ($\text{C}_2\text{H}_2\text{O}$), explained by protonation at C-3 and subsequent cleavage of two C–C bonds at position 2/4¹³⁵, results in fragment ions at m/z 245 $[\text{M}+\text{H}-\text{C}_2\text{H}_2\text{O}]^+$. This 2/4 cleavage does not occur for flavonols where the C-3 is oxygenated. Additional characteristic fragment ions corresponding to the extra loss of $\text{C}_2\text{H}_2\text{O}$ or C_2H_2 are observed at m/z 203 for $[\text{M}+\text{H}-2\text{C}_2\text{H}_2\text{O}]^+$ and 219 for $[\text{M}+\text{H}-\text{C}_2\text{H}_2\text{O}-\text{C}_2\text{H}_2]^+$ respectively.

4.5.3 DTMS and DTMS/MS of kaempferol

Low-energy CID spectra of kaempferol, fisetin and luteolin shows the presence of two peaks at m/z 258 and 259. The peak at m/z 258 has a higher relative intensity in the case of kaempferol. DTMS/MS analyses were performed on a sector instrument to obtain a better insight into the fragmentation pattern of kaempferol. Figure 4.9 shows the DTMS spectrum for kaempferol ($\text{IE}=16\text{eV}$). The electron ionisation yields the radical molecular ions $\text{M}^{\cdot+}$ at m/z 286 and the deprotonated molecule $[\text{M}-\text{H}]^+$ at m/z 285. Isolation and fragmentation of these ions in an MS/MS experiments (collision energy of 8KV) shown in Figure 4.10 yields in both cases fragments assigned to the losses of CO (M-28) and CO+H (M-29) observed respectively at 258/257 and 257/256. In the light of this, we have good reasons to believe that the two peaks at m/z 259 and 258 in the LDI-ITMS/MS of $[\text{M}+\text{H}]^+$ correspond to the losses of CO and CO+H respectively. It is likely that that the proximity of two hydroxyl groups (in position 3 and 5) around the carbonyl (in position 4) enhances the probability of a CO+H loss in the case of kaempferol. This probability is smaller in the case of luteolin and fisetin, which only have one hydroxyl group in the vicinity of the carbonyl (in position 5 and 3 respectively).

4.5.4 Multiple-stage LDI-ITMS of quercetin and morin, apigenin and genistein

MS/MS experiments were conducted under identical conditions with two supplementary sets of flavonoid isomers: (1) morin and quercetin and (2) apigenin and genistein. The two flavonols morin and quercetin differ in the position of a single hydroxyl group, situated on the C-ring in position 2' and 3' respectively. Apigenin and genistein, a flavone and isoflavone respectively, differ in the position of the phenyl group (B-ring) on the benzopyran-4-one (C-ring), in 2 and 3 respectively.

Under similar CID conditions, morin and quercetin (two flavonols) yields i,jB^+ fragment ions that are stereo-isomers of each other and can therefore not be discriminated. Unfortunately, fragmentation is not sufficiently structurally informative to infer the exact position of the two hydroxyl groups on the C-ring.

Although apigenin and genistein belong to different flavonoid groups, no diagnostic difference could be detected that would lead to a clear distinction between the two stereo isomers. Structurally informative fragmentation obtained in identical MS/MS experiments is not specific enough to determine the exact

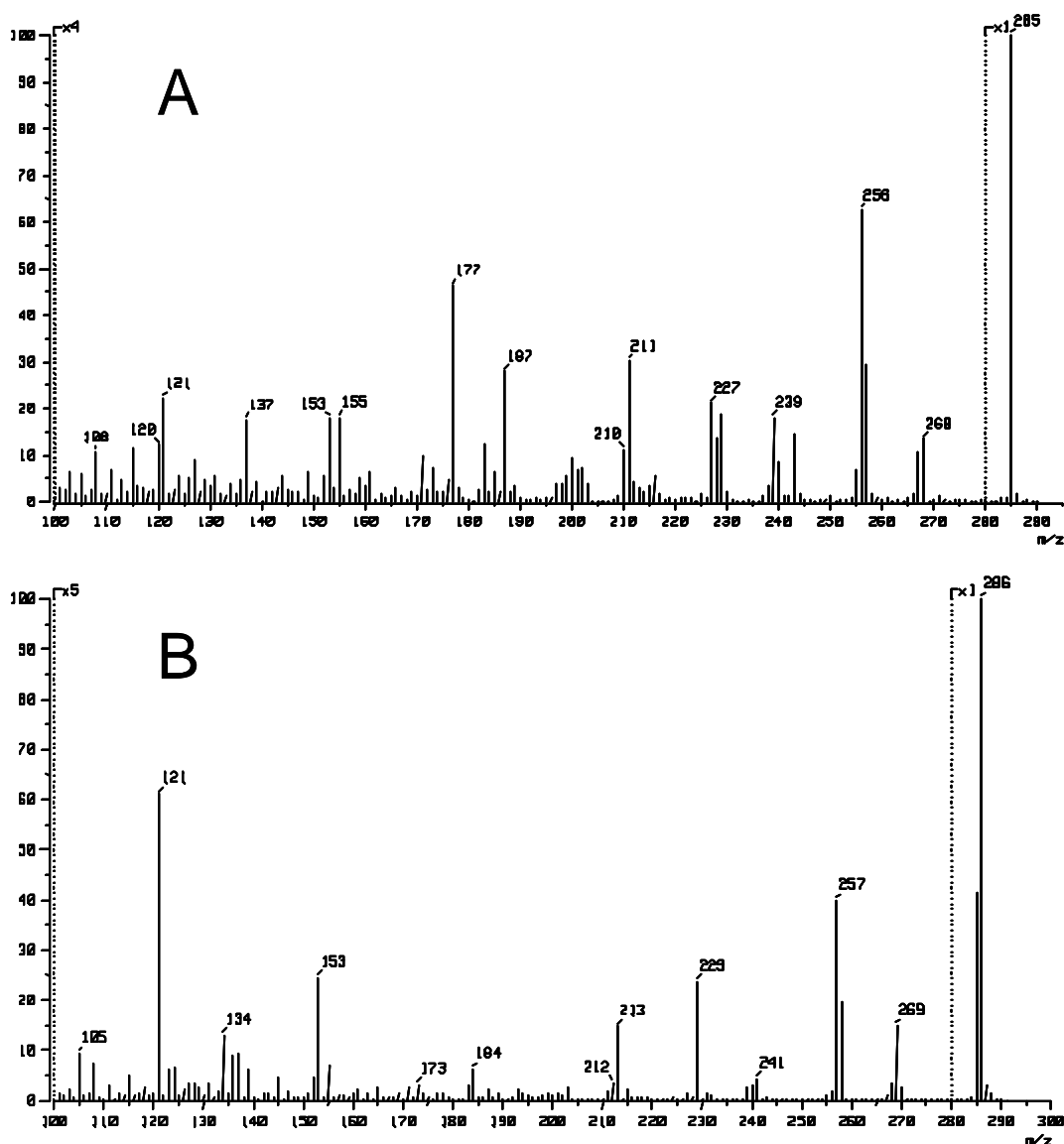


Figure 4.10 DTMS/MS of kaempferol performed at 16eV electron impact ionisation with a JEOL SX 102A double focusing mass spectrometer with B/E geometry. Fragmentation at 285 Da (A) and at 286 Da (B).

position of the phenyl group on the C-ring. It is therefore impossible to distinguish between the two isomeric precursors. In these two cases, the MS/MS methodology successfully employed in the previous section did not provide the means to distinguish between the structural isomers. This is problematic for diagnostic reasons because it would not be possible to make a distinction between apigenin from *Reseda luteola* L. and genistein from *Genista tinctoria* L.

4.5.5 Influence of the collisional energy on structural information in MS/MS

experiments

Since no structure specific ions could be obtained in the previous low collisional energy conditions, we investigated the effect of higher collisional energy on the spectral information. In the following experiment quercetin was investigated in MS/MS experiments at different excitation voltages.

Figure 4.11 shows three low-energy CID spectra at excitation voltages 1.6,

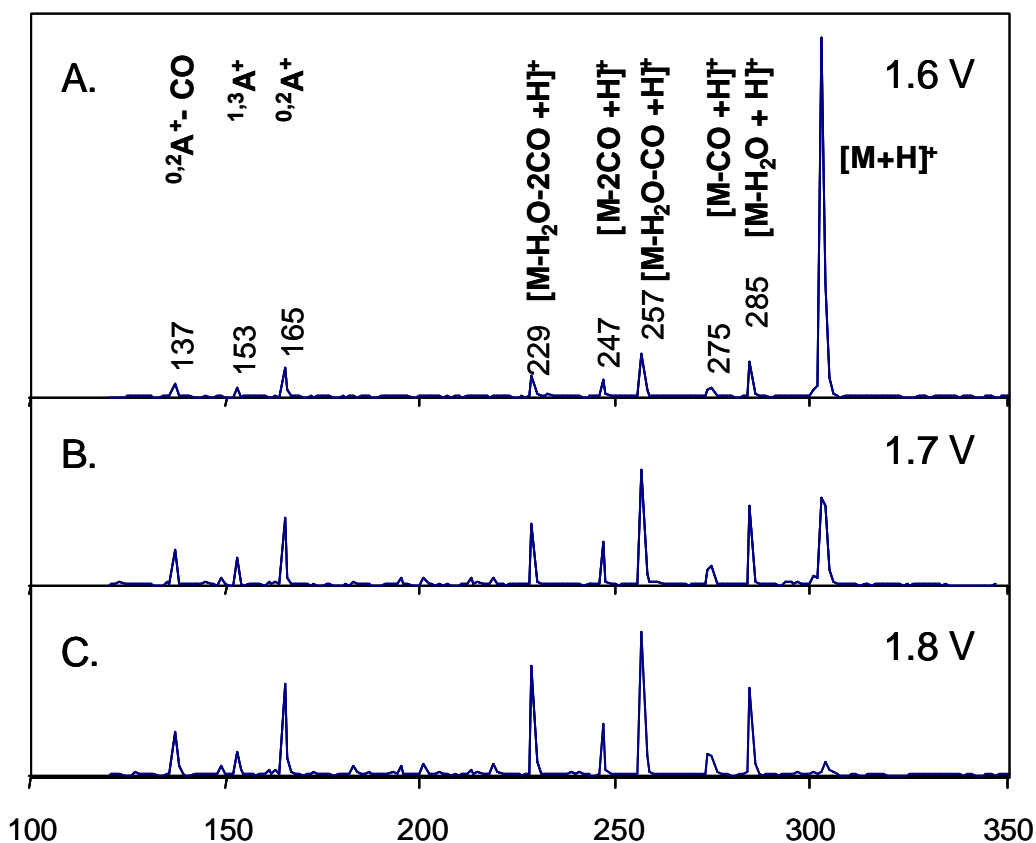


Figure 4.11 Low energy CID spectra at different excitation energies of the isolated pseudo-molecular ion of quercetin (m/z 303).

1.7 and 1.8 V, with the three spectra plotted on the same vertical scale to facilitate the comparison of peak intensities. In this figure we can clearly see distinct internal energy ranges. Figure 4.11.A at 1.6 V shows that the protonated molecule stays mostly intact and only few fragment ions are found. Increasing the collision energy improves the signal to noise ratio of the fragment peaks and provides optimal MS/MS conditions (Figure 4.11.B). Increasing the excitation amplitude even further to 1.8 V results in a decrease in precursor ions but does not enhance the formation of diagnostic fragment ions (Figure 4.11.C).

This experiment shows that the excitation amplitude has to be optimised for each multiple-stage MS experiment in the ion trap. Tuning of the collisional energy makes it possible to obtain an optimal ratio between dissociation products and precursor ions. The energies that were probed revealed no additional specific ions, but the quantitative differences observed with ITMS/MS could be linked to structural features in the analyte. If the energy regime in the ITMS could be calibrated accurately we think that it would be possible to obtain characteristic information about the different stereo-isomers of the same group.

4.6. Characterisation of flavonoid-O-glycosides

Flavonoids are often present as glycosides in plant extracts used for the preparation of dyes and pigments. A typical example is the case of black oak whose dyeing properties were discovered at the end of the 18th century. Quercitrin, a major compound of black oak is the quercetin-3-L-rhamnoside, which is a glycoside of quercetin. Interestingly, both quercetin and quercitrin are used to dye wool since the glycoside quercitrin and its aglycone quercetin do not have the same colouring characteristics (tint and lightfastness). On basis of data presented for the aglycone moiety quercetin, we explore in this section the LDMS characterization of flavonol-O-glycosides.

4.6.1 LDI

Figure 4.12.A is the LDI-ITMS spectrum of quercitrin at low laser power. Sodiated $[M+Na]^+$ and potassiated $[M+K]^+$ molecular ions are observed at m/z 470 and 486 respectively. No radical cations or protonated molecules are detected. The base peak is observed for the aglycone moiety (quercetin) with peaks at m/z 303 corresponding to the protonated ion and at m/z 325 for its sodium adduct. A few characteristic fragment ions of the aglycone moiety are also observed with very low intensity: cleavage of the C-ring in 1/3 leads to m/z 111 ($^{1,3}A^+-C_2H_2O$); and in

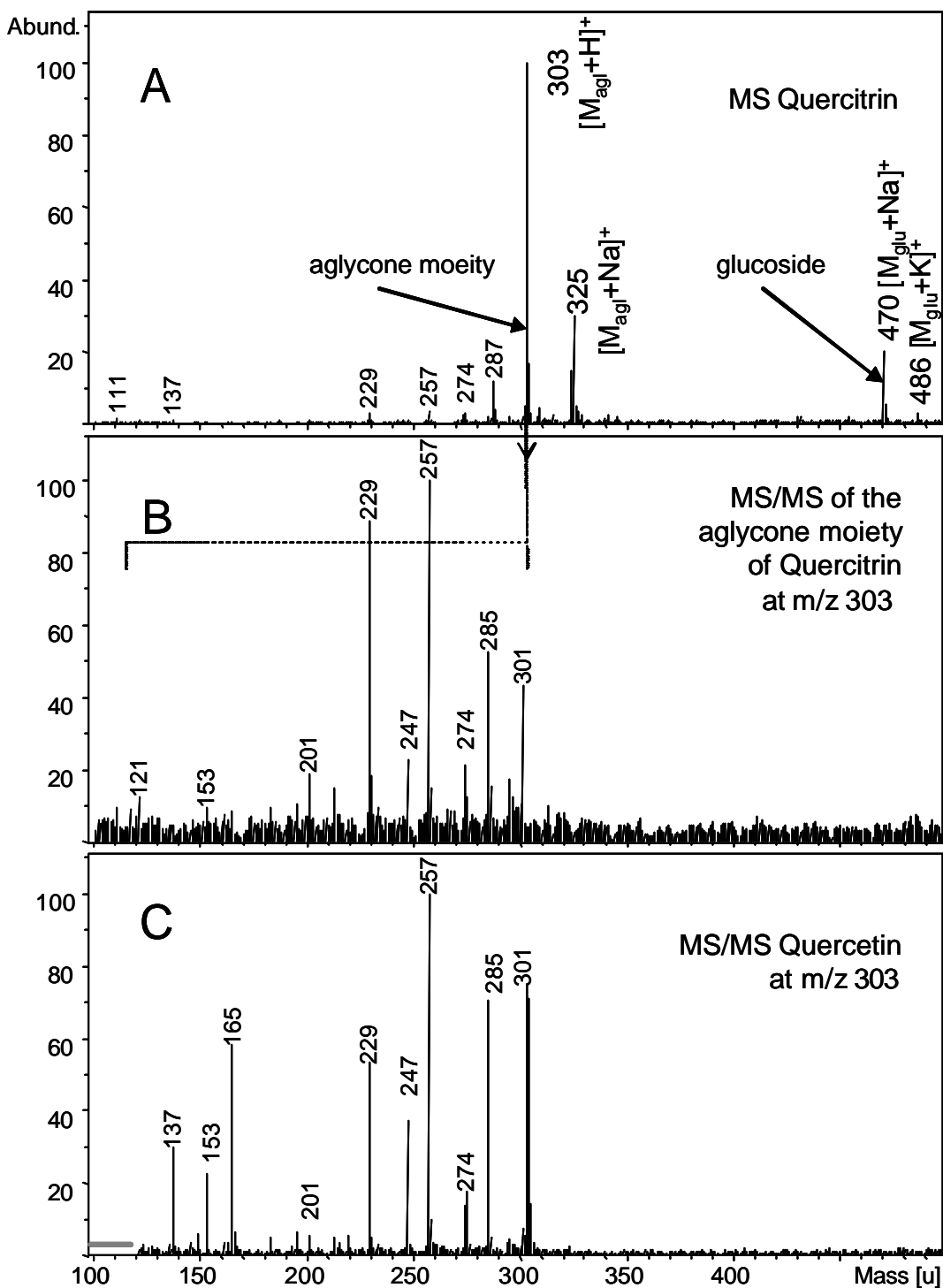


Figure 4.12 LDI-ITMS of quercitrin: the MS spectrum (A) displays both characteristic peaks for the glucoside and the aglycone moiety. The aglycone moiety at m/z 303 was further isolated and fragmented by CID in a MS/MS experiment (B). LDI-ITMS/MS of quercetin (C): isolation and fragmentation of the molecular ion at m/z 303.

0/2 to m/z 165 ($^{0,2}A^+$) and 137($^{0,2}A^+-CO$, or $^{0,2}B^+$). Additional ions corresponding to the loss of H_2O and CO are assigned as follows: $[M+H-H_2O]^+$ at m/z 285, $[M+H-COH]^+$ at m/z 274, $[M+H-H_2O-CO]^+$ at m/z 257, $[M+H-2CO]^+$ at m/z 247 and $[M+H-H_2O-2CO]^+$ at m/z 229. In summary, the fragmentation pattern of the glycoside is in perfect agreement with the fragmentation pattern of the aglycone.

4.6.2 MS/MS

Multiple-stage mass spectrometry was employed for the controlled fragmentation of the ions at m/z 303. CID of the isolated ions leads to the spectrum depicted in Figure 4.12.B. MS/MS of the precursor ions at m/z 303 closely matches the CID of the isolated molecular ion of quercetin shown in Figure 4.12.C. The signal-to-noise ratio for the diagnostic fragment ions of the aglycone is increased by roughly a factor of three in the MS/MS spectrum. This experiment demonstrates that the aglycone moiety of a glycoside has the same fragmentation

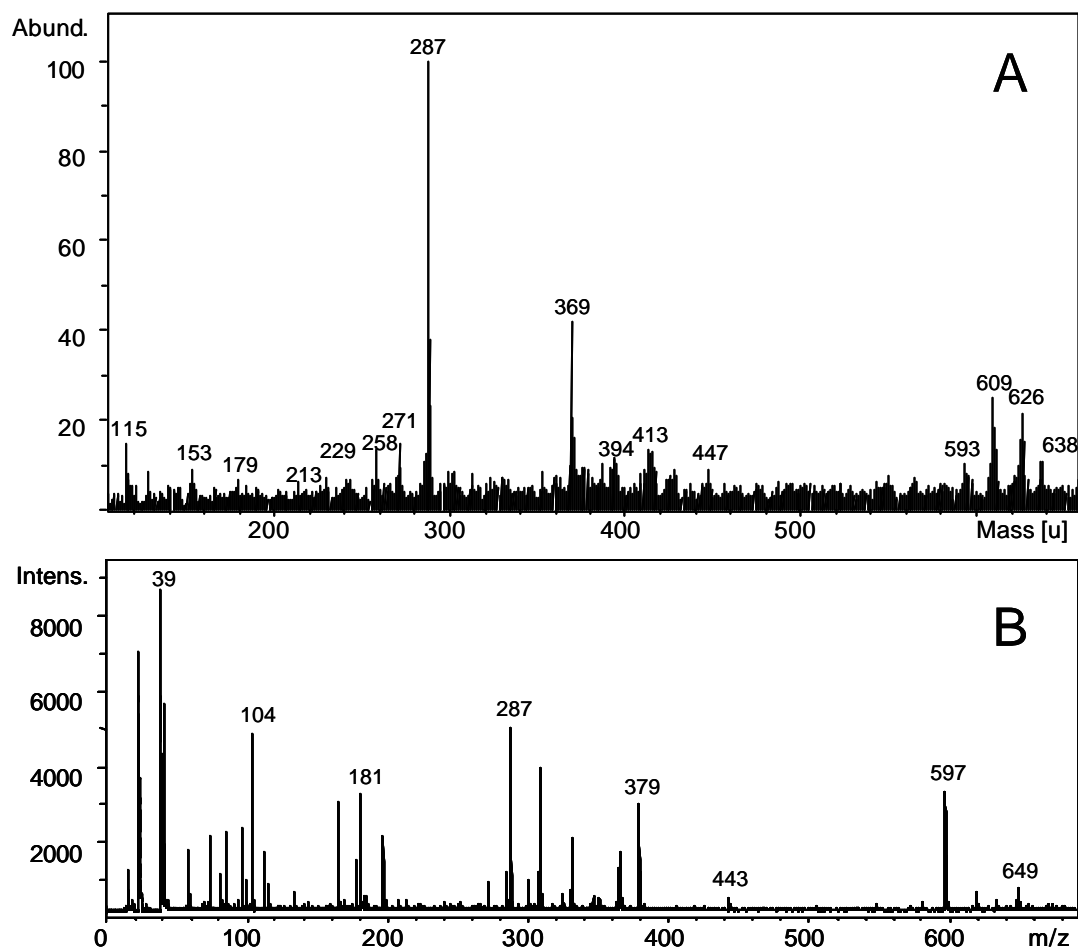


Figure 4.13 LDI-ITMS (A) and LDI-TOF-MS (B) of a *Reseda luteola* L. extract.

pattern as the reference aglycone. This experiment demonstrates the value of LDMS in the authentication of flavonoid-O-glycoside.

4.7. Analysis of complex samples

In this section we study the applicability of our LDMS approach to the analysis of complex samples such as flavonoid plant-extracts, mordanted pigments (colouring material fixed on a substrate) and paint reconstructions. Extracts of flavonoid plants and their lakes were prepared after traditional recipes.

4.7.1 Weld extracts

An extract of *Reseda luteola* L. was analysed in a LDI-ITMS experiment. The principal component of *Reseda luteola* L. is luteolin, in the form of aglycone, mono- and di-glycoside. Figure 4.13 shows the LDI-ITMS spectrum of a weld extract. The dominant peak is assigned to the protonated molecule of luteolin. Additional peaks in the mass range [100-300] are assigned to fragment ions of this protonated luteolin (153, 179, 213, 258, 271). The peak at m/z 369 is attributed to $[(M+2Na^++K^+)-2H^+]$. In the higher mass range a group of ions is assigned to dimeric species.

In an unknown sample, where an organic yellow is suspected, the detection

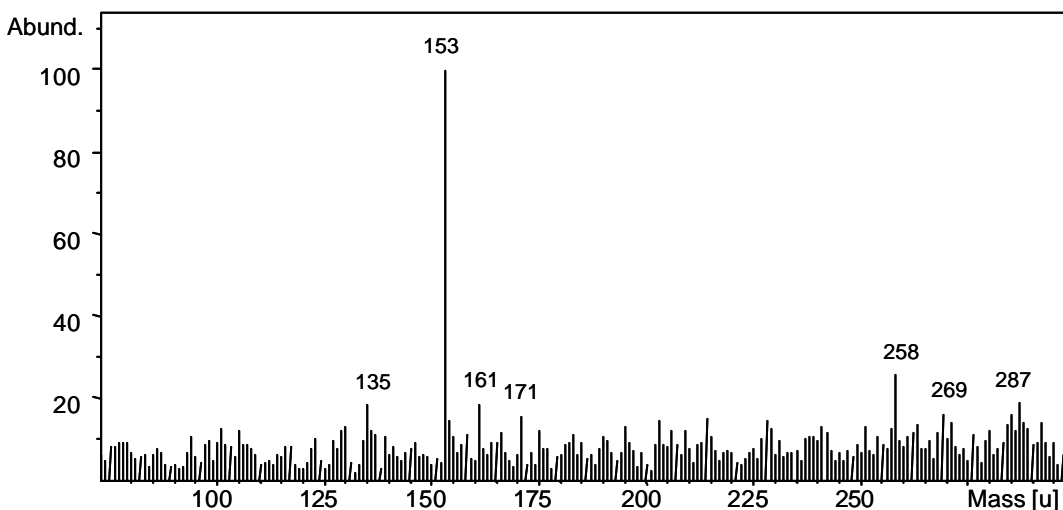


Figure 4.14 LDI-ITMS/MS of a *Reseda luteola* L. extract after isolation and fragmentation of the ion species at m/z 287. Peaks below 10% relative intensity are instrumental noise.

of this particular mass could however also suggest the presence of kaempferol or morin. The presence of fragment ions at m/z 153 and 179 already points to the presence of luteolin identified by ions of class $^{1,3}A^+$ and $^{0,4}B^+$. However, their low relative intensities make it rather improbable to reach the same conclusion in the case of a complex mixture, and in the absence of a predominant confirmatory fragment ion it would remain unclear which of the three isomers is present. Therefore, the m/z 287 ions were isolated and fragmented by CID in an MS/MS experiment with the ITMS. The resulting spectrum (Figure 4.14) reveals additional fragment ions characteristic of luteolin: $^{1,3}B^+$ at m/z 135, ($^{0,4}B^+-H_2O$) at m/z 161, as well as peaks at 241, 258 and 269. Additional structural information provided by MS/MS makes it possible to positively identify luteolin.

The LDI-TOF-MS spectrum of the weld extract also gives evidence for the presence of the protonated molecule of luteolin at m/z 287.

4.7.2 Flavonoid lakes

Neither LDI-ITMS (Figure 4.15) nor LDI-TOF-MS spectra revealed the complex form of the weld lake. The ITMS spectrum shows an intense peak at m/z 287 that is assigned to the protonated molecule of luteolin. Peaks in the dimeric regions of the TOF-MS spectrum support the presence of luteolin with peaks similar to its TOF-MS spectra. We infer that only the uncomplexed form of luteolin is desorbed and ionised.

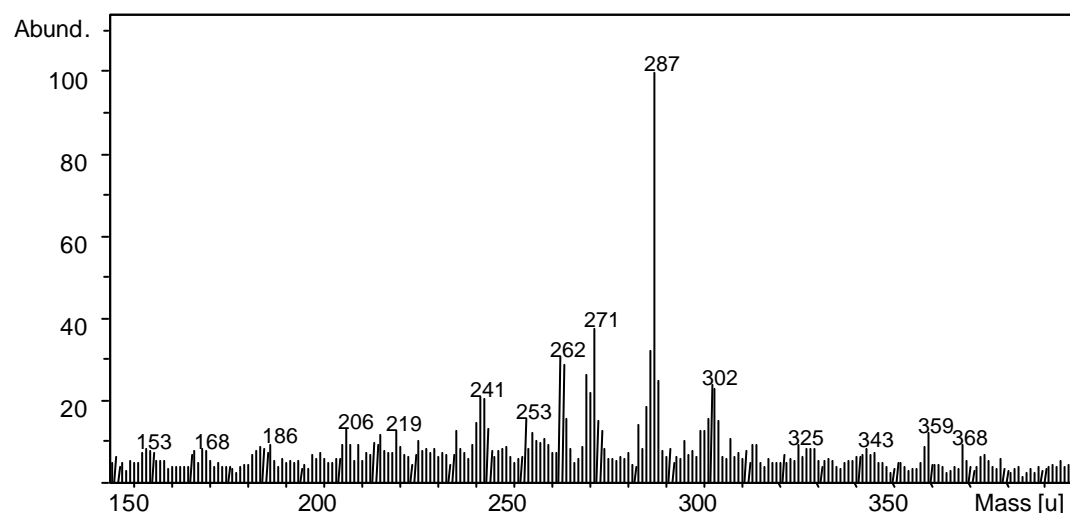


Figure 4.15 LDI-ITMS of a *Reseda luteola* L. lake

4.8. Analysis fibres dyed with flavonoids

Investigation of dyes from ancient fabric requires extracting sufficient colouring materials from the fibres prior to analysis. Spatially-resolved LDMS analysis was explored for the study of mordanted flavonoid directly at the surface of wool fibres. In this case the spatial resolution of the mass spectrometer is employed to target the surface of an individual fibre for analysis (see section 3.2) and the sample holder can be monitored during analysis to move the fibre while keeping it in focus of the laser beam.

An alum-mordanted quercetin dyed wool was analysed by LDI-TOFMS, and its spectrum is shown in Figure 4.16. Characteristic peaks of quercetin are observed at m/z 303 for the protonated molecule $[M+H]^+$, m/z 341 $[M+K]^+$, m/z 285 $[M+H-H_2O]^+$, m/z 591 $[2M-2H_2O+Na]^+$, m/z 629 $[2M-2H_2O-H+Na+K]^+$. Aluminium ions are detected at m/z 27. Again no complex form of the aglycone was identified in the TOF-MS spectrum. This experiment shows that organic flavonoids can be successfully identified by LDMS directly performed at the surface of a single wool fibre.

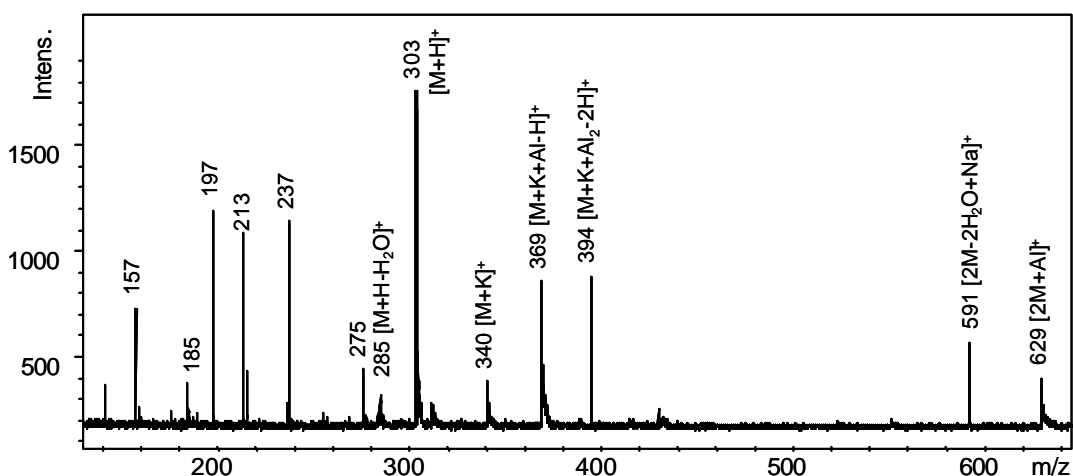


Figure 4.16 LDI-TOF-MS of an alum mordanted quercetin dyed wool.

4.9. *Investigation of cross-sectioned samples*

In spite of various attempts with reconstructions and easel painting samples, paint cross-sections containing flavonoid lakes could not be successfully analysed with LDMS. The limitations met with the study of flavonoid lakes discussed in the previous sections already cast doubt on the adequacy of the method for the identification of lake pigments in complex mixtures such as paint samples. The findings indicate though that surface analysis is possible and that the uncomplexed form of the lakes could be detected. Evidently, one explanation for the non-success of the analyses could be that the lake is not ionised whatsoever. Another hypothesis holds that the very small amount of material present at the surface of paint samples do not produce sufficient ions for detection. Further investigations discussed in the remainder of this thesis bear upon surface analysis of cross-sections comprising other types of colouring materials.

4.10. *Conclusion*

In this chapter we have employed laser desorption mass spectrometry (LDMS) in the analysis of flavonoids compounds traditionally encountered in artist's pigments and textile dyes. A series of characteristic flavonoids aglycones were successfully analysed both in LDI and MALDI. Ions in LDI are predominantly formed as protonated molecules and alkali adducts. Soft ionisation achieved with low laser power densities affords the formation of sufficient amounts of intact (pseudo-) molecular ions to subsequently perform MS/MS analyses. CID experiments produce diagnostic fragment ions – hardly observed or absent in the MS spectrum – that provide essential information for structural elucidation. Multiple-stage mass spectrometric capabilities of the ITMS were successfully employed to positively differentiate the three isomers luteolin, kaempferol and morin. However, MS/MS analyses cannot differentiate quercetin from morin, and apigenin from genistein. The MS/MS procedure was further applied to identify luteolin in a weld extract and to characterise the aglycone moiety of a flavonoid-O-glycoside. The potential for spatially-resolved analysis of LDMS was demonstrated with the analysis of a flavonoid at the surface of a wool fibre dyed according to traditional recipes. LDMS did not produce spectra that could lead to the identification of a complex form of a flavonoid in the form of a lake and investigation of paint cross-sections remained so far unsuccessful.

Chapter 5

An LDMS investigation of traditional colouring materials - Part II: Anthraquinones

In this chapter, LDMS was used for the investigation of red natural organic colouring materials traditionally used as artist's pigment and textile dye. It is shown that alizarin is amenable to characterization with ultraviolet LDMS but the interpretation of the spectra is not straightforward. Alizarin was detected in mixtures with linseed oil in naturally aged samples, as well as in two alizarin lakes samples. In-situ LDMS analyses of madder lakes at the surface of dyed wool fibres were demonstrated. Molecular structures are proposed to explain the coordination of characteristic ions detected in LDMS of alizarin lakes.

5.1. Introduction

Anthraquinone red organic colouring materials are known since antiquity and have been traditionally used as dyes for textiles and pigments for paintings^{16, 28}. Their manufacturing process and use bear a strong resemblance to flavonoids. The colouring material is extracted from plants or animals and rendered insoluble by preparation of a lake. Various possible biological sources, substrates and modes of preparation create a large range of potential chemical compositions of the original lake.

In easel paintings, red lakes were extensively used over opaque underlayers to add richness and depth to the painting of draperies. They were especially appreciated for their relative translucency when combined with the painting medium (the substrate itself is then transparent), allowing their use as a glaze. It is well known that red lakes present in museum objects are prone to severe degradation with ageing. Over the years original red colours irreversibly fade away. There is therefore a great need for better understanding of these degradation mechanisms. Unfortunately technical investigation is particularly problematical with samples that are microscopic in size, are build-up as a very complex stack of layers and/or contain only a very small amount of the colouring material. This chapter explores the analysis of red organic materials with LDMS.

First, reference materials were analysed including commercial alizarin as well as lakes of alizarin and madder prepared in the laboratory, to establish whether LDMS can detect anthraquinone. Then, artificially aged reconstructions of alizarin mixed with linseed oil were investigated to evaluate the applicability of the method to the detection of anthraquinones within a paint medium. Finally LDMS was employed for the *in-situ* identification of anthraquinone lakes on the surface of dyed wool fibres, using the accurate sample-positioning feature for spatially-resolved targeting of the laser beam onto the sample.

5.2. Anthraquinone pigments

5.2.1. Materials and practice

Among the large number of biological sources containing red organic colouring materials, a small group has been mostly used in Europe to produce

pigments for easel paintings and dyes for textiles (see Table 5.1). This group comprises red pigments of vegetable origin, such as madder roots and Brazil wood, and red pigments of animal origin such as cochineal, lac and kermes. History, preparation and use of red organic colouring materials have been discussed in the literature^{1, 2, 5, 17, 22, 23, 27, 144}.

	Name	Major component(s)
Plant origin	Madder roots (<i>Rubia tinctorium</i> L.)	Alizarin, Purpurin
	Brazil wood (<i>Caesalpinia brasiliensis</i> L.)	Brazilin
Animal origin	Kermes insect (<i>Kermes vermilio</i> Planchon)	Kermesic acid
	American cochineal (<i>Dactylopius coccus</i> O. Costa)	Carminic acid
	Polish cochineal (<i>Porphyrophora polonica</i> L.)	Carminic and kermesic acid
	Lac insect (<i>Kerr lacca</i> Kerr)	Laccaic acids

Table 5.1 *Principal sources of organic red colouring materials for the preparation of dyes and pigments.*

Red organic colouring materials are mostly anthraquinone dyestuffs. Anthraquinones have a molecular structure based on a quinone with two anellated benzene rings on either side¹⁴⁵. Substitutions on the two benzene rings give the particular colour properties to the pigment. Like flavonoids, anthraquinone dyestuffs are soluble in water and therefore must be prepared under the insoluble form of *lake* to be used as dyes or pigments. Dyestuffs are first extracted in solution from the biological source, and the resulting colouring material in solution is co-precipitated with an inert inorganic substrate. In this fashion, insoluble particles coloured with the dye are formed. These coloured particles are collected, washed and dried as a solid pigment. Possible substrates include calcareous materials such as chalk or gypsum, hydrated alumina derived from rock alum, and occasionally lead white. When alum was used, the product of the reaction is a complexation between the colouring material and the metal ion produced by alum. The technique is called *mordanting* since it is common to the dyeing of textile where the substrate, called *mordant*, is used to fix the dye on to the textile. Red colouring materials were usually re-extracted from dyed fabrics to produce pigments at lower costs. It is likely that fabrics dyed with different organic reds could have been used as a re-extraction source. The resulting pigment is then a mixture of coloured materials originating from different biological origins.

In this chapter, LDMS experiments have been conducted with colouring materials obtained from the madder plant *Rubia tinctorium* L.¹⁴⁶. Madder, a Rubiaceae plant, was the largest source for the manufacture of red pigments. Its root contains principally alizarin (shown in Figure 5.1) and several other anthraquinones in minor proportion such as purpurin, pseudo-purpurin, alizarin 2-methyl ester, rubiadin and munjistin¹⁴⁶. LDMS investigations were focussed here on the alizarin, the main colouring matter in the madder lakes.

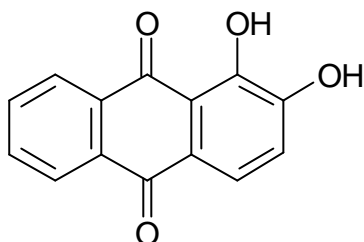


Figure 5.1 *Alizarin (m/z 240, $C_{14}H_8O_4$) is the principal compound of the red organic pigment extracted from the Rubiaceae plant *Rubia tinctoria*. Alizarin (1-, 2-dihydroxyanthraquinone) is a tri-cyclic aromatic diketone with two hydroxyl substituents.*

Alizarin is a transparent crimson, moderately saturated to moderately unsaturated. It is the most fugitive pigment still in common use^{31, 34, 35, 39}. It fades rapidly in tints, but is more stable in mass tone. Alizarin of synthetic nature is known in the Colour Index of the Society of Dyers and Colourists¹⁴⁷ under the name of PR83 (Pigment Red 83)*. Alizarin was one of the first synthesised organic pigments and was obtained by Graebe and Liebermann as early as 1871. Next, synthetic alizarin lakes have rapidly supplanted organic reds of natural production. Modern chemistry has found excellent light-fast replacements for fugitive anthraquinone red pigments, such as quinacridone and pyrrolidone. Despite of its lightfastness problems, traditional alizarin remains however a popular pigment among professional artists.

Molecular structures of red lake pigments found in painting are so far poorly understood. Generally the source of the red pigment is unknown and therefore the colouring matters that have been used as starting material. In addition the preparation method is also unknown and therefore the original composition of the resulting pigments. To compound the problem, it is most likely that degradation with time has induced severe molecular transformation to the pigment. Molecular structure for reference materials have been given by Kiel^{148, 149} who

* PR83 is the synthetic compound corresponding to the traditional organic pigment called madder lake. PR83 is the calcium lake (aluminium complex) of the 1,2-dihydroxyanthraquinone, commonly known as alizarin.

proposed $\text{CaAl}(\text{OH})(\text{Az})_2 \cdot x\text{H}_2\text{O}$ for the structure of an alizarin lake (Figure 5.2) prepared with the addition of an alkali and aluminium hydrate. Here covalent and coordination bonds fix the aluminium atom to two deprotonated alizarin molecules, with the additional adjunction of water molecules. The model adopted by Butler and Furbacher¹⁵⁰ proposes apart from aluminium that forms chemical bonds with alizarin, also calcium that bridges the alizarins by their 2-hydroxy groups.

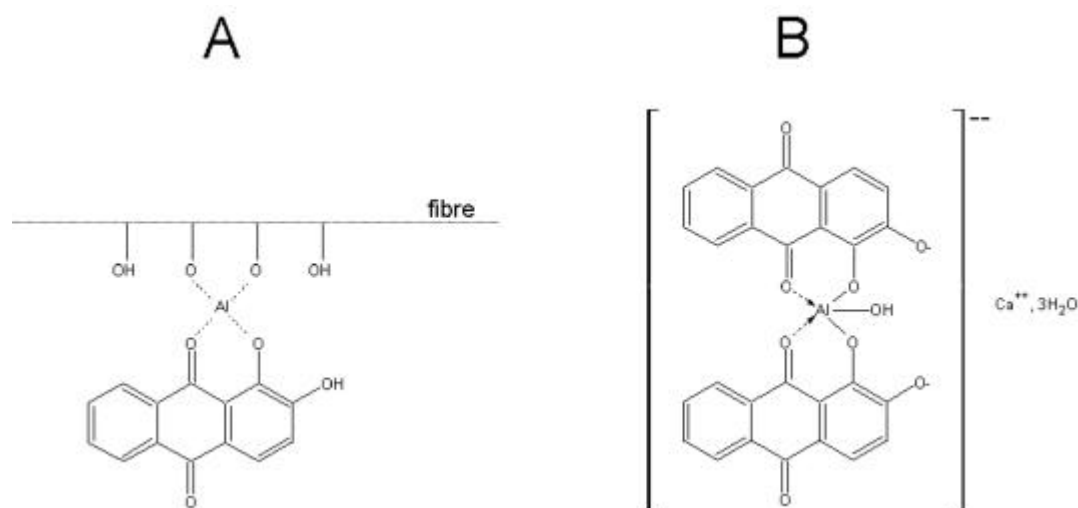


Figure 5.2 Alizarin lake bound to a fibre with a mordant (A) and lake pigment after precipitation in presence of alum and calcium (B), (after Kiel).

5.2.2. Molecular analysis of anthraquinone pigments

Current methods of analysis for the identification and characterization of red organic colouring materials in conservation sciences have been reviewed by Schweppe^{17, 146}. Determination of the molecular composition of red organic lakes in paintings and historical textile is problematical, for the same reasons as discussed for the flavonoids in the previous chapter.

Various analytical techniques are currently in use. Spectroscopic methods of investigation are UV-VIS¹⁴¹, solution spectrophotometry^{52, 54}, infrared spectroscopy with FTIR^{8, 53, 59, 67} and three-dimensional fluorescence⁵⁷. An investigation of colour changes has been reported by Kirby³². Chromatographic techniques, which afford the separation of the different anthraquinone components, have provided the most detailed molecular analysis so far. TLC⁷⁰ was mostly used in early days, whereas today HPLC^{71, 72-74, 76-79} stands out as a method of choice. In the case of dyed fibres, extraction of the dye is required prior to analysis⁸³. A

Chapter 5

common observation however is that chromatographic analyses could fail to identify anthraquinone components in complex samples obtained in too small quantity. When samples are not available for dissection, authentication of the red organic lake has been proposed by the elemental analysis of the substrate with techniques such as EDX and XRF. Lately, DT-MIKES and high-resolution DTMS has been successfully used by Van den Brink ¹⁵¹ to investigate ageing of alizarin in egg tempera matrices. The viability of LDMS has been demonstrated earlier by Bennett with L²TOF-MS ¹³³ and LDMS ⁸⁷.

5.3. Experimental

5.3.1. Instrumental set-ups and mass calibration

Anthraquinone samples were analysed by LDMS on the ITMS with a UV laser emitting at 355 nm and on the TOF-MS with a UV laser emitting at 337 nm. For a detailed description of both instruments we refer to Chapter 2.

A mass calibration for TOF-MS measurements was realised before each series of measurements to obtain optimal mass accuracy. Two samples of polyethylene glycol (PEG) with a molecular weight distribution of averaging m/z 400 and 1000 respectively served as calibrant. MALDI measurements were performed with a mixture of a 1mM ethanol solution of PEG and a 1M ethanol solution of DHB. The mixture was deposited on the surface of the probe and the ethanol vehicle was left to evaporate. Calibration was realised with peaks from the DHB and the PEG at regular intervals in the m/z range [0-1500].

By accurate positioning of the probe under the laser beam individual lake particles (typically 10-50 μm) or a single wool fibre can be easily targeted with a spatial resolution of 10-30 micrometers. The diameter and form of the laser beam as well as the camera output (sharpness, clarity and centring) were controlled before each set of analyses to guarantee optimal observation of the sample and accurate targeting with the laser.

5.3.2. Samples

Synthetic alizarin (1,2-dihydroxyanthraquinone) was obtained from Fluka. Commercial alizarin calcium lakes PR83 (aluminium complex) were provided by Tom Learner (Tate Gallery). An alizarin lake (reconstruction prepared and

gratefully supplied by Jana Sanyova, Royal Institute for Cultural Heritage, Brussels) was prepared by adding alum to a suspension of synthetic alizarin and subsequent neutralisation with the addition of potassium carbonate. The 25 years old naturally aged sample of alizarin in linseed oil paint was obtained from the Von Imhoff collection kept at the CCI (Ottawa). Fibres supposedly from ancient Peruvian civilisation⁶⁸, dyed with a red organic lake, were supplied by A. Wallert (Rijksmuseum, Amsterdam). Fibres dyed with a madder lake were provided by Dr. Quye (Edinburgh).

Alizarin was deposited on the stainless steel probe in solution (dissolved in a droplet of water). After evaporation of the solvent, alizarin forms thin particles adsorbed on the surface. Insoluble lakes and paint samples were adsorbed on the surface of the probe by deposition of a droplet of water with discrete particles in suspension, and subsequent evaporation of the water vehicle. Since anthraquinones lakes are insoluble in water it is supposed that only additives or contaminants are brought into solution during sample deposition.

The MALDI experiments were performed in a similar fashion as with flavonoid samples (see section 4.3.3) using 2,5-dihydroxybenzoic acid (DHB) as a matrix. A thin layer of the sample is first absorbed on the surface of the probe and subsequently, a thin matrix layer is deposited on top of the sample.

5.4. *LDI and MALDI of Alizarin*

5.4.1. *Synthetic alizarin*

The LDI-TOF-MS spectrum of synthetic alizarin ($C_{14}H_8O_4$; mw 240) at low laser power density is presented in Figure 5.3.A. The dominant peaks at m/z 241 and 242 are assigned to the protonated molecule $[M+H]^+$ and its C^{13} isotope. Sodiated and potassiated molecules $[M+Na]^+$ and $[M+K]^+$ are observed at m/z 263 (high intensity) and 279 (low intensity). Additional smaller peaks are assigned to the following species: $(M-H^?)Na^+$ at m/z 262, $[(M-H^?)Na]Na^+$ at m/z 285, $[(M-H^?)Na]K^+$ at m/z 301 (negligible). These ions are in agreement with the ion formation model proposed in Chapter 4 where labile hydrogen atoms are substituted by alkali atoms forming an organic salt.

The same synthetic alizarin analysed under MALDI-TOF-MS conditions at low laser power density is presented in Figure 5.3.B. Many of the main peaks are due to the DHB matrix. A strong $[M+H]^+$ ion of alizarin is observed while sodiated

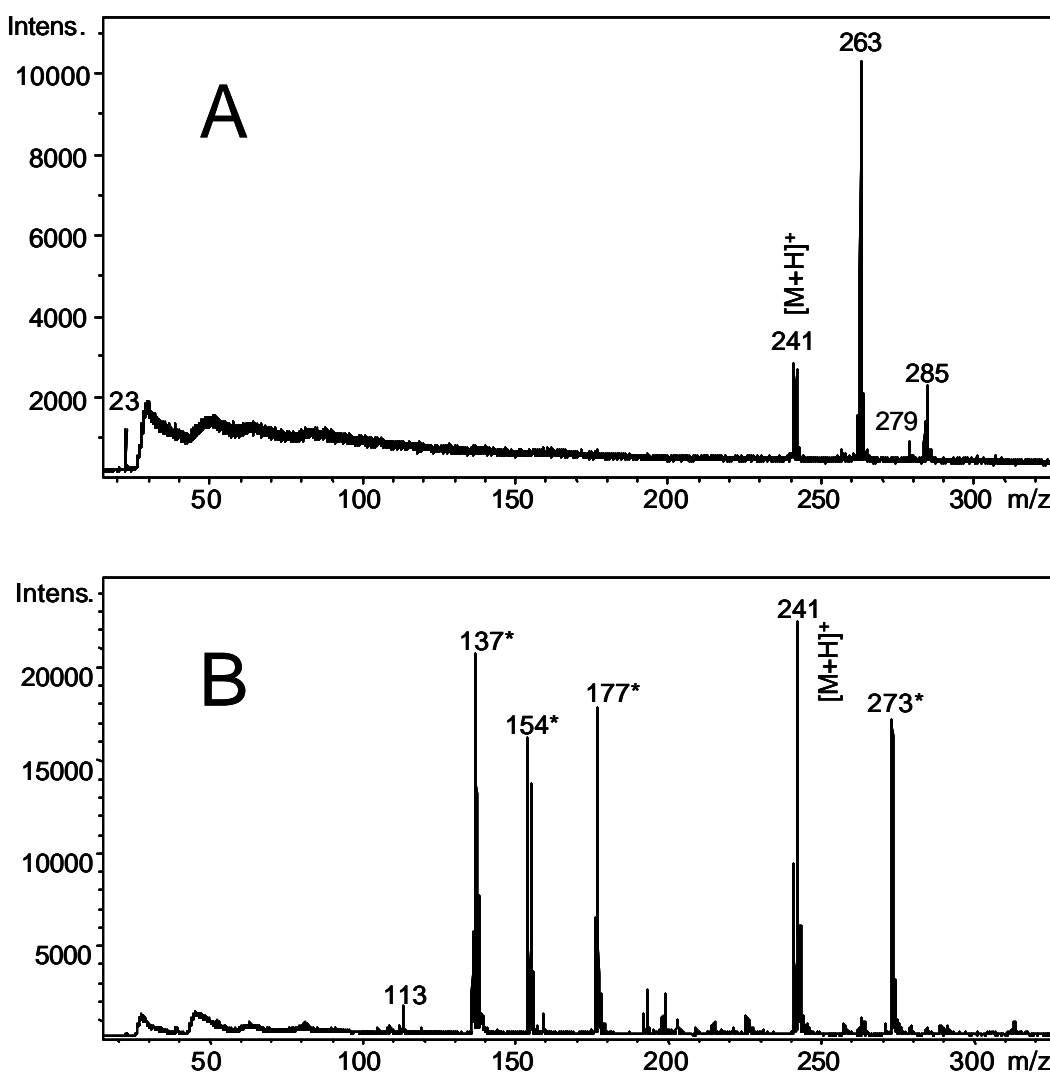


Figure 5.3 LDI-TOFMS (A) and MALDI-TOFMS (B) of alizarin at low laser power density.

or potassium ions are suppressed or absent due to the sample preparation method. Alizarin in very low concentrations however may be hard to discriminate from the matrix peaks (identified with an asterisk).

The LDI-ITMS spectrum of synthetic alizarin at low laser power density presented in Figure 5.4 is puzzling. In the mass range from 150-300 we observe a very low pseudo-molecular ion at m/z 241 that can be assigned to $[M+H]^+$ of alizarin. The ion at m/z 257 cannot be interpreted in a straightforward way. If we assume that the alizarin has taken up one oxygen implying that the sample is oxidatively degraded to purpurin, we can interpret the m/z 257 as an $[M+H]^+$ also. Mass differences of 16 Da between ions also appear at m/z 285 and 301 and at higher mass between the high intensity ions m/z 487, 503 and 519. The m/z 503 and m/z 519 can be nominally assigned to $[2M+Na]^+$ and $[2M+O+Na]^+$. The m/z

487 cannot be easily explained in the same manner. Further work using the MSⁿ capabilities of the ITMS to resolve this matter would have been the logical next step but this became impossible due to irreparable failure of the instrument.

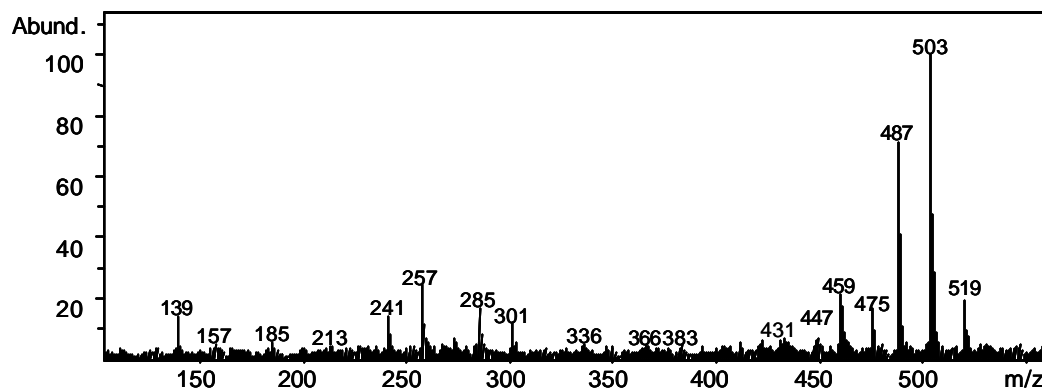


Figure 5.4 LDI-ITMS of alizarin at low laser power density.

The question was also explored whether alizarin could be traced when present in oil paint. Figure 5.5 shows the MALDI-TOF-MS spectrum of a 25-year-old paint-out of alizarin in linseed oil. The protonated molecule of alizarin is detected at m/z 241 $[M+H]^+$ between some peaks from the DHB matrix (identified with an asterisk) which demonstrates that alizarin can still be identified with LDMS when found mixed in an aged oil medium. There is also a very small peak for $[M+Na]^+$ at m/z 263. Other peaks of interest are indicative characteristic of the oil: diacylglycerols around 600 Da (labelled d) and triacylglycerols around m/z 900 Da (labelled t). These ions were also detected in commercial oil paint samples (data not shown). Similar ions have been reported by Van der Berg using MALDI-TOF-MS of linseed oil¹⁵². It should be noted that the ions observed are only a fraction of the total number of different triglycerides that are present.

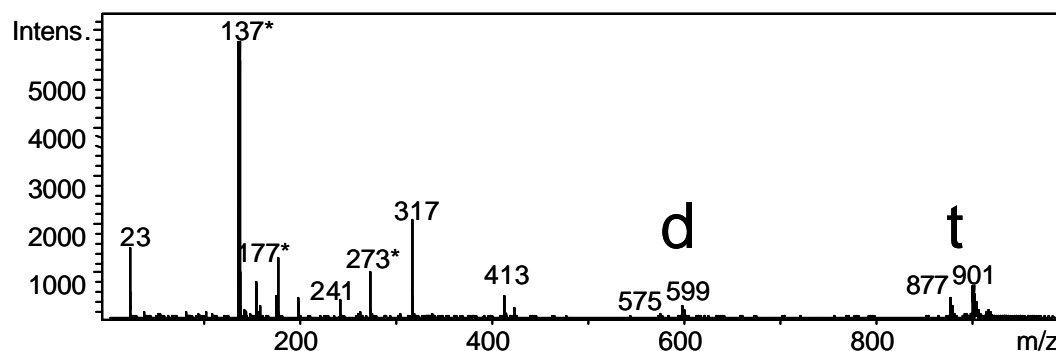


Figure 5.5 MALDI-TOF-MS of a 25 years old mixture of alizarin and linseed oil.

5.4.2. LDI of an alizarin lake

Alizarin is usually not used as such in paints but is present as lake pigment. In the view of the successful LDMS of the alizarin reference compound, the same sample methodology was applied to alizarin as lake pigment. The alizarin lakes were only investigated with LD-TOF-MS at 337 nm. Two different samples were investigated. One sample is an alizarin lake prepared in the laboratory (courtesy of J. Sanyova) whereas the second sample is PR83, a commercially available synthetic alizarin lake precipitated as calcium salt. The samples were investigated as received.

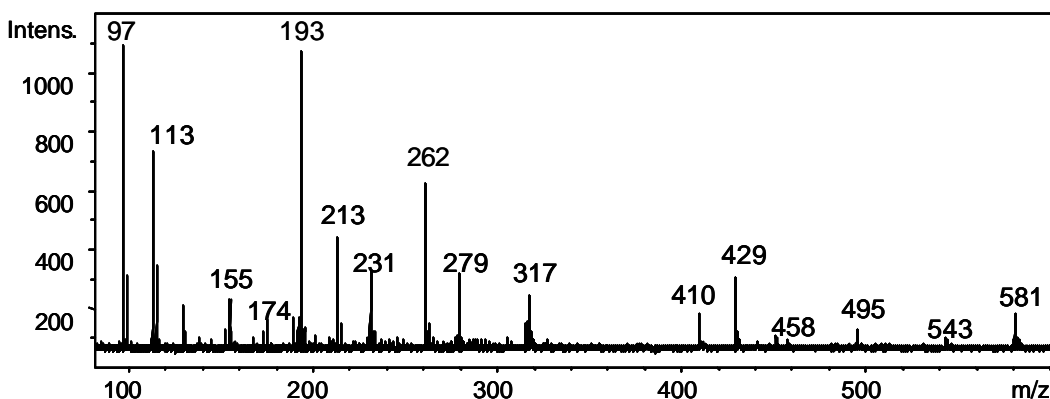


Figure 5.6 LDI-TOF-MS of an alizarin lake prepared in the laboratory

The LDI-TOF-MS spectrum at low laser power density of the alizarin lake prepared by Sanyova in the laboratory is presented in Figure 5.6. Many of the peaks cannot be directly related to the earlier data on free alizarin. Protonated alizarin is not observed. However, sodiated and potassiated alizarin is observed at m/z 262 $[M-H^2]Na^+$ and m/z 279 $[M-H^2]K^+$. The peaks at m/z 543 and 581 are also attributed to the alizarin lake. The peak at m/z 543 corresponds numerically to $[C_{28}H_{12}O_8,Al(OHNa)]^+$ and the peak at m/z 581 corresponds numerically to $[C_{28}H_{12}O_8,Al(OKNa)]^+$. These ions imply that two alizarin molecules are bridged by aluminium with sodium or sodium plus potassium as counter ions. According to the formula, four hydrogen atoms are involved in binding. In the case of m/z 581, one of the hydrogens is exchanged for potassium assuming that sodium is the ion forming atom for the MS. Therefore three of the hydroxyl groups of the alizarin must be involved in ionised form as bonds with aluminium. This explanation does not agree with the model proposed in the literature. The model proposed by Kiel^{148, 149} suggests that aluminium is only bound to one of the hydroxyl positions of the alizarin molecule and bonded with a weaker Van der Waals bond to the carbonyl of the alizarin. In the case of m/z 543, the potassium is replaced by a proton. There are no larger ions in the TOF-MS data that could elucidate other

forms of the complex. Several smaller ions were detected at m/z 495, 429, 410 and 317. The m/z 317 can be explained as a sodiated ion of alizarin aluminium hydroxide complex $[C_{14}H_8O_4, Al(OHNa)]$.

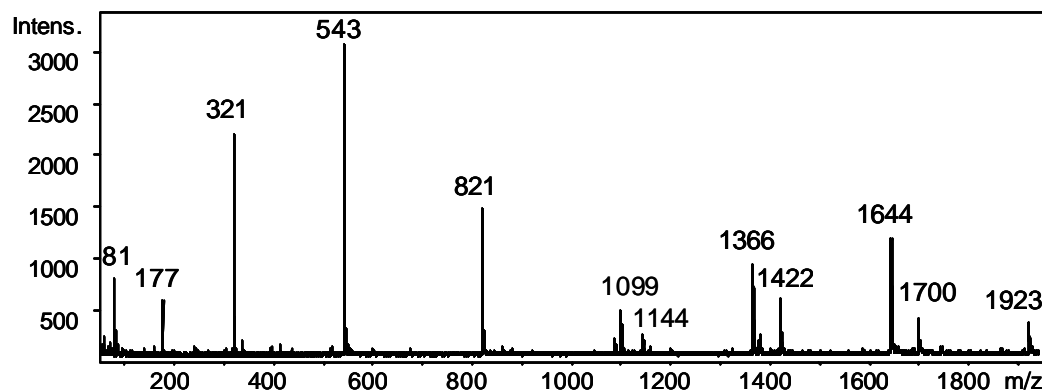


Figure 5.7 LDI-TOF-MS of an alizarin lake PR83.

The LDI-TOF-MS spectrum of the reference compound PR83, a calcium complex of alizarin aluminate in Figure 5.7 displays several dominant peaks with a mass difference of 278 Da up to mass m/z 1923. Peaks at m/z 821 and 1099 correspond to mass differences of 278 Da with respect to m/z 543. The peaks starting at m/z 1144 with 1422, and 1700 and the peaks starting at m/z 1366 with 1644 and 1923 also present mass increments of 278 Da. The mass difference of 278 Da can be assigned to a monomeric block $[C_{14}H_6O_4Ca]$. The model used by Butler and Furbacher¹⁵⁰ proposes that calcium not only binds alizarin molecules via the meta hydroxide group but also forms a bridge between the aluminium hydroxide that complexes two alizarins. Our spectrum supports the idea that calcium bridges the alizarin. The peak at m/z 321 is assigned to the ion $[C_{14}H_5O_4-Al-OCa]^+$ supporting the existence of aluminium in hydroxide form. The peak at m/z 543 is assigned to a calcium complex of an alizarin-aluminium-alizarin with the proposed formula of $C_{28}H_{12}O_4-Al-Ca$. This formula suggests that aluminium is not present in a hydroxide form and is bound to more than one hydroxy group of the alizarin. The ions at 821 and 1099 support the proposal that two calcium-alizarin complex units are connected to the structure of ion m/z 543. The ions at m/z 1144 and 1366 would be larger starter nuclei for the addition of Alizarin-Ca units. We infer that LDMS makes only a few ionisable parts visible of a more lake substance that probably consists of much larger complexes that are not easily ionised by laser induced ionisation.

5.5. *Alizarin lake in oil paint*

Samples from alizarin lake in aged oil paint obtained from a painting by Frank Stella did not produce any significant ions (data not shown). MALDI-MS with DHB produced a pattern of ions at m/z 413, 429, 441, 457, 471 and 485 but these have no apparent relationship to the MS data of alizarin nor to the alizarin lake standard samples. It is possible that a chemical treatment of the sample surface would have released ions reminiscent of alizarin or alizarin derived chemical compounds, but this was not the purpose of the experiment, which intended to explore the direct analysis with the laser beam. Remarkably, the same ion pattern was observed when MALDI-MS with a DHB matrix was applied to a synthetic madder lake prepared by Dr. J. Sanyova.

In view of these negative results, no experiments with lake pigmented layers in paint cross sections were undertaken.

5.6. *Analysis of natural dyed fibres*

LDMS analysis was also explored for the study of the surface of dyed wool fibres using a sample holder that allows targeting of the laser on the fibre. Two cases were investigated that involved dyeing with alizarin or with madder. Madder is not one substance but a mixture of alizarin and hydroxylated and acidic derivatives of alizarin.

Figure 5.8 shows the LDI-TOF-MS spectrum of an ancient Peruvian red dyed fibre provided by Dr. A Wallert (Amsterdam). A dominant peak is observed at m/z 241, which was assigned to the protonated molecule of alizarin. Sodiated or potassiated alizarin is not observed. There are quite a few other mass peaks in the

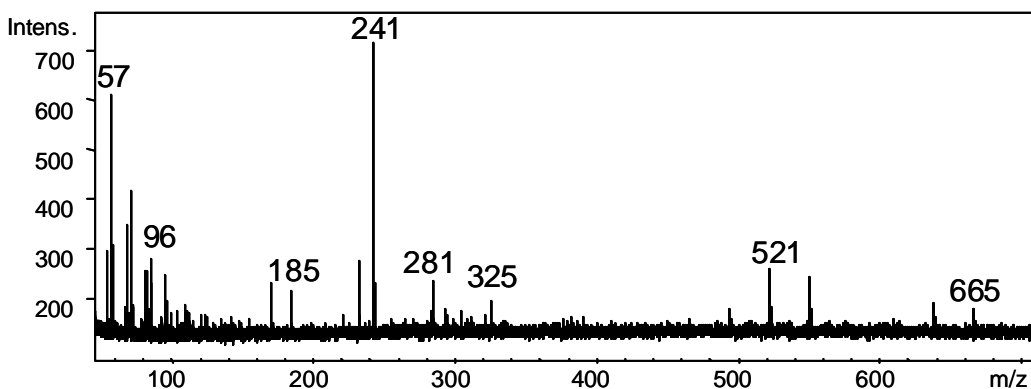


Figure 5.8 *LDI-TOF-MS of a fibre from an ancient Peruvian civilization dyed with red organic colouring material of unknown origin.*

spectrum that are not easily assigned. The m/z 521 is assignable to $[\text{C}_{28}\text{H}_{12}\text{O}_8\text{AlOH}]\text{H}^+$ which implies that an aluminium containing mordant would have been used. The main point of our result is that it seems feasible to analyse dye substance directly from a single fibre. However, fibres from controlled dye experiments are desirable for comparative studies.

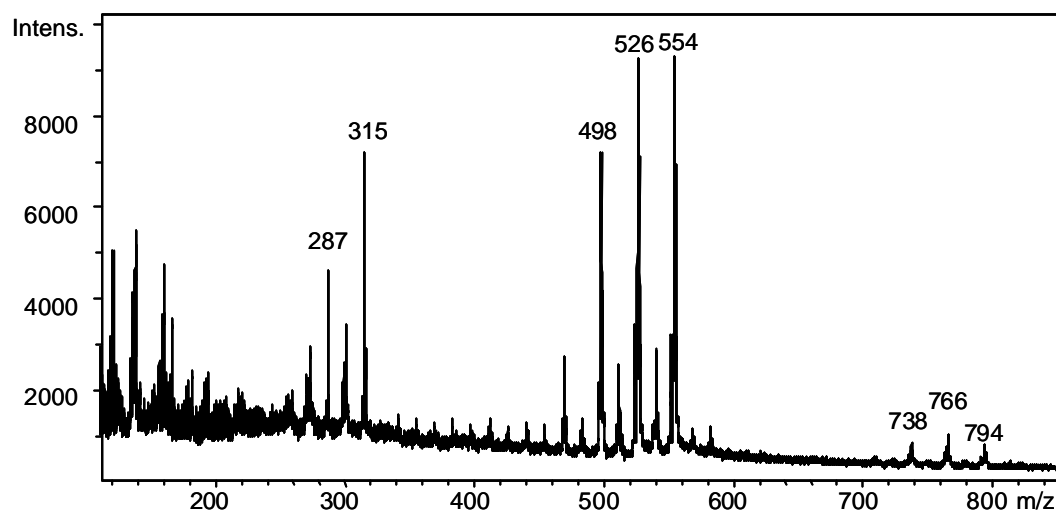


Figure 5.9 LDI-TOF-MS of a fibre dyed with a madder lake.

Figure 5.9 shows the LDI-TOF-MS spectrum of a fibre dyed with madder using an Al/Sn mordant provided by Dr. A. Quye (Edinburgh). The spectrum is remarkably different from the Peruvian fibre shown above. The spectrum shows peaks series around the 300, 470-560 and near 738-800 mass range. The mass difference between m/z 315 and 554 is 239 Da, while the difference between m/z 554 and 794 is 240 Da. These mass differences suggest that one or two alizarin molecules are grafted to a parent structure of 315 Da. Unfortunately, none of the ion structures proposed above for the alizarin experiments discussed earlier can be fitted to this ion. A formula $[\text{C}_{14}\text{H}_6\text{O}_6\text{-Al-OH}]\text{H}^+$ can be fitted to m/z 315 but no feasible structure is evident. An ion at m/z 287, which is 28 Da lower in mass, suggests that CO can be lost from the parent ion structure during analysis. Remarkably, the high intensity ions at m/z 470, 498, 526 and 554 also have mass differences of 28 Da and similarly the ions at m/z 738, 766 and 794.

These results demonstrate that although promising spectra can be obtained from dyed fibres, the interpretation of the ion distribution in the LDMS spectrum is not at all straightforward. Further studies would require a closer inspection of the dye compounds that actually bind to the fibre and a prior understanding of the nature of the coordination complex with other methods before LDIMS from a specific spot on the fibre is undertaken.

5.7. Conclusion

In this chapter we have employed laser desorption mass spectrometry (LDMS) for the analysis of anthraquinone compounds traditionally encountered in artists' pigments and textile dyes. Alizarin, a main component in madder dyestuff was successfully analysed with LDI and MALDI. Alizarin was also detected in a 25-year-old alizarin/linseed oil paint paint-out. LDMS spectra of alizarin lakes are shown to be far more complicated. The two lakes investigated show evidence for alizarin aluminium complexes. In the case of a commercial calcium alizarin lake (PR83) evidence for calcium bridged alizarin molecules could be deduced from the spectra as well. Anthraquinone lake pigments in aged oil paint failed to produce any relevant ions. Experiments with dyed wool fibres produced evidence for alizarin or complexes with alizarin showing the potential of the LDMS approach for these systems.

Although laser desorption approach is able to produce relevant ions in a number of the cases that were explored, the ion identification process needs further attention for example by analysis of ion under high resolution conditions in order to prove elemental composition or by MS/MS analysis.

Chapter 6

An LDMS investigation of traditional colouring materials - Part III: Indigoid dyes

LDMS is used for the investigation of indigo, a blue natural organic colouring material used traditionally as artist's pigment and textile dye. Fundamental studies of synthetic indigotin and natural indigo samples performed with TOF-MS and ITMS address the ion formation during the LDI process. Analysis of complex paint mixtures explores the influence of lead white and linseed oil on the LDI process of indigoids. The spatial resolution provided by a spot analysis with an ultraviolet laser beam makes it possible to directly identify indigo from the surface of wool fibres or from specific paint layers in cross-sections from painting reconstructions.

6.1. Introduction

6.1.1. Materials and practice

Indigo, one of the oldest natural dyestuffs, was known to ancient civilisations in Asia, Egypt, Greece, Rome, Britain, and Peru^{16, 28}. Indigo has been used to prepare traditional artist's pigments and textile dyes^{2, 16, 27, 153-155}. Accordingly, the Color Index of the Society of Dyers and Colorists¹⁴⁷ classifies indigo both as a pigment (CI Natural Blue 1) and as a vat dye for textile (CI Vat blue 1). The blue colouring material indigo* – indigotin - is the molecular species $C_{16}H_{10}N_2O_2$ with a structural formula shown in Figure 6.1.

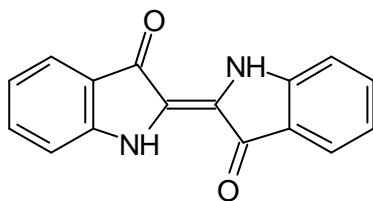


Figure 6.1 *Indigotin (MW 262Da, $C_{16}H_{10}N_2O_2$, C.I. vat blue 1; C.I. 73000) also commonly called indigo or indigo blue, is a blue colouring material traditionally prepared from plants extracts. The pigment is used as such and does not need a mordant.*

Indigoid dyestuffs, commonly named indigo, were traditionally obtained from plants. The main indigo-producing plants and their geographical distribution have been recently surveyed by Balfour-Paul¹⁵³. The indigo-plant *Indigofera tinctoria* L. grown in India and the woad *Isatis tinctoria* L. grown in Europe have been the most widely exploited biological sources. Synthetic indigo – indigotin - was among the very first synthetic pigments. It was produced as early as 1883 by Adolf von Baeyer and within only a few decades it almost completely replaced indigo of natural origin¹⁵³. Today synthetic indigo is produced on a large industrial scale and has obtained a worldwide popularity in Denim garments.

The manufacturing procedure of indigo dyestuff from woad and the indigo-plant implies a redox reaction. In a first step, fermentation of plant material[†] yields the reduced form of indigo, leuco-indigo (leucos = white bright) (Figure 6.2). In

* Indigoid dyestuffs are commonly referred to as indigo. Synthetic indigotin as well.

† Classification of indigo among *vat dyes* evokes the vats where fermenting was taking place.

the indigo-plant the precursor of the reduced form is indican (indoxyl- β -D-glucoside) whereas in woad it is also isatan B (indoxyl-5-ketogluconate). Enzymatic hydrolysis during fermentation breaks the glucoside or ester bonds yielding the indoxyl precursor molecule. Indigo is subsequently formed by oxidation on exposure to air (dehydrogenation with atmospheric oxygen) producing the blue colour.

Natural indigo was habitually traded in the form of lumps to be ground for use as pigment, or reduced again in an alkaline solution to obtain a dyeing bath. The dyeing procedure consists in steeping pieces of fabric in this leuco indigotin solution and to let them dry. Oxidation on air exposure fixes the colouring matter by absorption of the dyestuff onto the fibres. Note that this procedure does not imply the use of a mordant, as it is the case for yellow flavonoids and red anthraquinones (see Chapter 4 and 5).

In addition to variations inherent to the type of indigo-producing plants, their growth conditions and cultivation, the manufacturing process of the colouring material itself plays an important role in the quality of the artist's pigment. The indigo-plant produces indigo of higher purity than woad, but on the whole natural indigo always contains impurities originating from the plant material itself. Adulteration was common practice and pigments retailed under the label 'pure

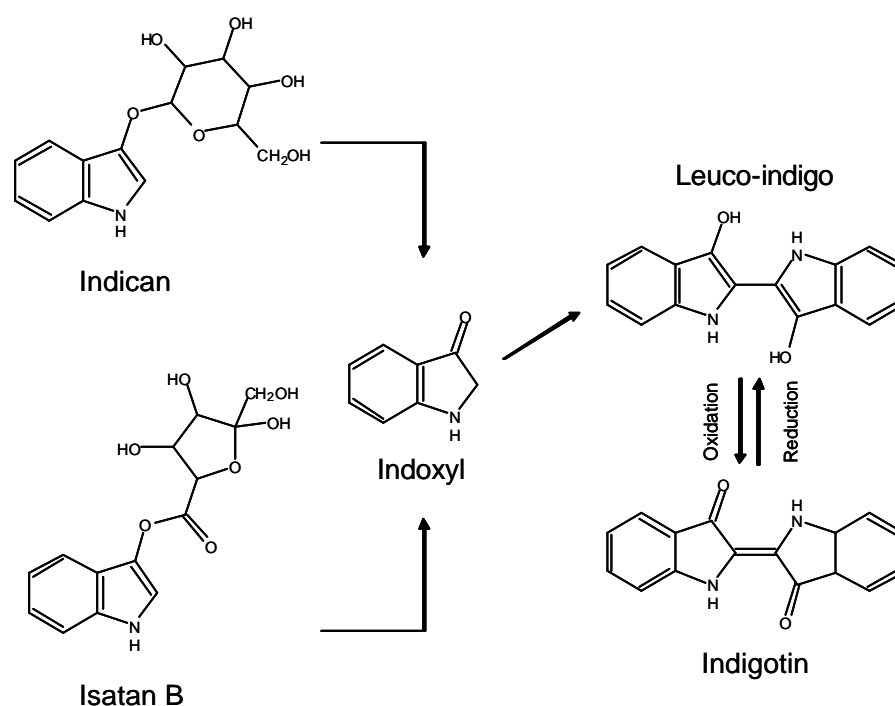


Figure 6.2 *Indoxyl released by fermentation from indican or isatan B oxidises to indigotin.*

Chapter 6

indigo' were in fact often mixed with impurities of various kinds, such as ashes, sand, soot, resin, etc ⁴⁹. In the pure form, natural indigo is a dark blackish blue powder. The colour of natural indigo can have a more coppery, reddish or violet tone depending on the biological origin and the manufacturing process.

6.1.2. Technical investigation of indigo in Conservation Sciences

Technical investigation of indigo in museum artefacts concern essentially ancient textiles and paintings, where indigo was used as early as the 15th century and probably even earlier.

Identification of indigo in paintings is very problematic since the pigment is generally found in very small amounts mixed with various other paint compounds and samples removed for technical investigation are often of microscopic size. Extraction and derivatization of indigo from dyed fibres for analysis ^{74, 141} is problematic because the indigo is only (partly) soluble in a small range of organic solvents. To compound the problem, indigo is a fugitive dyestuff that dramatically deteriorates with the passing of time. The blue colouring materials alters - mainly under the effect of light - into colourless products, a process called *fading* ³¹⁻³⁵. Little is known about degradation products of indigo and fading mechanisms in complex systems such as paintings ³⁶. The role of the manufacturing process, the preparation of the pigment-oil mixture, and the role of the media and additives on the degradation of indigo are still very poorly understood. Studies are underway to investigate the degradation of indigo by FTIR, mass spectrometry (DTMS and ESI-MS) and HPLC-MS ^{82, 156}.

Various analytical techniques that have been successfully used for the investigation of indigo in museum objects were reviewed in a monograph by Schweppe ⁴⁹. Non-destructive techniques such as Raman spectroscopy ^{51, 157}, infrared spectroscopy ⁶⁷, or UV/VIS spectroscopy ¹⁵⁸ can be used with negligible damage to museum artefacts. Unfortunately, these techniques often fail to ascertain the presence of indigo in complex samples, and cannot unravel complex molecular degradation processes. More detailed analytical information can be obtained when samples are removed for technical investigation. Sufficient material is rarely available to perform X-ray analysis, but chromatographic methods - such as TLC and HPLC ^{75, 76} - and mass spectrometry have been proved to be adequate techniques.

Mass spectrometry of indigo has been discussed earlier in the literature by different authors, notably by Mc Govern ¹⁵⁹ who has shown successful results with electron impact, and Gibbs ¹⁵⁸ who has identified indigo from ancient paper using

FAB after derivatization of the dyestuff. More recently, Van den Brink *et al.*⁴² have addressed discoloration of indigo in the paint matrix with DTMS.

6.1.3. LDMS of indigo and indigo-containing samples

Investigation of indigo presented in this chapter is part of a multidisciplinary project that aims at a better understanding of artists' use of indigo as well as the discoloration of the pigment in paintings¹⁶⁰. Here we will explore laser desorption mass spectrometry (LDMS) as an analytical tool for investigation of indigo in museum artefacts and paint reconstructions. Spatially-resolved LDMS is employed with the aim to develop *in-situ* mass spectrometric analysis of indigo at the surface of complex samples. More particularly we are interested in the analysis of indigo in individual layers of paint cross-sections, and in the direct identification from the surface of individual dyed fibres¹³⁸ without the need of extraction or derivatization.

Firstly, we have investigated the desorption and ionisation behaviour of indigo with LDMS using a nitrogen laser (337nm). Analyses concern indigo as pure reference compound and indigo in mixtures, i.e. in the presence of other inorganic pigments (lead white) and/or a binding medium (oil). Careful comparison between different natural and synthetic indigos examines the possibility to identify the nature or biological origin of the pigment. Particular attention will be given to the role of additional compounds in the LDI process. Deposition of matrix at the surface of indigo samples has been tested to determine whether the procedure can assist the LDI process and improves the analytical information. The ITMS analyser equipped with a Nd:YAG laser (355nm) was used to provide MSⁿ analysis (up to the fourth) in order to get a better insight into the fragmentation pattern of indigo in LDMS. The applicability of spatially-resolved LDMS is demonstrated for *in-situ* analysis of indigo at the surface of paint cross-sections and dyed fibres.

6.2. Experimental

6.2.1. Samples

Reference materials include synthetic indigo (Fluka), and natural indigo samples acquired from different manufacturers – namely Kremer, De Kat, and De

Spoel - all of which are declared to be manufactured from indigo plant *Indigofera tinctoria* L. Indigo is delivered in the form of a thin powder with differing grain sizes depending on the manufacturer.

“Mixed samples” include synthetic and natural indigo mixed with lead white (Kremer), linseed oil or both lead white and linseed oil. Lead white is basic lead carbonate $2\text{PbCO}_3 \cdot \text{Pb}(\text{OH})_2$, a white inorganic pigment that was commonly mixed with indigo to obtain lighter shades of the blue colour. The first set of sample was prepared in the laboratory. Indigo was mixed to lead white in different ratios (1/64 w/w, 1/32, 1/16, 1/8 and 1/4) and these mixtures were thoroughly ground in a mortar to obtain an homogeneous blend. Indigo and indigo/lead white mixtures were also blended in a droplet (a few microliters) of linseed oil and analysed immediately. The second set of samples was obtained from the collection of Ms. van Eikema-Hommes. These samples belong to a series of reconstruction experiments* that were undertaken to investigate variations induced in time by different parameters, such as the type of raw materials and their preparation, paint application, conservation and restoration treatments, light ageing, etc^{160, 44}.

The textile samples consist of two sets of dyed fibres: (1) wool fibres dyed with synthetic indigo in the laboratory (supplied by A. Quye, Edinburgh) and (2) wool fibres dyed with natural indigo from ancient Peruvian civilisation (supplied by A. Wallert, Rijksmuseum)⁶⁸. The first set of samples is part of a study conducted on the fading of fibres dyed with natural colouring materials.

6.2.2. Instrumental set-ups

Two instrumental set-ups were employed to perform LDMS studies of paint materials and paint cross-sections, one with a TOF-MS analyser and one with an ITMS analyser. For a detailed description of both instruments we refer to chapter 2.

Analysis were performed at two different wavelengths in the ultraviolet range: at 355 nm (Q-switched Nd:YAG laser) on the ITMS set-up and at 337 nm

* The complete collection of reconstructed samples includes various types of indigo (synthetic and natural) mixed in different proportions with different media (various types of oils, egg tempera, water, etc) and different types of additives (lead white, chalk, verdigris, smalt, etc). Samples were prepared in duplicate by application of the mixture on a cardboard with different layer thickness. Each sample was artificially aged under controlled conditions, a copy being saved as reference. These experimental specimens have been studied in parallel with case studies of seventeenth century Dutch paintings, notably concerning the use of indigo by Frans Hals.

(N₂ laser) on the TOF-MS set-up. Desorption and ionisation was performed directly (LDI) or with the assistance of a matrix (MALDI). Measurements were performed either in positive or in negative mode.

Comparative measurements were also performed with Direct Temperature Mass Spectrometry (DTMS) on a sector instrument Jeol SX102-102A (BEBE) to obtain better insight into the effects of ionisation and fragmentation processes. Samples are deposited at the tip of a direct insertion probe fitted with a resistively heatable platinum/rhodium (9/1) filament (100 µm diameter). The probe filament was temperature programmed to heat at a rate of 0.5 A min⁻¹ (approximately 8°C s⁻¹) to a final temperature of about 800°C. Ions were generated by electron impact ionisation (EI).

6.2.3. Sample preparation

Indigo samples were either analysed as thin particles absorbed at the surface of a stainless steel probe, or *in-situ* that is by direct LDI of the surface of the sample (cross-sections and fibres).

To absorb particles of indigo on the surface of the probe, a suspension of indigo in water was prepared and a few microliters were deposited with a pipette. Subsequent evaporation of the water vehicle left the particles adsorbed at the surface of the probe. Indigo/lead white mixtures are deposited onto the surface of the probe in a similar manner. Suspensions of pigment in (wet) uncured oil were deposited as a thin film on the probe. Surface tension keeps the fluid mixture in position during measurement (the surface of the probe is positioned vertically in the TOF-MS configuration). By accurate positioning of the probe under the laser beam individual particles of indigo (typically 10-50 micrometers) were easily targeted.

The other samples were analysed *in-situ*. For indigo-containing mixtures painted on a cardboard, touch-dry pieces of the paint film were cut out from the cardboard. The piece was then fixed to the surface of the probe with a droplet of Technovit (a light curing resin) to perform *surface analysis*. Alternatively the sample was embedded and sectioned to investigate as *cross-sections* clamped in the cavity of the probe. Wool fibres dyed with indigo were clamped at their two ends in the probe cavity. Individual fibres can be fastened in close contact with the metallic substrate provided that the two ends are correctly secured (see Chapter 4).

DHB (dihydroxybenzoic acid) was used as a matrix to perform MALDI experiments. With thin films of indigo on a probe, a solution of DHB in ethanol was deposited on top of the layer of indigo and left to dry. In this fashion, thorough

Chapter 6

and homogeneous blending of the matrix with the sample is not obtained, but the procedure is presumed to match closely the conditions of matrix deposition in the case of MALDI of paint cross-sections. For cross-sectioned samples, matrix (20 μ l of a 0.1M DHB solution in water) was deposited on the surface of the sample by means of a home-build nitrogen driven pneumatic spray system.

6.2.4. Mass calibration

A mass calibration for TOF-MS measurements was realised before each series of measurements to obtain optimal mass accuracy, especially in the presence of lead white. Two samples of polyethylene glycol (PEG) with a molecular weight distribution of averaging m/z 400 and 1000 respectively served as calibrant. MALDI measurements were performed with a mixture of a 1mM ethanol solution of PEG and a 1M ethanol solution of DHB. The mixture was deposited at the surface of the probe and the ethanol vehicle was left to evaporate. Calibration was realised with peaks from the DHB and the PEG at regular intervals in the m/z range [0-1500].

6.3. Analysis of synthetic indigo

6.3.1. LDI-TOF-MS

Synthetic indigo (Fluka) was analysed at low laser power density with the TOF-MS. A high degree of analytical reproducibility was observed. Figure 6.3 shows a characteristic LDI-TOF-MS experiment at low laser power density with spectral data averaged over 10 shots. This spectrum illustrates clearly that synthetic indigo desorbs and ionises satisfactorily at a UV wavelength of 337nm. Different types of ions are observed that correspond to different ionisation mechanisms. A first group of dominant peaks is assigned to the radical cation $M^{\bullet+}$ at m/z 262, the protonated molecule $[M+H]^+$ at m/z 263, the sodium adduct $[M+Na]^+$ at m/z 285 and the potassium adduct $[M+K]^+$ at m/z 301. At higher mass range we observe the sodiated dimer $[2M+Na]^+$ at m/z 547. The presence of these different types of indigo ions is evidence for simultaneous ionisation processes. $M^{\bullet+}$ is the result of multi-photon ionisation (MPI)^{* 161}. For protonated molecules, we propose that

* Ionisation potential of indigo has been measured in the gas phase to 7,31 eV (Bauer *et al.*) indicating that photon ionization requires at least two photons at UV wavelength of 337nm

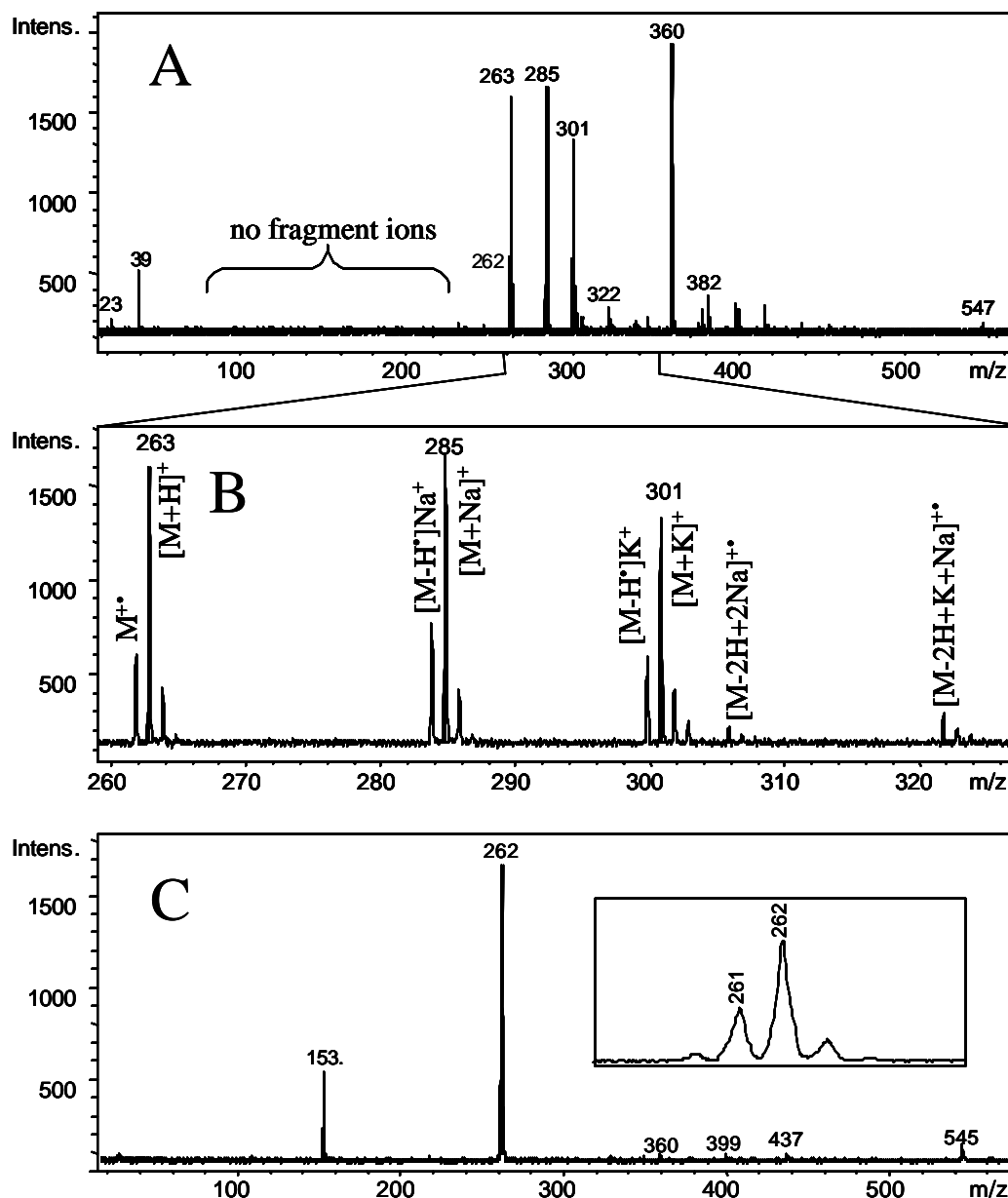


Figure 6.3 (A and B) LDI-TOF-MS in the positive mode of synthetic indigotin at low laser power; (C) LDI-TOF-MS in the negative mode.

indigo acts as its own proton donor. Lability of the hydrogen atoms in the indigo molecule is explained by the formation of an intramolecular oxygen-hydrogen bond, between $-CO$ and $-NH$ groups of the two heterocyclic rings (Figure 6.4). In all likelihood, stability of this structure is provided by the combined planar nature of the indigo molecule and its excited electronic state. The sodium and potassium

(3,68eV) and 355nm (3,49eV). Desorption and ionisation of indigo in the condensed phase most likely necessitates more than two photons.

adducts are explained by cationization with Na and K from salt contaminants in the sample or on the probe surface. This is supported by peaks at m/z 23 and 39 assigned to Na^+ and K^+ . Peaks at m/z 284 and 300 are assigned to the species $[\text{M}-\text{H}]\text{Na}^{2+}$ and $[\text{M}-\text{H}]\text{K}^{2+}$.

Formation of these ions is explained by formation of excited species $[\text{M}-\text{H}]^?$ followed by alkali addition¹¹¹. Supportive evidence is provided by the negative ion spectrum shown in Figure 6.3.C. Intense peaks at m/z 262 and 261 are assigned to the radical anion M^{2-} and to the deprotonated molecule $[\text{M}-\text{H}]^-$. Formation of $[\text{M}-\text{H}]^-$ results by electron capture from the intermediate species $[\text{M}-\text{H}^?]$. The great simplicity of the negative ion spectrum suggests that this mode is to be preferred for rapid identification.

An additional group of peaks in the positive mode at m/z 306, 322 and 338, is assigned to the species $[\text{M}-2\text{H}+2\text{Na}]^{2+}$, $[\text{M}-2\text{H}+\text{K}+\text{Na}]^{2+}$ and $[\text{M}-2\text{H}+2\text{K}]^{2+}$. We propose here a cation exchange during the ablation process (Figure 6.4). In this unusual ion formation mechanism, the two labile hydrogen atoms of the radical cation are exchanged for alkali cations present in the solid phase. The resulting ablated species are in all probability di-salts where the alkali is attached through an ionic bond.

An as-yet-unidentified peak in Figure 6.3.A is observed at m/z 360. In a higher mass range, related ions are observed at m/z 378 ($360+\text{H}_2\text{O}$), 382 ($360-\text{H}+\text{Na}$), 398 ($360-\text{H}+\text{K}$), 400 ($360+\text{H}_2\text{O}-\text{H}+\text{Na}$), 416 ($360+\text{H}_2\text{O}-\text{H}+\text{K}$). The

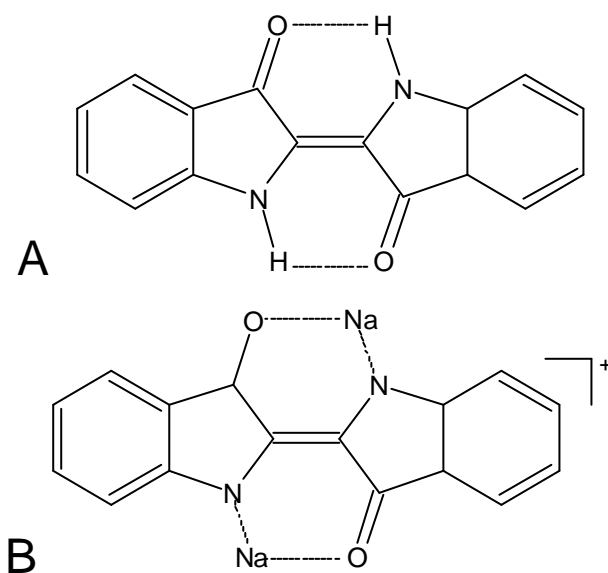


Figure 6.4 Cation exchange under laser MPI conditions leads to the substitution of hydrogen with sodium, potassium or lead atoms during the LDMS experiment.

relative abundance of these ions increases with a higher laser power. The presence of these adducts suggests that m/z 360 is the radical cation of an impurity in the indigo sample. Enhanced desorption and ionisation of this component by REMPI (resonance-enhanced multi-photon ionisation) at the particular wavelength used in the experiment is proposed to account for the high intensities. This hypothesis is supported by low voltage DTMS spectra, where a compound with a molecular weight of 360 is absent.

LDI-TOF-MS spectra obtained at low laser power do not display numerous characteristic fragment ions, as for instance in DTMS analyses. Synthetic indigo was therefore analysed at the maximum laser power density of the nitrogen laser (ca. $70\mu\text{J}/\text{pulse}$) in an attempt to induce fragmentation (spectra not shown). Predictably, the spectrum obtained under this condition shows a significant increase of the relative intensities in the range m/z [360-500]. In the mass range [0-300] however, no fragment ions could be detected with a relative intensity above 1%, giving evidence for a particularly soft ionisation mechanism.

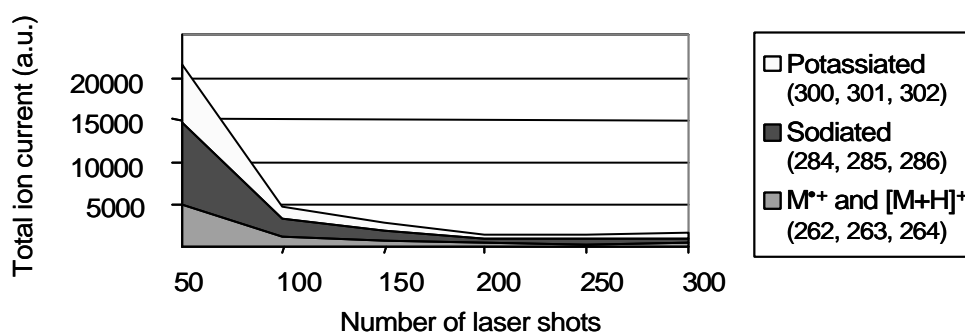


Figure 6.5 *Relative ion abundance in sequential bunches of 50 laser shots during LDI-TOF-MS of synthetic indigotin.*

LDI-TOF-MS of synthetic indigo was conducted for the duration of 300 laser shots at a fixed position of the probe surface. Spectra were averaged for cycles of 50 successive laser shots. Comparison of the mass spectra shows that the spectral information is quite reproducible in time. The ratio between the three principal peaks $[\text{M}+\text{H}]^+ / [\text{M}+\text{Na}]^+ / [\text{M}+\text{K}]^+$ stays approximately the same. In the course of the measurements the number of ions per shot (total ion current) decreases substantially. This is illustrated in Figure 6.5 by plotting the evolution in time of three prevalent groups of ions: $\text{M}^{\cdot+}$ and $[\text{M}+\text{H}]^+$ (with their corresponding isotopes*) for m/z 262, 263 and 264; $[\text{M}-\text{H}^{\cdot}]\text{Na}^+$ and $[\text{M}+\text{Na}]^+$ for m/z 284, 285 and 286; and $[\text{M}-\text{H}^{\cdot}]\text{K}^+$ and $[\text{M}+\text{K}]^+$ for m/z 300, 301 and 302. Figure 6.5 shows

* The peaks at 264, 286 and 302 correspond to the isotopic distribution of indigo, essentially due to the presence of the carbon isotope ^{13}C . ^{12}C and ^{13}C are in a 100:1.1 ratio.

Chapter 6

that the absolute intensity of these three groups of characteristic ions decreases with successive bunches of 50 shots. The total ion current of the different series of ions decreases proportionally with each other, and only moderate variations of the ratio between relative intensities are observed (<10%). The total ion current evens out at 1500 Da after 200 shots and sufficient signal is still observed after 500 shots.

Similar measurements signal averaged in smaller bunches of laser shots (1, 5 and 10 shots) confirm the initial downward slope of the curve. More than 40% of the ions are produced in the first 10 shots of a bunch of 50 laser shots. The decrease of the total ion current can be justified by sample consumption, but we believe that the modification of the surface condition of the sample also contributes significantly to this phenomenon. From these experiments we come to the conclusion that best analytical information is recorded during the initial laser shots. When sufficient density of material is present at the surface of the probe, it is possible to move the sample to offset the diminution of relative intensity. This alternative is however not conceivable in the case of spatially-resolved analysis of heterogeneous materials where moving the sample often implies a different analyte composition.

6.3.2. MALDI-TOF-MS

As expected, peaks dominating the LDI spectra are also observed in the MALDI spectra (Figure 6.6): m/z 262, 263, 264 for the radical cation and protonated molecule; m/z 284, 285, 286 for the sodiated species; m/z 300, 301, 302 for the potassiated species. The ions at m/z 360, 361, m/z 378, 382, 398, 400 and 416 remain unidentified. The relative ratio between radical cations and protonated molecules is comparable to the LDI spectra. This is evidence supporting the

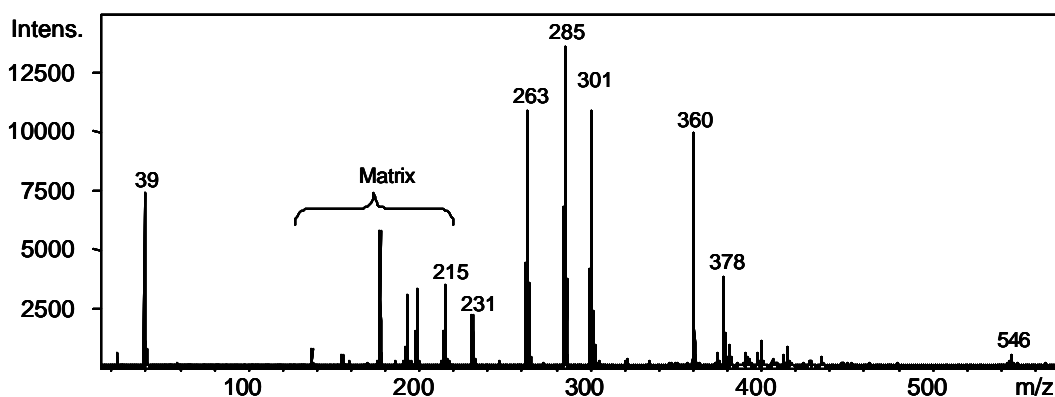


Figure 6.6 MALDI-TOF-MS of synthetic indigotin.

ionisation mechanism proposed for LDI with dominant proton transfer from indigo itself (indigo acting as its own matrix). The absolute intensity in MALDI is only moderately higher than in LDI. Typically the factor of amplification of the signal goes from 1,5 to 5. This difference is attributed to the fashion in which the matrix mixes with the analyte after surface deposition. The ratio of the sodium and potassium adduct to the protonated indigo was found to be roughly similar. Thus, the use of a MALDI matrix does not significantly improve the analytical information. On the contrary it introduces peaks characteristic of the matrix, which may complicate the interpretation of the spectra in unknown samples.

6.3.3. Multiple-stage LDI-ITMS

Synthetic indigo was further investigated by multiple-stage mass spectrometry (MS^n) with the ITMS in order to get a better insight into the fragmentation pattern. In the ITMS experiment, the sample was desorbed and ionised with a Nd:YAG laser working at 355 nm. At low laser power, indigo desorbs satisfactorily, supporting the observation that the molecule is a good chromophore in this ultraviolet range. Figure 6.7 shows the LDI-ITMS spectrum of indigo at low laser power. The spectrum displays dominant peaks for the protonated molecules $[M+H]^+$ at m/z 263 and the radical cation M^{2+} at m/z 262.

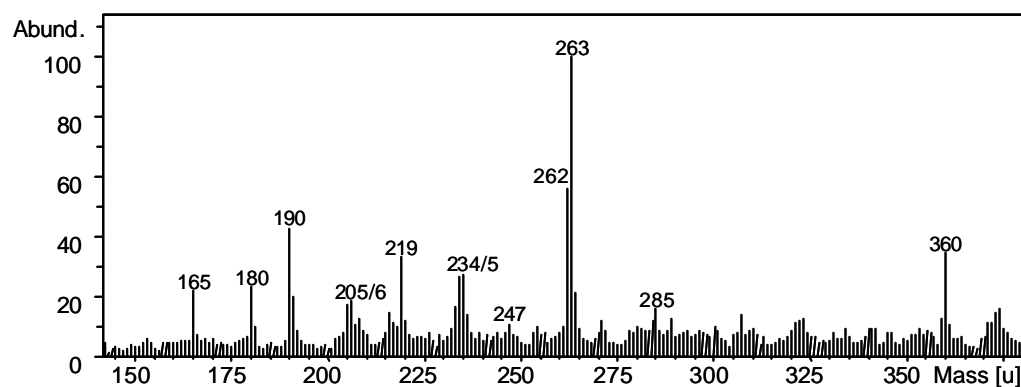


Figure 6.7 LDI-ITMS of synthetic indigotin at low laser power

Fragment ions were assigned as follows: $[M+H-CO]^+$ at m/z 235 and $[M-CO]^+$ at m/z 234, $[M-2CO]^+$ at m/z 206 and $[M-H-2CO]^+$ at m/z 205. Assignment of the peak at m/z 219, which corresponds to a loss of 43 Da, is not straightforward (see below). Peaks at m/z 165, 180 and 190 remain unidentified.

An MS^n experiment was performed by first isolating protonated molecules at m/z 263, followed by collision-induced dissociation (CID)*. Figure 6.8 shows the result of a MS^n experiment conducted in four stages. CID of the protonated molecule in Figure 6.8.A yields $[M-CO]^+$ at m/z 234, $[M-2CO]^+$ at m/z 206, and $[M-CO-COH]^+$ at m/z 205. The peak at m/z 246 is not identified. The presence of a peak at m/z 219 confirms this ion as a fragmentation product of indigo and is not an impurity. We propose a loss of $[CHNO]$ from the molecular ion, but this cannot be verified with current experiments. CID of the isolated fragments at m/z 234 and 235 in Figure 6.8.B yields $[M-CO-COH]^+$ at m/z 205 and $[M-2CO]^+$ at m/z 206. CID of fragment ions m/z 205 and 206 in Figure 6.8.C yields fragment ions at m/z 178 with an assigned elemental composition $C_{13}H_8N$. The peaks at m/z 169 and 196 remain unidentified.

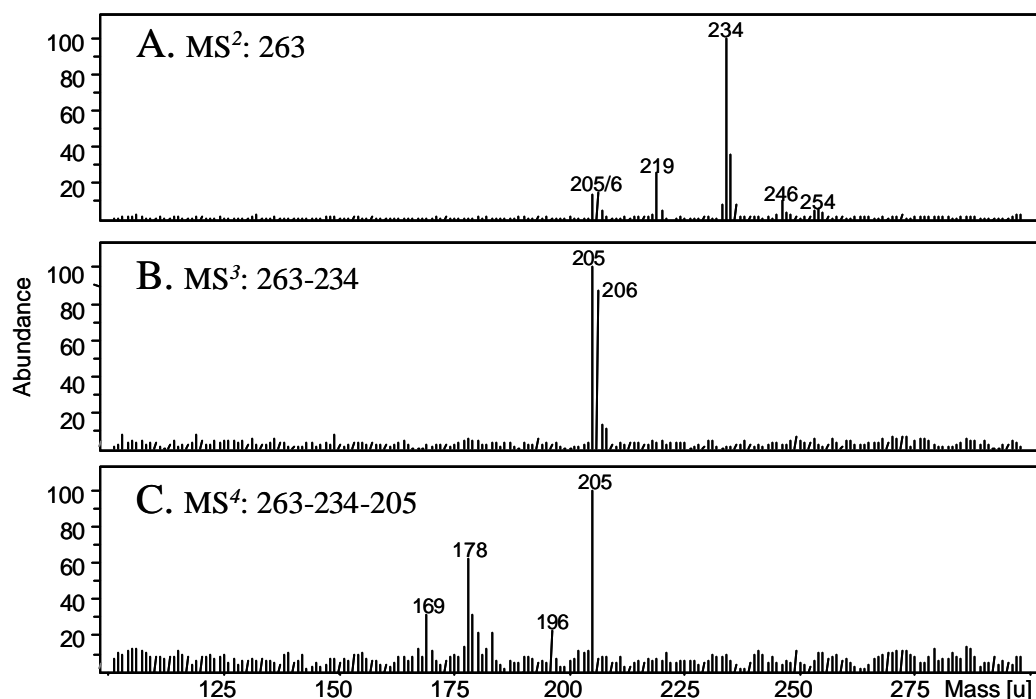


Figure 6.8 Multiple-stage LDI-ITMS of synthetic indigotin (Fluka): (A) MS^2 of the protonated ions at m/z 263, (B) MS^3 of the fragment ions of m/z 263 at m/z 234, and (C) MS^4 of the fragment ions of m/z 234 at m/z 205.

* The isolation capabilities of the ITMS in this experiment have a mass range of approximately 10Da, which means that the protonated molecule is not isolated from the radical cation. Spectra of the isolated species revealed however a minor contribution of the radical cation. In the CID experiment only protonated molecules at m/z 263 are excited and fragmented.

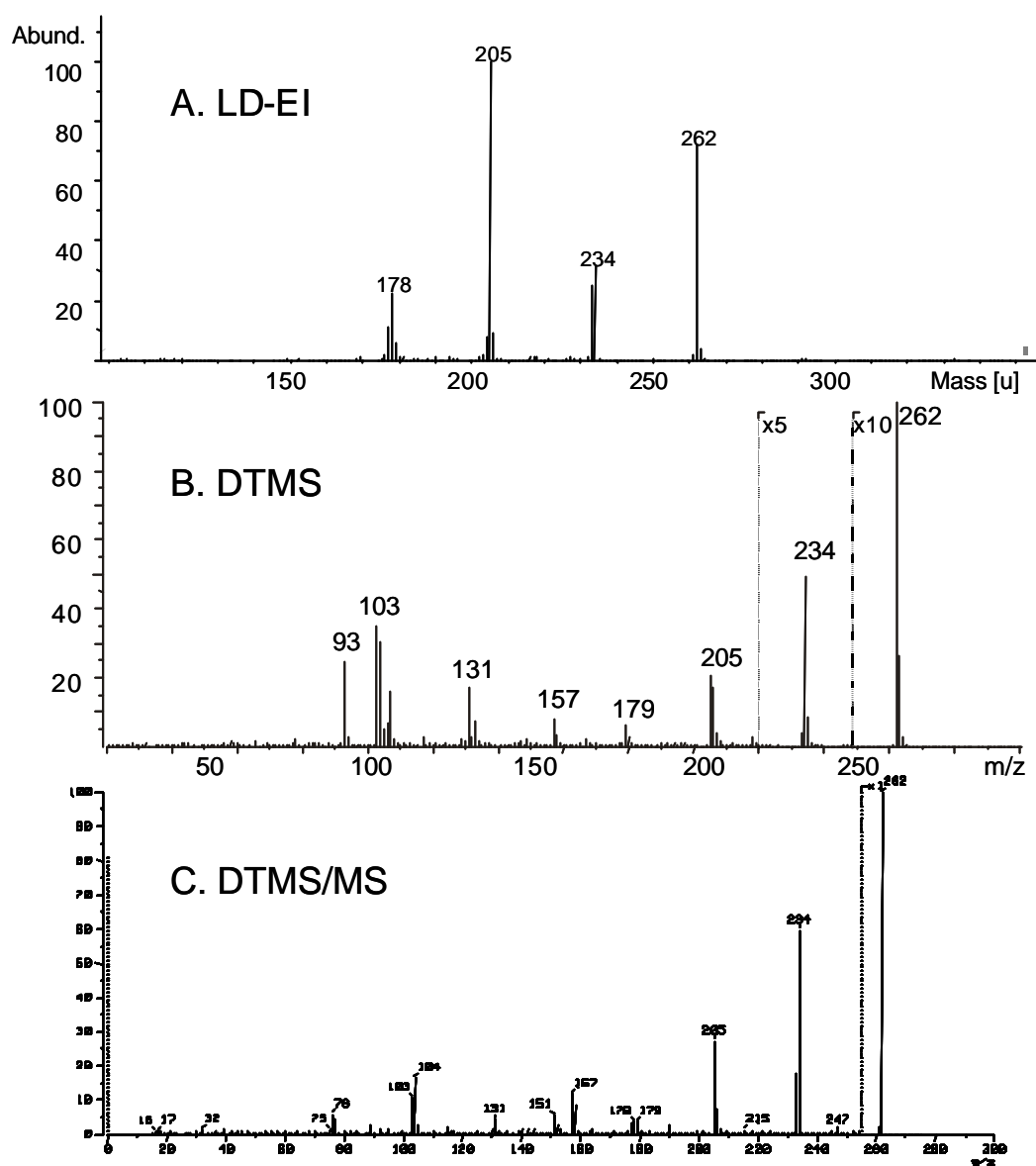


Figure 6.9 (A) *LDI-post EI*, (B) *DTMS* and (C) *DTMS/MS* of synthetic indigotin (Fluka).

Chapter 6

6.3.4. LD-EI with the ITMS

When post-EI ionisation (25eV) is used, the spectrum of synthetic indigo (Figure 6.9.A) displays four major peaks at m/z 178, 205, 234 and 262. Additional peaks are observed at 115 and 138, 165. These results are in good agreement with EI proposed by Gibbs *et al.*¹⁵⁸ and DTMS(/MS) with 16eV EI ionisation (Figure 6.9.B and C).

6.3.5. Conclusion

In this series of experiments, LDMS proves to be a successful technique for the investigation of synthetic indigo. An UV laser beam employed at a low power density produces soft ionisation that affords positive identification of the molecular species. LDI-TOF-MS spectra display intense peaks for protonated, sodiated and potassiated species. Negative ion spectra are simpler in appearance, with only one peak for indigo. Use of a DHB matrix did not improve the analytical information. Fragmentation is negligible under the TOF-MS conditions but is observed in ITMS experiments where the analyte is subjected to higher internal energy deposition conditions. The use of multiple-stage MS in the ITMS made it possible to follow the fragmentation route in a MS^4 experiment.

6.4. Analysis of natural indigos

Natural indigo is the manufactured product obtained from the transformation of plant materials. According to the biological source and the manufacturing process various additional compounds may be present in the resulting pigment. In the following experiments, a series of three natural indigo pigments obtained from different suppliers were analysed by LDMS under the same conditions. The three pigments are reportedly obtained from the same biological source (indigo-plant *Indigofera tinctoria* L.), but details of their manufacturing process have not been disclosed to us.

Figure 6.10.A displays the LDI-TOF-MS spectrum of natural indigo (de Kat) measured at low laser power density. In comparison with synthetic indigo, only a negligible contribution of sodium and potassium adducts (respectively at m/z 285 and 301) is observed indicating that lower concentrations of these alkali are present in the sample. The unidentified peak at m/z 360 detected earlier in

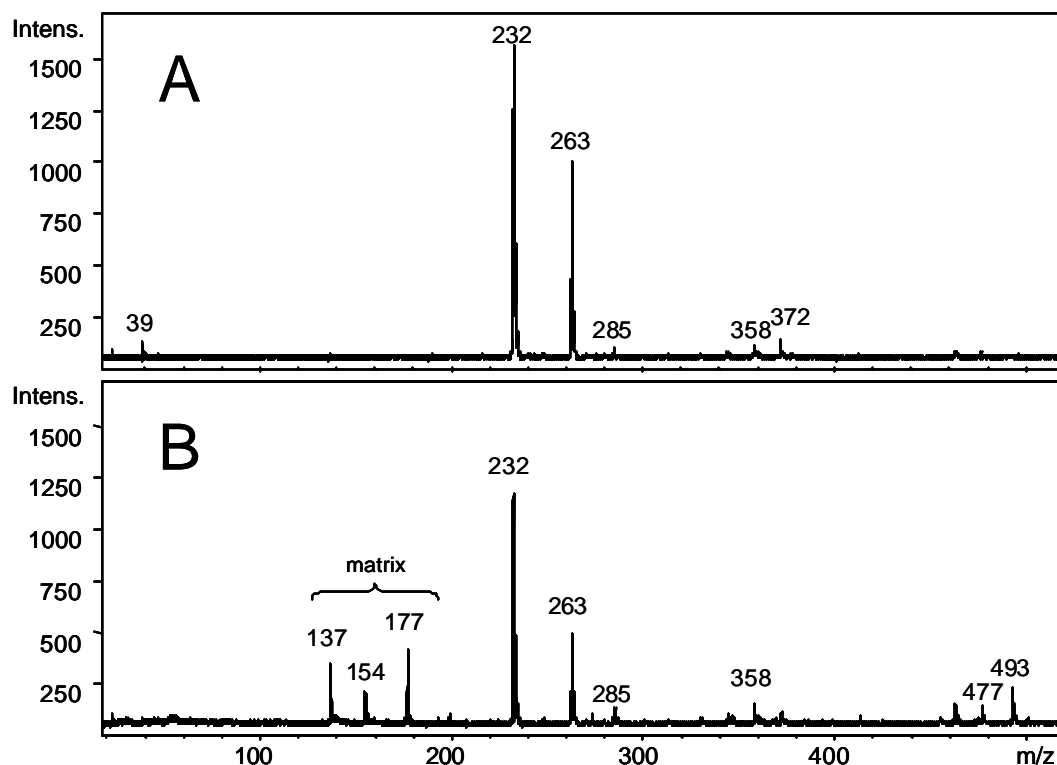


Figure 6.10 (A) LDI-TOF-MS and (B) MALDI-TOF-MS of natural indigo (*de Kat*).

synthetic indigo has here much smaller ion intensity. Natural indigo displays a dominant peak at m/z 232 that remains unidentified. Since this ion is also observed in DTMS experiments, we strongly suspect the presence of an additional compound. Presence of a peak at m/z 232 in MALDI spectra (Figure 6.10.B), where the formation of fragments ions is not likely, strongly supports this assumption. As is the case for synthetic indigo, MALDI spectra closely match the LDI spectra. Sodium and potassium adducts (m/z 285 and 301) as well as species observed in the range [450-500] have a higher intensity. The negative mode spectra reveal peaks at m/z 261 and 262 for the deprotonated molecule and radical anion.

On the basis of LDI and MALDI-TOF-MS analyses, no molecular signature could be identified in natural indigo that would identify the different manufacturers (De Spoel and Kremer). It is supposed that the unidentified m/z 232 ions is not the product of indigo fragmentation but rather an additional compound which production is enhanced in LDI. It may therefore possibly serve as marker for indigos of natural origin.

6.5. LDMS of indigo at the surface of dyed fibres

In fibres dyed with indigo, the colouring material is fixed to the fibre by oxidation in air, and no mordant is used. Since LDMS of indigo is relatively straightforward, we have investigated whether indigo present at the surface of a fibre can be desorbed and ionised in an LDI experiment.

Two sets of dyed fibres were analysed in a spatially-resolved experiment: (1) wool fibres dyed in the laboratory with indigo (unspecified origin) and (2) wool fibres dyed with natural indigo (uncertain biological origin) from an ancient Peruvian civilisation⁶⁸. Accurate aiming of the laser made it possible to interrogate one single fibre (10-30 μ m).

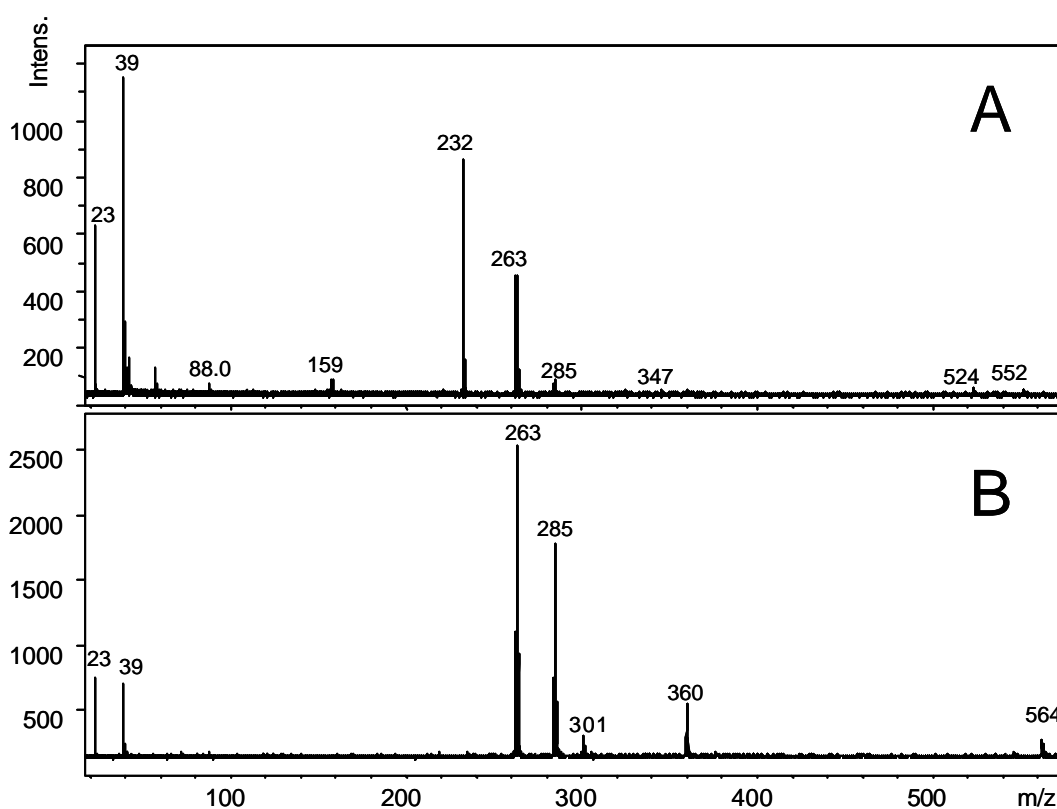


Figure 6.11 LDI-TOF-MS of (A) wool fibres dyed in the laboratory with indigo (B) wool fibres dyed with natural indigo from ancient Peruvian civilisation (sample provided by A. Wallert).

A bunch of wool fibres dyed in the laboratory with indigo were analysed by sampling one single spot and averaging the mass spectral information over 25 shots. Characteristic spectra were obtained near the LDI density threshold, but LDI at slightly higher power densities visibly improve the signal-to-noise ratio. The LDI spectrum (Figure 6.11.A) displays a particularly clear distribution of peaks

with characteristic ions readily attributed to natural indigo (m/z 232, 263, 285 and 524). A mass shift (up to ca. 1 mass unit) was observed in certain positions of the sample, and that required internal calibration after analysis. The poor mass accuracy was attributed to the position of the fibre on the probe. The part of the fibre sampled during LDMS might significantly bulge out of the probe cavity, inducing a shift in the time of flight (see section 3.2.). Experiments were also conducted with one single fibre clamped on the probe. Results are identical, although the relative intensity of the ions is strongly diminished, which makes the identification of the dyestuff less certain.

LDMS of wool fibres dyed with natural indigo from ancient Peruvian civilisation were successful as well. Figure 6.11.B shows the LDI-TOF-MS of indigo samples directly from the surface of one single fibre. Characteristic peaks are found at 262 $[M]^{2+}$, 263 $[M+H]^+$, 284 $[M-H^2]Na^+$, 285 $[M+Na]^+$, 300 $[M-H^2]K^+$, 301 $[M+K]^+$, 360. The spectrum is very clear and no degradation product could be identified here. The absence of a peak at m/z 232 combined with the presence of a peak at m/z 360 questions the authenticity of the natural origin of the indigo.

In conclusion, LDMS appears to be a suitable technique for rapid *in-situ* identification of indigo at the surface of dyed fibres. The procedure does not necessitate any preparation of the analyte. The analytical method is non-destructive, and does not necessitate prior extraction or derivatization of the dyestuff. At low laser power, indigo desorbs preferentially and spectra positively attest the presence of indigo. No interference is observed from the fibre material. Although analysis of an individual fibre is possible, analyses will be preferentially performed with multiple fibres. Positioning in the sample holder is much easier than for an individual fibre, and aiming of the laser is simplified because of the larger surface of material exposed.

6.6. LDMS of indigo in oil paint

In paintings, indigo is rarely used as a pure substance but occurs in mixtures with other painting materials. Because the presence of the additional paint materials might influence the LDI behaviour of the blue organic pigment, we explored LDMS of indigo in the presence of (1) lead white (basic lead carbonate), an inorganic pigment and drier of oil paint, and (2) linseed oil, a prevalent medium used in easel painting. Samples consist of indigo mixed with either lead white or with oil, and with both lead white and oil. Reconstructions were made on artists' board painted with thin films of such mixtures.

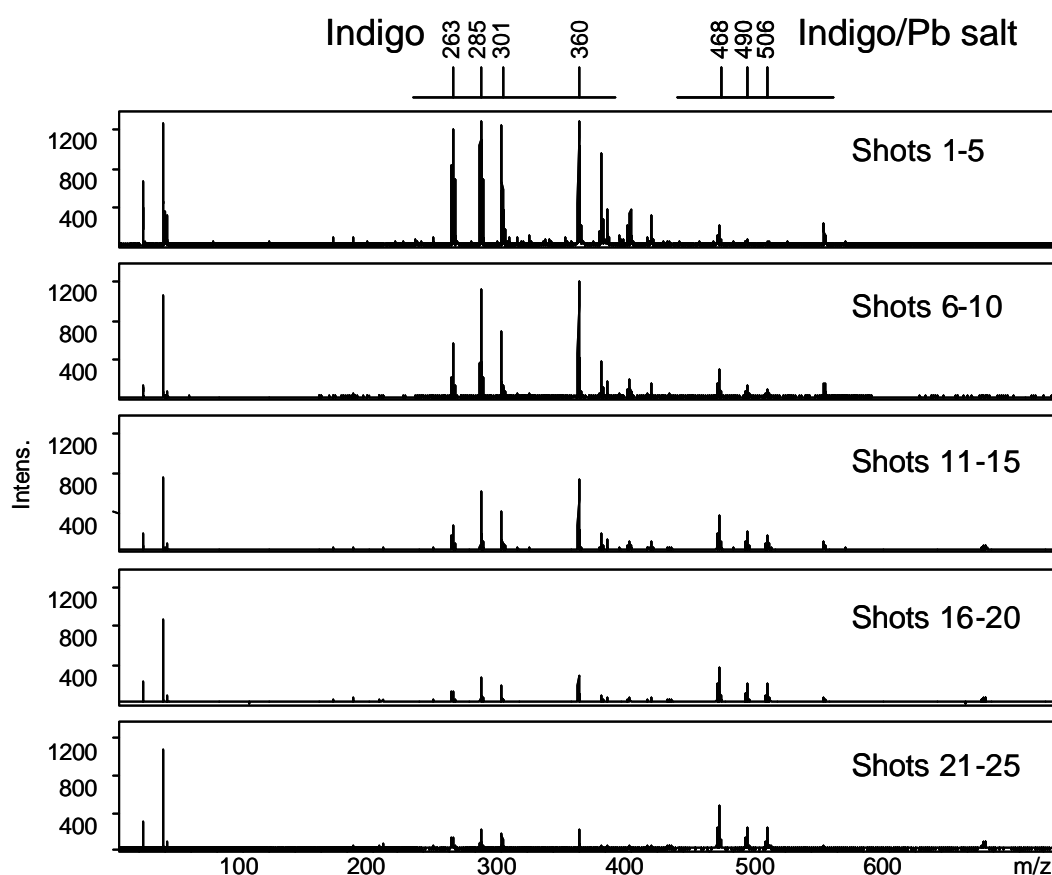


Figure 6.12 *LDI-TOF-MS of a 1:8 (w/w) indigo/lead white mixture. In the first shots indigo is predominantly observed with peaks corresponding to protonated (m/z 263), sodiated (m/z 285), and potassiated (m/z 301) species. Later, indigo is observed as indigo-lead salts (m/z 468, 490 and 506).*

These complex samples were investigated by LDI and MALDI-TOF-MS in different forms: (1) no preparation; (2) paint material removed from its support (carved out with a scalpel), ground, and prepared as a suspension in water; (3) paint material removed from its support, embedded in a supportive resin and cross-sectioned. Reference spectra of pure lead white were acquired in LDI and MALDI-TOF-MS for comparison (data not shown).

6.6.1. LDMS of indigo/lead white mixtures

The first LDI-TOF-MS experiment concerns a 1:8 (w/w) synthetic indigo/lead white mixture. Analysis was conducted at low laser power density with multiple laser shots in close succession (frequency of ca. 2Hz) on one fixed position in the sample. A series of spectra were registered averaging mass spectral

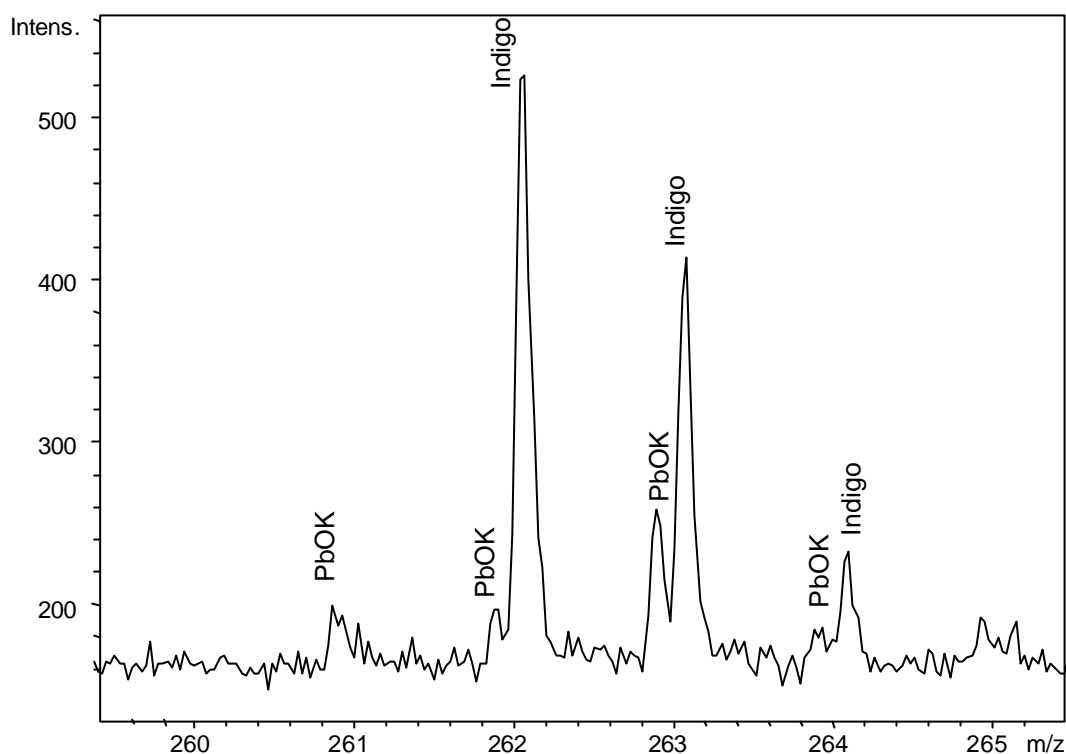


Figure 6.13 LDI-TOF-MS of a 1:8 indigo/lead white mixture in the mass range m/z [260-265], showing the isotopic distribution of $PbOK^+$ and indigo.

information for every 5 laser shots. From this set of spectra (Figure 6.12), different characteristic features of LDMS of indigo/lead white mixtures can be pointed out.

At low laser density, desorption and ionisation is intense showing a good response at the UV laser wavelength (337nm). Surprisingly, the spectral information significantly varies in time. In the first spectrum averaging the initial five laser shots, the molecule of indigo can be readily identified. Characteristic peaks at m/z 262, 263 and 264 can be assigned to the radical cation and protonated molecule; m/z 284, 285 and 286 are assigned to sodiated species; m/z 300, 301 and 302 are assigned to potassiated species. We also observe the unidentified species at 360 and 361, 382 (360-H+Na) and 398 (360-H+K). At this stage, characteristic peaks for lead white are observed with very low relative intensity.

In the following shots with the same power density, the absolute intensity of the diagnostic ions of indigo decreases significantly, whereas the intensity of the lead white derived ions increases. Notice in Figure 6.13 that TOF-MS provides the necessary resolution to separate $[PbOK]^+$ from indigo, which shows up in the same mass range with a theoretical difference of only 0.14 m/z (Table 6.2). The LDI of lead white itself produces a broad set of characteristic ions assigned to the lead ion

species	m/z*	species	m/z	species	m/z
Pb ⁺	208	(PbO) ₄ ⁺	894	(PbO) ₅ K ⁺	1155
(PbO)Pb ⁺	430	(PbO) ₄ Na ⁺	917	(PbO) ₆ ⁺	1340
2PbO ⁺	446	(PbO) ₄ K ⁺	933	(PbO) ₄ Pb ₂ O ₃ ⁺	1356
(PbO) ₂ Pb ⁺	654	(PbO) ₅ ⁺	1116		

Table 6.1 Dominant lead white derived ions detected in a LDI-TOF-MS analysis of a 1:8 indigo/lead white mixture (* m/z of the most abundant isotopic peak is indicated).

Isotope	Indigo		PbOK	
	Da	relative int.	Da	relative int.
M	262.07	83	260.93	22
M+1	263.07	15	261.93	20
M+2	264.07	2	262.93	50

Table 6.2 Theoretical isotopic distribution of indigotin C₁₆H₁₀N₂O₂, and PbOK.

(m/z 207) and various lead oxides (see Table 6.1). The presence of lead in these compounds is easily identified because of the characteristic isotopic distribution of the lead atom*. We speculate that the great variety of lead related species is the result of laser induced chemical reactions in the ablation region. The presence of Pb⁺ points to redox processes. The appearance of elemental Pb on the surface has been proposed in a study of the reduction mechanism induced by an IR laser by Pouli *et al.*¹⁶². It is also known that PbO is formed when lead white is heated at low temperature and that higher temperature converts PbO to Pb₃O₄¹⁶³. We suggest that lead white decomposes after repeated exposure of the lead white to the UV laser into PbO and PbCO₃ by releasing water and CO₂. Clusters of PbO are indeed seen in the spectra (see Table 6.1). It is unclear whether Pb⁺ is produced directly from Pb²⁺ or indirectly from metallic lead. Further evidence for changes in the surface composition is deduced from the presence of sodiated and potassiated lead oxide clusters.

* Abundance for isotopic peaks of lead is as follow: ²⁰⁴Pb (1,4%) ²⁰⁶Pb (24,1%) ²⁰⁷Pb (22,1%) ²⁰⁸Pb (52,4%).

With the increase of the number of laser shots the ions indicative of salt $[M-H^2]Pb^+$ become more prominent in the spectra with a multiplet of peaks ranging from m/z 467 to 471 (m/z 469 is the highest peak). Peaks at m/z 491 and m/z 507 correspond to a mass difference of 22 and 38 Da respectively. These peaks are attributed to the ions $[M-2H+Pb+Na]^+$ and m/z 506 $[M-2H+Pb+K]^+$. Similarly, a peak at m/z 674 is assigned to $[M-2H+2Pb]^+$. The isotopic distributions of these ions closely match the theoretical distribution (Figure 6.14). Formation of these ions is in good agreement with the mechanism proposed earlier (section 6.3.1.) in which indigo form bridges with metal ions. $[M-H^2]Pb^+$ is formed by addition of lead to the species $[M-H^2]$. Other indigo containing ions are explained by the cation exchange mechanism proposed above (Figure 6.4), which results in the substitution of one or two labile hydrogen atoms. Whereas the abundance of sodium and potassium substituted species decreases with the succession of laser shots, the abundance of mono and di-lead substituted species increases.

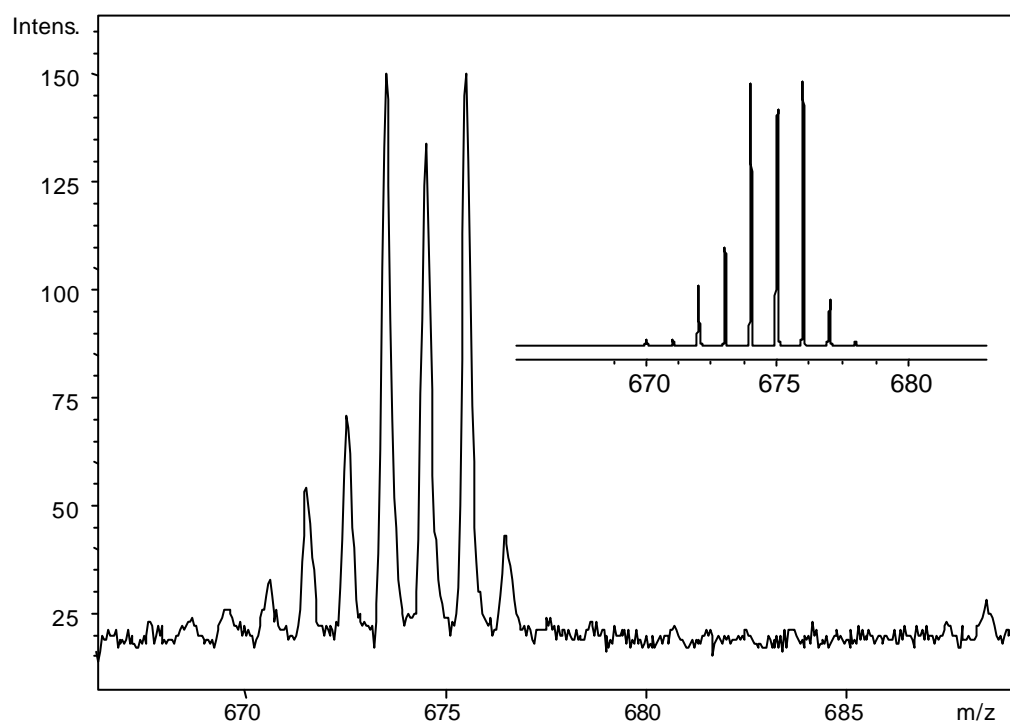


Figure 6.14 *LDI-TOF-MS of a 1:8 indigo/lead white mixture in the range m/z [665-690]. Isotopic distribution of the series of peaks around m/z 675 matches the theoretical distribution of $[C_{16}H_{10}N_2O_2-2H+2Pb]^{2+}$ shown in inset.*

Evolution in time of the mass spectral signal for the 1:8 indigo/lead white mixture is illustrated in Figure 6.15, which shows the total ion current (TIC) for two groups of pseudo-molecular ions of indigo: sodium adduct species (m/z 284-286), and lead adduct species (m/z 466-469). The summed TIC of the Na adducts

decreases over the successive laser shots, whereas the lead adducts increase. This is evidence for a preferential desorption of the indigo molecule in the first laser shots, followed by the appearance of newly formed lead complexes. This delay in detection supports the assumption that formation of lead species results from laser-matter interaction in the condensed-phase during experiments with multiple laser shots in close succession. We suspect that this interaction depends on the energy deposition during the LDI process. In the following experiments the sample was therefore investigated at different laser power densities averaging a fixed number of shots.

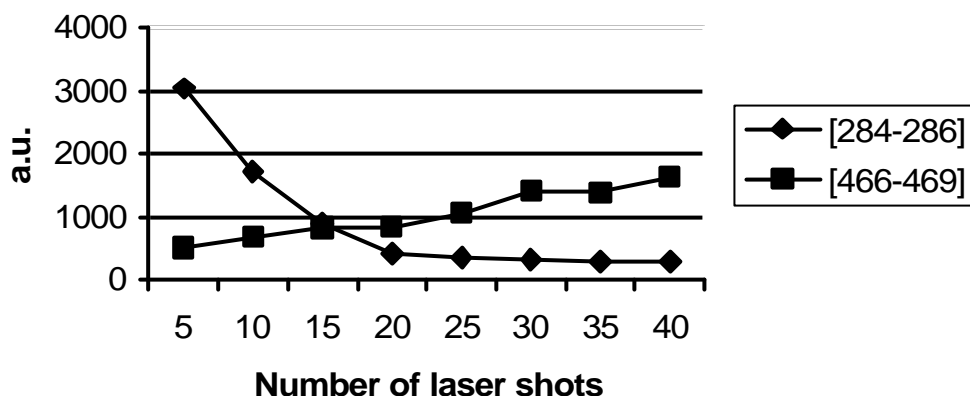


Figure 6.15 LDI-TOFMS of a 1:8 indigo/lead white mixture: total ion current of indigo pseudo-molecular ions: sodiated species (284-286) and lead species (466-469).

6.6.2. Effect of laser power density

The desorption and ionisation process for an indigo/lead white mixture (1:16) was investigated in a LDI-TOF-MS experiment at different laser power density, as illustrated in Figure 6.16. The relative contribution of ions derived from the lead white increases with higher laser power density. Absolute intensities of sodiated indigo species decrease whereas absolute intensities of lead-adduct indigo species increase. The species with lead and sodium (at m/z 490) and lead and potassium (at m/z 506) maximise at attenuation 29 with no increase after attenuation 20. This feature is explained by a higher laser-matter interaction at high energy. The stronger increase in relative intensity of Pb^+ in comparison with Na^+ and K^+ gives statistically more probability of a lead substitution.

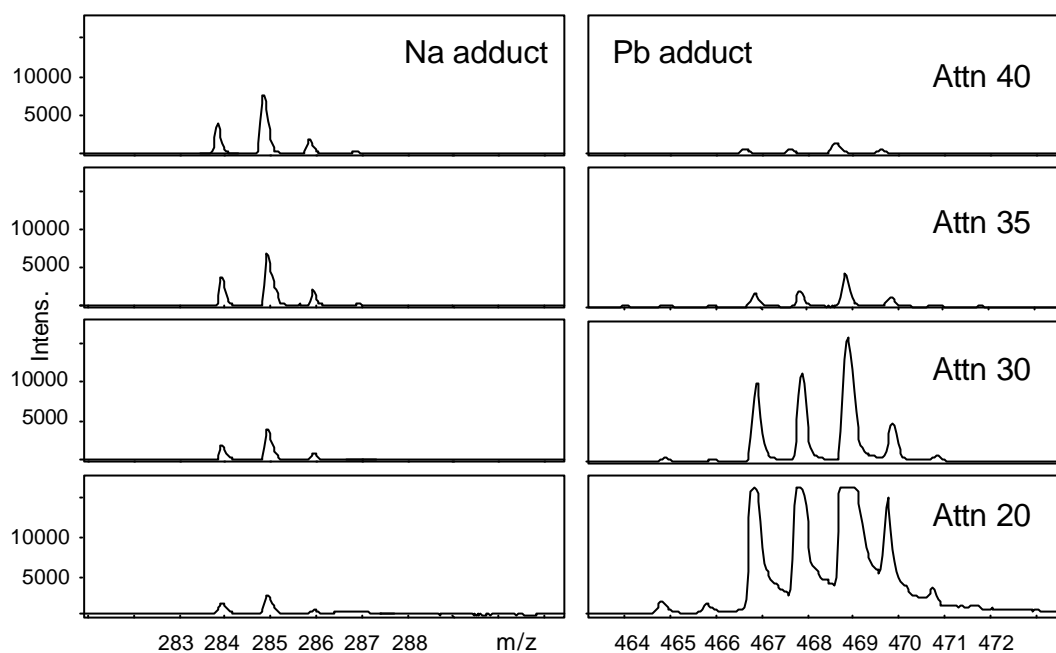


Figure 6.16 *Effect of the laser power density on the formation of Na and Pb adduct and substituted species: sodiated species decrease with increasing laser power density, whereas lead species increase dramatically (the detector saturates at attn 20).*

6.6.3. Influence of the ratio of lead white to indigo

A set of samples with natural indigo (de Kat) and lead white in different ratios was analysed by LDI-TOF-MS as shown in Figure 6.17. The set includes natural indigo and pure lead white, plus mixtures of the two compounds in ratio of indigo to lead white 1:4, 1:8, 1:16, 1:32 and 1:64 (w/w). A low amount of lead white, e.g. 1 to 4 (indigo/lead white) does not affect the mass spectrum of indigo very much. Since natural indigo is used we see the m/z 232 as a major peak (see section 6.4). Indigo become less obvious to identify in the spectrum of the sample with the ratio 1:32. The spectrum of pure lead white shows lead, lead oxide and lead oxide clusters with sodium and potassium. These same ions begin to appear in the spectrum of a mixture with a 1:8 ratio of indigo to lead white. Evidence for indigo lead $[M-H^2]Pb^+$ at m/z 469 is recognizable in the mixtures with the ratios 1:4 to 1:32.

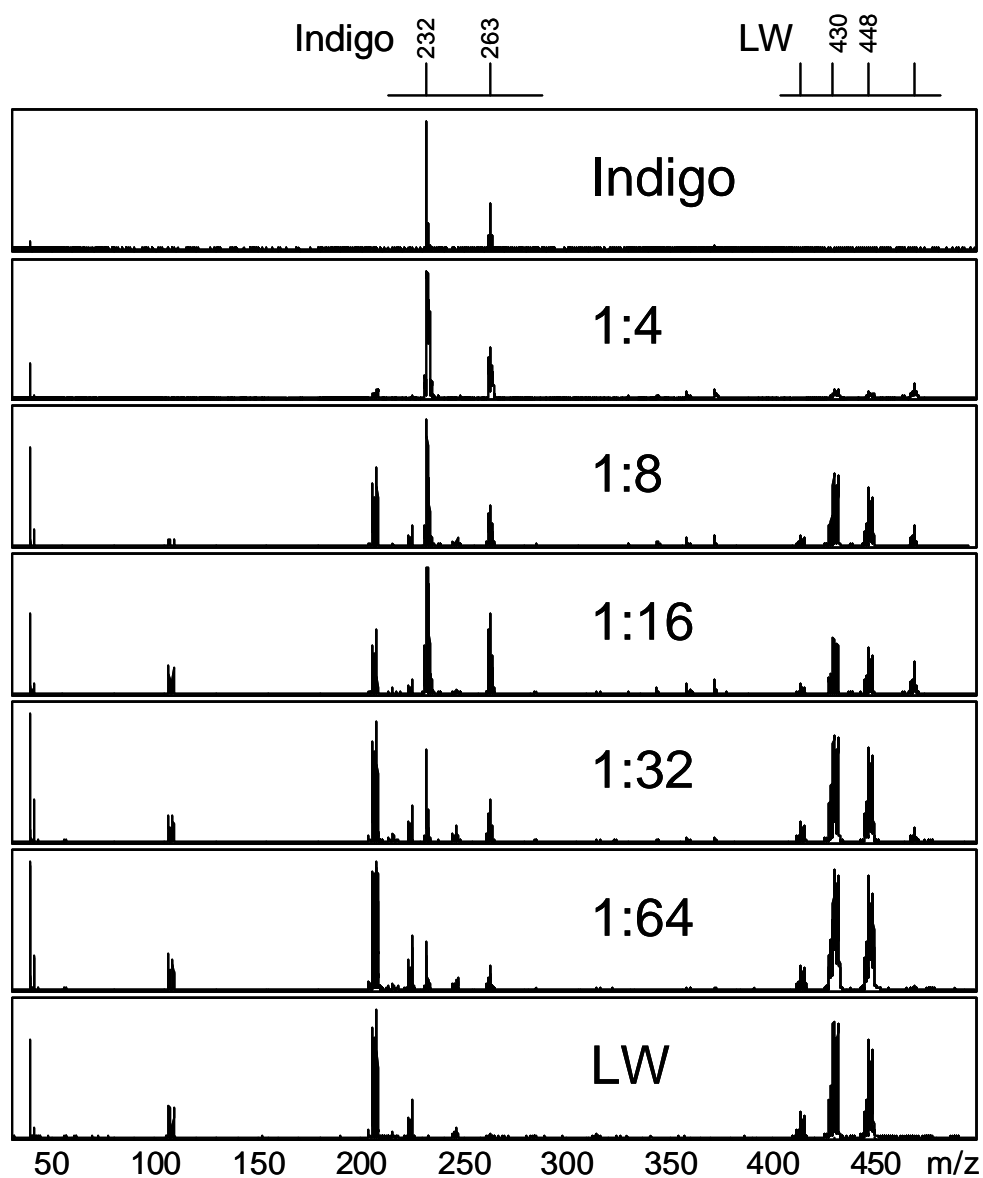


Figure 6.17 *Semi-quantitative analysis of natural indigo and lead white (LW) mixtures.*

6.6.4. LDMS of aged indigo/linseed oil mixtures

Two reconstructed films of indigo in oil were investigated by LDMS. The first sample (supplied by M. Eikema) was prepared with 1g of synthetic indigo mixed in 1.5 ml cold pressed linseed oil, painted on artist's board, and artificially aged. The second sample is a reconstructed mixture of synthetic indigo in cold pressed linseed oil (originating from the Von Imhoff collection kept at the

Canadian Conservation Institute, Ottawa) that has undergone a natural ageing of 25 years old. In both cases, a chip of the paint layer was carved out of the support and either analysed as such (*in-situ*) or was finely grounded in a mortar and deposited on the surface of the probe as a suspension in water.

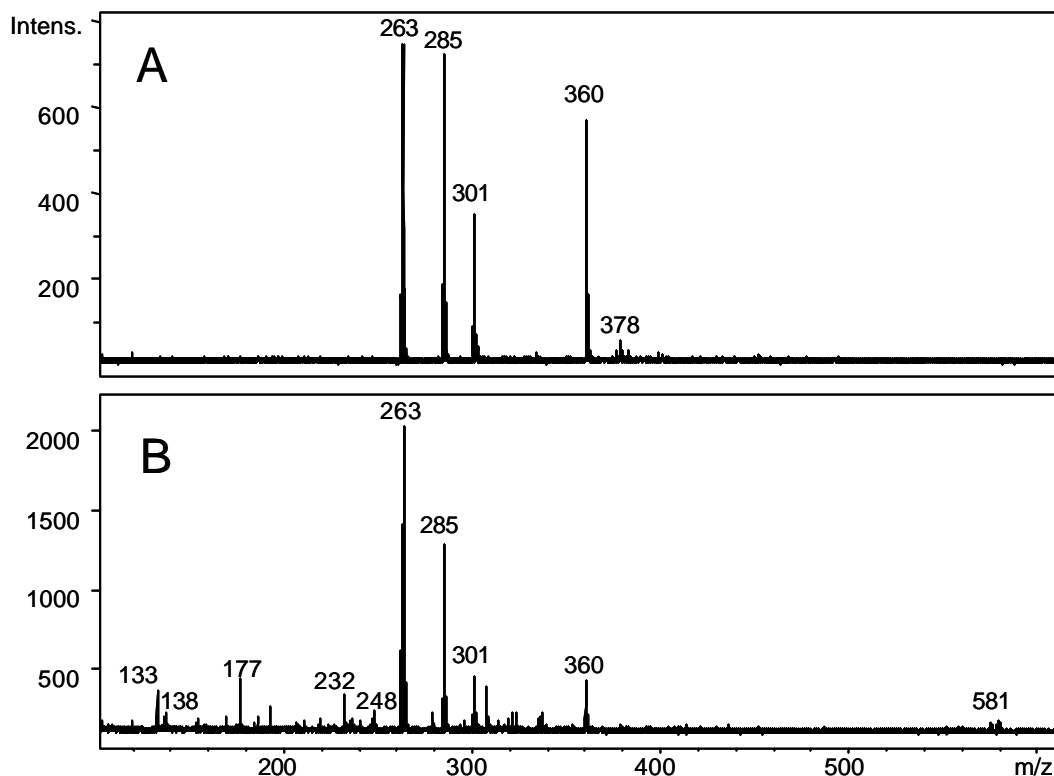


Figure 6.18 LDI-TOF-MS of synthetic indigotin mixed in oil: sample artificially aged (A) and sample naturally aged for 25 years (B).

The LDI-TOF-MS spectrum of the first sample by averaging on 10 laser shots is shown in Figure 6.18.A. It displays a series of peaks that can be readily attributed to indigo and afford its positive identification. Characteristic ions are found at m/z 262, 263, 284, 285, 300, 301, 334, 360, 378, and 398. No molecular signature relating to ageing could be identified. The spectrum is particularly clear, displaying no fragment ions or dimers. In the negative mode an intense peak at m/z 262 supports this identification. MALDI of the cardboard after spraying with DHB also leads to positive identification thanks to peaks at m/z 263, 284, 301, 360, but no additional structural information was identified.

The LDI-TOF-MS spectrum of the second sample is shown in Figure 6.18.B. Again, indigo is readily identified with peaks at m/z 262, 263, 284, 285, 300, 301, 306, 322, 360. When the sample is ground and deposited as a suspension, the absolute intensity of the signal is threefold higher. Peaks at m/z 232 and 248 suggest the presence of degradation products. Tryptantrin (m/z 248), a degradation product of indigo, has been identified by DTMS and HPLC in aged indigo¹⁵⁶. The

presence of m/z 232 suggests at this stage that the ion could be a degradation product of indigo.

6.6.5. LDMS of an indigo/linseed oil/lead white mixture

Two types of reconstructed samples of indigo/lead white/oil mixtures were investigated by LDMS analysis.

The first sample was prepared in the laboratory by mixing indigo and lead white (1:16 w/w) and then adding a droplet of linseed oil to this mixture. This mixture made with *uncured* oil was directly deposited on the probe for LDI-TOF-MS. The spectrum was recorded for a period of 60 laser shots (60s) averaging the mass spectral data for every 5 shots. In the first spectrum corresponding to the initial 5 laser shots, indigo can be identified as main component with peaks at m/z 263, 285, 301 and 360. This observation is supported by the mass spectrum in the negative mode with a peak observed at m/z 262. In the subsequent spectra however, no characteristic ions of indigo are observed anymore and only lead-related peaks are present. The absolute intensity of the lead peak Pb^+ increases as shown in Figure 6.19. Delay in the formation of Pb^+ can be justified by the necessary thermal effect of repeated laser shots in close succession. In this case no lead adducts of indigo were observed. This result demonstrates that indigo desorbs preferentially in the first laser shots, but soon leaves way to lead related species. We propose that after surface ablation in the first shots, no more indigo is present at the surface. In addition we suspect a *surface curing* effect of the UV laser on the

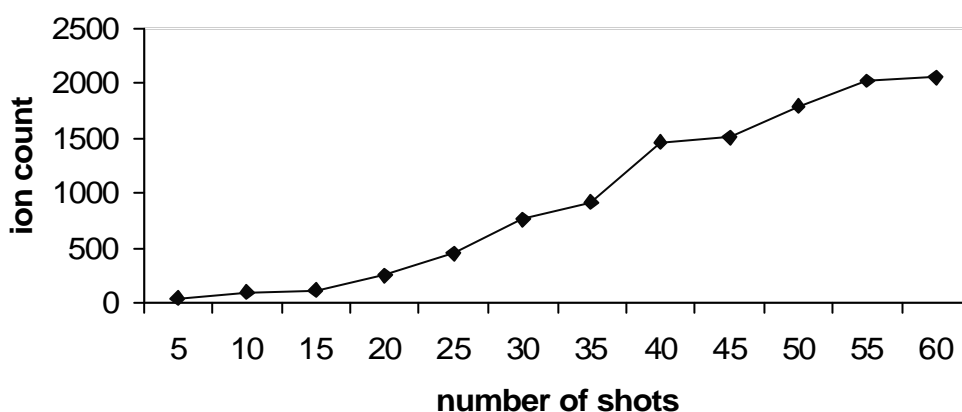


Figure 6.19 Evolution of the absolute intensity of the peak Pb^+ in an indigo-lead white-linseed oil mixture during an LDI-TOF-MS analysis. Data averaged every 5 laser shots.

linseed oil. Polymerisation of the oil at the surface would seal off the surface and prevent further indigo to being ablated in the successive laser shots.

The second sample was prepared with synthetic indigo and lead white 1:16 blended in cold pressed linseed oil. This mixture was painted on an artists' board with a paint layer thickness of ca. 30 μm and the layer was sampled when touch-dry. LDI-TOF-MS was performed by directly targeting the surface of the cardboard with the laser. A spectrum representing 50 shots averaged, shown in Figure 6.20, displays characteristic peaks for indigo at m/z 263, 285, 301, 360, 378, 382, 399 and 469. The lead adduct of indigo is detected at m/z 469, with its characteristic isotopic distribution. Lead related species, namely PbO , PbONa , Pb(PbO)K are also identified.

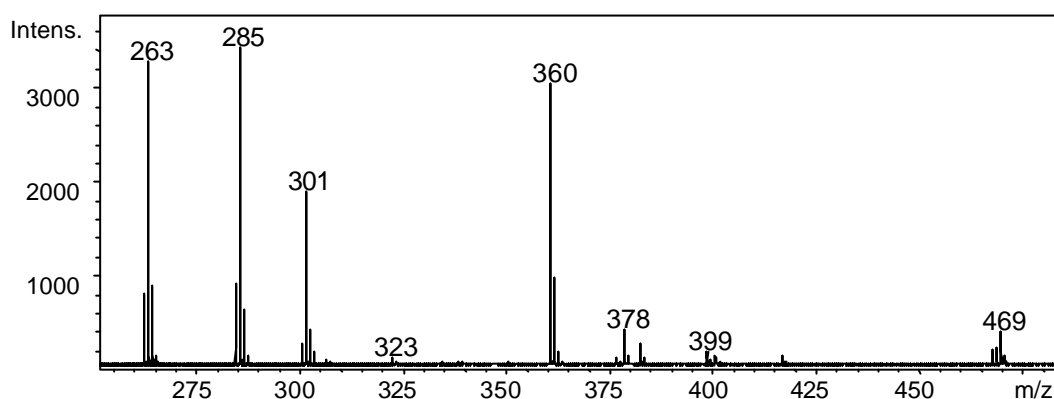


Figure 6.20 LDI-TOF-MS of an indigo and lead white mixture (1:16) blended to cold pressed linseed oil.

6.6.6. Conclusion

In this series of LDMS experiments, we have shown that indigo could be identified when thoroughly mixed with the pigment lead white, as well as at the surface of a sample of linseed oil paint that contains lead white. We have observed that preferential desorption of indigo is realised in the first laser shots whereas lead substituted indigo and lead white related peaks are produced at a later stage. At low laser power only negligible fragmentation is observed. We assume that laser-matter interaction at the surface of the sample is responsible for chemical modification in the condensed-phase. This accounts for the increase in time of lead-related species during multiple shot analyses, including notably the formation of lead adducts of indigo. Experiments conducted with increasing laser power density have shown the role of the energy deposition within this process.

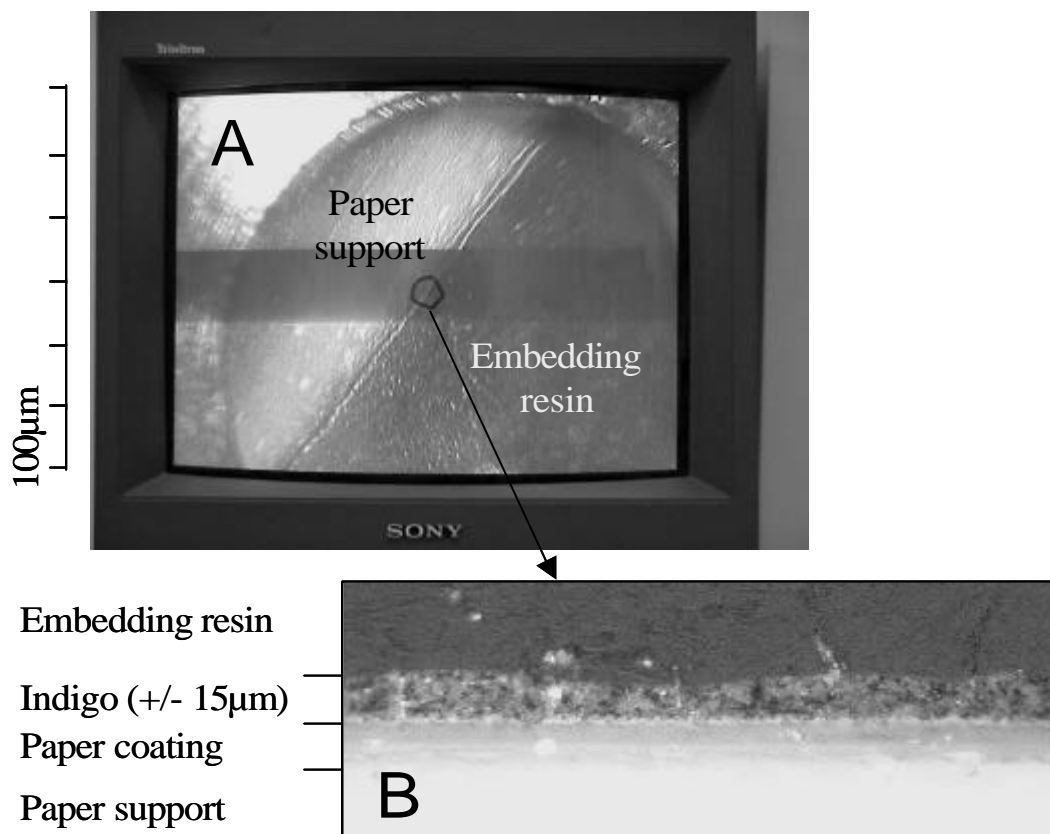


Figure 6.21 *Spatially-resolved laser desorption of an embedded paint cross-section containing a mixture of indigo and lead white in linseed oil. Image obtained with the CCD camera (A); detail showing the indigo layer painted on the cardboard paper (B).*

6.7. *Spatially-resolved LDMS of cross-sections*

LDMS has given very promising results when the surface of samples and indigo-containing mixtures are examined. Because samples removed from easel paintings are usually available in the form of embedded cross-sections, it was necessary to investigate if the methodology of LDMS would work with sectioned samples. Two samples investigated in section 6.6., i.e. thin films painted on artist's board, were therefore further investigated as sectioned samples. Figure 6.21 shows the surface of a cross-sectioned sample as observed with the viewing system of the LDMS. Particular attention was given to the polishing procedure because the smoothness of the surface* is crucial to the success of the analysis. In a second series of experiments, a thin film of matrix was deposited by pneumatic spraying

* Absence of residual embedding material on the surface of the sample must be ensured.

on the surface of the sectioned samples to investigate if this procedure could enhance the analytical information when MALDI would be performed.

The first sample is a mixture of indigo in oil painted on a cardboard paper as already described in section 6.6.4. The indigo/oil layer was investigated in a spatially-resolved experiment, and mass spectral information was averaged over 100 laser shots. Indigo is identified with peaks at m/z 262, 263, 284, 285, 300, 301, 360, 378. In the negative mode peaks are observed at m/z 261 and 262. The signal-to-noise ratio is much smaller compared to direct analysis on the cardboard. The absolute intensity is approximately twofold smaller for 10 times the same number of laser shots. We assume that this phenomenon can be explained by the smaller amount of material available at the surface of the sample. Only indigo present at the surface is detected. As a matter of fact, deposition of matrix at the surface of the sample did not improve the analytical information.

The second sample is a mixture of indigo and lead white in oil painted on a cardboard paper, already described in section 6.6.5. The cross-section was analysed by LDI-TOF-MS in the positive and negative mode, the spectra are

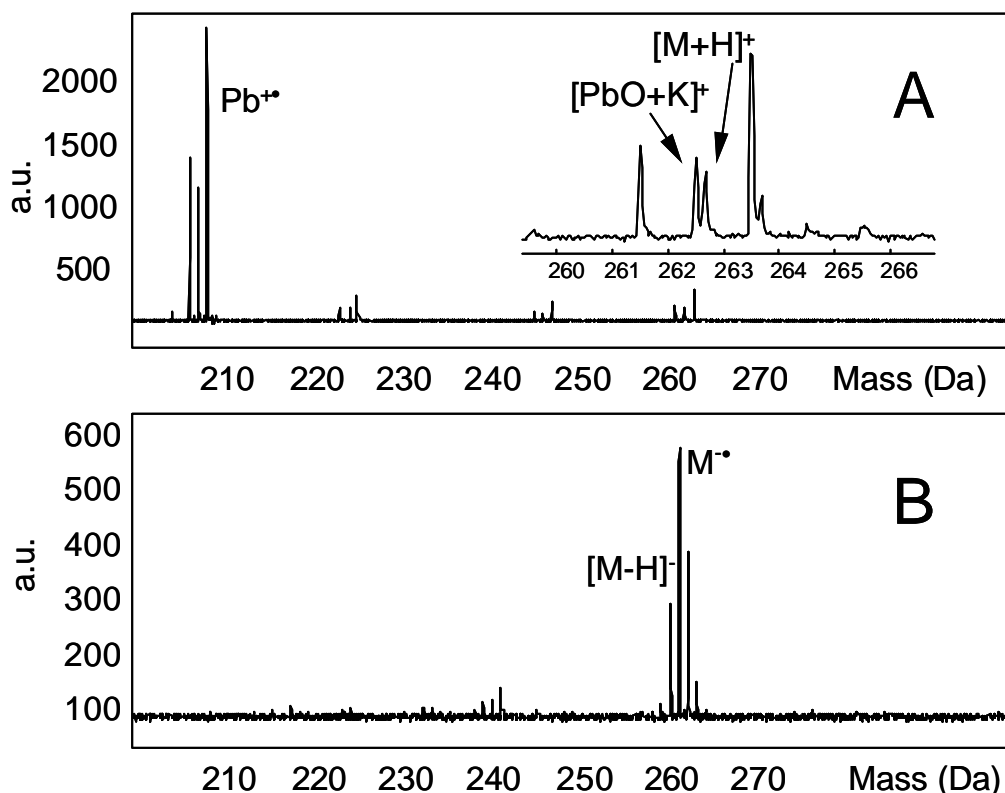


Figure 6.22 *Spatially-resolved LDMS of the surface of the cross-section of an indigo/lead white/oil reconstruction shown in Figure 6.23. Positive ion mode, 10 shots on indigo layer (A); negative mode, 19 shots on indigo layer (B).*

shown in Figure 6.22. Indigo is identified thanks to peaks at m/z 262, 263, 284, 285, 301 and 360. Lead white is identified with a series of peaks (assigned to Pb^+ , PbOH^+ , PbONa^+ , PbOK^+ , Pb_2^+ , Pb(PbO)^+ , $(\text{PbO})_2^+$, Pb(PbO)K^+ , Pb(PbO)_2^+ , $(\text{PbO})_3\text{H}^+$, Pb(PbO)_3^+ , $(\text{PbO})_4^+$). It is apparent in Figure 6.22 that the TOF-MS provides sufficient resolution to separate PbOK from indigo. LDI-TOF-MS in the negative mode positively identifies indigo with its parent ion $[\text{M-H}]^-$ at m/z 261. Here no overlapping exists with lead related peaks. Formation of indigo ions was not always successful. We assume that indigo is only detected, where particles are present at the surface of the cross-section. It might be possible that indigo at the surface suffers from the grinding and polishing process.

In conclusion, we have shown that indigo can be identified in a thin layer ($15\mu\text{m}$) of a complex mixture directly at the surface of a paint cross-section. This experiment demonstrates that LDMS should be a feasible approach to the investigation of easel painting samples prepared as thin cross-sections. With soft materials as indigo it seems wise to keep the sample preparation as mild as possible to avoid *surface scouring*.

Unfortunately indigo could not be detected so far in samples obtained from 17th century paintings. One explanatory hypothesis assumes that only indigo present at the surface of the cross-section could be detected. This would mean that in the samples investigated no indigo was present at the surface. Further investigation will be needed to confirm this assumption.

6.8. Conclusion

This chapter demonstrates the successful use of LDMS as method of investigation of indigo. First, we have shown that indigo is readily amenable to characterisation by LDMS as a pure compound. Different ionisation mechanisms were identified that lead to the formation of intact molecular species. Spectra are simple in appearance although additional unidentified compounds are observed. Spectra recorded in the negative mode are in good agreement, and are not complicated by peaks related to lead compounds. Indigo of natural origin was also successfully investigated with LDMS. Again, additional components were detected but those could not be identified. No distinctive molecular signature could be identified that relates to indigo of different manufacturers. Natural and synthetic indigo were differentiated but the mass spectrometric signature, however, cannot be assigned to specific structures yet. The multiple MS capability of the ITMS was employed to interrogate the fragmentation pattern of indigo molecular ions.

Indigo has been identified in painted films in the presence of oil or lead white. When mixed with lead white a strong contribution of the lead related species was observed. Lead adducts of indigo were detected in a multiple laser shot experiments with increasing intensity as a function of time. We suspect that significant induced surface modifications are induced in the condensed phase under the action of the UV laser.

Spatial resolution provided by the UV laser beam was proved to allow the direct authentication of indigo from the surface of wool fibres and of cross-sectioned paint samples. In sectioned samples, a large attenuation in the signal intensity was observed in comparison to “bulk” analysis. Irregular production of the ions from the surface of sectioned samples emphasises the importance of the surface preparation*. Use of a thin film of matrix deposited at the surface of the section did not improve the results, which suggests that indigo might not be present at the surface anymore due to surface scouring.

The non-success of LDMS for the analysis of cross-sections with 17th century paintings questions whether the technique can be used at all for the analysis of museum samples. Analysis of paint cross-sections was however demonstrated for indigo with reconstructed samples. Therefore the low concentrations and uneven distribution of the pigment at the surface of the samples looks the most likely explanation. The next chapter will discuss further attempts in the surface analysis of museum samples with modern materials.

* A homogenous distribution of photon flux across the laser beam is another crucial factor.

Chapter 7

LDMS of modern synthetic artists' pigments

LDMS was applied to the analysis of synthetic organic pigments employed in modern artists' paints. UV-LDI and MALDI-TOF-MS were successfully used for the identification of a series of reference organic pigments belonging to the azo pigments, phthalocyanine, quinacridone, dioxazine, perylene and diketopyrrolo-pyrrole. Analyses were then extended to the investigation of commercial acrylic and oil tube paints where the pigment is mixed in a binding medium. Results show that a nitrogen laser (337nm) used at low power density selectively desorbs and ionises synthetic pigments present in a binding medium. This makes LDMS a particularly attractive method for the investigation of complex samples where FTIR analysis fails because of strong interferences with additional materials found in the paint (binders and fillers). We will show that sufficient resolution of the mass analyser makes it possible to recognise the different substitution patterns of chlorine and bromine in phthalocyanines, whereas sensitivity and mass detection range makes it possible to identify trace amounts of PEG and PPG used as additives.

7.1. Introduction

The production of first synthetic pigments goes back to the mid 19th century with the beginning of the era of scientific chemistry^{18, 29}. Organic synthetic pigments have been mostly used as artist's materials since the 1950s. A considerable number of pigments has been synthesised in the laboratory attaining at present several tens of thousands of different compounds. Within a particular chemical class, wide variations of the colour properties are obtained with the introduction of additional chromophore or auxochrome groups*. Only a small portion of these compounds, however, has been marketed²⁹, and even a smaller range used in artist's materials. The history and use of modern organic pigments by painters has been recently surveyed by De Keijzer²¹. Prevalent chemical classes are azo pigments (reds, oranges and yellows), phthalocyanines (blues and greens) and quinacridones (violets, reds, oranges) and to a lesser extent dioxazine, perylene and anthraquinones. Today, modern synthetic pigments are ubiquitous and retailed off-the-shelf in the form of paint tubes, i.e. already mixed with an oil or synthetic binding medium (such as acrylic, polyvinyl acetate, polyester, etc)^{19, 164}.

Synthetic organic pigments usually have a well-known structure, their nomenclature is standardised, and they are listed in the Colour Index (C.I.)¹⁴⁷ published by the Society of Dyers and Colourist. Each pigment is given a C.I. generic name and a C.I. constitution number, e.g. PR122, which stands for pigment red number 122. Commercially available artists' paints, however, are formulated according to proprietary methods, and their exact compositions are often unknown. A great diversity of suppliers exists, and it is not uncommon that various commercial names refer to the same organic pigment. For instance the quinacridone pigment PR122 is retailed under diverse appellations such as *magenta*, *rose violet*, or *purple*. Poor labelling of paint materials by manufacturers often add to the confusion concerning their composition.

Various analytical methods of analysis have been successfully used for the study of synthetic organic pigments^{18, 47, 52, 87-89, 133, 165, 166}. Physical and structural characterization is essentially addressed by microscopic techniques and X-ray diffraction, whereas chemical analysis and colour measurement is performed by spectroscopic methods, such as VIS spectrophotometry, IR, NMR, electron spin resonance, emission resonance and MS. The use of MS for the analysis of synthetic colorants has been surveyed by Van Bremen⁸⁴, with a particular

* A chromophore is an arrangement of atoms that gives rise to colour, e.g. the functional groups of $-N=N-$, $>C=C<$, $>C=O$, whereas an auxochrome is a group that affects the spectral regions of strong absorption in chromophores, e.g. $-NH_2$, $-OH$, $-Br$, $-Cl$, $-NO_2$.

emphasis on the benefits of various ionisation methods. Admittedly, LC-MS and GC-MS are useful techniques for the analysis of dyes in complex mixtures since mass spectrometry can be carried out with additional chromatographic separation. LDMS is a promising technique for the direct analysis of synthetic dyes absorbed on surfaces (including covalently bound colorants). Bennett *et al.*⁸⁷ used UV-LDMS (265nm) to detect dyes present in a multicomponent mixture. Dale *et al.*^{88, 133} used two-step laser desorption photo-ionisation (L²TOFMS) to examine azo, anthraquinone, phthalocyanine and coumarin dyes. A pulsed IR laser (wavelength 10.6µm) was used to vaporise the samples as intact molecules, which were subsequently photo-ionised using either 193- or 266-nm UV laser radiation. Sullivan *et al.*⁸⁹ used negative MALDI for the analysis of polysulfonated azo dyestuffs. The value of MS/MS analysis for structural determination was also demonstrated with the production of fragment ions when only molecular ion species are formed as ionised species¹⁶⁷.

In easel paintings, authentication of modern organic pigments is an analytical challenge because of the small scale and great complexity of the samples. Organic pigments are found entangled in complex mixtures of components of the synthetic polymeric or oil medium, inorganic pigments, extenders and various additives¹⁶⁸. Only little information is provided by optical or microscopical investigations because of the fine division of the particles, leaving spectrometric and spectroscopic techniques as methods of choice. FTIR is a particularly useful method to conservation scientists^{19, 64}, since most of the modern artists' pigments can be identified from the FTIR fingerprint. FTIR offers the possibility to investigate *in situ* the surface of multi-layered samples prepared as sections. In practice, however, the pigment concentration is often so low in a paint layer that it is virtually impossible to detect them. In addition, many samples removed from museum easel paintings have an FTIR spectrum dominated by the binder and fillers (e.g. chalk or barium sulphate)*, so much so that the sharp organic pigments peaks are often hard to distinguish from noise¹⁹. FTIR is therefore a good analytical tool for *bulk composition*. Py-GC(-MS)^{81, 169} is quite successful in the investigation of pyrolytic fragments of most azo pigments but inadequate for the investigation of other pigments. The use of Py-GC has been demonstrated by Sonoda *et al.* for the investigation of acrylic paints (reference samples and samples removed from modern paintings). Recently DTMS^{19, 170} has been shown to be a very effective technique for modern paint analysis. Organic

* The outcome of FTIR analyses depends strongly on the type of additives (fillers, binders and pigments) found in the paint. For instance, FTIR usually fails to identify phthalocyanines in acrylic polymer emulsions because the characteristic peaks of the pigment are totally hidden by the extenders. In the particular case of Liquitex paints, however, fillers are of the silica type and found in small amounts. They do not interfere excessively with the peaks from organic pigments and FTIR analyses are feasible.

Chemical class	C.I. Pigment name	C.I. Constitution number	Molecular Weight (MW) ¹
Azo (Naphtol)	PR 188	12467	642
Azo (Diarylide)	PY 83	21108	816
	PV 19	73900	312
	PR 122	73915	340
Quinacridone	PR 209	73905	378
	PR 207	73906	312 + 378
(Quin. Quinone)	PR 206	73920	312 + 342
Dioxazine	PV 23	51319	588
Perylene	PR 178	71155	750
Diketopyrrolo-Pyrrole (DPP)	PR 254	56110	356
Anthraquinone	PR 83	58000:1	240
Phthalocyanine	PB 15	74160	575
	PG7	74260	1118 (M _{av} 1127)
	PG36	74265	see table 7.3

¹ Here we give the mono-isotopic molecular weight MW_m. In the case of the chlorinated compound PG7, MW_m is given for Cu-C₃₂N₈Cl₁₆. MW_{av} is the average molecular weight

Table 7.1 Reference compounds.

pigments can be identified at extremely low concentration and in the presence of binder (medium) and fillers (additives). DTMS can resolve the components of a heterogeneous sample using a temperature ramp¹⁷¹.

In this chapter we explore LDMS as a tool for the molecular identification of modern synthetic organic pigments. Analyses are performed with LDI and MALDI either in the positive or in the negative mode. The first series of measurements concerns a set of reference pigments belonging to the principal chemical classes of synthetic artist's pigments, namely azo pigments, phthalocyanine, quinacridone, dioxazine, perylene and diketopyrrolo-pyrrole. In a second stage, commercial paints (acrylic and oil media) containing one or several of these pigments will be analysed. We will notably demonstrate that mass spectrometry can easily distinguish the different substitution patterns in

phthalocyanines, which enables the differentiation of the different commercial blues and greens. In a last stage we will employ LDMS for the *in situ* investigation of cross-sectioned multi-layered systems. This latter category concerns reconstructed models prepared in the laboratory and microscopic samples removed from works of art.

7.2. Samples

A series of reference compounds covering the principal chemical classes encountered in synthetic organic pigments were analysed by LDMS. Samples are listed in Table 7.1, and are classified according to their chemical constitution. In Table 7.1, each reference pigment is given with its Colour Index ¹⁴⁷ generic name and number. For example PY83 stands for Permanent Yellow number 83, from which its chemical composition and molecular mass can be looked up in the Chemical Index. The table also includes the molecular weight of the colouring material(s).

A rough distinction can be made between azo pigments, and non-azo pigments also known as polycyclic pigments ¹⁸. Azo pigments under investigation can be further classified according to their structural characteristics into disazo pigments (diarylide yellows) and naphthol AS pigments (naphthol reds). Other samples fall into the category of polycyclic pigments and belong to one of the following chemical classes: phthalocyanine, quinacridone, perylene, anthraquinone, dioxazine, and diketopyrrolo-pyrrole.

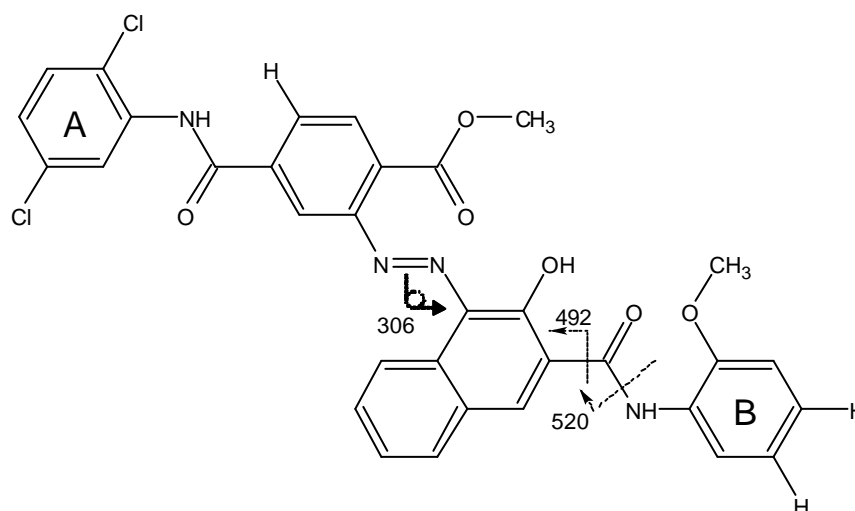


Figure 7.1 Azo pigment red PR188 (naphthol), Molecular composition and monoisotopic weight, $C_{33}N_4O_6Cl_2H_{24}$, MW 642 Da. Fragment ions refer to the MS fragmentation.

Chapter 7

7.2.1. Azo pigments

Artists' azo pigments are produced in many different colours, most importantly reds, orange and yellows. They can be classified in monoazo and disazo pigments, with one or two azo functions ($-N=N-$) respectively. Two prevalent classes of artist's azo pigments are the diarylide yellow pigments and the naphthol red pigments. In this chapter one pigment of each class has been analysed by LDMS: (1) Naphthol red PR 188, an intense yellowish red pigment with very good lightfastness properties. It is a naphthol red pigment (Figure 7.1). (2) Hansa yellow PY 83, the standard pigment within the reddish yellow range. It is a diarylide yellow pigment of which the structure is presented in Figure 7.2. It possesses excellent fastness properties, which make it almost universally applicable

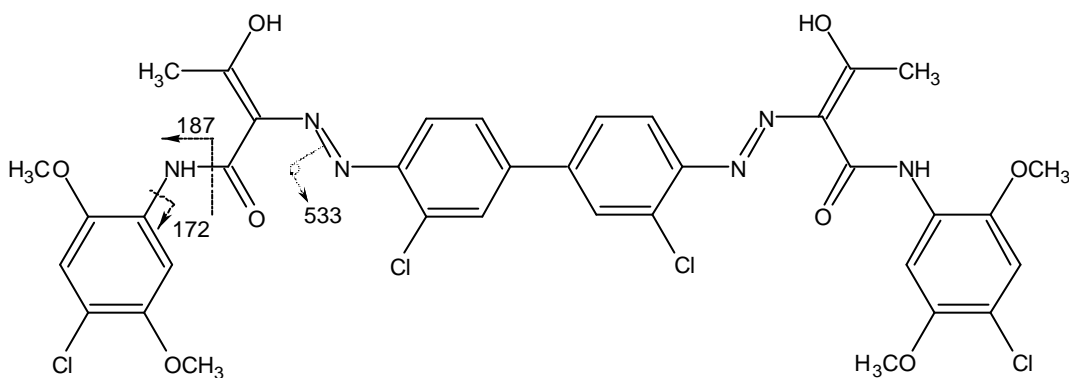


Figure 7.2 Azo pigment yellow PY83 (diarylide), $C_{36}N_6O_8Cl_4H_{32}$, MW 816 Da.

7.2.2. Phthalocyanines

Artists' phthalocyanine pigments are blue and green. The phthalocyanine structure is a tetra-aza-tetrabenzoporphine and artists' pigments are all based on the copper (II) complex structure shown in Figure 7.3. This molecule ($Cu-C_{32}N_8H_{16}$) is the copper phthalocyanine blue PB15. The blue colour of phthalocyanines can be altered to various shades of bluish and yellowish green by substitution with chlorine and/or bromine atoms on the four outer benzene rings. PG7 are chlorine-substituted phthalocyanines ($Cu-C_{32}N_8H_{16-n}Cl_n$). The number of substitutions is generally $n=15$, but 14 and 16 are also possible. Figure 7.4 shows the $n=16$ substituted molecule. PG36 is a chlorine and bromine-substituted phthalocyanine. The more chlorine atoms are replaced by bromine, the yellower the colour becomes.

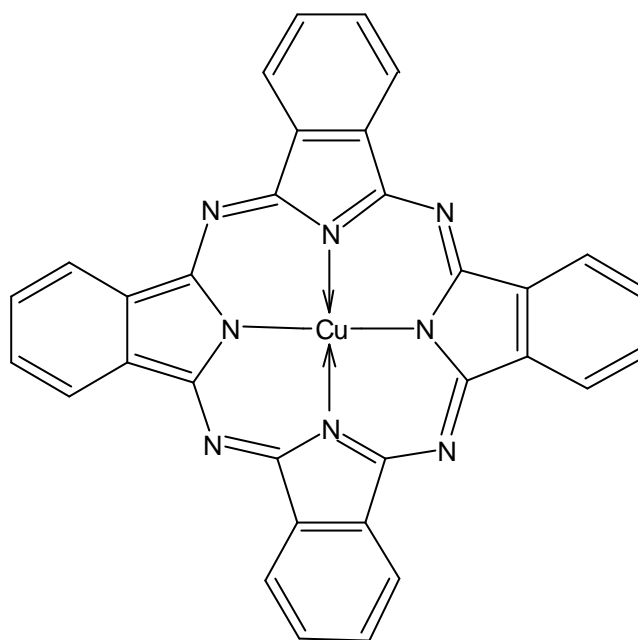


Figure 7.3 *Phthalocyanine blue PB15, Cu-C₃₂N₈H₁₆, monoisotopic molecular weight MW_m 575 Da (average molecular weight MW_{av} 576 Da).*

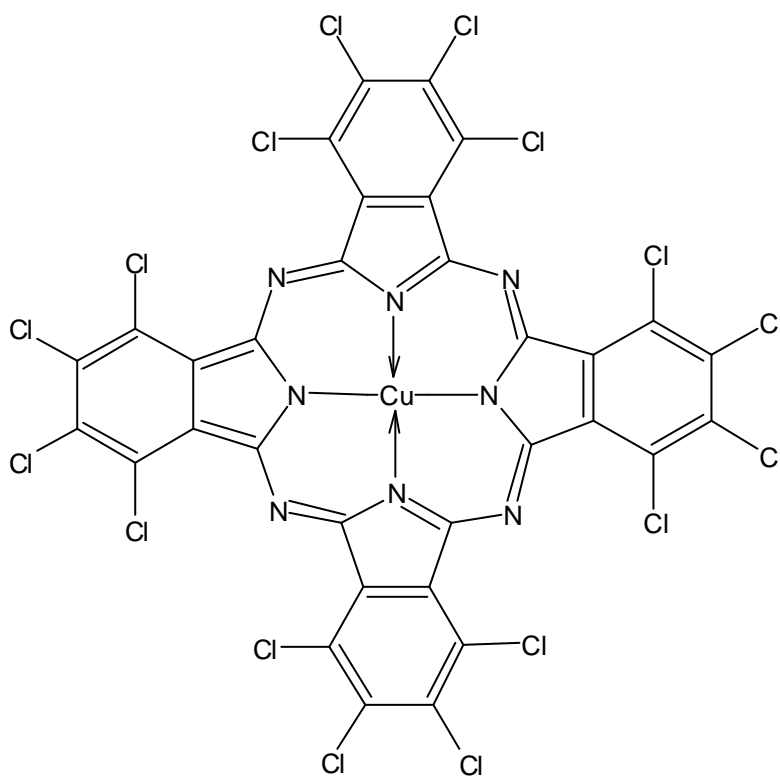


Figure 7.4 *Phthalocyanine green PG7: Cu-C₃₂N₈Cl₁₆, MW_m 1118 Da (dominant isotopic peak MW_d 1127 Da).*

Phthalocyanine can be identified by FTIR, but the technique does not give sufficient structural information to indicate the substitution pattern in the molecule nor the presence of additives. Besides, FTIR often fails to characterise phthalocyanine pigments in paints because of the low pigment concentration (phthalocyanines have a high hiding power). In addition, other paint compounds, such as fillers/extenders and binders can produce strong interference with the pigment signal. There is therefore a great need for a technique that would positively identify phthalocyanines in a cross-section when FTIR remains unsuccessful.

A variety of phthalocyanine-containing pigments, obtained from different manufacturers, were analysed by LDMS. High resolution of the TOF-MS is used for the characterisation of chlorinated and brominated phthalocyanines (PG7 and PG36). Two PG7 samples obtained from Winsor & Newton (Harrow, UK) (PG7WN), and Cornelissen (London) (PG7C) and were analysed in order to investigate whether a difference in composition could be detected.

7.2.3. Quinacridones

Quinacridone pigments represent a large range of pigments, all based on the same structure, a linear system of five anellated rings shown on Figure 7.5.A. This molecule itself is a violet shade, pigment PV19 (quinacridone violet). Many other pigments of different colours and shades, from deep reds to golden oranges, are produced by substitutions on the two end benzenes. PR122 is the 2,9-dimethylquinacridone ($C_{22}H_{16}N_2O_2$) (Figure 7.5.B). It offers a very clean bluish shade of red, which is usually referred to as pink or magenta. PR207 is a mixed

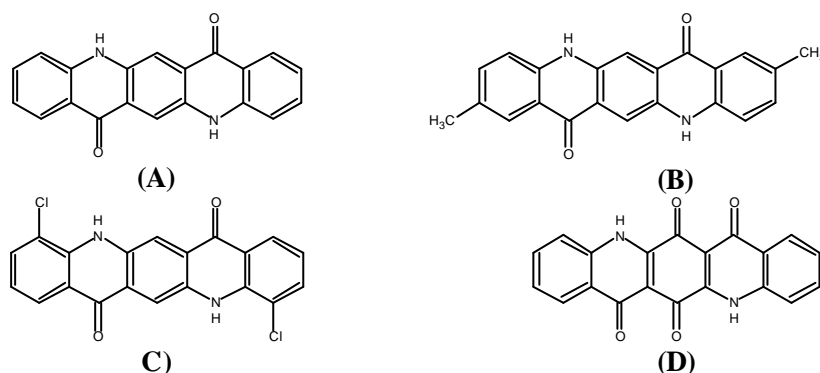


Figure 7.5 (A) quinacridone PV19, $C_{20}H_{12}N_2O_2$, MW 312 Da;
 (B) 2,9 di-methylated quinacridone PR122, $C_{22}H_{16}N_2O_2$, MW 340 Da;
 (C) 4,11 di-chlorinated quinacridone, $C_{20}H_8N_2O_2Cl_2$ MW 378 Da;
 (D) quinacridone quinone, $C_{20}H_{10}N_2O_4$, MW 342 Da.

phase pigment made from unsubstituted and 4,11-substituted dichloro-quinacridone (Figure 7.5.C). PR209 is the 3,10-dichloro-quinacridone, mixed with 1,8 and 1,10-dichloro-quinacridone. PR206 is a mixed crystal phase of unsubstituted quinacridone with quinacridone quinone (Figure 7.5.D). Recent studies have shown that Py-GC-MS fails to characterise quinacridone-containing acrylic paints¹⁹.

7.2.4. Perylene red pigment

Perylene pigments are diimides of perylene tetracarboxylic acid. PR178 ($C_{48}H_{26}N_6O_4$) is the perylene red with a molecular structure as shown in Figure 7.6.

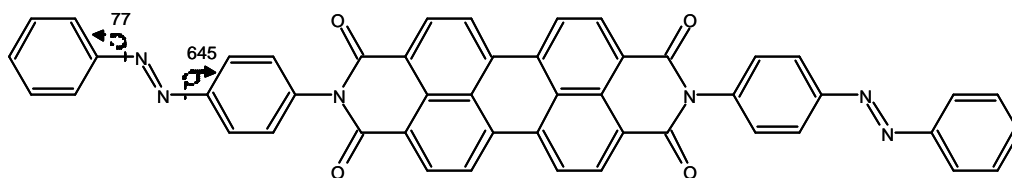


Figure 7.6 Perylene PR178, $C_{48}H_{26}N_6O_4$, MW 750 Da.

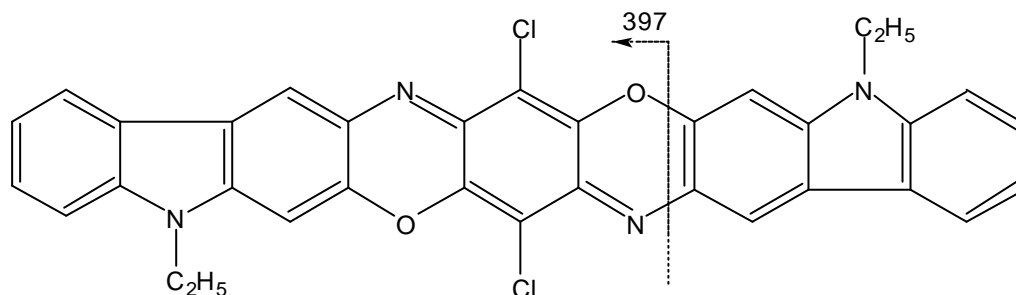


Figure 7.7 Dioxazine PV23, $C_{34}H_{22}N_4O_2Cl_2$, MW 588 Da.

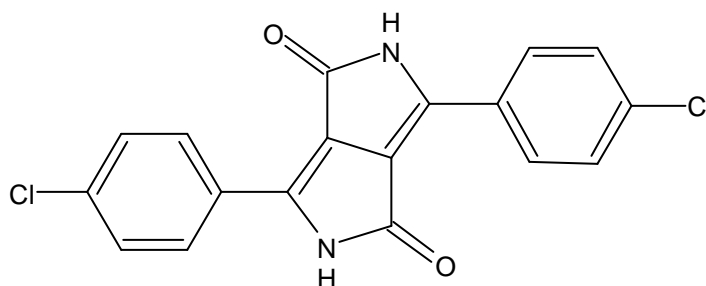


Figure 7.8 Diketopyrrolo-pyrrole (DPP) PR254, $C_{18}H_{10}N_2O_2Cl_2$, MW 356 Da.

Chapter 7

7.2.5. Dioxazine pigment violet PV23

The dioxazine violet pigment PV23 ($C_{34}H_{22}N_4O_2Cl_2$) is a bluish violet shade commonly referred as carbazole violet. It is derived from triphenodioxazine, a linear system of five anellated rings. Its molecular structure is shown in Figure 7.7. The pigment is particularly important in systems based on TiO_2 /rutile. PV23 is a favourite shading pigment for use in emulsion paints, and is used to lend a reddish tinge to phthalocyanine blue shades. LD/FTMS spectra of PV23 have been presented by Aaserud ¹⁷².

Manufacturer	Name	Pigment(s) (C.I. name)
Liquitex	Light Magenta	PR207, PR188 (PW6 ¹)
	Medium Magenta	PR122 (PW6)
	Vivid Orange	PY83, PR188
	Brilliant Purple	PV23 (PW6)
	Phthalocyanine Blue	PB15
	Phthalocyanine Green	PG7
Golden	Pyrrole Red	PR254
Grumbacher	Perylene Red	PR178
	Thalo Blue	PB15
Lascaux	Permanent blue	Unspecified Phtalo
Flashe (Lefranc & B.)	Hoggar blue	Unspecified Phtalo
Polyflashe (Lefranc & B.)	Brilliant blue	Unspecified Phtalo
Winsor & Newton	Permanent Green	Unspecified Phtalo
Van Gogh Oil Paint (Talens)	Permanent Red Violet	PR122, PV23
	Rose Madder	PR83, PV19

¹ PW6 is titanium white.

Table 7.2 Acrylic (or PVA) emulsion paints.

7.2.6. *Diketopyrrolo Pyrrole Pigment Red PR 254*

The basic skeleton of this recently developed group of pigments consists of two fused five-membered rings, each of which contains a carbonamide moiety in the ring. PR254 ($C_{18}H_{10}N_2O_2Cl_2$), with a molecular structure as shown in Figure 7.8, provides medium shades of red.

7.2.7. *Acrylic polymer emulsions (commercial tube paints)*

The vast majority of acrylic media used for artists' materials are emulsion paints, also referred to as dispersion paints. These consist of finely dispersed droplets of acrylic polymer in a continuous water phase that is stabilised by surfactants. The polymer component is usually a copolymer of methyl methacrylate (MMA) and a softer acrylate monomer such as ethyl- (EA) or butyl acrylate (BA), although styrene-acrylic and vinyl acetate-acrylic copolymers can also be used. Acrylics fuse as the water evaporates, and pigments particles remain trapped in the dry film.

A series of acrylic emulsion paints containing at least one of the aforementioned synthetic pigments were investigated by LDMS. Samples are listed in Table 7.2 and given by their commercial name. They are classified according to their manufacturer and brand name since the nature of the acrylic medium is assumed to be consistent within the same product series: Liquitex (Piscataway, NJ, USA), Lefranc & Bourgeois (Le Mans, France), Golden (New Berlin, NY, USA), Grumbacher (Bloomsbury, NJ, USA), Lascaux (Brüttisellen, Switzerland), Pigment composition is given as indicated on the paint tubes.

Samples from a sculpture and two modern easel paintings discussed in section 7.6.2 were kindly provided by Tom Learner (Tate Gallery, London).

7.3. *Experimental conditions*

MS studies of modern organic pigments were performed by LDI and MALDI with a TOF-MS instrument. For a detailed description of both instruments we refer the reader to chapter 2.

Samples were investigated as a thin film or as cross-sections in the TOF-MS instrument, a commercial Bruker Biflex TOF-MS (Bruker-Franzen Analytik, Bremen). We refer the reader to Chapter 2 for a detailed description of the sample preparation and the different possible configurations of the probe. Thin films were

deposited either at the surface of a stainless steel probe, or at the surface of a TLC plate coated with cellulose. TLC probes and embedded paint cross-sections are placed in a home-built sample holder. A calibrant is deposited at the same level as the sample surface. The probe is introduced in the ionisation chamber through a vacuum lock and positioned in the focus of a N₂ laser beam (working at 337 nm). Microscopic probe positioning is achieved thanks to an XY manipulator and the digital output of a CCD (Charge Coupled Device) camera for observation. Desorption and ionisation were performed directly (LDI) or with the assistance of a DHB matrix (MALDI) and measurements were performed either in positive or in negative mode.

In LDMS experiments, reference samples were deposited as a thin or thick film either on a stainless steel probe or on TLC plates coated with cellulose (reference components only). A few micrograms of the sample were mixed with ethanol. The suspension was homogenised using a vortex mixer. About 5 microliters of this solution or suspension were deposited onto the probe with a pipette and dried in vacuum. For thick films a few micrograms of pigment were deposited directly on the surface and a few microliters of ethanol were deposited to simultaneously disperse and adsorb the sample on the surface of the probe. Pigmented paint in an acrylic or oil medium were applied directly onto the surface of the probe and spread with the tip of a scalpel to obtain a thin film. When sufficient material was available, it was rather painted with a thin brush. MALDI experiments were performed using exclusively 2,5-dihydroxybenzoic acid (DHB) as the matrix. A thin layer of the sample is first absorbed on the surface of the probe as for LDI experiments. Subsequently a thin matrix layer was deposited on top of the sample. This approach was chosen to mimic as much as possible the way in which a matrix would be applied when analysing a paint cross-section.

7.4. *Analysis of reference samples*

In this section, a series of reference organic pigments were investigated by LD-TOF-MS. Reference samples were obtained from various manufacturers or were provided by Tom Learner (Tate Gallery). Samples are either single compounds (e.g. PY83) or mixtures of different compounds (e.g. PR206). For each sample analyses were carried out with LDI and MALDI, both in the positive and the negative mode. Laser power density was tuned just above the desorption ionisation threshold.

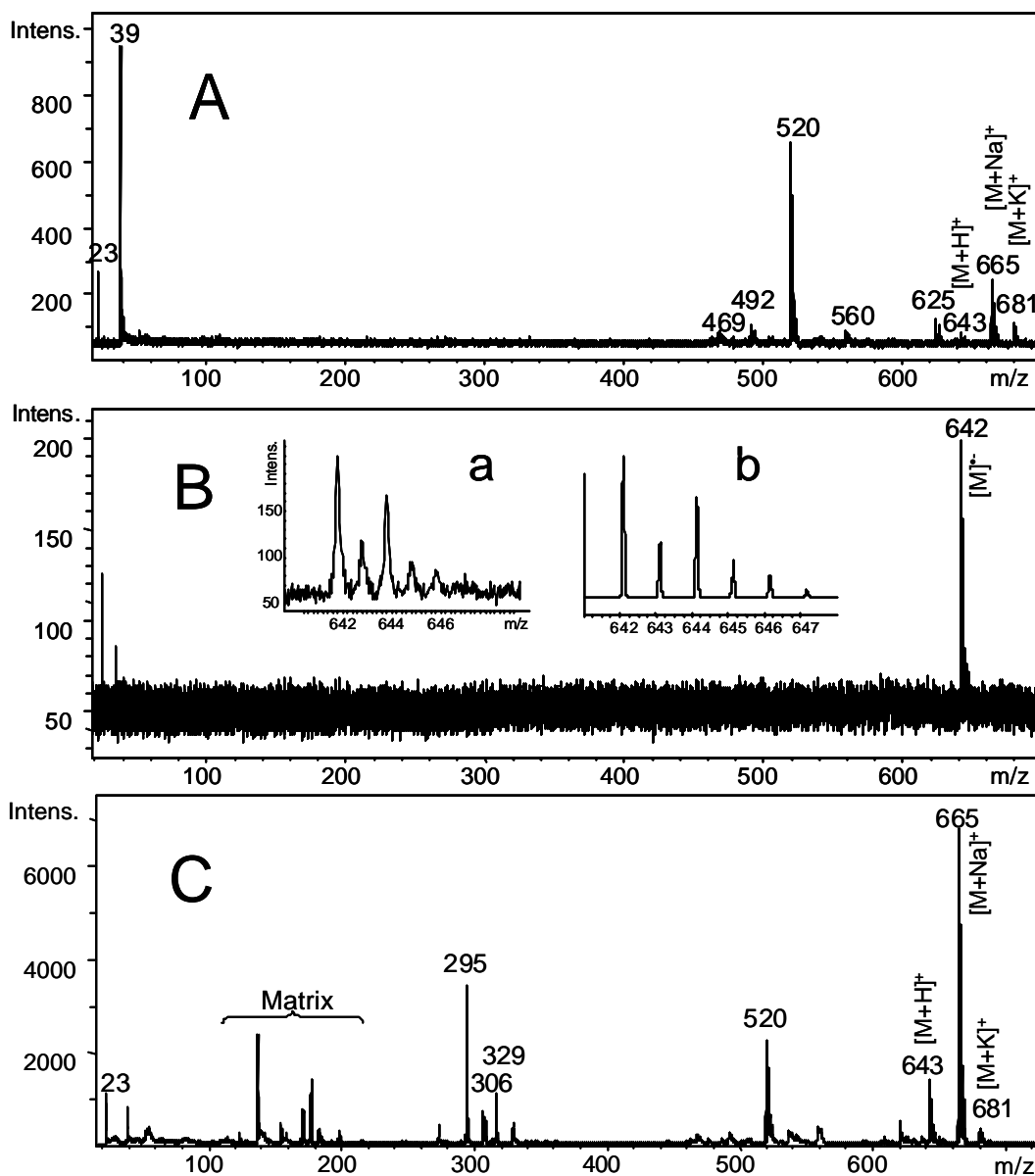


Figure 7.9 TOF-MS of naphthol AS pigment red PR188: positive LDI (A), negative LDI (B and inset a), theoretical isotopic distribution of PR188 $C_{33}N_4O_6Cl_2H_{24}$ (inset b), and MALDI (C).

7.4.1. Naphthol AS pigment red PR188

Naphthol AS pigment red PR188 ($C_{33}N_4O_6Cl_2H_{24}$) successfully desorbs and ionises under the LDI conditions (low laser power density, nitrogen laser working at 337nm). The positive ion spectrum of naphthol red PR188 (MW 642 Da) is simple in appearance (Figure 7.9.A). The sodiated species $[M+Na]^+$ is observed at

m/z 665 and potassiated species $[M+K]^+$ at 681, whereas the protonated molecule at m/z 643 is observed with only a small relative intensity. This suggests that the most likely mechanism for ionisation is that of cation attachment. Dominant peaks are observed at m/z 23 and 39 for the sodium and potassium ions. Loss of a hydroxyl radical OH^\cdot from the parent radical cation (m/z 642) is observed at m/z 625*. The dominant peak at m/z 520 results from cleavage of the amide bond on the side of the B ring (Figure 7.1). No ions from cleavage of the amide bond on the side of the A ring (with the two chlorine substitutions) could be detected. Cleavage of the phenyl–amide bond (on the side of the B ring) yields m/z 492 (small relative intensity). The peak at 469 is unidentified. The negative ion spectrum (Figure 7.9.B) shows exclusively a base peak assigned to the radical ion $[M]^{2-}$ at m/z 642. No characteristic fragment ions are observed, except peaks at m/z 35 and 37 which are assigned to chlorine anion.

The positive MALDI spectrum (Figure 7.9.C) shows dominant peaks for the protonated (m/z 643), sodiated (m/z 665, base peak) and potassiated (m/z 681) molecules. Surprisingly, an additional group of peaks is detected in the mass range [270-330], which was not observed in LDI. We assume that odd-electron ions at m/z 306 result from the photolytic cleavage of the azo bond by resonant absorption of the chromophore group (m/z 329 is assigned to the sodiated species). Cleavage of the azo bond is only possible after isomerisation of ($-N=N-$) to ($=N-N-$). Similar fragmentation has been reported for other azo containing anions using desorption ionisation methods⁸⁷. In the mass range [1000-1800] a sequence of peaks with regular interval of 44 Da gives evidence for the presence of polyethylene glycol (PEG) with average molecular weight MW_{av} of 1300 Da. PEG is probably a wetting agent in the pigment sample.

7.4.2. Diarylide pigment yellow PY83

In the positive ion spectrum of the diarylide pigment yellow PY83 ($C_{36}N_6O_8Cl_4H_{32}$) (Figure 7.10.A), protonated molecules are observed at m/z 817 with low relative intensity. A stronger signal (3 to 5 times higher) is obtained in MALDI (with DHB as a matrix) (Figure 7.10.B), with the sodiated parent ion at m/z 839. The dominant peak is observed at m/z 187 corresponding to the β -cleavage of the amide bonds with transfer one hydrogen atom (Figure 7.2). Loss of the aromatic side group by cleavage of the N-phenyl bond with transfer one hydrogen atom yields m/z 172 (small relative intensity). Cleavage of the azo bond yields m/z 533 indicating retention of the positive charge on the chlorinated

* LDI induces fragmentations in the molecule, which have been indicated numerically without implying any mechanisms.

fragment. In the mass range [400-800] of the MALDI spectra a sequence of peaks with regular interval of 44 Da gives evidence of the presence of polyethylene glycol (PEG), which is supposed to be present as additive in the pigment.

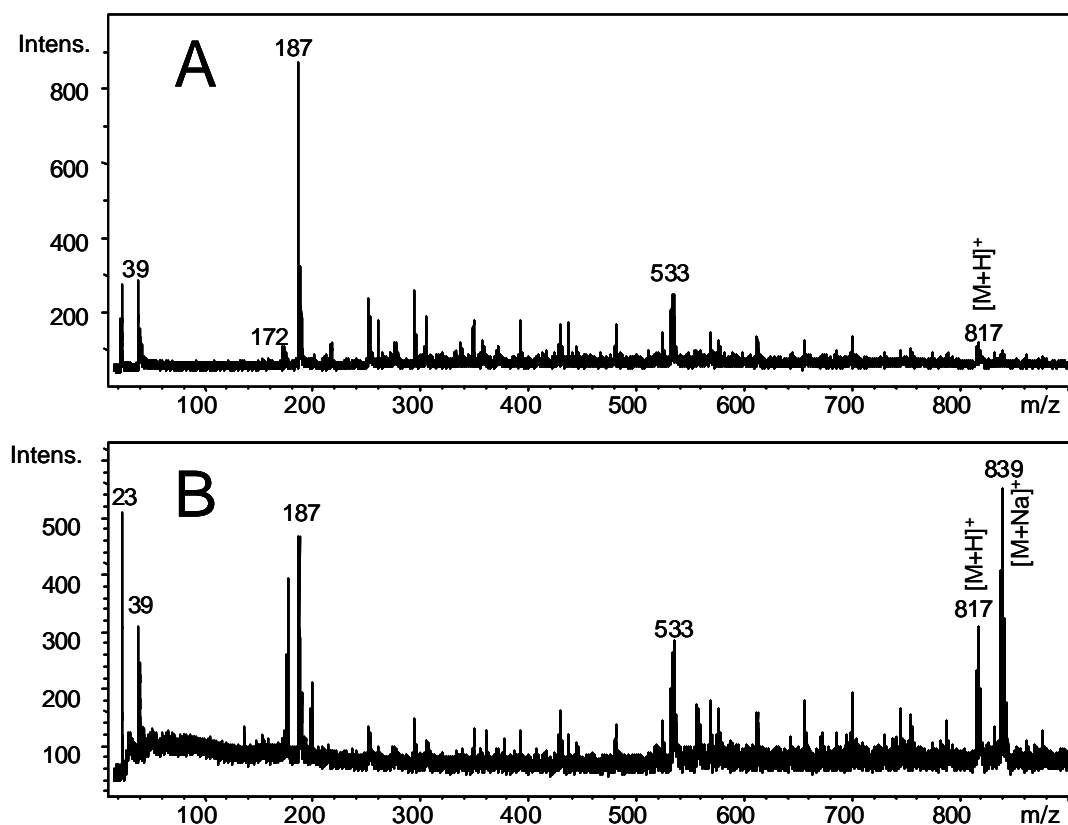


Figure 7.10 TOF-MS of diarylide pigment yellow PY83: LDI (A) MALDI (B).

7.4.3. Cu-Phthalocyanine green PG7 (chlorine substituted)

Cu-phthalocyanine green PG7 from two different suppliers were successfully desorbed and ionised in an LDI experiment. Figure 7.11.A shows the LDI mass spectrum of PG7C (Cornelissen) in the mass range [m/z 800-1400]. The dominant series of peaks at m/z 1127* is assigned to the hexadeca-chlorinated phthalocyanine species $\text{Cu-C}_{32}\text{N}_8\text{Cl}_{16}$, (labelled Cl_{16} in the figure). Additional series of peaks are assigned to various other chlorine substitutions of the copper phthalocyanine $\text{Cu-C}_{32}\text{N}_8\text{H}_{16-n}\text{Cl}_n$. Values of n are identified for dominant peaks at

* $\text{Cu-C}_{32}\text{N}_8\text{Cl}_{16}$ has a monoisotopic mass $\text{MW}_{\text{int}} = 1118$ Da with a relative abundance of 0.6%, whereas the dominant isotopic peak $\text{MW}_{\text{d}} = 1126$ Da has an abundance of 16.1% (see inset Figure 7.11.A).

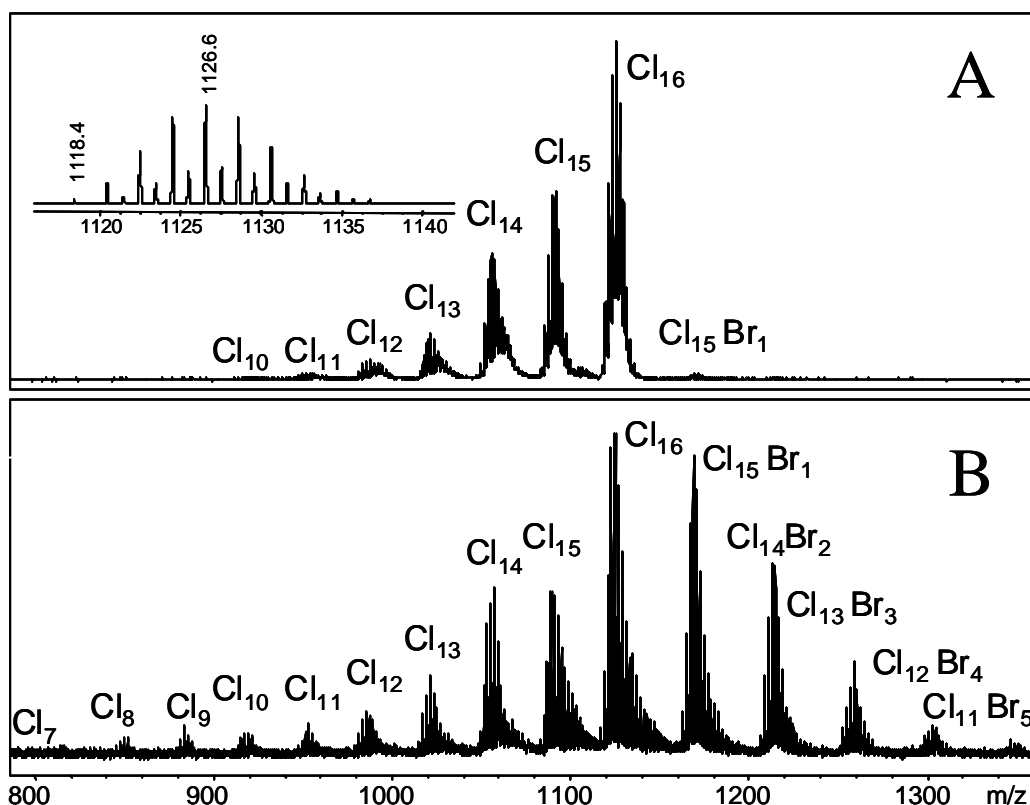


Figure 7.11 *Phthalocyanine green PG7: supplier Cornelissen (A) and supplier Winsor & Newton (B). In inset, the theoretical isotopic distribution $\text{Cu-C}_{32}\text{N}_8\text{Cl}_{16}$, with the monoisotopic (MW_m 1118 Da) and the dominant isotopic peaks (MW_d 1126 Da).*

m/z 1092 ($n=15$), 1056 ($n=14$), 1022 ($n=13$), 990 ($n=12$), 956 ($n=11$), 922 ($n=10$). A sequence of peak series is also observed in the mass range [500-600] that can be assigned to the unsubstituted copper phthalocyanine $\text{Cu-C}_{32}\text{N}_8\text{H}_{16}$ ($n=0$). We assume that the different species are present in the sample as such and are not the result of fragmentation and rearrangement during the LDI process. If this were the case fragment ions of the different brominated species would be expected with an analogous distribution (e.g. $\text{Cl}_{15}\text{Br}_1$ would yield $\text{Cl}_{14}\text{Br}_1$, $\text{Cl}_{13}\text{Br}_1$, and so forth, which is not the case). In the mass range of [0-500] a series of ions are detected that remain unidentified: 102, 158, 165, 176, 199, 220, 305, 319, 327, 341, 437, 493, 518, 560. We do not expect extensive fragmentation under our LDI conditions.

A series of peaks around $MW_d=1169$ are attributed to $\text{Cu-C}_{32}\text{N}_8\text{Cl}_{15}\text{Br}$, giving evidence for a phthalocyanine containing bromine substituent. This is ascertained in the negative mode, where characteristic distribution of peaks at m/z 35, 37 and 79, 81 is assigned to the chlorine and bromine atoms. Note that the

nomenclature PG7 does not imply that brominated substituents are present. In MALDI spectra no additional structural information was identified.

PG7WN has a LDI spectrum (Figure 7.11.B) in good agreement with PG7C. In the mass range [800-1600], however, a significantly different substitution pattern is observed. Additional substituted species are identified at m/z 887 ($n=9$) and 853 ($n=8$). Bromine/chlorine substituted species $\text{Cu-C}_{32}\text{N}_8\text{H}_{16-m-n}\text{Br}_m\text{Cl}_n$ are observed for the following (m,n) values: (5, 11) at m/z 1348, (4, 12) at m/z 1304, (3, 13) at m/z 1260, (2, 14) at m/z 1216, (1, 15) at m/z 1172. In the negative ion mode a characteristic distribution of peaks at m/z 35, 37 and 79, 81 can be assigned to chlorine and bromine resulting from elimination from the substituents.

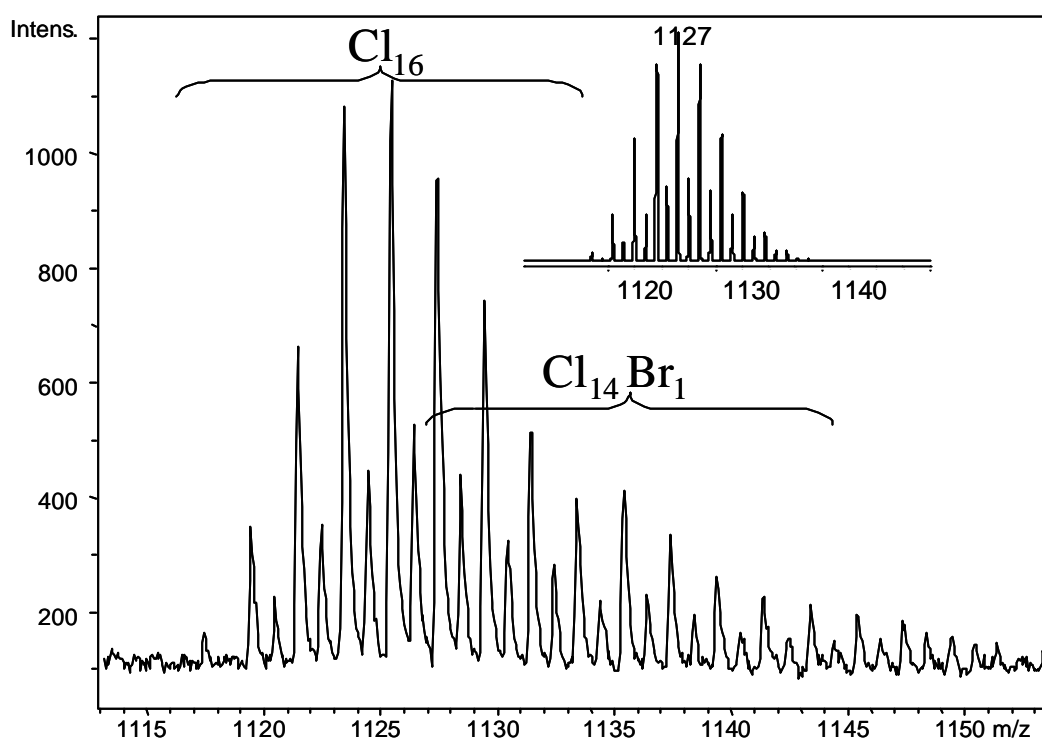


Figure 7.12 Detail of phthalocyanine green PG7 in Figure 7.12. In inset, the theoretical isotopic distribution of the hexadecachlorinated Cu-phthalocyanine $\text{Cu-C}_{32}\text{N}_8\text{Cl}_{16}$ (MW_d 1126). A shoulder in the peak sequence gives evidence for the presence of $\text{Cu-C}_{32}\text{N}_8\text{HBrCl}_{14}$ (MW_d 1136).

Figure 7.12 shows the mass range [m/z 1115-1150] in more detail. The dominant peaks are characteristic of the hexadeca-chlorinated phthalocyanine species $\text{Cu-C}_{32}\text{N}_8\text{Cl}_{16}$. A close look at the theoretical isotopic distribution of the molecule (shown in the inset) reveals a shoulder around m/z 1136 in combination

with peaks in excess of 1140. This is indicative of the substituted species $\text{Cu-C}_{32}\text{N}_8\text{HBrCl}_{14}$ (1,14).

The distribution of brominated species gives evidence for the presence of all the different chlorine substituted species in PG7, rather than being the result of chlorine loss during the LDI process. If this were the case, a similar chlorine loss would be expected for the brominated species. In the mass range [0, 500] a similar series of ions that remain unidentified are detected as for PG7C: m/z 102, 158, 165, 176, 199, 220, 305, 319, 327, 341, 437, 493, 518, 560.

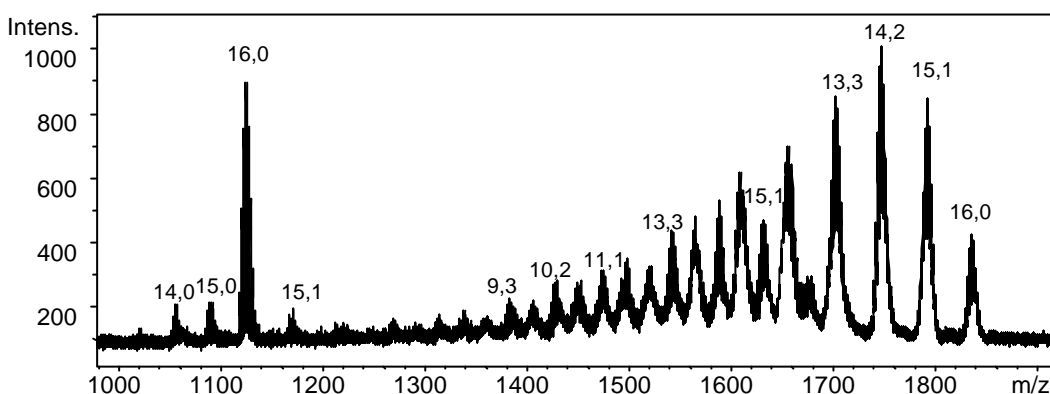


Figure 7.13 *Phthalocyanine green PG36, $\text{Cu-C}_{32}\text{N}_8\text{H}_{16-m-n}\text{Br}_m\text{Cl}_n$ (mass peaks of the ions are labelled with their m,n values).*

7.4.4. *Cu-Phthalocyanine green PG36 (chlorine and bromine substituted)*

Figure 7.13 shows the LDI-TOF-MS spectrum of PG36. This spectrum bears much resemblance to the spectrum of PG7. The series of ions in the range [0-600] is in good agreement with PG7, with notably a peak at m/z 575 assigned to the unsubstituted copper phthalocyanine. In the mass range [800-1200] a sequence of peaks is attributed to the isotopic distribution of the chlorinated species: $n=16$ at m/z 1126, $n=15$ at m/z 1092, $n=14$ at m/z 1058, $n=13$ at m/z 1023. Bromine and chlorine substituted species $\text{Cu-C}_{32}\text{N}_8\text{H}_{16-m-n}\text{Br}_m\text{Cl}_n$ are identified at m/z 1171 (1, 15) and 1216 (2, 14). In the mass range [1200, 2000], a sequence of characteristic peaks of PG36 is observed that corresponds to brominated and chlorinated species. The hexadeca-brominated species $\text{Cu-C}_{32}\text{N}_8\text{Br}_{16}$ (16,0) is observed with a series of peaks about m/z 1838. Other species are detected for (m,n) values at the m/z values listed in Table 7.3, with sodiated adducts indicated in brackets. A difference of 34Da establishes that we are here dealing with a mixture of different brominated

m/z	(m,n)	m/z	(m,n)	m/z	(m,n)
1794	15,1	1590	12,2	1385 (1408)	9,3
1749	14,2	1545 (1568)	11,3	1341 (1364)	8,4
1705	13,3	1518	12,0	1314	9,1
1680	14,0	1474 (1497)	11,1	1270 (1293)	8,2
1634 (1657)	13,1	1430 (1453)	10,2		

Table 7.3 *Cu-C₃₂N₈H_{16-m-n}Br_mCl_n species identified in the LDI-TOF-MS of PG36. Sodiated adducts are indicated in brackets.*

and chlorinated species and that the distribution observed is not the result of Cl losses (in which case we would observe a difference of 35Da).

7.4.5. Quinacridones: PV19, PR206, PR207 and PR209

The LDI of the unsubstituted quinacridone PV19 (C₂₀H₁₂N₂O₂,) (Figure 7.14.A) is dominated by an intense peak for the protonated molecular ion at m/z 313, and a minor contribution for the sodiated adduct at m/z 333. Dimers [2M+H]⁺ are observed at m/z 625 with the sodium adduct [2M+Na]⁺ at m/z 647. The negative mode (data not shown) presents a dominant peak at m/z 311 assigned to [M-H]⁻ suggesting that quinacridone ionises according to a similar mechanism as described for indigo with the analyte acting as its own matrix (proton donor).

The quinacridone PR209 (Figure 7.14.B) displays dominant peaks of the protonated and sodium species at m/z 381 and 403. Dimeric species observed in the range [650-750] are assigned to [2M-HCl]⁺ at m/z 724 and [2M-2HCl]⁺ at m/z 688. In the negative mode peaks are attributed to the radical ion and deprotonated molecules with a characteristic quadruplet.

The quinacridone mixture PR207 (Figure 7.14.C) shows a peak for the unsubstituted quinacridone at m/z 313 and 335 (sodiated), the di-chlorinated species at m/z 381 and 403 (sodiated), and a mono-chlorinated species at m/z 344 and 366 (sodiated). The negative mode provides supportive evidence with peaks at m/z 311 and the quadruplet at 379 (data not shown).

Quinacridone PR206 (Figure 7.14.D) shows the quinacridone m/z 313 and the quinacridone quinone at m/z 343 (protonated), 365 (sodiated), 381 (potassiated) and 387 (di-sodiated). The MALDI spectrum reveals the presence of

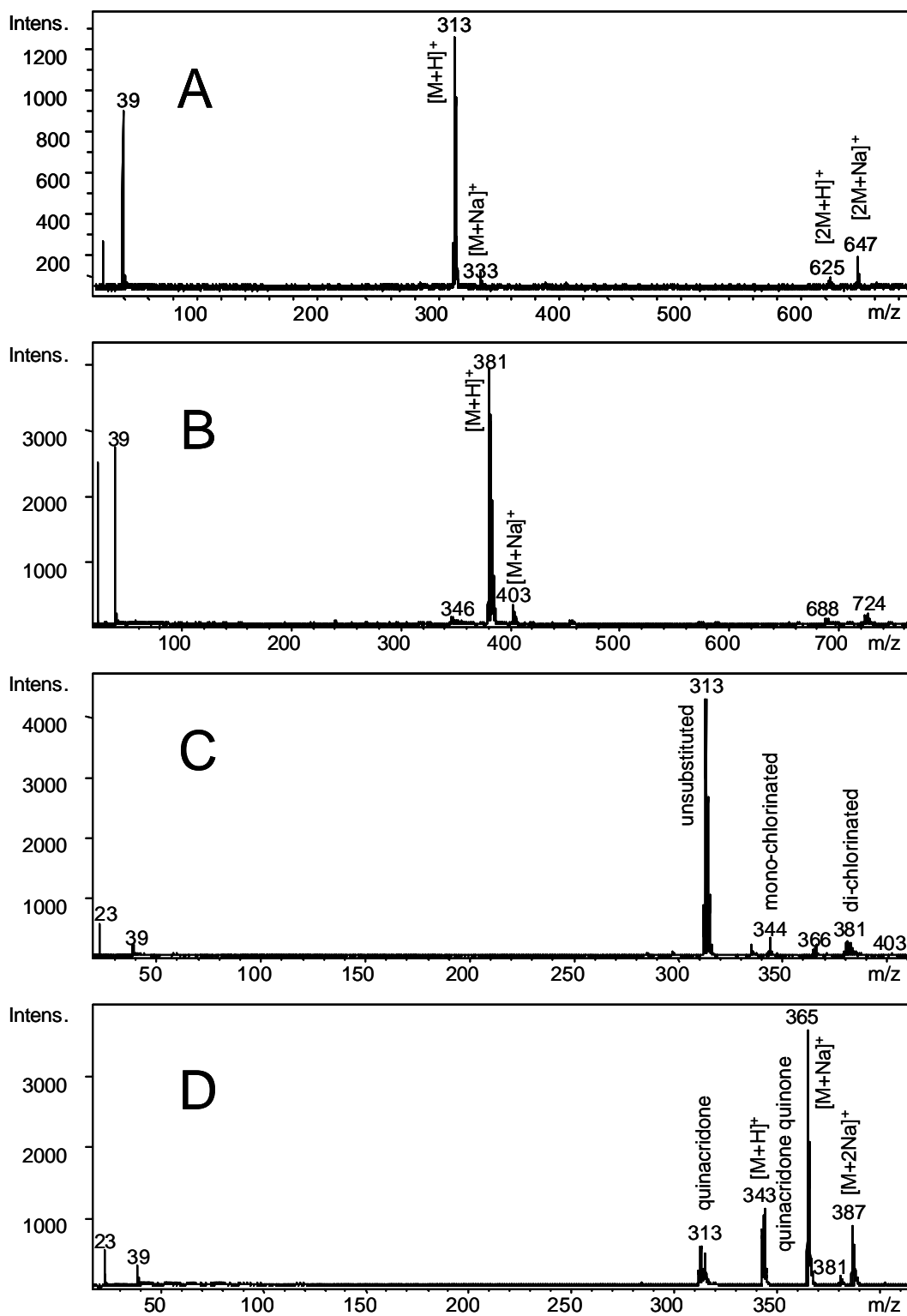


Figure 7.14 LDI-TOF-MS of quinacridone: PV19 (A); PR209 (B); PR207 (C); PR206 (D).

the same molecule specific ions and points to additional compounds that remain unidentified.

7.4.6. Perylene pigment red: PR 178

The LDI spectrum of perylene pigment red PR178 ($C_{48}H_{26}N_6O_4$) (Figure 7.15) displays a dominant peak at m/z 751, assigned to the protonated molecule. There are several fragmentation pathways opened by LDI which are thought to be caused by solid-phase absorption of UV photons. Loss of H_2 is observed at m/z 749. Fragmentation of the amine-phenyl bonds yields m/z 77 and 645 (Figure 7.6). Both ions correspond to a moiety that does not include the $N=N$ bonds. The peak at m/z 540 is assigned to the loss of two phenyl radicals by fragmentation of the amine-phenyl bonds on both sides of the molecule. The peak at m/z 556 is assigned to the fragmentation of the amine on one side and the fragmentation of the amine-phenyl group on the other side of the molecule. Multiple loss of a carbonyl is observed at m/z 722 (750-28), 630 (658-28) and 617 (645-28). A peak at m/z 1393 is believed to be the radical cation of an unidentified photo-synthesised compound.

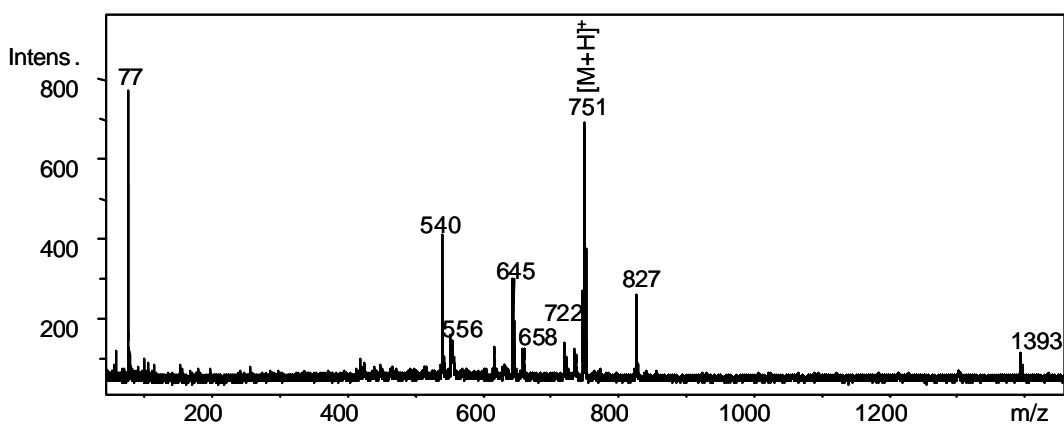


Figure 7.15 LDI-TOF-MS of perylene pigment red PR178.

7.4.7. Dioxazine pigment violet PV23

Dioxazine pigment violet PV23 ($C_{34}H_{22}N_4O_2Cl_2$) (Figure 7.16.A) displays a dominant peak at m/z 589 for the protonated molecule, with a typical Cl pattern. Dominant peaks at m/z 554 and m/z 520 are assigned to the loss of chlorine atoms.

Chapter 7

A peak at m/z 575 is assigned to the loss of a methyl group. In the negative mode (Figure 7.16.B), fragment ions are only observed for the loss of one ethyl group at m/z 559 and two ethyl groups at m/z 530. An additional peak is observed at m/z 397 numerically assigned to the fragment ion resulting from cleavage of the O-C and N-C linkages in the six membered heterocycle (Figure 7.7).

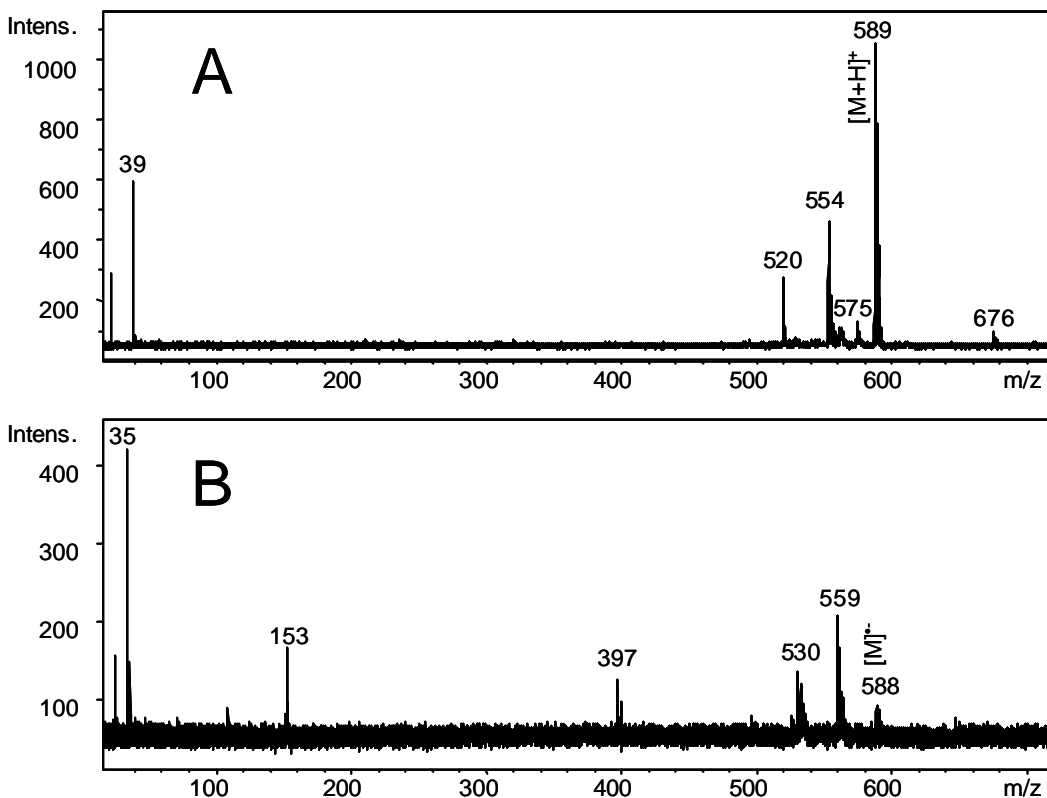


Figure 7.16 LDI-TOF-MS of dioxazine PV23: positive mode (A) and negative mode (B).

7.4.8. Diketopyrrolo Pyrrole Pigment Red PR 254

Diketopyrrolo Pyrrole Pigment Red PR254 ($C_{18}H_{10}N_2O_2Cl_2$) (Figure 7.17) displays a dominant peak at m/z 357 with a characteristic isotopic distribution assigned to the protonated molecule. Peaks at m/z 379 and 401 are assigned to sodiated and di-sodiated species $[M+Na]^+$ and $[M-H+2Na]^+$. Fragment ions are accounted by the loss of CO at m/z 330 and Cl at m/z 322. The small peak at m/z 138 is attributed to $C_6H_6N_2O_2$ resulting the loss of both C_6H_4Cl groups, a process that we postulate to occur in the solid phase by exposure to UV photons.

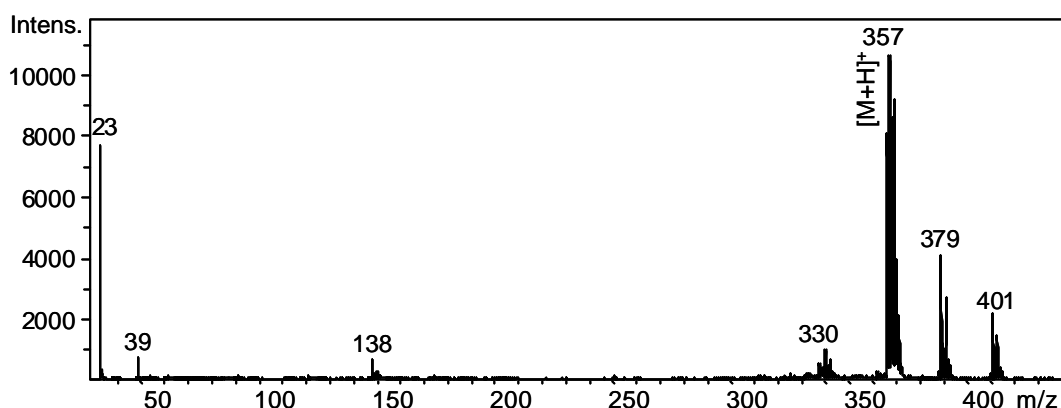


Figure 7.17 LDI-TOF-MS of diketopyrrolo pyrrole pigment red PR254.

7.4.9. Conclusions

This set of measurements demonstrates that a series of pure pigments from the major chemical classes of modern synthetic pigments were all amenable to characterisation by LDI and MALDI-TOF-MS. Using a nitrogen laser (337nm) at low power density, mass spectra reveal a soft ionisation process. Dominant peaks are observed for the intact molecular or pseudo-molecular ion, and fragmentation was observed only to a limited degree. Negative ion spectra produce complementary information in the case of the brominated and chlorinated species. The use of a matrix did not significantly increase the desorption and ionisation of the pigment, but made it possible to reveal the presence of additives such as PEG and PPG in the pigments. In many spectra, additional peaks could not be assigned on basis of the molecular structure of the pure pigments. We assume that additional compounds are being made due to exposure to the UV light.

7.5. Acrylic polymer emulsions and oil paints

7.5.1. Phthalocyanine acrylic emulsion paints

A set of different phthalocyanine-blue emulsion paints was examined. According to the label, the Grumbacher sample is known to contain PB15 ($\text{Cu-C}_{32}\text{N}_8\text{H}_{16}$) plus the red pyrrole PR254 ($\text{C}_{18}\text{H}_{10}\text{N}_2\text{O}_2\text{Cl}_2$). The three other paints from Lascaux, Flashe and Polyflashe contain unspecified phthalocyanine pigments. A typical LDI-TOF-MS spectrum is shown in Figure 7.18 in the case of the

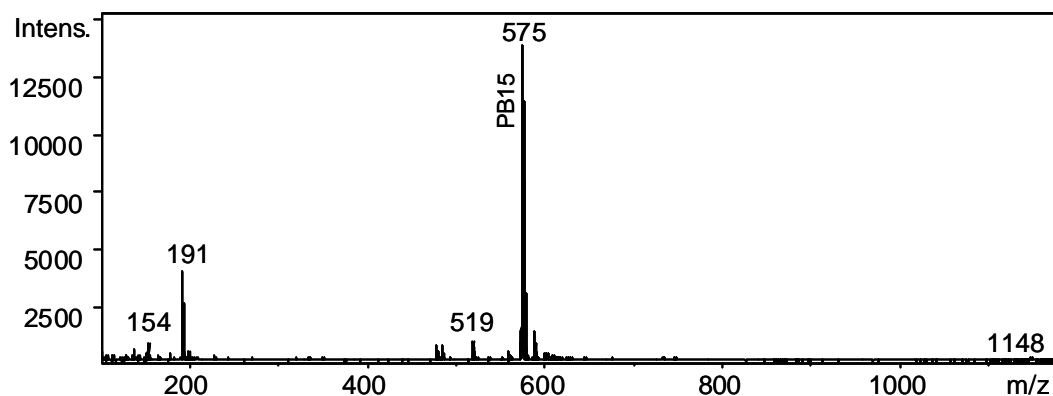


Figure 7.18 LDI-TOF-MS of a phthalocyanine blue emulsion paint (Thalo blue from Grumbacher) shows a dominant peak at m/z 575 for $\text{Cu-C}_{32}\text{N}_8\text{H}_{16}$ characteristic of the pigment blue PB15.

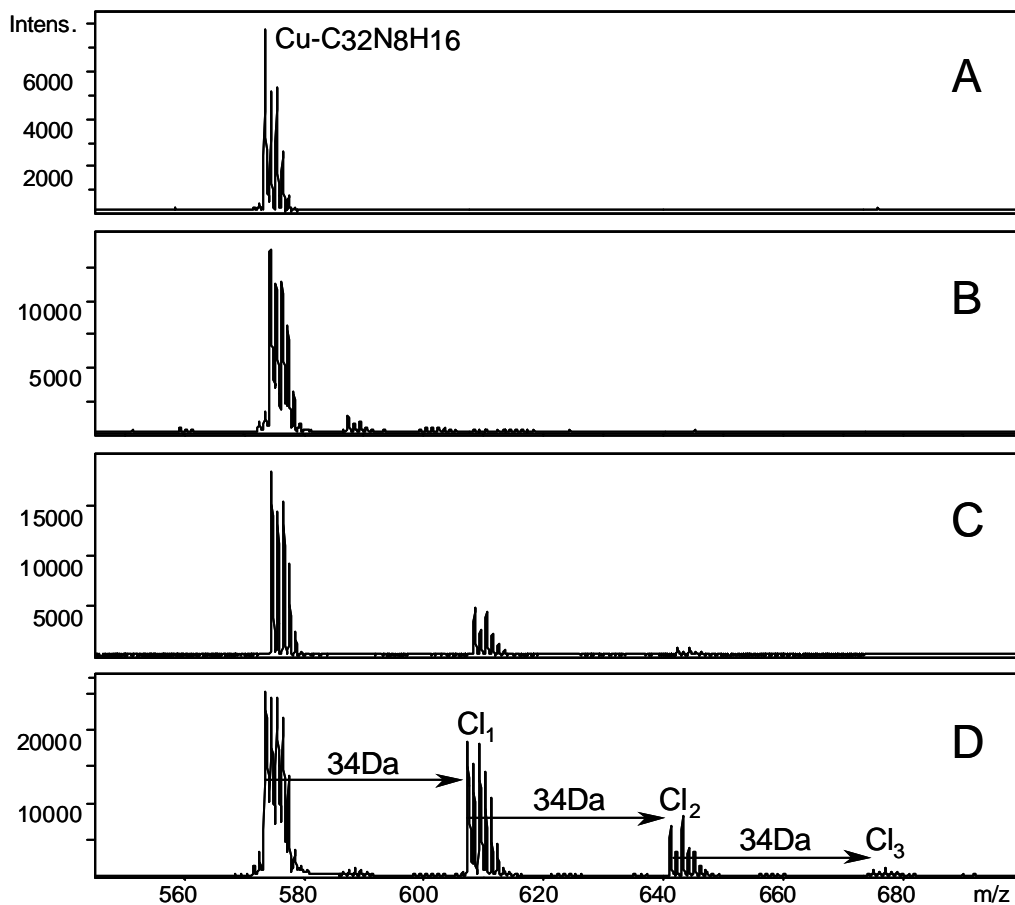


Figure 7.19 Detail of the LDI-TOF-MS of four different phthalocyanine blue emulsion paints: (A) Polyflashe brilliant blue, (B) Grumbacher thalo blue, (C) Flashe hoggar blue and (D) Lascaux permanent blue, showing their characteristic distribution of mono-, di- and tri-chlorinated phthalocyanine (marked Cl_1 , Cl_2 and Cl_3).

Grumbacher sample. The spectrum displays dominant peaks at m/z [574-576] assigned to the blue pigment $\text{Cu-C}_{32}\text{N}_8\text{H}_{16}$ (PB15).

The four emulsion paints under investigation display characteristic differences. Figure 7.19 shows in parallel the four LDI-TOF-MS spectra in the mass range m/z [550-700]. The Polyflashe sample shows a particularly “clean” spectrum (Figure 7.19.A), suggesting that pure $\text{Cu-C}_{32}\text{N}_8\text{H}_{16}$ was employed in the manufacture of the emulsion paint. In the spectra of the other paint samples (Figures 7.19.B to D), additional peaks are observed indicative of the presence of chlorinated or brominated phthalocyanine compounds. These additives modify the physical and chemical properties of the emulsion paint, and give the colour a more greenish shade. The Flashe and Lascaux spectra reveal the presence of mono- di- and tri-chlorinated species at m/z 609 and 643 and 677, marked Cl_1 , Cl_2 and Cl_3 on the spectrum. The Grumbacher and Flashe samples display a series of peaks around m/z 1146, which are assigned to the dimer (data not shown). In this mass range, the Lascaux sample displays a series of peak at m/z 1146, 1180 and 1214. The isotopic distribution of the series of peak at m/z 1146 indicates the presence of a dimeric species (rather than a brominated species such as $\text{Cu-C}_{32}\text{N}_8\text{H}_2\text{Cl}_2\text{Br}_2$). The species at m/z 1180 and 1214 correspond to two additional chlorine substitutions.

No characteristic peaks of the medium could be observed in the LDI-TOF-MS of these diverse phthalocyanine emulsion paints. Structural information concerns exclusively the pigment. This selectivity is a great advantage to analytical purposes. Selective desorption and ionisation of the pigment can be explained by a strong response of the pigment to the ultraviolet laser light, and conversely by a

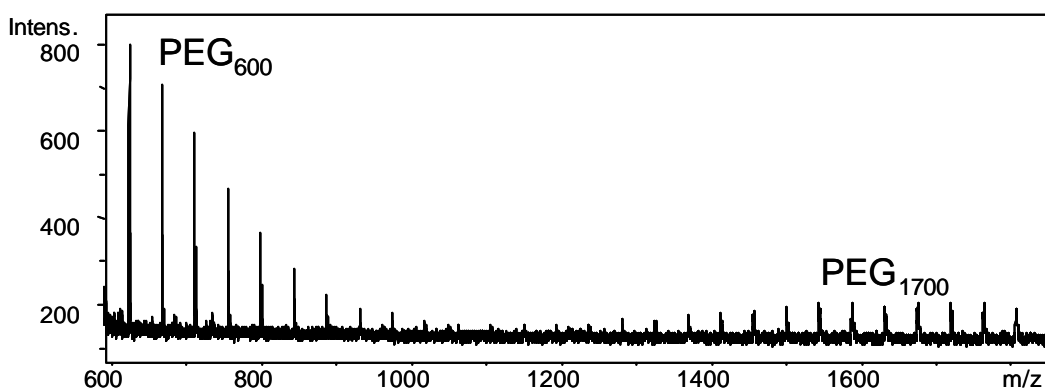


Figure 7.20 MALDI-TOF-MS of phthalocyanine blue emulsion paint (Grumbacher) in the mass range [600-1800] Da showing a sequence of peaks with regular interval of 44 Da, characteristic of polyethylene glycol (PEG) additives with average molecular weight of 600 Da and 1700 Da.

poor response of the medium itself. This feature is highly beneficial to the investigation of the pigment since it is habitually present in very small proportions and difficult to identify in FTIR because its signal is masked by the medium.

In MALDI spectra, a series of peaks with regular increment of 44 Da are assigned to the polymeric compound PEG (polyethylene glycol). PEG is present with average molecular weight of m/z 600 and 1700 in the Grumbacher sample (Figure 7.20), m/z 1000 in the Polyflashe, and m/z 600 in the Lascaux sample. No PEG was detected in the Flashe sample. PEG is a common additive to acrylic paints to improve dispersion in the emulsion. LDMS is a very sensitive method for the detection of PEG. In addition to the high ionisation efficiency of PEG, it is assumed that the sample preparation in MALDI experiments contributes to the high abundance of the ions. When the matrix is applied, PEG is probably extracted from the paint by the solvent (ethanol) and migrates to the surface of the sample where it concentrates prior to analysis. MALDI does not facilitate the production of characteristic peaks of the medium*.

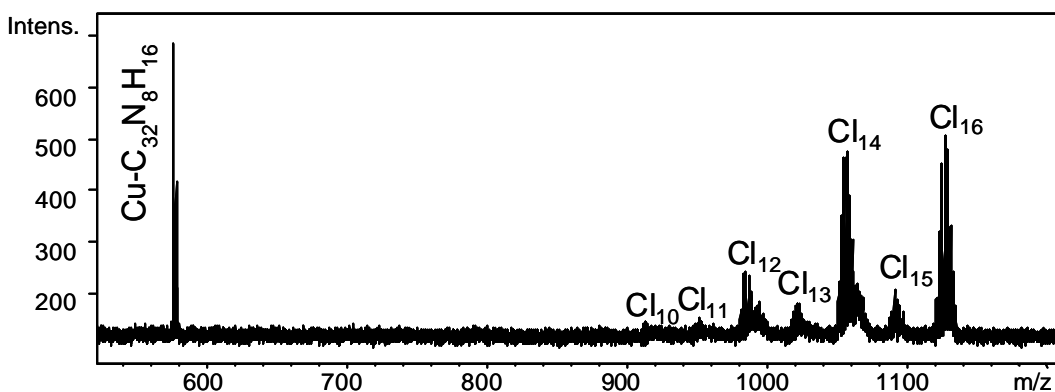


Figure 7.21 LDI-TOF-MS of a phthalocyanine green emulsion paint (Winsor&Newton), with peaks labeled according to their degree of chlorine substitution.

Similar results are obtained with phthalocyanine-green acrylic emulsion paint from Winsor & Newton (London), as shown in Figure 7.21. Dominant peaks are assigned to $\text{Cu-C}_{32}\text{N}_8\text{H}_{16}$ (576 Da) and $\text{Cu-C}_{32}\text{N}_8\text{Cl}_{16}$ (1127 Da). Additional peaks found in the mass region m/z [900-1200] are assigned to different chlorinated species with $n=[10-13]$. In the mass region [1050-1070], it is possible to distinguish ions at m/z 1058 and at m/z 1064 corresponding to the signals of the

* Acrylate media have very high molecular mass ($\text{MW} > 500,000$ Da). They are not expected to ionise under the conditions of the experiments and cannot be detected in this mass window. DTMS studies of acrylic emulsion have been recently reported¹⁷³.

chlorinated species $\text{Cu-C}_{32}\text{N}_8\text{Cl}_{14}\text{H}_2$ and $\text{C}_{32}\text{N}_8\text{Cl}_{16}$. $\text{C}_{32}\text{N}_8\text{Cl}_{16}$ corresponds to the elimination of Cu from the parent molecule. It is not clear whether the copper can be eliminated as a result of the analytical methodology.

7.5.2. Acrylic emulsion paints with azo, quinacridone, dioxazine, perylene, DPP and anthraquinone

Following the example of the phthalocyanine containing paints, a series of acrylic emulsion paints were interrogated with LDMS. The general appearance of the spectra confirms findings described in the previous section. The LDI process results in the selective desorption and ionisation of the organic pigments, whereas the acrylic medium is not observed. Under MALDI conditions the presence of PEG or PPG is occasionally detected in addition.

Identification of the pigments is based on comparison of LDI and MALDI spectra with the data gathered for pure compounds. Since the spectra present an uncomplicated profile, the identification is generally straightforward.

Light magenta (Liquitex): in LDI (Figure 7.22) the naphthol red PR188 ($\text{C}_{33}\text{N}_4\text{O}_6\text{Cl}_2\text{H}_{24}$) is identified with two dominant peaks at m/z 665 and 520 assigned to the sodiated pseudo-molecular ion and a fragment ion resulting from the cleavage of the amide bond. Peaks at m/z 543 and 559 are assigned to the sodiated and potassiated fragments. According to specification the quinacridone PR207 should be present but mass spectrometric evidence for this compound could not be obtained. At higher laser power, a PEG 1500 can be detected in trace amounts.

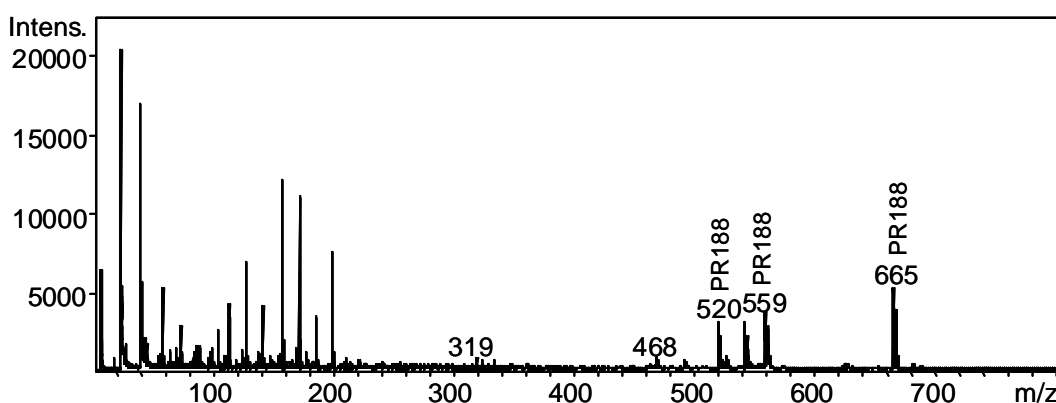


Figure 7.22 LDI-TOF-MS of light magenta paint (*Liquitex*).

Medium magenta (Liquitex): the LDI spectrum (Figure 7.23) shows the protonated molecule of di-methylated quinacridone PR122 ($C_{22}H_{16}N_2O_2$) at m/z 341 along with a peak at m/z 313 assigned to $C_{20}H_{12}N_2O_2$ from protonated quinacridone PV19. In MALDI, PEG with average molecular weight $MW_{av}=1700$, and PPG with $MW_{av}=1200$ are identified as additives.

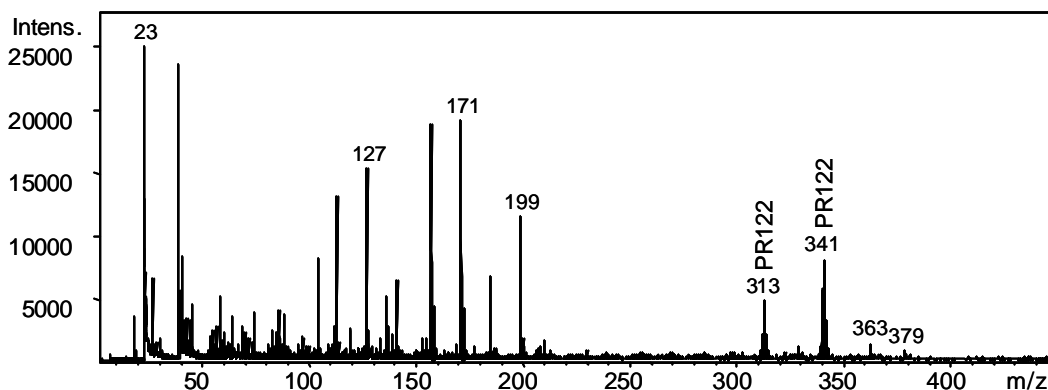


Figure 7.23 LDI-TOF-MS of medium magenta paint (Liquitex).

Vivid orange (Liquitex): the LDI mass spectrum (Figure 7.24) reveals the presence of the two pigments PY83 ($C_{36}N_6O_8Cl_4H_{32}$) at m/z 187, 251, 276 and 533, and PR188 at m/z 520 and 665 (low intensity). In MALDI pseudo-molecular ions of the two pigments could be seen at m/z 665 for PR188 and 817 and 839 for PY83. PEG with average molecular weight $MW_{av}=1700$, and PPG with $MW_{av}=700$ are detected.

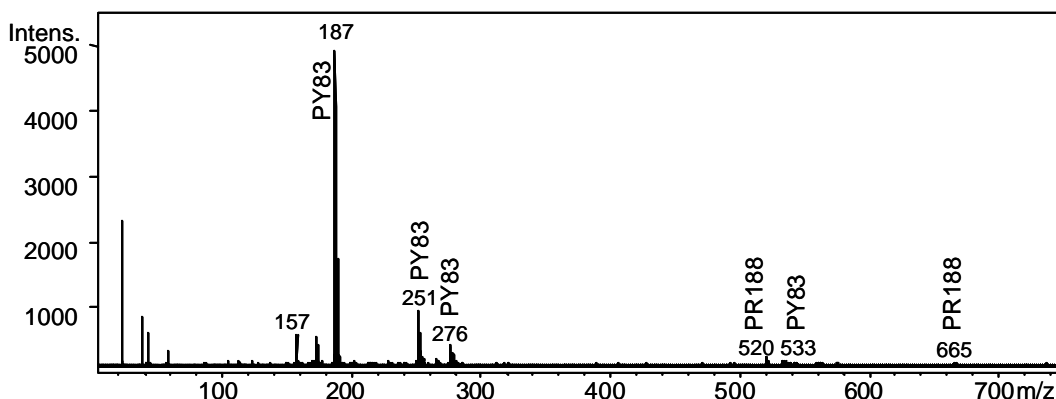


Figure 7.24 LDI-TOF-MS of vivid orange paint (Liquitex).

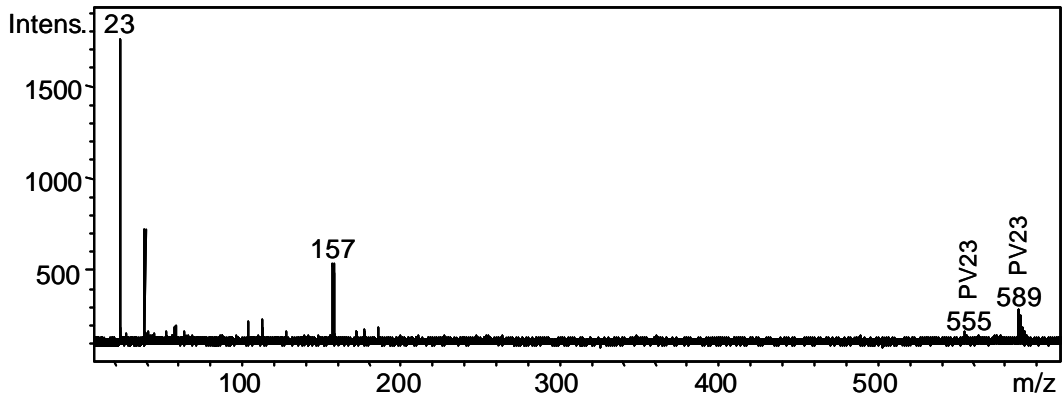


Figure 7.25 LDI-TOF-MS of brilliant purple paint (Liquitex).

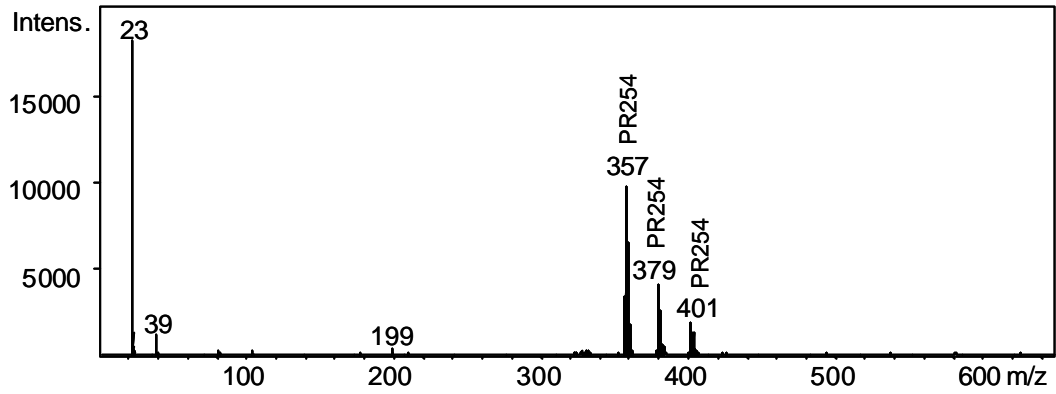


Figure 7.26 LDI-TOF-MS of pyrrole red paint (Golden).

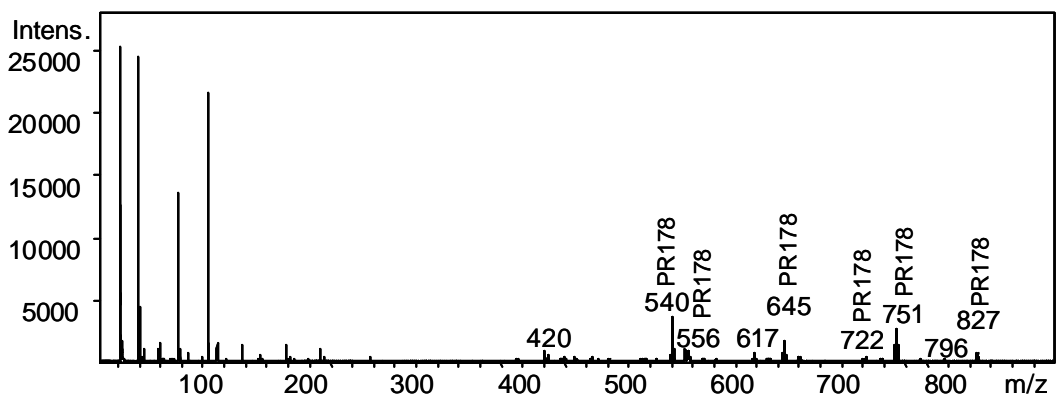


Figure 7.27 LDI-TOF-MS of perylene red paint (Grumbacher).

Brilliant purple (Liquitex): (Figure 7.25) PV23 ($C_{34}H_{22}N_4O_2Cl_2$) is identified in the paint with peaks at m/z 589 and 555 assigned to the protonated molecule and an ion due to loss of a chlorine radical. In MALDI, PEG with average molecular weight $MW_{av}=1650$ is identified as an additive.

Pyrrole red (Golden): (Figure 7.26) PR254 ($C_{18}H_{10}N_2O_2Cl_2$) is identified with peaks at 357, 379 and 401. In the MALDI spectrum, PEG with average molecular weight $MW_{av}=600$ and $MW_{av}=1700$ are identified as additive.

Perylene red (Grumbacher): the LDI spectrum (Figure 7.27) is in good agreement with the spectrum of the pure compound PR178 ($C_{48}H_{26}N_6O_4$) (Figure 7.15). The pigment can be identified by a large number of diagnostic peaks (m/z 540, 556, 645, 722, 751, 827). In the MALDI spectrum, PEG with average molecular weight $MW_{av}=1700$ is identified as additive.

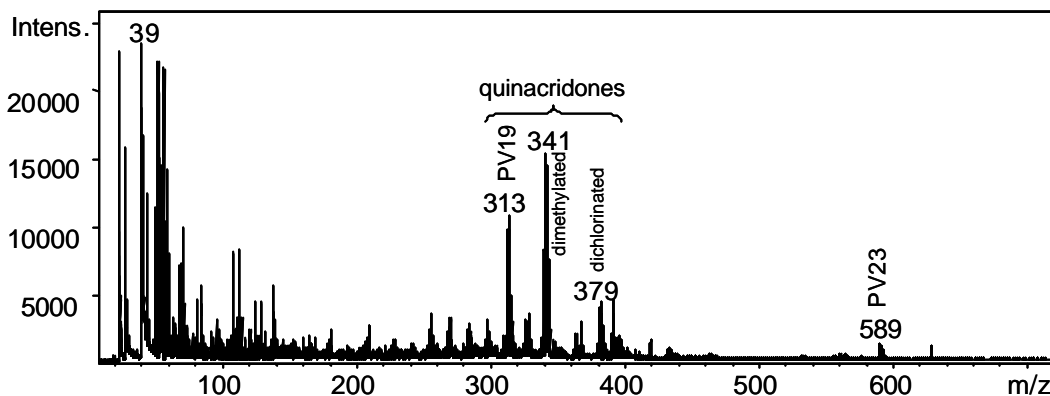


Figure 7.28 LDI-TOF-MS of permanent red violet oil paint (Van Gogh series from Talens).

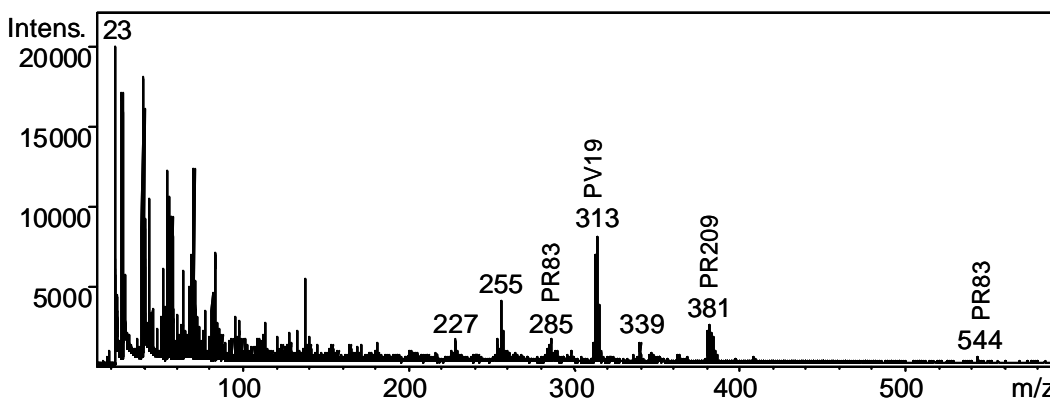


Figure 7.29 LDI-TOF-MS of rose madder oil paint (Van Gogh series from Talens).

7.5.3. Oil paints

Two oil paints from the series Van Gogh, Royal Talens (Apeldoorn) were investigated.

Permanent Red Violet (Van Gogh): (Figure 7.28) Evidence for quinacridone is found at m/z 313, 341 and 379, indicating the presence of quinacridone, and the di-methylated and di-chlorinated species. The dioxazine PV23 ($C_{34}H_{22}N_4O_2Cl_2$) was identified with a mass peak at m/z 589.

Rose madder (Van Gogh): (Figure 7.29). The quinacridone PV19 ($C_{20}H_{12}N_2O_2$) is identified with peaks at m/z 313, the dichloroquinacridone PR209 is identified with peaks at 381 and the anthraquinone PR83 is identified with peaks at m/z 285 and 544

From these analysis we can conclude that desorption and ionisation is also successful with modern pigments in an oil medium but the LDI efficiency is quite low and the process is far less selective than in the case of acrylic emulsions.

7.5.4. Conclusions

In this section we have demonstrated the applicability of LDMS for the identification of commercially available tube paints containing modern pigments. Laser desorption ionisation leads to the formation of the intact molecular ion, which afford a straightforward identification of the pigments. Fragment ions are rarely observed if at all, and no diagnostic ions of the medium (acrylic or oil) have been identified. The presence of unidentified peaks in the higher mass range was explained by the presence of unknown additional compounds in the paint formulation.

LDI provides a selective desorption and ionisation technique for the investigation of the modern pigments by mass spectrometry. This feature looks particularly promising for the *in-situ* identification of cross-sectioned samples since current methods of investigation (FTIR) often fail to identify the pigment because of strong interference of additional paint materials. Ionisation efficiency was proved to be poorer in oil media than in acrylic emulsion ones.

LDMS experiments with blue phthalocyanine acrylic paints have demonstrated that the degree of halogenation of the blue pigment can be determined in a similar way as already described for pure pigments. A variety of substitution patterns have been identified showing the degree of impurity of the PB15 ($Cu-C_{32}N_8H_{16}$). Different patterns of halogenation were identified for pigments in acrylic emulsion obtained from different manufacturers.

Some pigments indicated by the manufacturer were not detected in the acrylic emulsion or oil paints. This can have various reasons. Unfortunately no information was available about the quantity of these pigments in the tube.

The use of a MALDI matrix did not significantly increase the desorption and ionisation of the pigment, but made it possible to selectively ionise additives such as PEG and PPG in the paint formulation. These compounds play a role as compatibility agent in the emulsion.

7.6. *Spatially-resolved LDMS analysis of cross-sectioned paint samples*

One added benefit of our LDI-TOF-MS set-up is the possibility to perform spatially resolved analysis with a resolution down to 10 micrometers. In this section we explore the applicability of the LDMS approach to the study of multi-layered samples. Paint reconstructions were prepared by superimposing thin layers of two different phthalocyanine acrylic emulsion paints. LDMS of this system was used to test the applicability of the technique to the study of the surface of cross-sectioned samples, and assess the spatial-resolution. The technique was further applied to the study of paint samples removed from easel painting supplied by the Tate Gallery.

7.6.1. *Reconstructed stacks of phthalocyanine layers*

A multi-layer model was prepared by superimposing thin layers of two different emulsion paints, namely Liquitex phthalocyanine blue (PB15, $\text{Cu-C}_{32}\text{N}_8\text{H}_{16}$) and Liquitex phthalocyanine green (PG36). The sample was left to cure until being touch-dry and was then embedded and cross-sectioned. The sectioned sample viewed under the microscope shows a succession of uniform layers of circa 100 micrometers in thickness. Previous experiments have shown that the phthalocyanine blue emulsion paint can be easily distinguished from phthalocyanine green. A dominant contribution of the multi-halogenated species in the green compound is not observed in the blue compound. The laser beam was aimed at the middle of a blue layer. The spectral information is in perfect agreement with spectra of the individual tube paint analysed as thin film deposited on a metal plate. PB15 is positively identified with a series of peaks at m/z 576 (base peak) and m/z 479, 520, 560 (low relative intensity).

From this result we can conclude that LDMS is a suitable technique for the investigation of modern paint material in the form of an embedded cross-section. The preparation of the sample did not hinder the authentication of the blue phthalocyanine PB15. Selective desorption still holds for sectioned samples, and no characteristic ions of the medium could be identified. In addition we have shown that the spatial resolution of the LDI-TOF-MS set-up affords the characterisation of an individual layer of approximately 100 micrometers. No interference of the adjacent layer was observed in this case. Spatial-resolution in this series of experiments was roughly estimated to 20-50 microns.

7.6.2. Samples removed from easel paintings

Spatially-resolved LDI-TOF-MS was further employed for the investigation of two samples obtained from the Tate Gallery. The first sample is from the sculpture *Dunstable Reed* (T01361) of Phillip King (1934-). A layer of magenta colour was sampled with the laser. The LDMS spectrum reveals the presence of protonated quinacridone PV19 ($C_{22}H_{16}N_2O_2$) with a peak at m/z 313.

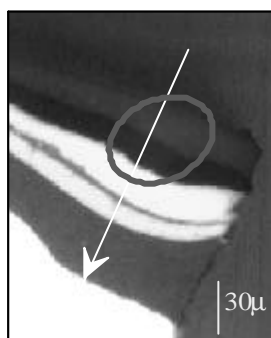


Figure 7.30 Surface of a cross-sectioned sample (*“Interior with a picture”* of Patrick Caulfield, Tate Gallery T07112) analyzed by spatially-resolved MS analysis. The estimated diameter of the laser beam (grey circle) overlaps several coloured layers.

The second sample was taken from the painting *Interior with a picture* (T07112) of Patrick Caulfield (1936-). The cross-sectioned sample displays a series of layers as shown on Figure 7.30. Spatially-resolved analysis was used for the identification of the different layers^{171, 90}. A series of spectra was taken as a line scan from the top layers to the back layers. Undoubtedly, the composition of the spectral information changes according to the position where the sample is aimed at. Best results were obtained for the top layers of the paint. The two pigments PY3 and PR170 can be readily identified in the LDI-TOF-MS spectrum (Figure 7.31) by comparison with the LDMS of the corresponding pure pigments¹³⁸. When deeper layers of the sample are analysed, the signal corresponding to this

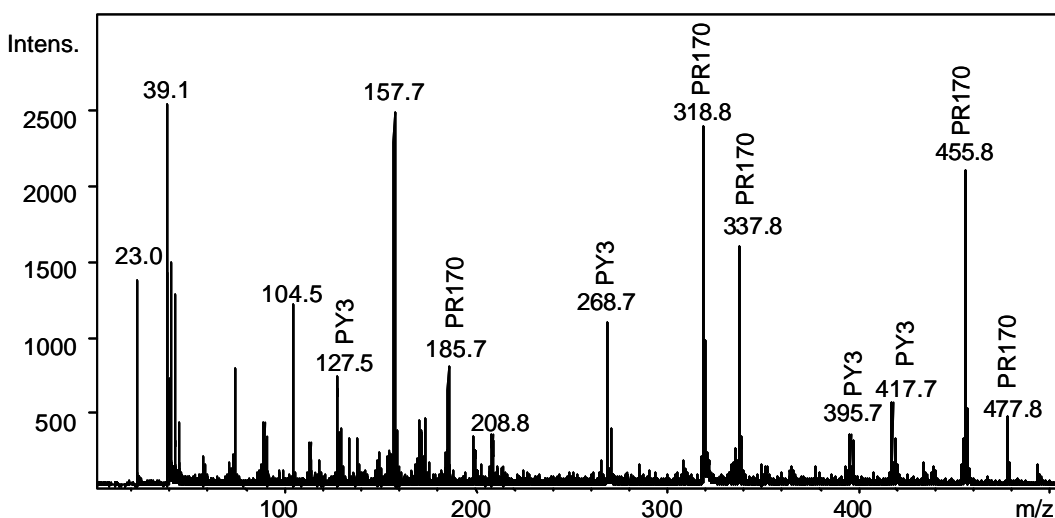


Figure 7.31 LDI-TOF-MS of the top layer of the Caulfield sample (T07112.N). The spectrum displays characteristic ions for the two pigments PY3 and PR170.

two pigments decreases and finally disappears. This phenomenon is accounted for by the size of the laser beam, which desorbs and ionises areas covering several layers (Figure 7.30).

The spectra of a series of samples from the paintings *Black on Maroon* (T01164) and *Red on Maroon* (T01165) of Mark Rothko (1903-1970) remained so far inconclusive.

7.7. Conclusions

This work demonstrates the effectiveness of LDMS methodology for the analysis and characterization of modern pigments used in easel paintings. We have paid particular attention to the investigation of a series of modern organic pigments that are difficult or simply not amenable to characterisation with FTIR because of strong interferences of additives. *In-situ* sampling was performed with organic pigments deposited as a thin film at the surface of a substrate (metallic and TLC cellulose plates). Best results were observed with LDI in the positive mode. Only little structurally relevant ions were observed in the negative mode. Spectral information provided by the desorption ionisation method is characterized by the production of quasi-molecular ions (protonated, sodiated and potassiated) with little fragmentation due to photolytic cleavage. Mass resolution of the TOF-MS analyser affords unambiguous molecular formula determination of multi-chlorinated and brominated species by assigning their different isotopes. Analysis of quinacridone pigments shows that it is possible to simultaneously identify

different compounds in a mixture (multi-component analysis). In MALDI experiments, additives of PEG and PPG were characterised. MALDI is therefore a suitable method to interrogate the purity of the sample. The disadvantage of MALDI spectra, however, is the dramatic increase of peaks at low masses that can obscure the analyte signal. In acrylic emulsion paint, pigments are selectively desorbed at low laser power density. LDMS does not yield signals characteristic of the medium, as it is the case in DTMS experiments¹⁹. Spatially-resolved experiments at the surface of paint cross-sections shows that it is possible to positively identify the presence of a pigment - or a mixture of pigments - in an individual layer of ca. 30 micrometers¹⁷¹.

In summary, LDMS is a selective tool for dye analysis in synthetic paints. Two important advantages of the use of a focussed laser for sampling is the minimal preparation prior to mass spectral analysis, as well as the ability to locally desorb and ionise organic pigments with a spatial resolution down to about 20 micrometers. The technique is therefore very attractive for the study of easel painting samples since only a few micrograms of material are needed and it offers the possibility to investigate the surface of cross-section *in-situ* with a high spatial resolution. So far however, not all painting samples were successfully analysed and further investigation will be needed to establish the reasons of this limitation. The LDMS approach looks however promising for the rapid authentication of modern pigment and for investigation of complex samples that FTIR fails to identify. In particular, LDI-TOF-MS is appropriate for the investigation of pigments whereas MALDI-TOF-MS is more suitable for the investigation of certain paint additives.

Chapter 8

Improvements in surface preparation of paint cross-sections necessary for advanced imaging techniques *

A new polishing procedure is presented for the preparation of paint cross-sections with enhanced surface quality. As a result, chemical surface analysis by Fourier Transform Infrared (FTIR) imaging spectroscopy and Laser Desorption Ion Trap Mass Spectrometry (LDMS) is now possible. Surface quality is demonstrated by FTIR-imaging, Differential Interference Contrast (DIC) microscopy and Interferometric Profiling.

* This chapter is based on the publication: Wyplosz, N., Koper, R., Van den Weerd, J., Heeren, R., Boon, J.J. Improvements in surface preparation of paint cross-sections necessary for advanced imaging technique Art et Chimie, La Couleur, Paris 16-18 September 1998, CNRS Editions.

8.1. Introduction

In the last decades, Fourier Transform Infrared Spectroscopy (FTIR) and Mass Spectrometry (MS) have found an important place in the scientific examination of works of art ⁵. These techniques only require minute amounts of sample to perform analysis at the molecular level. They are well suited for the analysis of microscopic samples removed from easel paintings and have found particular use in the study of binding media and other organic materials.

Typical samples removed from easel paintings have microscopic size and present a complex superimposition of layers, each composed of different materials mixed together. Restoration treatments and degradation induced by the passing of time may add further to the intricacy. It is desirable to understand complex phenomena such as the changes upon aging of the different organic compounds, the interactions of the different materials within one layer or between adjacent layers, or the side effect of restoration treatments.

One of the major difficulties in the investigation by FTIR and MS is to relate the molecular information about the various materials to their distribution within the sample. For MS the different layers of a sample are habitually dissected manually and analyzed separately. Separation is often inaccurate or simply unachievable, and no spatial resolution is available within the isolated paint fragments. For FTIR, the structural information can be conserved by investigating sectioned samples. Sectioning is a routine procedure common to other spectroscopic and microscopic techniques and extensive collections of cross-sections already exist in conservation laboratories. Samples are first embedded in a supportive medium (usually a transparent synthetic resin) and sectioning is achieved by polishing from one or two sides, or by microtoming. Cross-sections are made to be observed in reflection and thin-sections in transmission ⁶². Higher quality visual information is obtained with thin-sections but for practical reasons cross-sectioning is often preferred: microtoming is problematical with brittle paint materials and polishing from the both sides is admittedly demanding.

In our laboratory, novel instrumentation is being developed for the rapid local chemical analysis of the surface composition of paint sections with a spatial resolution better than 10 μm . FTIR-imaging microscopy affords for the first time the rapid visualization of the distribution of functional groups at the surface of paint sections. A Laser Desorption Ion Trap Mass Spectrometer (LDMS) allows the study of embedded paint sections by mass spectrometry.

Many samples obtained from conservation laboratories were proved to have a thin layer of embedding material left on top of the sample section after polishing. Albeit the presence of this thin film is unimportant in visual microscopy, it hampers surface chemical analyses. A new surface preparation was developed in order to remove the embedding material from the surface of the paint sections and to ensure that the actual paint is being examined with a surface analytical technique.

8.2. FTIR-imaging and Laser Desorption Ion Trap Mass Spectrometry

The novel FTIR-imaging spectrometer consists of a Michelson interferometer equipped with a step-scan mirror, an FTIR-microscope and a 64x64 pixels Mercury-Cadmium-Telluride (MCT) infrared-camera (spectral range 4000-900 cm^{-1})¹⁷⁴. In the MCT infrared-camera each pixel is an independent detector. A 400x400 μm surface area from a paint cross-section is imaged through the microscope onto the camera providing a diffraction limited spatial resolution of approximately 6 μm for a pixel in the central wavelength region. One single measurement with the MCT infrared-camera provides simultaneously 4096 FTIR-spectra at different positions resulting in high-resolution FTIR chemical images.

MS characterization of microscopic objects can be obtained by vaporizing material with focused laser pulses (LDMS)⁹⁹. An external ion source Quadrupole Ion Trap Mass Spectrometer (ITMS) was built on this principle for the analysis of paint cross-sections. Material is locally removed from the surface of a section with the help of a laser (UV or IR). The accurate targeting of the laser is realized with the help of a micro-positioning system and a visual microscope. The spatial resolution of the ablation is defined by the spot size of the laser beam (ca. 10 μm). Ionisation is either performed directly by the laser (laser desorption and ionisation) or with the help of an electron beam (laser desorption and post electron ionisation). The injection of the ions generated externally to the ITMS is achieved by homebuilt ion optics. ITMS affords the determination of ion structures by serial MS analysis (MS^n)¹²³.

8.3. Evidence of smearing

A series of samples obtained from various conservation laboratories were analyzed by FTIR-imaging. A visual microscopic image of the surface area viewed

by the MCT-camera was collected on the same microscope with a CCD camera mounted on the triocular. Areas of interest were selected on the optical image and the corresponding IR-spectra were displayed (Figures 8.1 and 8.2). Unfortunately the embedding resin strongly interfered almost everywhere at the surface of the sample. The embedding material typically shows up at 1750 cm^{-1} through its carbonyl group (C=O).

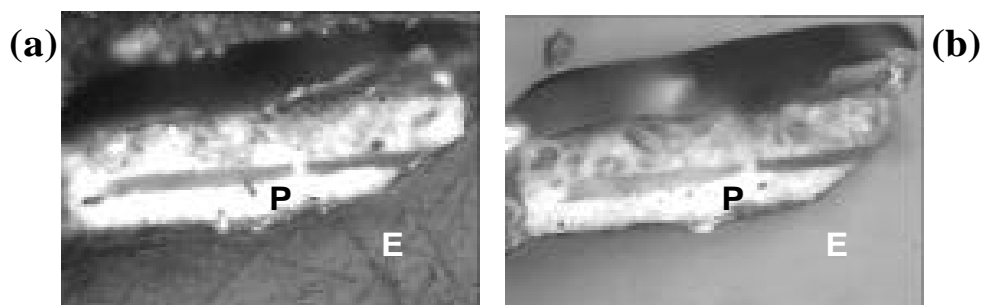


Figure 8.1 *Optical microscopy (a) before and (b) after re-polishing (see Figure 8.3. for FTIR-images)*

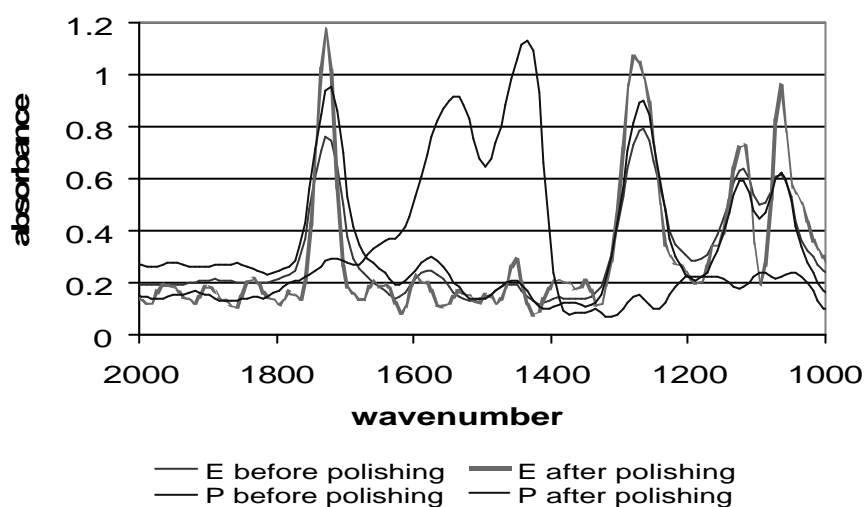


Figure 8.2 *Single pixel FTIR spectra in the $[2000-1000\text{cm}^{-1}]$ range for pixel E (in grey) and pixel P (in black) before (thin line) and after (thick line) re-polishing (see Figure 8.1.).*

False colour FTIR-images (seen here in black and white) displaying the relative absorption intensities for each pixel at particular spectral bands revealed blurred contrast (Figures 8.3.a and 8.3.c). This prevents totally the imaging of the different functional groups' distribution at the surface of the section. The bad

quality of the contrast could be either attributed to the masking of the surface section by some embedding material or to an excessive corrugation of the surface. An image viewing absorption at 1750 cm^{-1} indicates the presence of embedding material (through its C=O group) covering the paint surface.

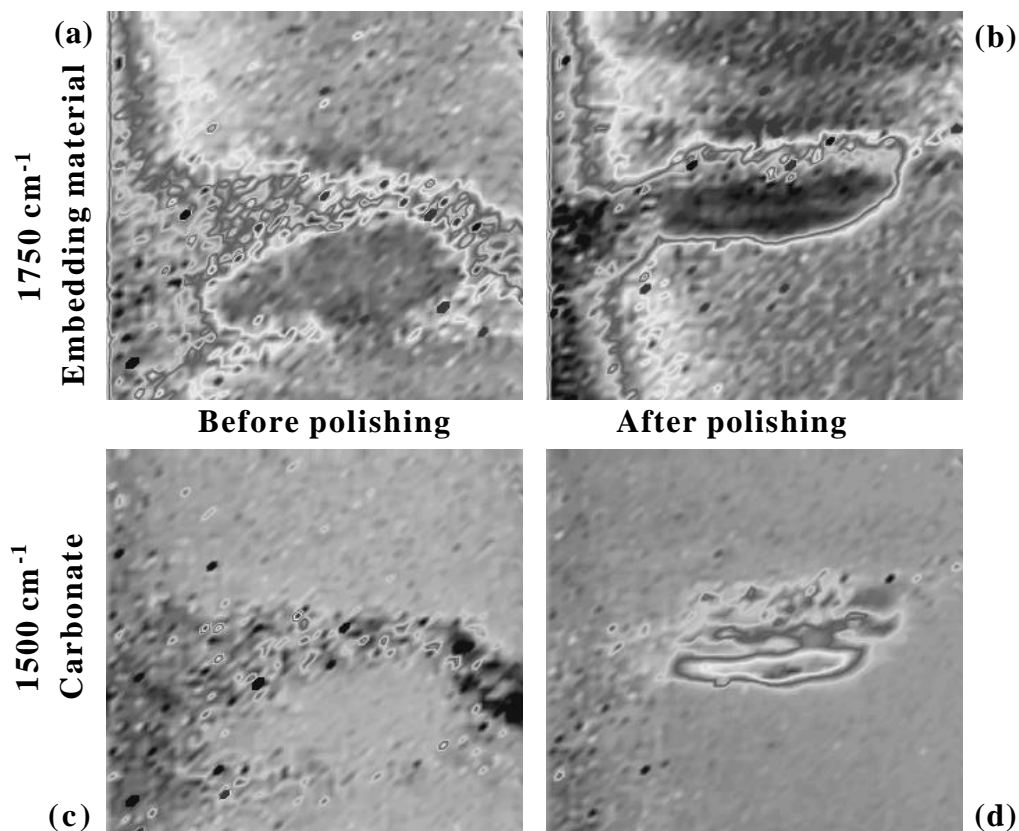


Figure 8.3 FTIR-imaging at 1750 cm^{-1} (a) before re-polishing and (b) after re-polishing, at 1500 cm^{-1} (c) before re-polishing and (d) after re-polishing. (see Figure 8.1. for optical images).

Observation by Differential Interference Contrast microscopy (DIC) ¹⁷⁵ disclosed scattered smears of embedding material on top of the paint section. A DIC picture shows a typical cross-section as received from a conservation laboratory (Figure 8.4.a). A thin transparent film of embedding material is revealed by the narrow tracks left on the surface during polishing by the abrasive. Standard microscopic observation is not sufficient to make this film perceptible (e.g. in Figure 8.1).

Often overlooked or considered as a negligible hindrance, smearing is sufficient to substantially worsen the FTIR-imaging and LDMS analytic results (for LDMS it hinders the laser desorption of the paint material). A surface

preparation method was thus sought to remove the smears of embedding material. Fast Ion Milling (FIM) ¹⁷⁶ or cryo-microtoming was tried, but the most convincing procedure appears to be lapping with rolling alumina.

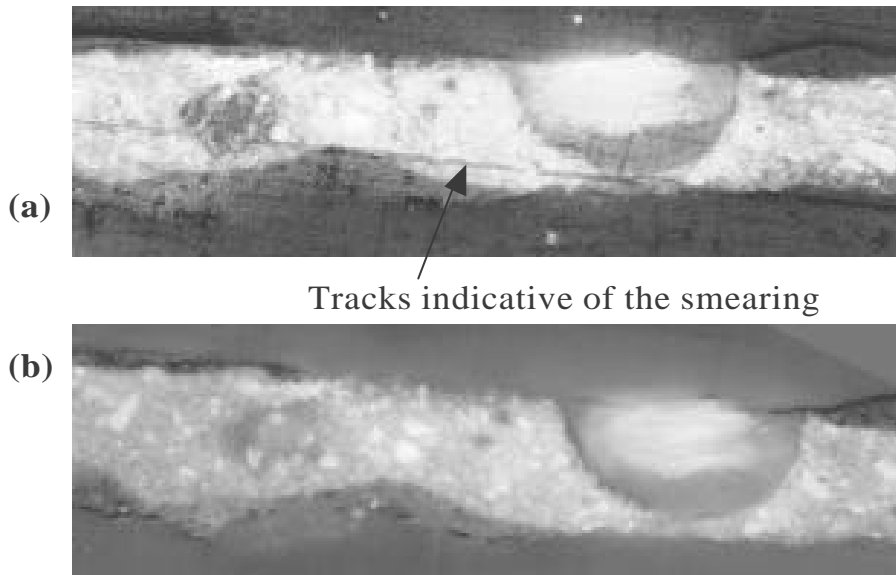


Figure 8.4 *Differential Interference Contrast (DIC) microscopy (a) before, (b) after re-polishing with rolling alumina.*

8.4. *A new sample preparation*

Samples are embedded in a cylindrical block of Technovit 2000 LC (Heraeus Kulzer, Wehrheim). A cylinder was chosen simply because it fits well our sample holder. Technovit 2000 LC is a one component acrylic light curing resin ¹⁷⁷. It cures in ca. 30 minutes at a low temperature (<32°C), does not fluoresce or infiltrate the sample excessively, and is slightly toxic. The major drawback is the slight shrinking during curing.

A three-step procedure was devised to embed samples. A silicone mould (Elastosil M-4500, Wacker, Munich) with three different types of cavities was manufactured (Figure 8.5) in order to cast different block of resins: (8.5.a) 3mm x Ø8mm cylinders, (8.5.b) halves of the same cylinder, and (8.5.c) truncated halves. A block of resin is first prepared using the hole (8.5.c). The bottom side of the manufactured block is perfectly flat despite the shrinking of the resin (Figure 6a). The block is placed in the hole (8.5.b), flat side on the top; the paint sample is positioned correctly on this side (Figure 8.6.b). Technovit 2000 LC is particularly

Sample preparation of paint cross-sections

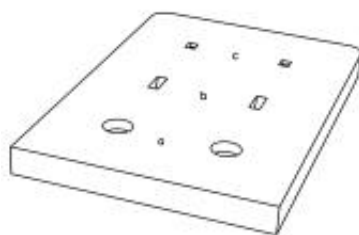


Figure 8.5 *Silicone mould*

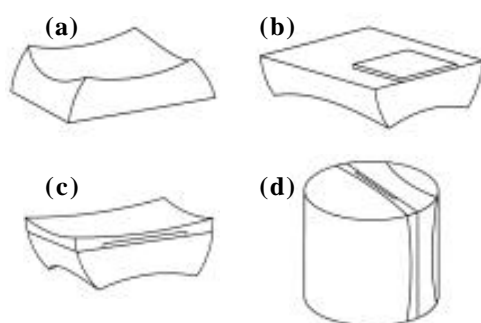


Figure 8.6 *Technovit 2000 LC blocks*

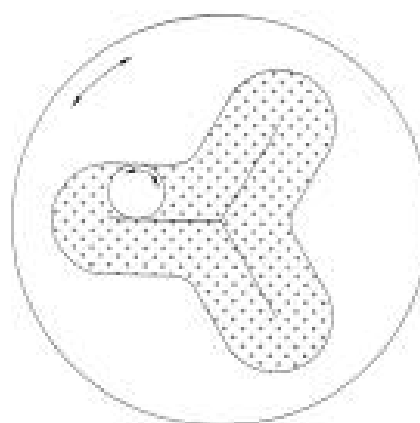


Figure 8.7 (A) *Sample holder on the rotating wheel and (B) polishing wheel.*

convenient since it stays workable until it is placed under blue light (440 nm) where tiny amounts solidify within minutes. The sample can be first accurately positioned in a droplet of resin which is cured and the block is subsequently completed (Figure 8.6.c). The block (8.6.c) is then placed in the hole (8.5.a) and the whole cylindrical block is eventually completed (Figure 8.6.d).

The cylindrical block is fixed on a homebuilt sample holder (Figure 8.7.A). The sample holder enables to adjust the surface of the section precisely parallel to the polishing wheel. The vertical position of the resin block can also be regulated in order to apply a minimal and uniform pressure during polishing. The block is first sectioned by grinding the block on a series of fixed-abrasive papers. The grain size is lowered down to grit 1200 (grain size 14 μm). To ensure an omnidirectional cutting, the sample holder is engaged in a three-branched pathway (Figure 8.7.B). The turning of the wheel induces a slow-rotational self-motion of the sample holder in the pathway. After this rough preliminary polishing, the cross-section is re-polished on rolling alumina. A continuous stream of water droplets containing 50 nm grain size alumina in suspension is deposited over a rotating thin cloth. For the comparison, 4000-grit abrasive paper has a grain size of 5 μm (Figure 8.8). The sample holder is placed on the rolling alumina and checked under DIC at regular intervals until complete removal of the smearing film is achieved (Figure 8.4.b).

Already existing cross-sections of other forms (e.g. parallelepipedic) or

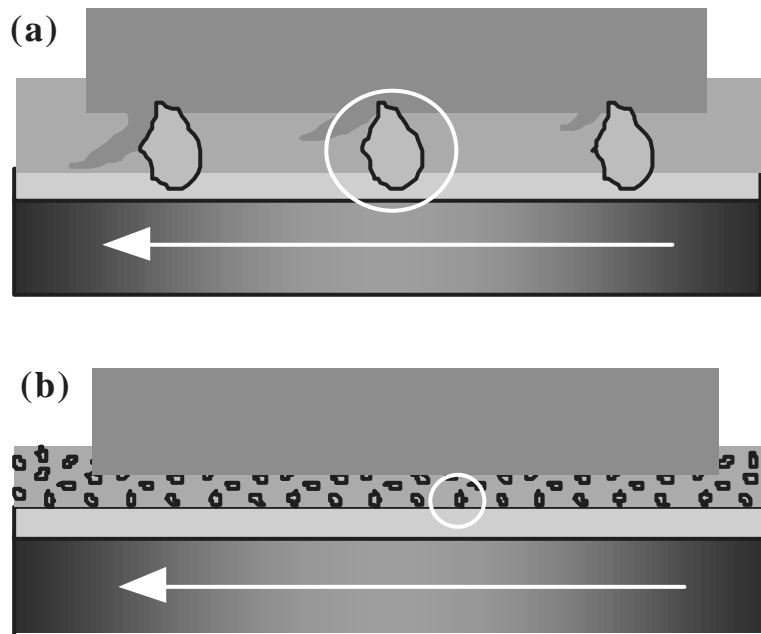


Figure 8.8 (a) Grinding with fixed abrasive on a cloth (grain size 5 μm), (b) Lapping with rolling abrasive in a lubricant: (50 nm rolling Al_2O_3 in water).

made from other common types of resins were also successfully re-polished with rolling alumina.

8.5. Analyses after polishing

The re-polishing significantly enhances optical microscopy's contrast (Figure 8.1). On the FTIR-image at 1750 cm^{-1} (Figure 8.3.b) no interference of the embedding material is found in the region of the paint section and the outline of the sample/embedding material interface is sharp. The IR-spectrum of the pixel corresponding to the point P reveals now the paint material. Interestingly the spectrum of the pixel corresponding to the point E (embedding material) is also better. This can be accredited to a decrease in corrugation of the sample after re-polishing (a smooth surface has a predominant specular reflection behaviour whereas a rough surface has a predominant diffuse reflection behaviour). At the point P, the presence of the functional group carbonate (CO_3) is inferred from its characteristic absorption band around 1500 cm^{-1} . The distribution of carbonate at the surface of the section is shown on the image (8.3.d).

Atomic Force Microscopy (AFM) ¹⁷⁸, a technique capable of revealing surface corrugation down to the nanometric scale (the alumina grain size is 50 nm), was tried to obtain information on the surface morphology of the paint section after

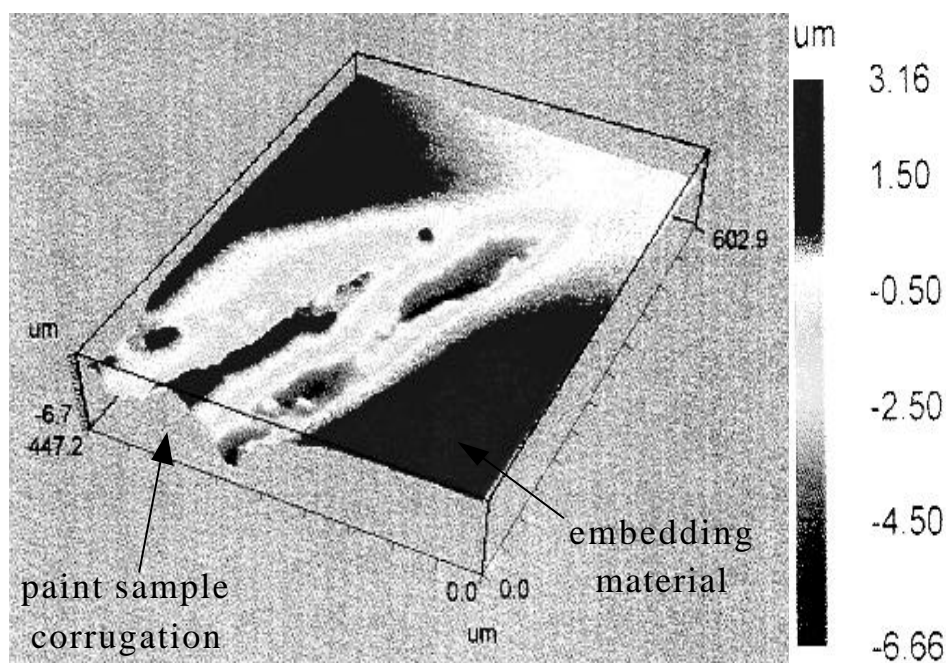


Figure 8.9 Interferometric profilometry reveals the surface corrugation of a sample after polishing with rolling alumina.

polishing. Unfortunately the scanning of the paint surface was inconclusive. Failing of the AFM was ascribed to the inadequacy of our instrument (Nanoscope II, Digital Instruments) to analyze corrugation in excess of 5 μ m. Interferometric profilometry¹⁷⁹, a non-contact analytical surface technique was subsequently employed. Figure 8.9 shows the surface of a sample after polishing with rolling alumina. The microscopic amplitude of the surface corrugation could be attributed to the distinct abrasion rates of the different materials within each layer.

8.6. Conclusion

The surface condition of most samples we obtained from conservation laboratories was insufficient for correct FTIR-imaging and LDMS analyses because of the smearing of embedding material during polishing. A new polishing procedure for embedding paint cross-sections using a homebuilt sample holder and lapping with 50 nm grain size rolling alumina suspended in water was developed. It was proved suitable both for the preparation of new samples in Technovit 2000 LC and the re-polishing of already existing samples. Paint cross-sections prepared in this manner were successfully analyzed by FTIR-imaging. Good surface chemical contrast can now be obtained in reflection mode by viewing functional groups' distributions. Since the sample preparation also opens the way to spatially-resolved LDMS of paint sections, dissection of sample will not be necessary anymore in future MS analyses.

8.7. Acknowledgements

We are grateful to Herman Ficke, Dick Glastra van Loon, Hans Zijlenmaker and Muriel Geldof (AMOLF) for their technical assistance, to Optilas (Alphen aan den Rijn) for the use of a WYKO RST-Plus Interferometric Profilometer, Tom Kruis (T.U Delft) for FIM, to Petria Noble (Mauritshuis), Prof. van Asperen de Boer and Karin Groen (MOLART) for supplying paint samples (16th to 19th century).

Bibliography

1. Bomford D, Brown C, Roy A, Kirby J, White R. *Art in the Making: Rembrandt*: National Gallery London, 1988.
2. Bomford D, Dunkerton J, Gordon D, Roy A, Kirby J. *Art in the Making - Italian Painting before 1400*: National Gallery London, 1989.
3. Bomford D. *Conservation of Paintings. Pocket Guides*: National Gallery London, 1997.
4. Ferretti M. *Scientific Investigation of Works of Art*: ICCROM, 1993.
5. Mills JS, White R. *The Organic Chemistry of Museum Objects*, 2nd Edition. Oxford: Butterworth-Heinemann, 1994.
6. Schramm HP, Hering B. *Historische Malmaterialien und ihre Identifizierung*. In: Schiessl U, ed. *Bücherei des Restaurators*: Ferdinand Enke, 1995.
7. Baer NS, Low MJD. *Advances in Scientific Instrumentation for Conservation: An Overview, Science and Technology in the Service of Conservation*, Washington, 1982. IIC.
8. Flieder F. *Mise au point des techniques d'identification des pigments et des liants inclus dans la couche picturale des enluminures de manuscrit*. *Studies in Conservation* 1968; 13:49-86.
9. Mairinger F, Schreiner M. *New Methods of Chemical Analysis - A Tool for the Conservator, Science and Technology in the Service of Conservation*, Washington D.C., 1982. IIC.
10. Thompson DV. *The Practice of Tempera Painting, Materials and Methods*: Dover, 1936.
11. Thompson DV. *The Materials and Techniques of Medieval Painting*: Dover, 1956.
12. Wehlte K. *Werkstoffe und Techniken der Malerei*: Otto Maier, 1967.
13. Mayer R. *The Artist's Handbook of Materials & Techniques*: Faber & Faber, 1991.
14. Gettens RJ, Stout G. *Painting Materials, A Short Encyclopaedia*: Dover, 1966.
15. Laurie AP. *The Painter's Methods and Materials*: Dover, 1960.
16. Cardon D, Du Chatenet G. *Guide des teintures naturelles*: Delachaux et Niestlé, 1990.
17. Schweppe H, Roosen-Runge H. *Carmine - Cochineal Carmine and Kermes Carmine*. In: Feller RL, ed. *Artists' Pigments: A Handbook of their History and Characteristics*. Vol. 1: Cambridge University Press, 1986:255-283.
18. Herbst W, Hunger K. *Industrial Organic Pigments. Production, Properties, Applications*: VCH, 1997.
19. Learner TJS. *The Characterisation of Acrylic Painting Materials and Implications for their Use, Conservation and Stability*. London: University of London, 1996.
20. De Keijzer M. *Microchemical analysis of synthetic organic artist's pigments discovered in the twentieth century*, 9th Triennial Meeting of ICOM Committee for Conservation, 1990.
21. De Keijzer M. *A survey of red and yellow modern synthetic organic artist's pigments discovered in the 20th century and used in oil colours*, 12th Triennial Meeting of ICOM Committee for Conservation, Lyon, 29 August - 3 September, 1999. James & James.
22. Kirby J. *The Preparation of Early Lake Pigments: a Survey*, Dyes on Historical and Archaeological Textiles, 6th Meeting, Leeds, September, 1987.
23. Kirby J, White R. *The Identification of Red Lake Pigment Dyestuffs and a Discussion of their Use*. *National Gallery Technical Bulletin* 1996; 17:56-69.
24. Feller RL. *Artists' Pigments*. Vol. 1. Cambridge: Cambridge University Press, 1986.
25. Roy A. *Artists' Pigments*. Vol. 2. Oxford: Oxford University Press, 1993.
26. Fitzhugh EW. *Artists' Pigments*. Vol. 3. Oxford: Oxford University Press, 1997.
27. Harley RD. *Artists' Pigments c. 1600-1835. Technical Studies in the Arts, Archaeology and Architecture*. London: Butterworth Scientific, 1982.
28. Schweppe H. *Handbuch der Naturfarbstoffe*: Ecomed, 1992.
29. McLaren K. *The Colour Science of Dyes and Pigments*: Adam Hilger, 1983.
30. Wittke G. *Farbstoffchemie. Serienbücher Chemie*: Diesterweg & Sauerländer, 1992.
31. Kirby J, Saunders D, Cupitt J. *Colorant and colour change, Early Italian Paintings Techniques and Analysis*, Symposium, Maastricht, 9-10 October, 1996. Limburg Conservation Institute.

Bibliography

32. Kirby J, Saunders D. Sixteenth- to eighteenth-century green colours in landscape and flower paintings: composition and deterioration, *Painting techniques History, Materials and Studio Practice*, Contribution to the IIC Dublin Congress, 1998.
33. Johnston-Feller RM. Reflections on the Phenomenon of Fading. *Journal of Coatings Technology* 1986; 58:33-50.
34. Johnston-Feller R, Bailie CW. An analysis of the optics of paint glazes: fading. *Science and Technology in the Service of Conservation* 1982:180-185.
35. Padfield T, Landi S. The light-fastness of the Natural Dyes. *Studies in Conservation* 1966; 11:181-196.
36. Phenix A. The fading of indigo as an artist's pigment: some technical notes. Unpublished results: AMOLF, 1998.
37. Quye A, Wouters J, Boon JJ. A Preliminary Study of Light-ageing Effects on the Analysis of Natural Flavonoid-dyed Wools by Photodiode Array HPLC and by Direct Temperature Mass Spectrometry, 11th Triennial Meeting of ICOM Committee for Conservation, Edinburgh, 1-6 September, 1996. Black & Black.
38. Rioux JP. Caractérisation de pigments décolorés dans des tableaux de Van Gogh peints à Auvers-sur-Oise, 12th Triennial Meeting of the ICOM Committee for Conservation, Lyon, 29 August - 3 September, 1999. Black & Black.
39. Saunders D, Kirby J. Light-induced Colour Changes in Red and Yellow Lake Pigments. *National Gallery Technical Bulletin* 1994; 15:79-97.
40. Townsend JH, Tennent NH. Colour Transparencies: Studies on Light Fading and Storage Stability, 10th Triennial Meeting of the ICOM Committee for Conservation, Washington, D.C., 1993.
41. Thomson G. *The Museum Environment*: Butterworth-Heinemann, 1986.
42. Van den Brink O, Van Eikema Hommes MH, Boon JJ. Discoloration of Indigo in the Paint Matrix, Fourth Infrared Users' Group Meeting (IRUG4) in Conservation Science, Bonnefanten Museum, Maastricht, February 14-18, 2000.
43. Whitmore PM, Cass GR. The Fading of Artists' Colorants by Exposure to Atmospheric Nitrogen Dioxide. *Studies in Conservation* 1989; 34:85-97.
44. Van Eikema Hommes M. *Historical Paintings Recipes and their Relevance for the Scientific Study of Paintings.*: University of Amsterdam, 2002.
45. Plesters J. Cross-sections and Chemical Analysis of Paint Samples. 1956:110-157.
46. Ferreira ESB, Quye A, McNab H, Hulme AN, Wouters J, Boon JJ. The analytical characterization of flavonoid photodegradation products: A novel approach to identifying natural yellow dyes in ancient textiles, 12th Triennial Meeting of ICOM Committee for Conservation, Lyon, 29 August - 3 September 1999, 1999. James & James.
47. Peters AT, Freeman HS. *Analytical Chemistry of Synthetic Colorants*. Advances in Color Chemistry Series. Vol. 2: Chapman & Hall, 1995.
48. Stoecklein W, Goebel R. Application of cathodoluminescence in paint analysis. *Scanning Microscopy* 1992; 6:669-678.
49. Schweppe H. Indigo and Woad. In: Fitzhugh EW, ed. *Artists' Pigments: A Handbook of Their History and Characteristics*. Vol. 3: Oxford University Press, 1997:81-108.
50. Wallert A. Identification of Flavonoid Type Yellows in Small Paint Samples by Solution Absorption and Fluorescence Spectrophotometry, *Dyes in History and Archaeology*, 13th annual meeting, Edinburgh, 1994.
51. Guineau B. Non-destructive analysis of organic pigments and dyes using Raman microprobe, microfluorometer or absorption microspectrophotometer. *Studies in Conservation* 1989; 34:38-44.
52. Billmeyer FW, Kumar R, Saltzman M. Identification of Organic Colorants in Art Objects by Solution Spectrophotometry. *Journal of Chemical Education* 1981; 58:307-313.
53. Masschelein-Kleiner L, Heylen JB. Analyse des laques rouges anciennes. *Studies in Conservation* 1968; 13:87-97.
54. McJunkin D. Cochineal and Lac: a Simple Method for Estimating Mixtures, *Dyes in History and Archaeology*, 12th annual meeting, Brussels, 1993.
55. Messinger JM. Ultraviolet-fluorescence Microscopy of Paint Cross Sections. *Journal of the American Institute for Conservation* 1992; 31:267-274.

56. Shimoyama S, Noda Y. Non-destructive Three-Dimensional Fluorescence Spectrum Technique, Dyes in History and Archaeology, 12th annual meeting, Brussels, 1993.
57. Shimoyama S, Noda Y. Non-Destructive Determination of Plant Dyestuffs used for Ancient Madder Dyeing, Employing a Three-Dimensional Fluorescence Spectrum Technique, Dyes in History and Archaeology, 13th annual meeting, Edinburgh, 1994.
58. Clark RJH. Raman microscopy: application to the identification of pigments on medieval manuscripts. *Chem. Soc. Rev.* 1995; 24:187.
59. Kirby J. A Spectrophotometric Method for the Identification of Lake Pigment Dyestuffs. *National Gallery Technical Bulletin* 1977; 1:35-45.
60. Pilc J, White R. The Application of FTIR-Microscopy to the Analysis of Paint Binders in Easel Paintings. *National Gallery Technical Bulletin* 1995; 16:73-84.
61. Derrick MR, Doehne EF, Parker AE, Stulik DC. Some new analytical techniques for use in conservation. *Journal of the American Institute for Conservation* 1994; 33:171-184.
62. Derrick MR. Infrared Microspectroscopy in the Analysis of Cultural Artefacts. In: Humecki HJ, ed. *Practical Guide to Infrared Microspectroscopy*. Vol. 19. New York: Marcel Dekker, 1995:287-322.
63. Hul-Ehrnreich Vt. Infrared Microspectroscopy for the Analysis of Old Painting Materials. *Studies in Conservation* 1970; 15:175-182.
64. Langley A, Burnstock A. The analysis of layered paint samples from modern paintings using FTIR microscopy, 12th Triennial Meeting of ICOM Committee for Conservation, Lyon, 29 August - 3 September, 1999. Black & Black.
65. Low MJD, Baer NS. Application of Infrared Fourier Transform Spectroscopy to Problems in Conservation. *Studies in Conservation* 1977; 22:116-128.
66. Wilkinson JM, Locke J, Laing DK. The Examination of Paints as Thin Sections Using Visible Microspectrophotometry and Fourier Transform Infrared Microscopy. *Forensic Science International* 1988; 38:43-52.
67. Gillard RD, Hardman SM, Thomas RG, Watkinson DE. The Detection of Dyes by FTIR Microscopy. *Studies in Conservation* 1994; 39:187-192.
68. Wallert A, Boytner R. Dyes from the Tumilaca and Chiribaya Cultures, South Coast of Peru. *Journal of Archaeological Science* 1996; 23:853-861.
69. Wallert A. Pigment and organic colorants: Two case studies, Early Italian Paintings Techniques and Analysis, Symposium, Maastricht, 9-10 October, 1996. Limburg Conservation Institute.
70. Taylor GW. The chemistry of madder dyeing: application of semi-quantitative TLC, Dyes in History and Archaeology, 10th annual meeting, London, 1991.
71. Wouters J. High Performance Liquid Chromatography of Anthraquinones: Analysis of Plant and Insect Extracts and Dyed Textiles. *Studies in Conservation* 1985; 30:119-128.
72. Wouters J, Verhecken A. The scale insect dyes (homoptera:coccoidea) species recognition by HPLC and diode-array analysis of the dyestuffs. *Annales de la Société Entomologique de France* 1989; 25:393-410.
73. Wouters J, Verhecken A. The coccid insect dyes: HPLC and computerized diode-array analysis of dyed yarns. *Studies in Conservation* 1989; 34:189-200.
74. Wouters J, Verhecken A. Potential taxonomic applications of HPLC analysis of coccoidea pigments (homoptera:sternorhyncha). *Belg. J. Zool.* 1991; 121:211-225.
75. Wouters. A new method for the analysis of blue and purple dyes in textiles, Dyes in History and Archaeology, 10th annual meeting, London, 1991.
76. Halpine SM. An improved dye and lake pigment analysis method for high-performance liquid chromatography and diode-array detector. *Studies in Conservation* 1996; 41:76-94.
77. Halpine SM. Analyses of artists' materials using High-Performance Liquid Chromatography, Early Italian Paintings Techniques and Analysis, Symposium, Maastricht, 9-10 October, 1996. Limburg Conservation Institute.
78. Koren Z. An efficient HPLC Analysis Scheme for Plant and Animal Red, Blue and Purple Dyes, Dyes in History and Archaeology, 13th annual meeting, Edinburgh, 1994.
79. Quye A, Wouters J. An application of HPLC to the identification of natural dyes, Dyes in History and Archaeology, 10th annual meeting, London, 1991.

Bibliography

80. Boon JJ, Pureveen J, Rainford D, Townsend JH. "The Opening of the Wallahalla, 1842": Studies on the Molecular Signature of Turner's Paint By Direct Temperature-Resolved Mass Spectrometry (DTMS). In: Townsend J, ed. *Turner's Painting Techniques in Context*. London, 1995:35-45.
81. Sonoda N. Characterization of Organic Azo-Pigments by Pyrolysis-Gas Chromatography. *Studies in Conservation* 1999; 44:195-208.
82. Keune K. Doctoral dissertation (in preparation): University of Amsterdam.
83. Tiedemann EJ, Yang Y. Fiber-safe extraction of red mordant dyes from hair fibers. *Journal of the American Institute for Conservation* 1995; 34:195-206.
84. Van Breemen RB. Mass Spectrometry. In: Peters AT, Freeman HS, eds. *Analytical Chemistry of Synthetic Colorants*. Vol. 2: Chapman & Hall, 1995:96-116.
85. Brune D, Hellborg R, Whitlow HJ, Hunderi O. *Surface Characterization*: Wiley-VCH, 1997.
86. Stoeckli M, Farmer TB, Caprioli RM. Automated Mass Spectrometry Imaging with a Matrix-Assisted Laser Desorption Ionization Time-of-Flight Instrument. *Journal of the American Society for Mass Spectrometry* 1998; 10:67-71.
87. Bennett JA, Schweikert EA, Van Vaeck L, Adams FC. Analysis of multicomponent dye samples with laser microprobe mass spectrometry. *J. Trace and Microprobe Techniques* 1990; 7:279-292.
88. Dale MJ, Costello KF, Jones AC, Langridge PRR. Investigation of Porphyrins and Metalloporphyrins Using Two-Step Laser Mass Spectrometry. *Journal of Mass Spectrometry* 1996; 31:590-601.
89. Sullivan AG, Gaskell SJ. The Analysis of Polysulfonated Azo Dye-stuffs by Matrix-assisted Laser Desorption/Ionization and Electrospray Mass Spectrometry. *Rapid Communications in Mass Spectrometry* 1997; 11:803-809.
90. Van der Weerd J. *Microspectroscopic analysis of traditional oil paint*. Amsterdam: University of Amsterdam, 2002.
91. Lubman DM. *Lasers and Mass Spectrometry*. Oxford Series on Optical Sciences. Vol. 1: Oxford University Press, 1990.
92. Van Hecke GR, Karukstis KK. *Laser-Assisted Mass Spectrometry. A Guide to Lasers in Chemistry*: Jones and Barlett Publishers, 1998:153-168.
93. Van Vaeck L, Van Roy W, Struyf H, Poels K, Gijbels R. Laser-microprobe mass spectrometry. In: Brune D, Hellborg R, Whitlow HJ, Hunderi O, ed. *Surface Characterization, A User's Sourcebook*: Wiley-VCH, 1997.
94. Van der Doelen GA. *Molecular studies of fresh and aged triterpenoid varnishes*. Amsterdam: University of Amsterdam, 1999.
95. Van den Berg JDJ, Boon JJ, Van den Berg KJ, Fiedler I, Miller MA. Identification of an Original Non-Terpenoid Varnish from the Early 20th Century Oil Painting "The White Horse" (1929), by H. Menzel. *Analytical Chemistry* 1998; 70:1823-1830.
96. Boon JJ, Van Och J. A Mass Spectrometric Study of the Effect of Varnish Removal from a 19th Century Solvent-sensitive Wax Oil Painting, 11th Triennial Meeting of ICOM Committee for Conservation, Edinburgh, 1-6 September 1996, 1996. James & James.
97. Van den Brink OF, Boon JJ, O'Connor PB, Duursma MC, Heeren RMA. Matrix-assisted laser desorption/ionization Fourier transform mass spectrometric analysis of oxygenated triglycerides and phosphatidylcholines in egg tempera paint dosimeters used for environmental monitoring of museum display conditions. *Journal of Mass Spectrometry* 2001; 36:479-492.
98. Finney RW, Jones AM. Direct Analysis of Wood Preservatives in Ancient Oak from the Mary Rose by Laser Microprobe Mass Spectrometry. *Studies in Conservation* 1993; 38:36-44.
99. Van Vaeck L, Struyf H, Van Roy W, Adams F. Organic and Inorganic Analysis with Laser Microprobe Mass Spectrometry. *Mass Spectrometry Reviews* 1994; 13:189-232.
100. Van Rooij GJ. *Laser Desorption Analyses in Trapped Ion Mass Spectrometry Systems*. Amsterdam: University of Amsterdam, 1999.
101. Heeren RMA, Boon JJ, Noble P, Wadum J. Integrating imaging FTIR and secondary ion mass spectrometry for the analysis of embedded paint cross-sections., 12th Triennial Meeting of ICOM Committee for Conservation, Lyon, 29 August - 3 September, 1999. James & James.
102. Andrews DL. *Lasers in Chemistry*: Springer-Verlag, 1997.
103. Posthumus MA, Kistemaker PG, Meuzelaar HLC. Laser Desorption-Mass Spectrometry of Polar Nonvolatile Bio-Organic Molecules. *Analytical Chemistry* 1978; 50:985-991.

104. Conzemius RJ, Capellen JM. A review of the applications to solids of the laser ion source in mass spectrometry. *International Journal of Mass Spectrometry and Ion Physics* 1980; 34:197-271.
105. Cotter RJ. Lasers and Mass Spectrometry. *Analytical Chemistry* 1984; 56:485A-504A.
106. Hillenkamp F. Laser Desorption Techniques of Nonvolatile Organic Substances. *International Journal of Mass Spectrometry and Ion Physics* 1982; 45:305-313.
107. Johnstone RAW, Rose ME. *Mass Spectrometry for Chemists and Biochemists*: Cambridge University Press, 1996.
108. Hanley L, Kornienko O, Ada ET, Fuoco E, Trevor J. Surface Mass Spectrometry of Molecular Species. *Journal of Mass Spectrometry* 1999; 34:705-723.
109. Todd PJ, Schaaff TG, Chaurand P, Caprioli RM. Organic ion imaging of biological tissue with secondary ion mass spectrometry and matrix-assisted laser desorption/ionization. *Journal of Mass Spectrometry* 2001; 36:355-369.
110. Van der Peyl GJQ. *Desorption and Ionization Processes in Laser Mass Spectrometry*. Amsterdam: University of Amsterdam, 1984.
111. Zenobi R, Knochenmuss R. Ion Formation in MALDI Mass Spectrometry. *Mass Spectrometry Reviews* 1998; 17:337-366.
112. Wright SJ, Dale MJ, Langridge-Smith PRR, Zhan Q, Zenobi R. Selective in Situ Detection of Polymer Additives Using Laser Mass Spectrometry. *Analytical Chemistry* 1996; 68:3585-3594.
113. Miller JC. *Laser Ablation, Principles and Applications*. Springer Series in Materials Sciences 28. Vol. 28: Springer-Verlag, 1994.
114. Rubahn H-G. *Laser application in surface science and technology*: Wiley, 1999.
115. Berkenkamp S, Menzel C, Karas M, Hillenkamp F. Performance of Infrared Matrix-assisted Laser Desorption/Ionization Mass Spectrometry with Lasers Emitting in the 3 micrometer Wavelength Range. *Rapid Communications in Mass Spectrometry* 1997; 11:1399-1406.
116. Van den Haag E. *Pyrolysis mass spectrometry of lignin polymers*. Amsterdam: University of Amsterdam, 1995.
117. Voumard P, Zhan Q, Zenobi R. A new instrument for spatially resolved laser desorption/laser multiphoton ionization mass spectrometry. *Review of Scientific Instruments* 1993; 64:2215-2220.
118. Tanaka K, Waki H, Ido Y, Akita S, Yoshida Y, Yoshida T. Protein and Polymer Analyses up to m/z 100 000 by Laser Ionization Time-of-flight Mass Spectrometry. *Rapid Communication in Mass Spectrometry* 1988; 2:151-153.
119. Karas M, Bachmann D, Bahr U, Hillenkamp F. Matrix-Assisted Ultraviolet Laser Desorption of Non-Volatile Compounds. *International Journal of Mass Spectrometry and Ion Processes* 1987; 78:53-68.
120. Cotter RJ. *Time-of-Flight Mass Spectrometry, Instrumentation and Applications in Biological Research*: American Chemical Society, 1997.
121. Louris JN, Cooks RG, Syka JEP, Kelley PE, Stafford GC, Todd JFJ. Instrumentation, Applications and Energy Deposition in Quadrupole Ion-Trap Tandem Mass Spectrometry. *Analytical Chemistry* 1987; 59:1677-1685.
122. March RE. An Introduction to Quadrupole Ion Trap Mass Spectrometry. *Journal of Mass Spectrometry* 1997; 32:351-369.
123. March RE. Quadrupole Ion Trap Mass Spectrometry: Theory, Simulation, Recent Developments and Applications. *Rapid Communications in Mass Spectrometry* 1998; 12:1543-1554.
124. Miller PE, Denton MB. The Quadrupole Mass Filter: Basic Operating Concepts. *Journal of Chemical Education* 1986; 63:617-622.
125. Todd JFJ. Ion Trap Mass Spectrometer - Past, Present and Future. *Mass Spectrometry Reviews* 1991; 10:3-52.
126. Vestal M, Juhasz P. Resolution and Mass Accuracy in Matrix Assisted Laser Desorption Ionization-Time-of-Flight. *Journal of the American Society for Mass Spectrometry* 1998; 9:892-911.
127. Mc Lafferty FT, F. *Interpretation of mass spectra*: University Science Books, 1993.
128. Wallert A. *Natural Organic Yellows: Analysis and Documentary Evidence*. Recent Advances in the Conservation and Analysis of Artefacts 1987:297-302.
129. Markham KR. Flavones, Flavonols and their Glycosides. *Methods in Plant Biochemistry*, J.B. Harborne Ed. 1989.
130. Grayer RJ. Flavonoids. *Methods in plant biochemistry* 1989.

Bibliography

131. Mabry TJ, Markham KR. Mass Spectrometry of Flavonoids.78-126.
132. Claeys M, Li QM, Van den Heuvel H, Dillen L. Mass Spectrometric Studies on Flavonoid Glycosides. Applications of Modern Mass Spectrometry in Plant Science Research 1996.
133. Dale MJ, Jones AC, Langridge-Smith PRR. Laser Desorption Laser Photoionization Time-of-Flight Mass Spectrometry of Dyes. Analytical Chemistry 1993; 65:793-801.
134. Deng H, Van Berkel GJ. Electrospray Mass Spectrometry and UV/Visible Spectrophotometry Studies of Aluminum (III)-Flavonoid Complexes. Journal of Mass Spectrometry 1998; 33:1080-1087.
135. Ma YL, Li QM, Van den Heuvel H, Claeys M. Characterization of Flavone and Flavonol Aglycones by Collision-induced Dissociation Tandem Mass Spectrometry. Rapid Communication in Mass Spectrometry 1997; 11:1357-1364.
136. Ma Y-L, Vedernikova I, Heuvel Vd, H. C, M. Internal Glucose Residue Loss in Protonated O-Diglycosyl Flavonoids upon Low-Energy Collision-Induced Dissociation. Journal of the American Society for Mass Spectrometry 1999; 11:136-144.
137. Watson DG, Pitt AR. Analysis of Flavonoids in Tablets and Urine by Gas Chromatography/Mass Spectrometry and Liquid Chromatography/Mass Spectrometry. Rapid Communications in Mass Spectrometry 1998; 12:153-156.
138. Wyplosz N, Heeren RMA, Boon JJ. Analyses of natural organic pigments by ITMS, FTMS and TOFMS, 46th ASMS Conference on Mass Spectrometry and Allied Topics, Orlando, Florida, May 31- June 4, 1998.
139. Haefliger OP. New sample preparation for quantitative laser desorption mass spectrometry and optical spectroscopy. Review of Scientific Instruments 1998; 69:18281832.
140. Ma Y. Development and application of mass spectrometric methods for the structural characterization of flavonoid glycosides and other biologically active natural products. Antwerpen, 1999.
141. Taylor GW. Detection and Identification of Dyes on Anglo-Scandinavian Textiles. Studies in Conservation 1983; 28:153-160.
142. Dik J, Wallert, A. Two still-life paintings by Jan v. Huysum. In: Hermens E, Ouwkerk, A., Costaras, N., ed. Looking Through Paintings: The Study of painting Techniques and materials in Support of Art Historical research.
143. Ferreira SB, Quey A, Mc Nab H, Hulme AN. Photo-oxidation products of quercetin and morin as markers for the characterisation of natural flavonoid yellow dyes in ancient textiles, Dyes in History and Archaeology 18, Brussels, 1999.
144. Stoessel I. Rote Farblacke in der Malerei. 1985.
145. Van den Berg AJJ, Labadie RP. Quinones. Methods in Plant Biochemistry 1989.
146. Schweppe H, Winter, J. Madder and Alizarin. In: Press OU, ed. Artists' Pigments: A Handbook of Their History and Characteristics. Vol. Vol. 3, 1997:109-142.
147. Colour Index. Bradford: The Society of Dyers and Colorist, 1971.
148. Kiel EG, Heertjes PM. Metal Complexes of Alizarin - I. The structure of the Calcium-Aluminium Lake of Alizarin. Journal of the Society of Dyers and Colourists 1963; 79:21-27.
149. Kiel EG, Heertjes PM. Metal Complexes of Alizarin - II. The structure of some metal complexes of alizarin other than Turkey Red. Journal of the Society of Dyers and Colourists 1963; 79:61-64.
150. Butler IS, Furbacher RJ. Chemistry and Artists' Pigments. Journal of Chemical Education 1985; 62:334-336.
151. Van den Brink OF. Molecular changes in egg tempera paint dosimeters as tools to monitor the museum environment.: Doctoral Dissertation, University of Amsterdam, 2001.
152. Van den Berg J. Analytical chemical studies on traditional linseed oil paints.: University of Amsterdam, 2002.
153. Balfour-Paul J. Indigo: British Museum Press, 1998.
154. Clark RJH, Cooksey CJ, Daniels MAM, Withnall R. Indigo, woad, and Tyrian Purple: important vat dyes from antiquity to the present. Endeavour, New Series 1993; 17:191-199.
155. Seefelder M. Indigo, Kultur, Wissenschaft und Technik: Ecomed, 1994.
156. Novotna P, Boon JJ, Van der Horst J, Pacakova V. Photodegradation of indigo in dichloromethane solution. J. Coloration Technology 2003; 199:1-7.

157. Burgio L, Clark RJH. Library of FT-Raman spectra of pigments, minerals, pigment media and varnishes, and supplement to existing library of Raman spectra of pigments with visible excitation. *Spectrochimica Acta Part A* 2001; 57:1491-1521.
158. Gibbs J, Jordan JG, Seddon KR, et al. The in situ identification of indigo on ancient papers. *Eur. Mass Spectrom.* 1995; 1:417-421.
159. McGovern PE, Lazar J, Michel RH. The analysis of indigoid dyes by mass spectrometry. *JSDC* 1990; 106:22-25.
160. Hendriks E, Van Eikema Hommes M, Levy-van Halm K. Indigo used in the Haarlem Civic Guard Group Portraits by Frans Hals, Painting techniques, history, materials and studio practice, IIC Dublin Congress, 1998.
161. Bauer H, Kowski, K., Kuhn, H., Luetke, W., Rademacher, P. Photoelectron spectra and electronic structures of some indigo dyes. *Journal of Molecular Structure* 1998; 445:277-286.
162. Pouli P, Emmony, D.C., Madden, C.E., Sutherland, I. Analysis of the laser-induced reduction mechanisms of medieval pigments. *Applied Surface Science* 2001; 173:252-261.
163. Gettens RJ, Kühn, H., Chase, W.T. Lead White. In: Roy A, ed. *Artists' Pigments*. Vol. 2. Oxford: Oxford University Press, 1993.
164. Morgans WM. *Outlines of Paint Technology*: Edward Arnold, 1990.
165. Van Berkel GJ, McLuckey SA, Glish GL. Electrospray Ionization of Porphyrins Using a Quadrupole Ion Trap for Mass Analysis. *Analytical Chemistry* 1991; 63:1098-1109.
166. Hinks D, Lewis DM. Capillary electrophoresis of dyes. *European Chromatography and Analysis* 1993:9-11.
167. Brumley WC, Brilis GM, Calvey RJ, Sphon JA. Collisional activation mass spectra of M^+ ions of azo dyes containing 2-naphthol. *Biomedical & Environmental Mass Spectrometry* 1989; 18:394-400.
168. Stoye D. *Paint, Coatings and Solvents*.: VCH, 1993.
169. Sonoda N, Rioux J-P, Duval AR. Identification des matériaux synthétiques dans les peintures modernes. *Studies in Conservation* 1993; 38:99-127.
170. Boon JJ, Wyplosz N, Marino B, Duursma M, Van der Horst J, Learner TJS. Mass spectrometric identification of pigments and media in modern paintings, CD-ROM A011183, 49th ASMS meeting on mass spectrometry and allied topics, Chicago, IL, 27-31 May, 2001.
171. Boon JJ, Keune K, Learner T. Identification of pigments and media from a paint cross-section by direct mass spectrometry and high-resolution imaging mass spectrometric and microspectrometric techniques, 13th ICOM Triennial Meeting, Rio de Janeiro, 2002. Vol. 1.
172. Aaserud DJ, Simonsick WJ. *Modern Mass Spectrometry for coatings*. *Progress in Organic Coatings* 1998; 34:206-213.
173. Boon JJ, Learner T. Analytical mass spectrometry of artists' acrylic emulsion paints by direct temperature resolved mass spectrometry and laser desorption ionisation mass spectrometry. *Journal of Analytical and Applied Pyrolysis* 2002; 64:327-344.
174. Lewis EN, Treado PJ, Reeder RC, et al. Fourier Transform Spectroscopic Imaging Using an Infrared Focal-Plane Array Detector. *Analytical Chemistry* 1995; 67:3377-3381.
175. Nomarski G, Weill AR. Application à la métallographie des méthodes interférentielles à deux ondes polarisées. *Revue de Métallurgie* 1955; 52:121-128.
176. Robinson K, Pugh PJA, Walker JF, Newcomb SB. Applications of Focused Ion Beam Milling in Biological Electron Microscopy. *European Microscopy and Analysis* 1997:21-22.
177. Krupa A, Waentig F. Zur Untersuchung von Holzoberflächen mit transparenten Überzügen. *Restauro* 1995; 4:244-247.
178. Binnig G, Quate CF, Gerber C. Atomic Force Microscope. *Physical Review Letters* 1986; 56:930-933.
179. Caber PJ. Interferometric profiler for rough surfaces. *Applied Optics* 1993; 32:3438-3441.

Summary

Conservation scientists have been studying easel painting materials for decades, generally focussing on problems related to the preservation of the works of arts, or the history of artists' techniques. Investigation of easel painting is no easy task and a major problem that plagued previous technical investigations is the high intricacy of the paint samples. On the one hand painting materials are intricate mixtures of molecules that have undergone complex transformations with ageing, and on the other hand sampling is highly problematical because works of art are precious and unique artefacts.

This thesis discusses the use of laser desorption mass spectrometry, known in short as LDMS, as a novel technique of analysis in the field of conservation science, and more particularly for the investigation of natural and synthetic organic pigments encountered in easel paintings. LDMS is a technique that has been advantageously used in the past by physicists and chemists for the study of surfaces. Here, this promising technique has been applied for the first time to the analysis of artists' paint materials and the investigation of samples in cross-section. Analysis focussed on the study of organic pigments present in old masters' and modern easel paintings.

Adaptation of the LDMS technique to the study of easel painting materials has required various technical developments. A sample holder was specially designed to make the analysis of samples of microscopic size or in the form of embedded cross-section possible. Preliminary studies addressed a series of experiments to test the performance and characteristics of two LDMS instruments, namely a commercial time of flight mass spectrometer (TOF-MS) and a home-build ion trap mass spectrometer (ITMS). The results of these experiments, discussed in Chapter 3 and 8, put to the light the main experimental benefits and disadvantages of each technique. The key advantage of using LDMS for the study of paint materials is the possibility to perform spatially resolved surface analysis of minute amounts of materials with a lateral resolution down to 10 micrometers. In practice, an essential requirement of the success of LDMS surface analysis appeared to be the correct preparation of the samples under investigation. Chapter 8 describes the efforts to improve the surface preparation of paint cross-sections. A new polishing procedure is presented that was employed to remove the smearing of embedding material resulting from sample sectioning. Various precision surface analytical techniques were used to ascertain the success of the method.

Several phenomena stemming from the use of a laser for sampling have particularly attracted our attention and are discussed in Chapter 3. The nature of the ions detected, hence the analytical information delivered by the measurements,

is directly connected to the choice of experimental parameters such as the characteristics of the sample surface, the laser power density, the pressure in the analytical instruments and the time-scale of the experiments. As a result of these observations it became clear how experimental conditions had to be optimised in order to obtain the highest amount of information during LDMS analysis. The surface of cross-sectioned samples must be smoothly polished and present the smallest possible corrugation. In terms of laser power density, it was established that minimum amounts of energy were the best guarantee for good analytical information and limited sample consumption. Tests performed on pure reference compounds showed that samples could be advantageously deposited on TLC plates coated with cellulose. Optimal desorption and ionisation conditions were obtained with multiple laser shots in close succession.

In Chapter 4 and 5, two ionisation techniques were examined for the LDMS analysis of flavonoid and anthraquinone reference materials, namely LDI and MALDI. LDI is the direct laser desorption and ionisation of the sample surface, whereas MALDI involves the added use of a strong chromophore (a matrix) to assist the LDI process. These experiments revealed several fundamental characteristics of LDMS experiments with organic pigments. LDI spectra showed that ions are predominantly formed as protonated molecules and simple- or multiple-alkali adducts. Unexpected formation of multiple-alkali adducts was accounted for by the modification of the surface of the sample induced by laser-matter interaction in the course of the experiment. Dimeric species were additionally observed whereas ion fragmentation was observed to be small to negligible. These experiments gave also evidence that *ablation* occurs during LDI rather than *desorption* (as the appellation of the technique suggests it). Finally the intensity of the signal shows that substantial amounts of ions are obtained with low laser power densities in LDI. This particular feature makes it possible to perform multiple-stage analysis (MS^n) with the ITMS set-up. This was proved to be particularly advantageous in cases where MS^n experiments added analytical information essential to structural identification. MALDI experiments were equally successful, but in view of the good quality of the LDI signal, MALDI did not provide additional analytical information.

From an analytical point of view, Chapter 4 and 5 established LDMS as a valuable tool in the analysis of flavonoid and anthraquinone pigments. All samples analysed were proven to respond positively to the LDI technique. MS/MS was proven to be capable of differentiating between three flavonoid isomers, luteolin, morin and kaempferol. Complex forms of alizarin (called lake) were successfully investigated with LDI although the interpretation of the spectra was not always straightforward. The potential for spot selected analysis of a focussed laser beam for LDMS sampling was proven to be successful for the analysis of a flavonoid at

Summary

the surface of a wool dyed fibre. On the other hand, LDMS analyses remained unsuccessful in several instances. In particular, LDMS-MS was unable to differentiate groups of flavonoid isomers such as quercetin from morin, or apigenin from genistein. LDMS spectra of flavonoid lakes were partially successful for the molecular characterisation of the complexed form. Finally, LDI was only successful in the identification of major compounds of flavonoid and anthraquinone plant extracts. Chromatographic techniques, notably HPLC can also identify minor compounds and therefore provide more information.

In Chapter 6, LDMS studies were extended to the blue pigment indigo. LDMS was proven to be a suitable technique for the differentiation between natural and synthetic indigo. To study LDMS of paint mixtures containing indigo, laboratory samples were prepared with indigo mixed with basic lead white and/or linseed oil. In lead white mixtures the LDI spectra revealed a strong contribution of lead related species. This suggests a chemical reaction between indigo and lead white in the condensed phase under the action of the UV laser. Spatially-resolved analysis was successful with the direct identification of indigo on dyed fibre and within cross-sectioned paint samples. A significant attenuation in the signal intensity was however observed in comparison with bulk analyses. Irregular production of the ions from the surface of sectioned samples emphasised the importance of surface preparation. Use of a thin film of matrix deposited on the surface of the section did not improve the results, suggesting a phenomenon of surface scouring during polishing of soft areas in which indigo is preferentially removed from the sample surface.

In Chapter 7, the effectiveness of the LDMS is demonstrated for the analysis and characterization of modern pigments. Mass resolution of the TOF-MS analyser is sufficient to afford molecular formula determination of multi-chlorinated and brominated species by assigning their different isotopes. Analysis of quinacridone pigments shows that it is possible to simultaneously identify different compounds in a mixture (multi-component analysis). In MALDI experiments additives to the paint in trace amount were detected, which shows that the technique is suitable for interrogation of the purity of the samples. Unfortunately, the dramatic increase of peaks at low masses in MALDI spectra can obscure the analyte signal. In acrylic emulsion paint, pigments are selectively desorbed at low laser power density. LDMS does not yield information about the medium, as is the case in DTMS experiments.

In conclusion, the experiments conducted in this thesis demonstrate that LDMS could be beneficially employed in the field of conservation science. The new possibilities offered by LDMS to investigate organic pigments by mass spectrometry directly from the surface of paint cross-sections represent a significant improvement. Spatially-resolved experiments at the surface of paint

cross-sections showed that it is possible to positively identify the presence of a pigment – or a mixture of pigments – in an individual layer of circa 10 micrometers. Furthermore the use of an ITMS mass analyser opens the way to investigation by MSⁿ. On the other hand this study establishes the condition and limitation in which LDMS could be used. It shows that the technique is limited by a range of complications introduced by the particularity of the laser sampling. Analysis is not straightforward and is not successful in all conditions. LDMS can therefore be only usefully employed in combination with other current analytical techniques such as microscopy and chromatography.

Samenvatting

Al tientallen jaren bestuderen conserveringswetenschappers de materialen die voorkomen in schilderijen. In het algemeen concentreren zij zich op de problemen met betrekking tot het bewaren van de kunstwerken of op de geschiedenis van de schildertechniek. Het onderzoek van schilderijen is niet eenvoudig; een groot probleem in "eerder" onderzoek is de complexiteit van schilderijmonsters. Niet alleen zijn schildersmaterialen mengsels van moleculen die complexe veranderingen hebben ondergaan ten gevolge van verouderingsprocessen, maar bovendien is het nemen van een monster van zoiets unieks en kostbaars als een schilderij zeer problematisch.

Dit proefschrift gaat over het gebruik van laser-desorptie massaspectrometrie (LDMS) als nieuwe analytische techniek voor conserveringswetenschap. In het bijzonder voor onderzoek aan natuurlijk en synthetische (kunstmatige) organische pigmenten (en kleurstoffen) die voorkomen in schilderijen. LDMS is in het verleden door natuurkundigen en scheikundigen met succes gebruikt voor de analyse van oppervlakken. In het hier beschreven werk is deze veelbelovende techniek voor het eerst toegepast op de analyse van kunstenaarsmaterialen en in het onderzoek van dwarsdoorsneden van verfmonsters. Het analytisch werk is geconcentreerd op de studie van organische pigmenten die voorkomen in moderne schilderijen en schilderijen van oude meesters.

De ontwikkeling van LDMS ten behoeve van het onderzoek van schilderijen vereiste een aantal technische aanpassingen. Om de analyse van microscopische monsters en van ingebedde verfdwarsdoorsneden mogelijk te maken is een speciale monsterhouder ontworpen. De prestaties en eigenschappen van twee instrumenten, een time-of-flight en een op AMOLF gebouwde ion trap massaspectrometer, zijn in een voorstudie geïnventariseerd. De resultaten van deze experimenten worden behandeld in de Hoofdstukken 3 en 8. Zij verschaffen inzicht in de voor- en nadelen van elk van de twee technieken. Het belangrijkste voordeel van het gebruik van LDMS voor onderzoek aan verfmaterialen is de mogelijkheid om met een hoog ruimtelijk oplossend vermogen (>10 micrometer) ruimtelijk opgeloste oppervlakte-analyse te doen aan zeer kleine hoeveelheden monster. De monstervoorbereiding bleek een essentiële factor voor het succes van oppervlakte-analyse met behulp van LDMS. Hoofdstuk 8 beschrijft de inspanningen die geleverd zijn om de voorbereiding van het oppervlak van verfdwarsdoorsneden te verbeteren. Het beschrijft een nieuwe polijstmethode die werd ontwikkeld om de verspreiding van inbedmateriaal ten gevolge van het doorsnijden van het monster te elimineren. De werking van deze methode is geverifieerd met verschillende nauwkeurige methoden voor oppervlakte-analyse.

Hoofdstuk 3 behandelt een aantal fenomenen die aan het gebruik van de laser voor bemonstering en analyse in de massaspectrometer zijn verbonden. De aard van de ionen, die worden gedetecteerd, en dus de analytische informatie, die voortkomt uit de metingen, is direct gerelateerd aan de keuze van de experimentele parameters. Voorbeelden daarvan zijn de oppervlakte-eigenschappen van het monster, de vermogensdichtheid van de laser, de druk in het instrument en de tijdschaal van de experimenten. Door deze bevindingen werd duidelijk hoe de experimentele condities moesten worden geoptimaliseerd om de grootste hoeveelheid informatie uit de LDMS te halen. Het oppervlak van de dwarsdoorsnedemonsters moet glad gepolijst zijn en een zo klein mogelijke ruwheid hebben. Studies van de vermogensdichtheid van de laser wezen uit dat minimale hoeveelheden energie de beste garantie waren voor hoge kwaliteit van de analytische informatie en een beperkte monsterconsumptie. Testen met pure referentieverbindingen lieten zien dat de analyse van monsters die op cellulose TLC-platen aangebracht zijn, goede resultaten oplevert. De beste desorptie- en ionisatieresultaten werden verkregen als de laserschoten elkaar snel opvolgden.

In hoofdstuk 4 en 5 worden twee ionisatiemethoden voor LDMS analyse van flavonoïde en anthrachinon-achtige referentiematerialen vergeleken, te weten LDI en MALDI. LDI is de directe laserdesorptie en ionisatie vanaf het monsteroppervlak; bij MALDI wordt een sterke chromofoor (matrix) aangebracht om ionvorming te bevorderen. Deze experimenten brachten een aantal fundamentele karakteristieken van LDMS aan organische pigmenten aan het licht. De LDI spectra lieten zien dat ionen voornamelijk gevormd worden als geprotoneerde moleculen en als enkelvoudige of meervoudige alkali-adducten. De onverwachte vorming van meervoudige alkali-adducten wordt verklaard als het gevolg van veranderingen in het monsteroppervlak door interactie tussen laserlicht en materie tijdens de analyse. Daarnaast werden dimere ionen waargenomen, terwijl de fragmentatie van ionen nauwelijks werd waargenomen. Deze resultaten gaven ook aan dat tijdens het LDI proces ablatie plaatsvindt en niet desorptie (zoals de naam van de techniek suggereert). Tenslotte werd uit de signaalintensiteit afgeleid dat grote hoeveelheden relevante ionen verkregen worden bij lage laserintensiteiten. Daardoor was het mogelijk om, gebruik makend van een ITMS instrument, een meervoudige massaspectrometrische analyse (MS^n) uit te voeren aan de ionen. Deze experimenten bewezen met name hun nut indien MS^n additionele analytische informatie verschafte, hetgeen essentieel was voor structuuridentificatie. MALDI experimenten overigens bleken eveneens succesvol maar gaven gezien de goede kwaliteit van het LDI signaal geen additionele analytische informatie.

Gezien vanuit de analyse, zetten hoofdstuk 4 en 5 LDMS neer als een waardevol gereedschap voor de analyse van flavonoïden en anthrachinon-achtige

Samenvatting

pigmenten. Alle monsters die geanalyseerd zijn gaven goede LDI-MS resultaten. MS/MS bewees zijn nut in het maken van onderscheid tussen de drie flavonoïde isomeren luteoline, morin(e) en kampferol. Gecomplexeerde vormen van alizarine zijn succesvol onderzocht met behulp van LDI alhoewel de alizarine-lak monsters zeer gecompliceerde spectra opleveren. Testen voor plaats opgeloste LDMS analyse gebruikmakend van een gefocusseerde laser bundel waren positief voor een flavonoïde op het oppervlak van een geverfde wolvezel. Daar staat tegenover dat LDMS analyse in sommige andere gevallen niet succesvol was. Het was bijvoorbeeld met LDMS/MS niet mogelijk om verschillende groepen flavonoïde-isomeren te onderscheiden, zoals quercitine van morine en apigenine van genistein. LDMS van flavonoïde lakken was ook niet succesvol voor de moleculaire karakterisering van de gecompliceerde vorm. Tenslotte moet worden opgemerkt worden dat met behulp van LDI (MS) alleen de belangrijkste componenten van flavonoïde en anthrachinone plantenextracten geïdentificeerd konden worden. Chromatografie (in het bijzonder HPLC) kan ook de componenten die in mindere mate aanwezig zijn identificeren en levert zo nog steeds meer informatie.

In hoofdstuk 6 wordt het LDMS onderzoek uitgebreid met het blauwe pigment indigo. LDMS blijkt een goede techniek om natuurlijke en synthetische indigo van elkaar te onderscheiden. Teneinde LDMS van indigohoudende verfmengsels te bestuderen werd indigo gemengd met loodwit en/of lijnolie. In mengsels met loodwit lieten de spectra een sterke bijdrage van loodgerelateerde pieken zien. Dit wijst op reacties tussen indigo en loodwit in de vaste fase die plaatsvinden onder invloed van de UV laser. Ruimtelijk opgeloste analyse was succesvol voor de directe identificatie van indigo op een geverfde vezel en in dwarsdoorsneden van verfmonsters. Er werd echter wel een significante vermindering van de signaalintensiteit waargenomen vergeleken met bulkanalyse. De onregelmatige ionenproductie van het oppervlak van dwarsdoorsneden benadrukte het belang van monstervoorbereiding. Het aanbrengen van een dunne laag matrix op het oppervlak van de dwarsdoorsnede leidde niet tot een verbetering van de resultaten. Dit duidt op een fenomeen van erosie aan het oppervlak dat plaatsvindt gedurende het polijsten van zachtere gebieden waarbij indigo preferent verwijderd wordt van het monsteroppervlak.

In hoofdstuk 7 wordt de waarde van LDMS gedemonstreerd voor de analyse en karakterisering van moderne pigmenten. De massaresolutie van de TOF-MS is toereikend voor bepaling van de molecuulformule van meervoudig gechlorideerde en meervoudig gebromeerde stoffen door gebruik te maken van de isotoopverdeling van deze elementen. De analyse van quinacridon pigmenten toont aan dat het mogelijk is om verschillende stoffen gelijktijdig in een mengsel te identificeren. Met de MALDI techniek konden sporen van additieven in pigmenten gedetecteerd worden, wat demonstreert dat techniek geschikt is voor het

onderzoeken van de zuiverheid van monsters. Jammergenoeg kan de hoge intensiteit van pieken bij lage massa in MALDI-spectra het signaal van de te onderzoeken componenten echter vertroebelen. Pigmenten in acrylaat emulsieverven worden selectief gedesorbeerd bij een lage vermogensdichtheid van de laser. In tegenstelling tot DTMS geeft LDMS geen informatie over het bindmiddel van deze verf.

Als eindconclusie kan gesteld worden dat de experimenten die in dit proefschrift beschreven staan laten zien dat LDMS nuttig kan worden toegepast in de conserveringswetenschap. De nieuwe mogelijkheden die door LDMS geboden worden voor massaspectrometrisch onderzoek van organische pigmenten direct aan het oppervlak van verfdwarsdoorsneden betekenen een belangrijke verbetering. Plaats opgeloste experimenten aan het oppervlak van verfdwarsdoorsneden toonden aan dat het mogelijk is een pigment, of een mengsel van pigmenten, positief te identificeren in een individuele laag van ongeveer 10 micrometer. Daarnaast biedt het gebruik van een ITMS de mogelijkheid tot MSⁿ onderzoek. Aan de andere kant identificeert deze studie de voorwaarden en beperkingen voor het gebruik van LDMS. Zij laat zien dat de techniek beperkt wordt door een aantal complicaties die hun oorsprong vinden in het bemonsteren met behulp van de laser. De analyse is niet zonder complicaties toe te passen en is niet onder alle omstandigheden succesvol. Hierdoor is het gebruik van LDMS met name nuttig in combinatie met andere gangbare analytische technieken zoals microscopie en chromatografie.

Résumé

La recherche en conservation étudie les problèmes relatifs à la bonne préservation des peintures, leur restauration ainsi qu'à l'histoire des matériaux et des techniques. L'investigation scientifique des œuvres peintes est très problématique car les échantillons disponibles pour analyse sont fort complexes. D'une part la couche picturale est constituée d'un mélange de matériaux qui subissent des transformations physico-chimiques au cours du temps, d'autre part la prise d'échantillon pose problème car les œuvres d'art sont des objets uniques et précieux.

Cette thèse étudie l'utilisation de la spectrométrie de masse par désorption laser (connue sous l'acronyme anglais LDMS pour *Laser Desorption Mass Spectrometry*) comme nouvelle technique d'analyse dans le domaine de la conservation scientifique, et plus spécifiquement pour l'étude des pigments organiques, naturels ou de synthèse, présents dans les peintures de chevalet. Le LDMS est une technique déjà connue et mise à profit par les physiciens et les chimistes, essentiellement pour l'étude des surfaces. Dans cette thèse, le LDMS a été appliqué à l'analyse des matériaux présents dans les peintures de chevalet, et de quelques échantillons sous forme de coupes transversales. Les analyses se concentrent plus particulièrement sur l'étude des pigments organiques en usage dans les peintures de maîtres anciens ou les peintures modernes.

L'application du LDMS à l'étude des peintures a nécessité divers développements techniques. Un porte-échantillon a été spécialement développé pour rendre possible l'analyse d'échantillons de taille microscopique ou sous la forme de coupes transversales. Des études préliminaires ont eu pour but l'évaluation des performances de deux instruments pour la spectrométrie de masse par désorption laser (LDMS), l'un avec un analyseur à temps de vol (TOF-MS) et l'autre construit spécifiquement à cet usage avec une trappe d'ions (ITMS). Les résultats de ces expériences présentés dans les chapitres 3 et 8 mettent en lumière les principaux avantages et inconvénients de chacune de ces deux approches. L'avantage primordial de l'usage du LDMS dans l'étude des peintures réside dans la possibilité de réaliser une analyse de surface avec des quantités infimes d'échantillons, et cela avec une résolution spatiale pouvant atteindre une dizaine de microns. Une préparation minutieuse des échantillons s'est révélé être une condition essentielle au succès de l'analyse de surface par LDMS. Le chapitre 8 décrit les efforts mis en œuvre pour améliorer la préparation de la surface des coupes transversales. Une nouvelle méthode de polissage est présentée qui est employée pour éliminer la fine couche de matériaux d'encapsulation qui vient

recouvrir la surface de l'échantillon lors du polissage. Diverses techniques d'analyse de surface ont été utilisées pour confirmer le succès de la méthode.

Divers phénomènes liés à l'utilisation d'un laser pour la production des ions ont retenu notre attention et sont discutés au chapitre 3. La nature des ions détectés, et de ce fait des informations livrées par l'analyse, est en rapport direct avec le choix des paramètres expérimentaux tels l'état de surface de l'échantillon, la puissance du laser, la pression régnant dans l'instrument d'analyse, ou encore de la durée de l'analyse. A la lumière de ces observations, il devint évident que les conditions expérimentales lors des analyses par LDMS peuvent être optimisées pour augmenter la précision des résultats. Les coupes transversales doivent être polies de la façon la plus égale possible afin de présenter un relief minimum. La puissance du laser sera choisie la plus basse possible afin de combiner de bons résultats d'analyse avec une déplétion minimum de l'échantillon. Des tests réalisés sur des matériaux de référence purs ont montré que les échantillons peuvent être avantageusement déposés sur des plaques pour chromatographie en couche mince couverte de cellulose. On a également établi que les conditions optimales de désorption et ionisation sont obtenues par séries de tirs successifs du laser.

Aux chapitres 4 et 5, deux techniques d'ionisation appelées respectivement LDI (*Laser Desorption and Ionisation*) et MALDI (*Matrix-Assisted Laser Desorption/Ionisation*), sont mises en oeuvre pour l'analyse LDMS d'échantillons de référence. La technique du LDI désigne l'ionisation-désorption par laser réalisée directement à la surface de l'échantillon, tandis que le MALDI fait en plus appel à l'adjonction d'un puissant chromophore (appelé matrice) pour assister le phénomène de LDI. Ces expériences ont révélé plusieurs caractéristiques fondamentales de l'étude par LDMS des pigments organiques. Les spectres LDI montrent que les ions sont principalement formés sous la forme de molécules protonées et comme ions adduits (addition simple et multiple d'atomes métalliques). La formation inattendue d'ions adduits est attribuée à la modification de la surface de l'échantillon, résultat de l'interaction photon-matière pendant l'expérience. Des dimères ont également été observés alors que la fragmentation ionique reste négligeable. Ces expériences apportent également la preuve que le LDI est un phénomène d'ablation plutôt que de désorption (comme l'appellation LDI le laisse littéralement entendre). Finalement on constate qu'avec le LDI, une quantité importante d'ions est obtenue à des intensités faibles du laser. Cette caractéristique permet de réaliser des analyses successives (MS^n) avec la trappe d'ions. Ceci s'avère particulièrement utile lorsque l'analyse MS^n peut apporter des informations supplémentaires essentielles à l'identification structurale des molécules. La technique MALDI est tout aussi satisfaisante mais au vu des bons résultats du LDI, elle n'apporte pas d'informations supplémentaires.

Résumé

Du point de vue analytique, les chapitres 4 et 5 établissent que le LDMS est une technique efficace dans l'analyse des pigments de la famille des flavonoïdes et des anthraquinones. La plupart des échantillons analysés ont montré une bonne réponse au LDI. Les analyses successives en MS-MS ont réussi à différencier trois flavonoïdes isomères, à savoir la lutéoline, la morine et le kaempferol. Des formes complexes de l'alizarine, appelée laque, ont été étudiées avec succès par LDI, mais l'interprétation des spectres en est difficile. L'utilisation d'un faisceau laser convergeant pour la formation d'ions permet une analyse LDMS résolue dans l'espace. Ceci est démontré pour l'analyse de teintures à la surface de fibres de laine. Cependant les analyses LDMS ne furent pas toujours couronnées de succès. En particulier le LDMS-MS fut incapable de différencier des flavonoïdes isomères comme la quercitine de la morine ou l'apigénine de la génistéine. Les spectres LDMS de laques de flavonoïdes sont aussi infructueux pour la caractérisation moléculaire de la forme complexée. Finalement le LDI ne s'est révélé concluant que pour l'identification des composants principaux d'extraits de plantes contenant des flavonoïdes ou des anthraquinones. De ce fait le LDMS n'égale pas à ce jour des techniques de chromatographie comme l'HPLC capable d'identifier des composés secondaires en très faibles quantités.

Au chapitre 6, les investigations par LDMS ont été étendues au pigment bleu indigo. Le LDMS est une technique adéquate à la différenciation entre indigo naturel et indigo synthétique. Pour l'étude par LDMS de mélanges de matériaux contenant de l'indigo, des échantillons furent préparés au laboratoire avec de l'indigo et du blanc de plomb et/ou de l'huile de lin. Dans les échantillons avec du blanc de plomb, les spectres LDI ont montré une forte contribution des espèces contenant du plomb. Cela semble indiquer une réaction chimique en phase condensée sous l'action du laser UV entre l'indigo et le blanc de plomb. Des analyses résolues dans l'espace ont été accomplies menant à l'identification de l'indigo directement à la surface de fibres teintées ou de coupes transversale d'échantillon de peinture. Une atténuation importante de l'intensité du signal fut cependant observée en comparaison avec les analyses directes. Une production irrégulière d'ions à la surface des coupes transversales souligne le rôle essentiel de la préparation de surface. L'utilisation d'un film mince de matrice pour MALDI déposé à la surface de la coupe n'a pas montré d'amélioration notable des résultats. Cela suggère que l'indigo présent dans les parties les moins dures à la surface de la coupe subit une déplétion accrue lors du polissage.

Au chapitre 7, l'efficacité du LDMS est démontrée pour l'analyse et la caractérisation de pigments modernes. La résolution en masse de l'analyseur à temps de vol TOF-MS est suffisante pour permettre la détermination de la formule moléculaire d'espèces polychlorées et polybromées en identifiant leurs différents isotopes. L'analyse de pigments de la famille des quinacridones montre qu'il est

possible d'identifier simultanément différents composés d'un mélange. En MALDI la détection d'additifs présents en trace montre que la technique est adaptée à l'évaluation de la pureté des échantillons. Malheureusement, dans les spectres MALDI, une augmentation importante des pics de faibles masses peut éclipser le signal de l'échantillon. Dans les émulsions acryliques, les pigments sont ionisés de manière sélective à faible puissance du laser. Le LDMS ne donne pas d'informations relatives au liant comme c'est le cas pour le DTMS.

En conclusion, les expériences menées dans cette thèse démontrent que la technique LDMS peut être utilisée avec succès dans le domaine de la conservation scientifique. Les possibilités d'étudier les pigments organiques par spectrométrie de masse directement à la surface de coupes transversales sont prometteuses. Des analyses par LDMS résolue dans l'espace ont démontré qu'il est possible d'identifier la présence d'un pigment ou plusieurs pigments dans une couche picturale d'une dizaine de microns seulement. L'utilisation d'une trappe d'ions ouvre de plus la voie à des analyses successives en MSⁿ. D'autre part, cette étude établit les conditions d'utilisation ainsi que les limites du LDMS pour l'étude des peintures. Elle montre que diverses complications surgissent quand un laser est utilisé pour la production des ions. Les analyses sont en général délicates et ne sont pas couronnées de succès dans tous les cas de figures. Le LDMS trouvera donc sa meilleure utilisation auprès d'autres techniques déjà en usage dans les laboratoires de recherche en conservation, notamment en combinaison avec la microscopie et la chromatographie.

Dankwoord

MERCI to my wonderful mass spectrometry team at AMOLF: Oscar van den Brink, Gisela van der Doelen, Klaas-Jan van den Berg, Ivana Pastorova, Inez van der Werf, Georgiana Languri, Sophie Peulvé, Sander Koster, Ahmed Al-Khalili, Xinghua Guo, Jaap van der Weerd, Katrien Keune, Stefan Luxembourg, Pete O'Connor, Prof. Dr. J.R.J. van Asperen-de Boer, Wim Muizebelt, Piet Kistemaker, Beatrice Marino, Dominique Scalarone, Vincent Klap, Janine de Maaijer, Tina Weeding, Liz Minor, Marcel Janson, Gerard van Rooij, René Koper, Theo van Diepen, Oscar van Hoof, Ken Sutherland, Petra Novotna. Special thanks to Jorrit van den Berg, my ever present neighbour in the crowded *kippenhok* room for your long-lasting camaraderie.

At first, I would naturally like to express my gratitude to my promotor Jaap Boon, who has been undoubtedly the cornerstone and ever-present motor of the MOLART project as a whole. Without your knowledge, dedication and enthusiasm for conservation sciences this vast inter-disciplinary venture would never have been possible. I owe you a special expression of thanks for your expertise, intellectual input and guidance throughout the writing of this thesis.

I am also deeply grateful to my co-promotor Ron Heeren for supervising the research discussed in these pages. His enthusiasm for mass spectrometry has been always highly inspiring.

Big thanks to Gert Eijkel, Jerre van der Horst, Annebeth Kraij-Kerkhoff, Jos Pureveen, Leo Spetter, Ad de Snaijer and Hans Zeijlenmaker for your craftsmanship and wizardry in solving all technical problems. Extra thanks to Marc Duursma, the best technician on earth, for your continuing enthusiasm and assistance.

Many thanks go out to the “inter-disciplinary” colleagues of the MOLART group who greatly contributed to the interest of the job. To the AMOLF people: Muriel Geldof, Alan Phenix, Lidwien Speleers and Linda Hartgring. To the people at SRAL in Maastricht: René Hoppenbrouwers, Hélène Dubois, Mireille te Marvelde and Anne van Grevenstein. Big thanks also to Renate Keller and Leslie Carlyle for your great contribution to the SRAL workshops. To the ICN people, especially Karin Groen and René Huigen. To the indigo expert Margriet van Eikema Hommes. To the Mauritshuis conservators Petria Noble and Jørgen Wadum. To the museum fellows Arie Wallert (Rijksmuseum), René Boitelle (Van Gogh museum) and Sibylle Schmitt (Kölnisches Stadtmuseum). Thanks to Anita Quye and Jana Novotna for providing samples.

Many thanks to the countless people at AMOLF for your great help and for the inspiring scientific discussions. Thanks to all for your intuitive understanding of my imperfect Dutch.

Many thanks to the members of the doctorate commission, in particular Jan Wouters and Steen Ingemann for your time and expert assistance during the writing of the thesis. Thanks to Ester Ferreira for reading the final text, Mark Clarke and Nicole de Waal for editing this book, your help is deeply appreciated.

I am very grateful to the ICCROM people for the course on Conservation Sciences in 1995 in Paris. To the NVMS people (Dutch society of mass spectrometry) for the great job they do organizing conferences and especially for supporting my trip to Barcelona for the IMSC.

The most special thanks to Charles Tumosa and Marion Mecklenburg for inviting me to the Conservation Analytical Laboratory of the Smithsonian Institution back in the summer of 1993. My internship in Washington, D.C. was the experience of a lifetime. Also special thanks to my long-time friends François and Françoise Péquignot (Musée des Beaux-Arts de Strasbourg) for their crucial encouragements to enter the fascinating world of conservation sciences. My sincerest gratitude to Stefan Wülfert for the great time I had at the Schweizerisches Institut für Kunstwissenschaft in Zurich in 1994, and my warmest thanks to the skilful and passionate team of restorers of the SIK. Also big thanks to Joyce Townsend, Stephen Hackney and Tom Learner for the grand time I had at the Tate Gallery in 1995 and their brilliant work. Many thanks to the many other very knowledgeable “Taters” I had the privilege to meet.

My thanks go finally to my parents Julien and Paule, to my brothers Benjamin and Jonathan, and to Christine and Orane for your love and support.

Curriculum Vitae

The author was born on November 16, 1970 in Paris. He obtained a first degree in Sciences at the University of Paris-Orsay (1991) and a diploma in Chemical Engineering at the European High Institute of Chemistry in Strasbourg (1995). He studied History of Art at the Paris-Sorbonne University (1989-1991) and the University of Strasbourg (1993-1995). He held internships at the Conservation Analytical Laboratory of the Smithsonian Institution, Washington D.C. (1993), at the Schweizerisches Institut für Kunstwissenschaft, Zürich (1994), and at the Tate Gallery, London (1995). He served in the French Army at the national military forensic lab (IRCGN), Rosny-sous-Bois. In 1996 he joined the FOM-Institute for Atomic and Molecular Physics in Amsterdam as Ph.D. student working for the MOLART project. Since 2001, he has been an examiner in the field of Industrial Chemistry with the European Patent Office, The Hague.